

A Thesis Submitted for the Degree of PhD at the University of Warwick

Permanent WRAP URL:

<http://wrap.warwick.ac.uk/101142>

Copyright and reuse:

This thesis is made available online and is protected by original copyright.

Please scroll down to view the document itself.

Please refer to the repository record for this item for information to help you to cite it.

Our policy information is available from the repository home page.

For more information, please contact the WRAP Team at: wrap@warwick.ac.uk

EXCITED STATE STUDIES OF INORGANIC COMPLEXES
BY LASER FLASH PHOTOLYSIS

by

Hisham Y. Al-Saigh

A thesis submitted for
the degree of
Doctor of Philosophy

Department of Chemistry and Molecular Sciences
University of Warwick

December 1983

*I dedicate this thesis to my Mother
and to the memory of my Father.*

ACKNOWLEDGEMENTS

I wish to thank Professor T. J. Kemp for his invaluable encouragement and interest throughout the work. I thank Dr. G. A. Salmon for his assistance in respect of the pulse radiolysis experiments cited in this thesis. I also thank Professor O. Traverso of the University of Ferrara, Italy, for supplying the platinum complex, Dr. N. G. Connelly of the University of Bristol for e.m.f. measurements and Dr. T. G. Brown of Preston Polytechnic for lifetime measurements on two complexes.

I am also grateful to the workshops of the Department of Chemistry and Molecular Sciences for help in both construction of apparatus and maintenance of the laser assembly.

I wish to acknowledge financial support from the University of Mosul, Mosul, Iraq.

ABSTRACT

This thesis is concerned with three distinct but inter-related problems in inorganic photophysics, namely (i) the photosensitisation of an important alkylcobalt(III) complex, (ii) the photophysics and photoelectron transfer reactions of two bis(bipyridine)-ruthenium(II) complexes and (iii) a preliminary study of a luminescent binuclear complex of platinum. The first two problems comprise the major part of the work and the literature survey is focused on these. The principal methods of investigation have been 347 nm laser flash photolysis (in emission and absorption), fluorimetry and quantum yield determination.

Photosensitisation of Alkylcobalt(III) Complexes: While alkylcobalamins and their model compounds, the alkylcobaloximes are known to photodissociate in high yield under visible light irradiation, the multiplicity and energy of the photoreactive state have not been identified. Now acidopentammine complexes of cobalt(III) are known to be photosensitised both by organic triplet states and by the 'solar energy' complex $[\text{Ru}(\text{bpy})_3]^{2+}$, indicating the dissociating state to have triplet character and to be of lower energy than signified by the absorption maxima. Accordingly we investigated the possibility of such sensitizers functioning in the case of the organocobalt(III) compounds both by measuring the kinetics of interaction between the donor triplet states and the alkylcobalt(III) compound by laser flash photolysis, which indicated that while donors with $E_T > 170 \text{ kJ mol}^{-1}$ were quenched very effectively, those with low values of E_T ($< 110 \text{ kJ mol}^{-1}$), such as rubrene and β -carotene, where virtually without effect ($k_q < 10^7 \text{ dm}^3 \text{ mol}^{-1} \text{ s}^{-1}$). The detailed picture, covering a comprehensive range of triplet donors, enables a Wilkinson plot to be compiled and hence a clear picture of the energies of the active states of the alkylcobalt(III) complex. This work was extended to a range of inorganic donors of widely varying reduction potential from which it became clear that the principal process of quenching is energy- rather than electron-transfer (although the latter might participate in favoured cases). A comparative study was carried out on *tris*-(acetylacetonato) cobalt(III). The laser kinetic studies were augmented by a series of quantum yield experiments using sensitizers with S_1 absorption well to the red of the band maxima of the CT transitions of the R-Co(III) species, but with very high values of ϕ_T .

Photophysics and Photoelectron Transfer Reactions of Bis(polypyridyl) Ruthenium(II) Complexes: We examined the temperature dependence of the luminescence lifetimes of the complexes $[\text{Ru}(\text{bpy})_2\text{acac}]^+$ and $[\text{Ru}(\text{bpy})_2\text{en}]^{2+}$ from 77 to $\sim 300 \text{ K}$ with the view of elucidating whether their comparatively very short lifetimes at ambient temperature are due to small activation barriers to deactivation, as shown by two groups for the well-known complex $[\text{Ru}(\text{bpy})_3]^{2+}$, or to large pre-exponential terms. In fact the activation barriers are very much lower than for $[\text{Ru}(\text{bpy})_3]^{2+}$ and the frequency terms are also somewhat lower, the overall behaviour is thus energy-controlled. However, sizeable solvent-isotope effects (up to ca. 2) are found indicating a considerable amount of CTS character in the electronic transition responsible for the deactivation step.

Studies of the quenching of these same Ru(II) complexes by a wide variety of electron acceptors, combined with electrochemical and lifetime measurements, indicates that whilst the behaviour of $[\text{Ru}(\text{bpy})_2\text{acac}]^+$ follows Weller theory for excited-state electron-transfer very closely, as does $[\text{Ru}(\text{bpy})_3]^{2+}$, the result for $[\text{Ru}(\text{bpy})_2\text{en}]^{2+}$ indicates a generally much faster quenching than predicted for full electron-transfer, indicating the possibility of either non-radiative exciplex formation or an initial one electron oxidation of the ligand, ethylenediamine.

Luminescence from a Binuclear Platinum Complex: The complex $[\text{Pt}(\text{PPh}_3)_2]_2$ luminesces not only at low-temperature (77 K), ~ 660 nm in glassy solvents (as recorded before), but also at ambient temperatures at ~ 460 -520 nm. The room temperature emission is strongly quenched by dioxygen, which indicates it to be spin-forbidden. Temperature studies indicate that there is no gradual shift in the emission band as the temperature is raised, but rather are two coexistent and distinct emissions at 460-520 and 660 nm.

ABBREVIATIONS

acac	acetylacetonato
bpy	2,2'-bipyridine
CA	cellulose acetate
CT	charge-transfer
CTTL	charge-transfer-to-ligand
CTTM	charge-transfer-to-metal
CTTS	charge-transfer-to-solvent
DMF	dimethylformamide
DMSO	dimethylsulphoxide
E _A	activation energy
E _T	Dimroth parameter
en	ethylenediamine
EPA	ethanol:isopentane:ether (2:5:5)
ESA	excited state absorption
e.s.r.	electron spin resonance
ISC	inter-system crossing
LF	ligand field
LMCT	ligand-to-metal charge-transfer
M-L	metal-ligand
MLCT	metal-to-ligand charge-transfer
MO	molecular orbital
MTHF	2-methyltetrahydrofuran
phen	1,10-phenanthroline
PMM	polymethylmethacrylate
PPh ₃	triphenylphosphine
py	pyridine
S	spin quantum number

SOC	spin-orbit coupling
T	temperature
T _g	glassing temperature
u.v.	ultra-violet
τ	lifetime
φ	quantum yield
λ	wavelength

CONTENTS

	Page
<i>Chapter 1</i>	<i>Introduction</i>
1.1	Historical and introductory remarks 1
1.2	Electronic absorption spectra of coordination compounds 4
1.3	Excited state processes of transition metal complexes 11
1.4	Quenching of excited-states by energy transfer 16
1.5	Bimolecular electron-transfer reactions of excited-states of transition metal complexes 21
1.6	Emission spectra of luminescent transition metal complexes 27
1.7	Theory of non-radiative processes 31
1.8	Kinetic schemes for luminescence 35
<i>Chapter 2</i>	<i>Selected Systems</i>
2.1	Cobalt(III) - A 3d ⁶ system 42
2.1.1	Absorption spectra and some photochemical aspects of Co(III) complexes 43
2.1.2	Photosensitised reactions of Co(III) complexes 51
2.1.3	Cobaloximes as models for vitamin B ₁₂ 55
2.1.4	Electronic spectra and photochemistry of alkylcobaloximes and alkylcobalamins 60

	Page
2.1.5 The photochemistry of tris-(acetylacetonato)cobalt(III)	68
2.2 Ruthenium(II); A system exhibiting 'heavy atom' luminescence	70
2.2.1 Absorption and luminescence spectra	72
2.2.2 The Crosby model for low-temperature luminescence of ruthenium(II) complexes	75
2.2.3 Photoredox reactions and quenching mechanisms	82
<i>Chapter 3</i>	<i>Experimental</i>
3.1 Instrumentation	89
3.1.1 Luminescence intensities and spectra	89
3.1.2 Laser flash photolysis	91
3.1.3 The optical bench	102
3.1.4 Other instrumentation used	104
3.2 Sample preparation	105
3.3 Purity of chemicals	109
3.4 Sample synthesis	110
3.5 Analysis of results	111
3.5.1 ESA and emission lifetime measurements	111
3.5.2 Analysis of Arrhenius-type data	112

	Page
<i>Chapter 4</i>	<i>Sensitisation and Quenching Processes of Alkylcobalt(III) Compounds</i>
4.1	Quenching of organic triplet states by ethyl(aquo)cobaloxime 114
4.2	Quenching of inorganic excited states by ethyl(aquo)cobaloxime 117
4.3	Sensitisation of the photo-decomposition of ethyl(aquo)-cobaloxime 118
4.4	Quenching of excited states by methylcobalamin 123
4.5	Quenching of excited states by tris-(acetylacetonato)cobalt(III) 124
4.6	Discussion 125
<i>Chapter 5</i>	<i>Luminescence Kinetics and Electron-Transfer Quenching of Bis(polypyridyl) Complexes of Ruthenium(II)</i>
5.1	Introductory remarks 132
5.2	Luminescence spectra and lifetime measurements in different solvents 134
5.3	Temperature-dependence studies of emission lifetime - Results 136
5.4	Luminescence kinetics: Discussion of results 139
5.5	Kinetics of luminescence quenching of polypyridyl complexes of Ru(II) by electron-transfer - Results 145
5.6	Kinetics of luminescence quenching by electron-transfer - Discussion 148

	Page
<i>Chapter 6</i>	
<i>Luminescence from a Binuclear Platinum Complex: A Preliminary Study</i>	155
<i>References</i>	161

CHAPTER 1
INTRODUCTION

The photosensitivity of inorganic compounds of all types has been appreciated from the earliest times. This subject has always drawn attention as an interesting area for qualitative study as in, for example, the photographic process, and now, increasingly, it has prompted quantitative investigations in view of its valuable applications to preparative chemistry¹. An illustration of how concepts relating to inorganic photochemistry have developed is provided by the simple example of aqueous iodide ion. In early work, the initial step in this process was proposed² to be formation of an iodine radical and a "free-solution electron". Following photoionisation the electron was thought to be ejected into the solution, where it was bound by electric polarisation of surrounding water molecules to yield its solvation energy, B . At that time (1928), there was no experimental evidence for "free-solution electrons" and this concept³ was discarded until increasing evidence in the 1950s led ultimately to the optical characterisation of the solvated electron by fast kinetic spectroscopy in 1961^{4,5}.

The nature of the radical produced was correctly deduced from the electronic absorption spectrum of I^- ion in water, where the separation of the two bands observed was recognised as being related to the $^2P_{1/2} - ^2P_{3/2}$ doublet splitting of gaseous iodine atoms⁶. Thus, to understand simple inorganic-ion photolysis, the

spectroscopic transition must be related to the nature of the excited state, which in turn must be related through scavenging processes or direct observation of reactive intermediates to the final product formation.

Mechanistic photochemistry has been an area of intense activity and rapid advances for the last twenty years. Early investigations dealing chiefly with organic systems were extended subsequently into reactions of organometallics and transition-metal complexes. This has come about partly through realisation of synthetic possibilities, both in conventional solution work and matrix isolation, and also through demand for the development of solar energy devices based either on conversion of water into combustible fuel or on provision of electrical power⁷. The increased availability of pulsed lasers, operating both in the ns and ps time domains, has stimulated measurements of ultrafast ($k > 10^{-6} \text{ s}^{-1}$) photophysical processes utilising both luminescence and excited-state absorption (ESA) detection modes. New facets of luminescence behaviour have emerged, including dual luminescence, several observations of non-exponential decay of certain complexes and the frequent occurrence of bimolecular electron-transfer processes.

An excited state decays by two types of processes, broadly termed as radiative and non-radiative. While luminescence studies yield direct information about radiative processes, they can give only indirect evidence concerning non-radiative pathways. To obtain useful

information about the nature and extent of the latter, it is necessary to monitor the effects on the luminescence of a system caused by systematic variation of environmental factors such as solvent, ligand field (LF) and temperature. Further information can be obtained by examining the effect of inter-molecular processes on the luminescence, usually in the form of quenching experiments, and by examining the photoreactivity of complexes, which can also be classified as a type of non-radiative process. One of the most important and general processes characterised has been the quenching or generation of an excited state by one-electron-transfer reactions⁸. By "quenching" it refers to (usually non-radiative) deactivation of an electronically excited molecule (excited state) by bimolecular interaction with a ground state molecule (quencher). Among the possible results of such quenching are one-electron transfer to or from the excited substrate, excitation energy-transfer from excited substrate to quencher, net chemical reaction (in substrate, quencher, or both), and net radiationless decay. As quenching via electron-transfer has become well studied, it has been found frequently that the same excited substrate can be quenched by electron donors and acceptors. It is a little ironic that the importance of these reactions was recognised only recently since it was established long ago that in photosynthesis an excited chlorophyll molecule mediates redox reactions which originate in one-electron-transfer reactions of the excited magnesium complexes⁹⁻¹¹.

1.2 ELECTRONIC ABSORPTION SPECTRA OF COORDINATION COMPOUNDS

The assignment of the various bands which appear in the absorption spectra of transition metal complexes is a very difficult problem because the absorption spectra reflect, of course, the complexity of the electronic structure of these molecules. It has been useful to classify the spectra of organic molecules according to the "orbital jump" involved. Thus, these are $\pi-\pi^*$, $n-\pi^*$, $\sigma-\sigma^*$, and so forth, transitions.

In order to make the problem easier in the case of transition metal complex spectra, it is convenient to describe each state by using its preponderant molecular orbital configuration, and then to make a classification of the electronic transitions according to the location of the MO's involved. Using this criterion, three types of electronic transitions may be distinguished as follows¹²:

- (i) Transitions between MO's mainly localised on the central metal. MO's of such a type are those deriving from metal d-orbitals (for example, the $t_{2g}(\pi)$ and $e_g(\sigma^*)$ MO's in Fig. 1.1. These transitions are usually called d-d or ligand field (LF) transitions.
- (ii) Transitions between MO's mainly localised at the ligands and MO's mainly localised on the central metal. For obvious reasons, these transitions are called charge transfer (CT) or electron transfer transitions. Depending



Notes on this

MO's

Legend Details

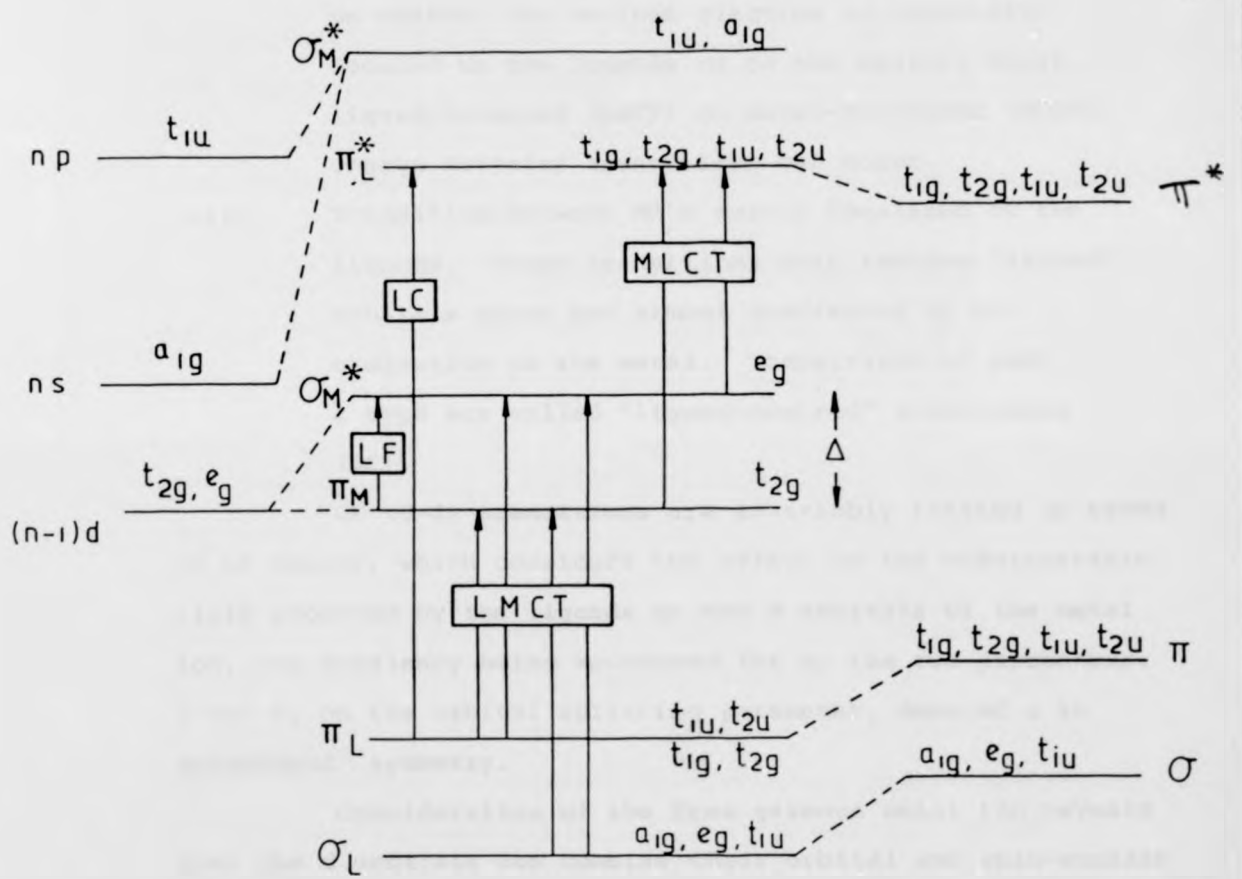
Figure 1.1 Molecular orbital scheme for an octahedral complex:

LF - ligand-field transitions,

LMCT - ligand-to-metal-charge-transfer,

MLCT - metal-to-ligand charge-transfer,

LC - ligand-centred transitions



Metal Orbitals

MO's

Ligand Orbitals

on whether the excited electron is originally located on the ligands or on the central metal, ligand-to-metal (LMCT) or metal-to-ligand (MLCT) charge transfer transitions can occur.

- (iii) Transitions between MO's mainly localised on the ligands. These transitions only involve "ligand" orbitals which are almost unaffected by coordination to the metal. Transitions of such a type are called "ligand-centred" transitions (LC).

LF (d-d) transitions are invariably treated in terms of LF theory, which considers the effect of the electrostatic field produced by the ligands on the d orbitals of the metal ion, any covalency being accounted for by the two parameters, B and C, on the orbital splitting parameter, denoted Δ in octahedral symmetry.

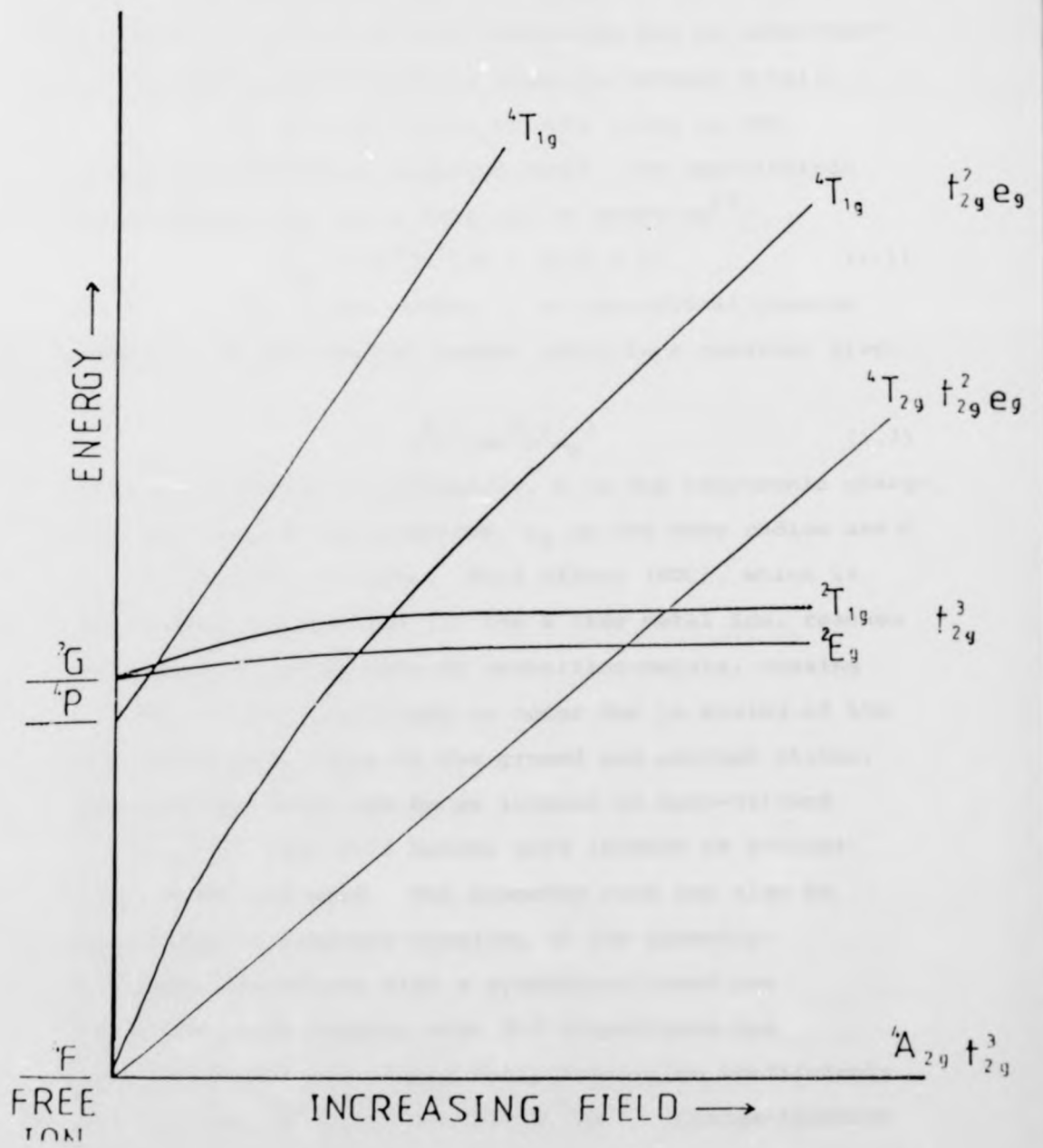
Consideration of the free gaseous metal ion reveals that the d-orbitals can combine their orbital and spin-angular momenta as predicted by Russell-Saunders coupling¹³ to produce a set of states which are designated by different term symbols and ordered according to Hund's rules¹³. The ligand field splits the d-orbitals into two sets, one containing the three orbitals d_{xy} , d_{yz} , and d_{xz} (t_2) and the other containing the axial orbitals $d_{x^2-y^2}$ and d_{z^2} (e). The splitting and relative positions of these sets depend upon the overall symmetry of the system and the LF strength. An indication of the latter can be obtained from the spectrochemical series.

For a strong field, terms corresponding to the

different orbital configurations ($t_{2g}^m e_g^n$) are derived from group theory. In reality, the ligand field is often of intermediate strength, and the ordering of the states can be predicted from a term diagram such as those developed by Tanabe and Sugano¹⁴, which correlate the two extreme cases depicted above. The treatment is illustrated as follows. Chromium(III) is a d^3 system and has the configuration t_{2g}^3 in O_h symmetry. Promotion of an electron will give rise to a $t_{2g}^2 e_g$ configuration. The terms for the t_{2g}^3 configuration are $^4A_{2g}$, 2E_g , $^2T_{2g}$, and $^2T_{1g}$, with the $^4A_{2g}$ term being the ground state by consideration of Hund's rule. The $t_{2g}^2 e_g$ configuration gives rise to a further set of quartet and doublet terms. The quartet states represent transitions between different orbitals whereas the doublet states refer merely to changes of electron spin within a single orbital. The ordering of these states for the appropriate ligand field strength can now be found by recourse to the d^3 term diagram, as shown in Fig. 1.2.

Transitions between any two of these states are fully allowed only when (i) there is no alteration in the spin quantum number ($\Delta S = 0$), and (ii) a change in symmetry is involved (Laporte-allowed) as satisfaction of these two conditions is required to achieve a non-zero transition moment integral for both the magnetic and electric dipole vectors of the exciting light, respectively. In the case cited above, as for all transition-metal complexes, there are no fully-allowed transitions between the ground and first excited states

Figure 1.2 Term diagram (lowest levels) for an octahedral d^3 metal complex (from reference 16).



as they are all Laporte-forbidden, and in the doublet case both Laporte- and spin-forbidden. d-d Transitions do, however, occur and their mechanism can be understood by considering the selection rules in further detail.

The spin selection is only valid in the absence of spin-orbit coupling (SOC), the one-electron SOC constant, ξ_{nl} for a free ion is given by¹⁵:

$$\xi_{nl} = CZ^4/n^3 l(l + \frac{1}{2})(l + 1) \quad (1.1)$$

where Z is the atomic number, l is the orbital quantum number, n is the orbital number and C is a constant given by

$$C = e^2 h^2 / 2m^2 c^2 a_0^3 \quad (1.2)$$

where h is Planck's constant/ 2π , e is the electronic charge, m is the mass of the electron, a_0 is the Bohr radius and c is the velocity of light. This effect (SOC), which is shown above in equation 1.1 for a free metal ion, reaches significance in the case of transition-metals, causing spin-forbidden transitions to occur due to mixing of the same spin-orbit terms in the ground and excited states; although they will not be as intense as spin-allowed transitions, they will become more intense as heavier metal atoms are used. The symmetry rule may also be broken due to vibronic coupling of the symmetry-forbidden transition with a symmetry-allowed one. These arguments suggest that d-d transitions are relatively weak and indeed their extinction coefficients (ϵ) are usually ca. 10 to 1000 $M^{-1}cm^{-1}$. Charge-transfer transitions are invariably both spin- and symmetry-allowed, and are therefore very intense with ϵ values

ca. 10^3 to 10^4 $M^{-1}cm^{-1}$ or greater.

The various type of charge transfer absorption spectra have been discussed by Dunn¹⁷, Jörgensen¹⁸, Schmidtke¹⁹, and Schläfer and Gliemann¹⁵. The transitions in question all involve a radical redistribution of electron density within the molecule. Systems in which excitation results in a transfer of electronic charge away from the ligands towards the metal centre are denoted ligand-to-metal charge transfer (LMCT) transitions. Excitations which result in an outward flow of electronic charge are denoted metal-to-ligand charge transfer (MLCT) and charge-transfer-to-solvent (CTTS). Jörgensen¹⁸ has proposed a semiempirical correlation of the energies of LMCT transition maxima with the electronegativity difference between metal and ligand, $X_L - X_M$, the d-orbital energy difference caused by ligand-field splitting, $10Dq$, the difference in the spin-pairing energy of the central metal in the ground and excited states, SSP , and the Racah parameter, B . Thus, the maximum of a LMCT transition is expressed as¹⁹

$$\bar{\nu}_{\max} = 30(X_L - X_M) + 10Dq + SSP + aB \quad (1.3)$$

In many complexes one would expect $X^- \rightarrow M$, LMCT transitions at different energies, depending on (1) whether the ligand electrons involved in the transition have a σ - or π -symmetry with respect to the metal-ligand bond; (2) whether the acceptor orbital is antibonding or non-bonding; and (3) the values, $10Dq$ and X_m , appropriate to the specific metal-centred acceptor orbital involved in the transition. Although one would generally expect $d_{x^2-y^2}$ and d_{z^2} orbitals

to differ in energy in $M^{III}L_5X$ complexes, the last point has not been carefully explored, and one generally uses an average optical electronegativity and an average value of $10 Dq$ if the transition involves an antibonding orbital. If non-bonding metal orbitals are involved, the $10 Dq$ term does not appear in the correlative equation³.

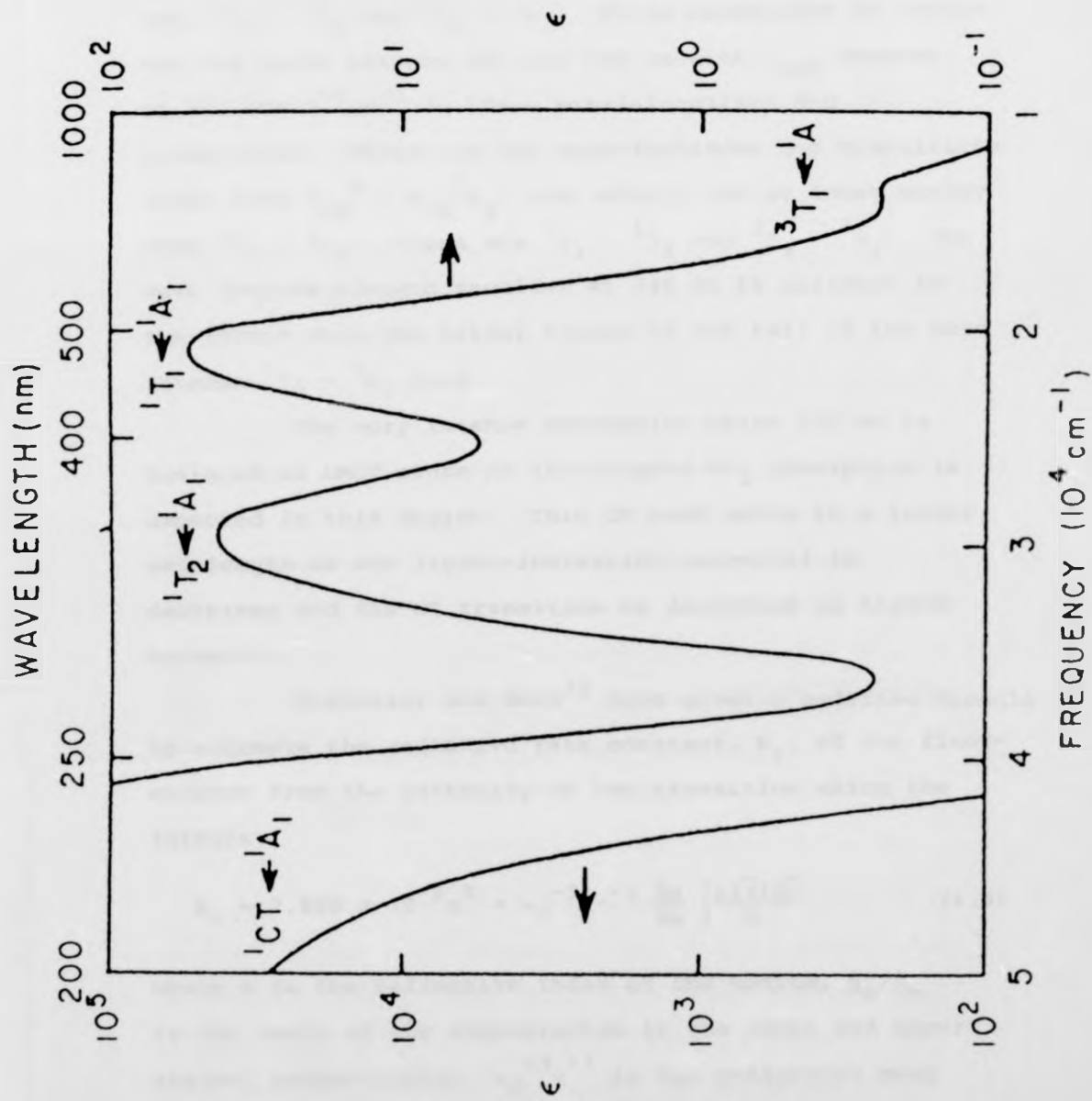
Charge transfers in the reverse direction, i.e. metal-to-ligand charge transfer (MLCT) transitions (Fig. 1.1), are likely to occur in complexes with central atoms having small ionisation potentials and ligands with easily available empty π^* orbitals. Ligands such as CN^- , CO , SCN^- and especially conjugated organic molecules possess empty π^* orbitals suited for such "inverted" transitions²⁰⁻²³. Regarding the central atoms, it is obvious that MLCT transitions will be favoured when the metal has a low oxidation state. For example, the bands in the visible of low-spin $[Fe(phen)_3]^{2+}$ are due to MLCT transitions, while those of low-spin $[Fe(phen)_3]^{3+}$ are due to LMCT transitions^{20,21}.

The energy of the CT band depicts the ease with which the metal ion is oxidised (MLCT) or reduced (LMCT), and its position will therefore depend upon the nature and oxidation state of the metal, and for readily oxidised or reduced metal cores may well completely envelop the low-intensity d-d bands, as in the case of $Ru(II)$ ²⁴ and $Co(III)$ ¹.

Both types of transition (d-d and CT) are depicted for $[Co(NH_3)_6]^{3+}$ in the absorption spectrum shown in Fig. 1.3. This species is d^6 , and magnetic measure-

Figure 1.3 Absorption spectrum of $[\text{Co}(\text{NH}_3)_6]^{3+}$
(from reference 3).

WAVELENGTH (nm)



ments indicate that it is a low-spin complex. There are two low-energy spin-allowed d-d transitions arising from $t_{2g}^6 \rightarrow t_{2g}^5 e_g$ in the spectrum of the spin-paired d^6 ion, ${}^1T_1 + {}^1A_1$ and ${}^1T_2 + {}^1A_1$. It is reasonable to assign the two bands between 350 and 500 nm with ϵ_{\max} between 10 and $100 \text{ M}^{-1} \text{ cm}^{-1}$ as these metal-localised d-d transitions. There are two spin-forbidden d-d transitions (also from $t_{2g}^6 \rightarrow t_{2g}^5 e_g$) that should lie at lower energy than ${}^1T_1 + {}^1A_1$; these are ${}^3T_1 + {}^1A_1$ and ${}^3T_2 + {}^1A_1$. The weak long-wavelength shoulder at 740 nm is assigned to the former with the latter hidden in the tail of the more intense ${}^1T_1 + {}^1A_1$ band.

The very intense absorption below 250 nm is assigned as LMCT since no intraligand NH_3 absorption is expected in this region. This CT band moves to a longer wavelength as the ligand-ionisation potential is decreased and the CT transition is described as ligand-to-metal.

Strickler and Berg²⁵ have given a modified formula to estimate the radiative rate constant, k_r , of the fluorescence from the intensity of the transition using the formula:

$$k_r = 2.880 \times 10^{-9} n^2 \langle \nu_f^{-3} \rangle^{-1} \frac{g_e}{g_n} \int \frac{\epsilon(\bar{\nu}) d\bar{\nu}}{\bar{\nu}} \quad (1.4)$$

where n is the refractive index of the medium, g_e/g_n is the ratio of the degeneracies in the lower and upper states, respectively, $\langle \nu_f^{-3} \rangle^{-1}$ is the reciprocal mean cube of the emission maximum and the integration is carried out over the entire absorption band. The

stringent conditions under which this equation holds, i.e. broad bands with a small Stokes shift and for a strongly allowed transition, make the equation of limited use in practice; where large Stokes shifts for emission are observed, e.g. in the cases of $[\text{Cr}(\text{urea})_6]^{3+}$ ²⁶ and Rh(III)phosphorescence²⁷, d-d bands are invariably weak. The treatment has, therefore, only any real use when absorption and emission bands are coincident, in which case the approximate form

$$k_r \sim 5 \times 10^{-9} \nu^{-2} \epsilon_{\text{max}} \Delta \bar{\nu} \quad (1.5)$$

gives an order of magnitude estimate of k_r .

A test for the Strickler-Berg modified formula was undertaken by Crosby and Demas²⁸ by estimating radiative lifetimes for some ruthenium and osmium complexes due to mixing of the states in the absorption bands, and they formulated a model based on SOC considerations in which the phosphorescence is considered to "borrow" intensity from fully-allowed transitions due to the loss of spin and orbital identity between the two states caused by SOC.

1.3 EXCITED STATE PROCESSES OF TRANSITION-METAL COMPLEXES

There are several processes which a molecule in an excited state can undergo. The excited state, when first generated by absorption of a light quantum, may be in a high vibrational state. This is usually the case with coordination compounds, as evidenced by the broadness of the absorption and emission bands and, where observable, the red shift of the latter relative to the

former¹. The accepted explanation is that the transitions obey the Franck-Condon principle in that the most favoured transition is to vibrational levels such that the most probable nuclear positions are not much different from those in the ground state. If a transition terminates at a high vibrational level of the excited state, the implication is that the zero vibrational level is one of significantly different geometry from that of the ground state²⁹.

A preliminary and very rapid process is then the thermal equilibration of the excited state to vibrational equilibrium with the medium; this probably occurs within a few vibrational periods. The equilibrated excited state may then return to the ground state by emission or by radiationless deactivation (internal conversion). Either form of return is usually to some high vibrational level of the ground state. Alternatively, the internal conversion may be to a lower state of the same multiplicity. Emission and radiationless deactivation may be somewhat hindered in the case of complexes, and suggested lifetimes have been around 10^{-7} sec³⁰, while internal conversion to a lower excited state is considered to be very fast. Thus excitation is normally thought to be followed by a rapid descent to the lowest excited state of the same multiplicity. It has been suggested, however, that this may not always be the case, especially with asymmetric complexes²⁹. Returning to the emission process, this is called fluorescence if the excited state and ground states are of the same multiplicity, and phosphorescence if

they are of different multiplicity.

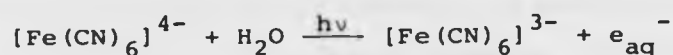
The excited state may also undergo a radiationless transition to a lower state of different multiplicity, i.e. intersystem crossing may occur, and this process is thought to have about the same probability as that of radiationless deactivation to the ground state, at least in the case of Cr(III)^{30,31}. The new state so reached may now have a relatively small emission probability since the phosphorescent return to the ground state is hindered by the change of multiplicity. The triplet states of organic molecules and the doublet state of Cr(III) are examples of such potentially long-lived states.

Finally, an excited state may undergo chemical reaction. If some particular bond is highly distorted in the nascent excited state, fairly prompt or predissociative cleavage would be a possibility. Alternatively, a thermally equilibrated excited state may undergo a rapid but otherwise essentially ordinary chemical reaction. In either situation, the nature of the chemical process should show some correlation with that of the excited state, and such correlations are in fact found. Thus, excitation to a ligand-field state tends to lead to heterolytic reactions, such as aquation which has been observed for a variety of complexes of Cr(III), Co(III), Pt(IV), Pt(II), and other metals. For example³²:

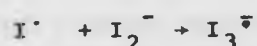
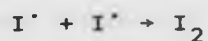
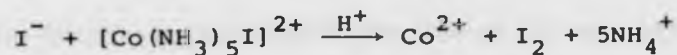
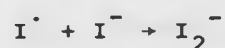
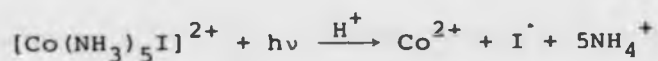


LMCT excited states tend to give redox decomposition in which the metal is reduced and either a ligand is oxidised (intramolecular oxidation-reduction

reactions), as in the well-documented case of Co(III) photochemistry³³, or solvent is oxidised. CTTS states tend to lead to oxidation of the metal or of the complex as a unit, accompanied either by reduction of the solvent or production of a solvated electron (intermolecular oxidation-reduction reactions), as in the example³⁴.



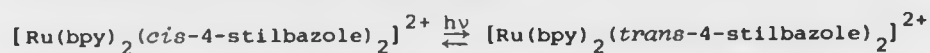
Photoreactions are frequently studied by chemical scavenging of the primary radicals produced, and the situation is often complicated by secondary radical reactions as in the case of $[\text{Co}(\text{NH}_3)_5\text{I}]^{2+}$ ³⁵



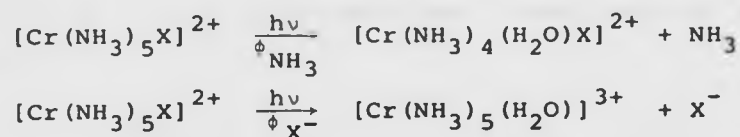
Oxidation of the metal core follows irradiation of the MLCT bands. This situation is uncommon as it requires the combination of a reducing metal and an oxidising ligand to be energetically accessible to near-u.v. light.

Finally, ligand-centred transitions, as expected, induce reactions typical of the ligand and

are therefore of no special interest from an inorganic point of view. One example is that of



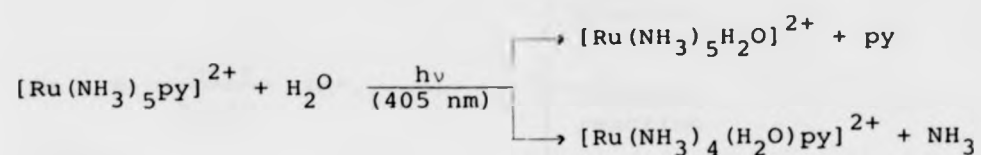
The independence of photosubstitution yields of Cr(III) complexes in O_h symmetry on excitation wavelength throughout the LF bands suggests that these reactions occur from a common state, that is, the lowest excited state of a given spin multiplicity. However, complexes such as $[\text{Cr}(\text{NH}_3)_5\text{X}]^{2+}$ ³⁷ (X = Cl, Br) have been shown to exhibit two reaction modes:



ϕ_{NH_3} is constant throughout the range of excitation, whereas ϕ_{X^-} shows an approximately 50-fold increase (0.005 to 0.3) on going toward the CT absorption bands, suggesting a small but finite CT component to the d-d bands, from which they "borrow" intensity. This example also illustrates that photochemical reactions are not simply accelerated thermal reactions, but can lead to unique products.

The intermixing of excited states in heavy-metal systems caused by SOC is elegantly demonstrated by the effect of ligand substitution upon the photochemical reactivity of $[\text{Ru}(\text{NH}_3)_5\text{X}]^{2+}$ ³⁸, where X is a series of substituted pyridines. Excitation into the MLCT band in aqueous acidic solution yields products which are

considered to originate from a common excited LF state.



Substitution of the aromatic ring causes the total quantum yield to vary from 0.003 to 0.02 and it is suggested that aromatic substitution by electron-withdrawing groups lowers the energy of the (unreactive) CT state below that of the LF state to give reduced reactivity. The implications of this example are that SOC is so large that inhibition of inter-state transitions is effectively removed, so that relaxation to the (photoreactive) lowest excited state is rapid.

1.4 QUENCHING OF EXCITED-STATES BY ENERGY TRANSFER

Electronic energy transfer involves the exchange of excess energy by physical processes to produce relaxation of the donor with no chemical change. Energy transfer is one mechanism of the bimolecular quenching of an excited-state molecule which may take place. The other mechanisms are chemical reaction and the deactivation of the excited-state by some (physical) catalytic action of the quencher (Fig. 1.4). Different quenching processes may also occur simultaneously which causes noticeable complications in the study of these systems.

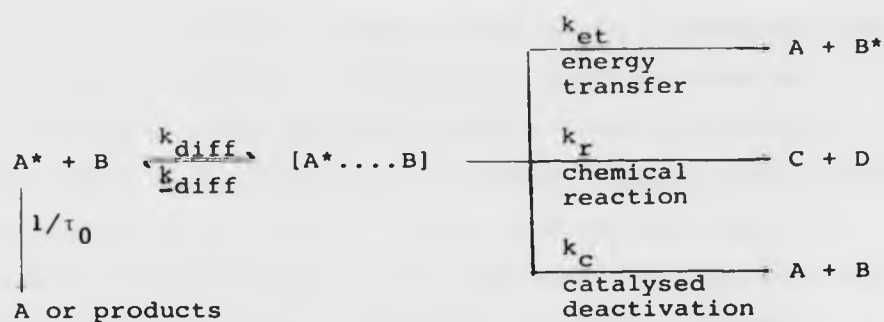


Fig. 1.4 Bimolecular quenching processes for an excited-state molecule

Intermolecular energy transfer leads to electronic excitation of the acceptor, which can then undergo any of the normal fates of excited species. One of these is decomposition, and photosensitised reactions are those in which dissociation or reaction takes place in a species other than that absorbing the radiation.

Photosensitisation offers several advantages compared to direct irradiation of the spectral absorption bands. For instance, it makes possible the population of a given excited-state of the acceptor complex with more sharply defined electronic energy, that is, with a smaller vibrational contribution than obtainable by direct light absorption. The use of photosensitisers of well-characterised donor levels affords fairly accurate identification of the thermally equilibrated excited state energies of the acceptor species and, often, gives rise to "cleaner" photoreactions, peculiar to the selectively populated thermally-equilibrated excited states. Quenching experiments yield quantitative information about intramolecular deactivation steps as

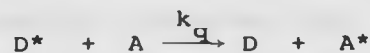
well as the nature of the excited state. Quenching can be used to completely suppress an excited state to facilitate a more detailed study of other processes. In general, sensitisation by energy transfer and quenching processes can be used³⁹ (i) to identify the reactive state of a molecule, (ii) to increase the quantum yield of a process, (iii) to increase the range of useful exciting wavelengths, (iv) to quench undesired photoreactions, and (v) to study the intimate mechanism of bimolecular processes. Sensitisation can also provide information on excited-state lifetimes, intersystem crossing efficiencies, and emission and reaction efficiencies.

Well-defined characterised organic triplet donors are often used in sensitisation studies, such as biacetyl, naphthalene, etc.³⁹. The desire to understand the factors influencing the mechanism of energy transfer has created an interest in the quenching of organic triplets by transition metal complexes^{40,41}. Inorganic complexes⁴² are also sometimes used as donors, although less convincingly, as many are not completely understood in fluid solution at ambient temperature due to general lack of photophysical data under these conditions.

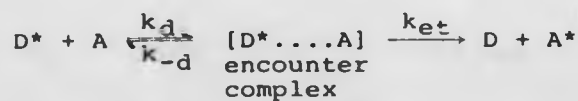
The sensitised solvation and phosphorescence of $[\text{Cr}(\text{CN})_6]^{3-}$ in dimethylformamide at room temperature⁴³ provides a good example of sensitisation by a series of donors of different energies. Energy-transfer from high energy donors (e.g. triplet xanthone), which can populate both $^4\text{T}_{2g}$ and the $^2\text{E}_g$ excited states, causes both photosolvation and phosphorescence, whereas

sensitisation with low-energy donors, such as $[\text{Ru}(\text{bipy})_3]^{2+}$, which are able to transfer energy only to the ${}^2\text{E}_g$ state, promotes only phosphorescence, implying that a higher state is photoactive, while the lower one is responsible for phosphorescence. It was also possible to establish that the efficiency of the ${}^4\text{T}_{2g} \rightarrow {}^2\text{E}_g$ intersystem crossing step of $[\text{Cr}(\text{CN})_6]^{3-}$ by means of the energy transfer technique⁴⁴, as being about 0.5.

There are two principal mechanisms for energy transfer, i.e. long-range resonance transfer, which occurs even in a rigid medium at high dilution³ when the donor is distant from the acceptor (by an average of 50-100^oA). The other mechanism, which is the most important one for transition metal complexes, is collisional transfer, which is characterised by the bimolecular quenching rate constant, k_q , of the excited state D^* by A. If it is assumed that energy transfer is the only mode of bimolecular quenching, then the kinetic scheme⁴⁵ is simply:



Such a process can be considered to involve two steps, viz.



i.e., diffusion together of the excited state and the quencher to give the so-called encounter complex, and then the energy transfer step which competes with the diffusion apart of the two molecules. The diffusion-

controlled rate constant, k_d , is given by the modified Stokes-Einstein equation

$$k_d = 8 kT/3000 \eta \quad (1.6)$$

where η is the viscosity of medium, k is the Boltzmann constant, and T is the absolute temperature, thus the energy transfer rate is an inverse function of viscosity. For a solvent such as water at room temperature, k_d is approximately $5 \times 10^9 \text{ M}^{-1} \text{ sec}^{-1}$, while for glycerine it is about $5 \times 10^6 \text{ M}^{-1} \text{ sec}^{-1}$ ³. The experimental quenching constant, k_q , can be found by use of the Stern-Volmer equation⁴⁶, which is derived by consideration of the quenching mechanism as an additional competing deactivation process of the excited level:

$$\frac{\phi^0}{\phi} = 1 + K^{SV}[Q] \quad (1.7)$$

where $[Q]$ is the quencher concentration, ϕ^0 is the photochemical yield in the absence of quencher, ϕ is the observed yield, and K^{SV} is given by

$$K^{SV} = k_q \tau \quad (1.8)$$

where τ is the phosphorescence lifetime of the complex under the experimental conditions used. The energy transfer efficiency, α_{et} , that is the fraction of encounters which results in energy transfer from D^* to A , as

$$k_q = k_d \left(\frac{k_{et}}{k_{-d} + k_{et}} \right) = k_d \alpha_{et} \quad (1.9)$$

$$\alpha_{et} = \frac{k_q}{k_d} \quad (1.10)$$

When the energy transfer process is diffusion controlled or nearly so for organic molecules in fluid solution, the

Table 1.1 Selected Examples of Energy Transfer Efficiency (a)

Donor	Acceptor	$k_q^{(b)} / \text{dm}^3 \text{mol}^{-1} \text{s}^{-1}$	$k_d^{(b)} / \text{dm}^3 \text{mol}^{-1} \text{s}^{-1}$	$\alpha = \frac{k_q}{k_d}$
$[\text{Ru}(\text{bipy})_3]^{2+}$	$[\text{Mo}(\text{CN})_6]^{4-}$	9×10^9	9×10^9	1
$[\text{Ru}(\text{bipy})_2(\text{CN})_2]$	O_2	5×10^9	7×10^9	0.7
Acridine	$[\text{Ni}(\text{NH}_3)_6]^{2+}$	3×10^8	7×10^9	0.04
$[\text{Ru}(\text{bipy})_3]^{2+}$	$[\text{Ni}(\text{gly})_2]$	4×10^7	7×10^9	0.006
Acridine	$[\text{Ni}(\text{H}_2\text{O})_6]^{2+}$	3×10^7	7×10^9	0.004
$[\text{Ru}(\text{bipy})_3]^{2+}$	$t\text{-}[\text{Cr}(\text{en})_2\text{F}_2]^+$	3×10^6	3×10^9	0.001
$[\text{Ru}(\text{bipy})_3]^{2+}$	$[\text{Cr}(\text{en})_3]^{3+}$	$\leq 1 \times 10^6$	4×10^8	< 0.002
$[\text{Cr}(\text{en})_3]^{3+}$	$[\text{Co}(\text{H}_2\text{O})_6]^{2+}$	2×10^5	$> 4 \times 10^8$	< 0.0005

(a) Aqueous solutions at $\sim 20^\circ\text{C}$. For some of these systems, experimental evidence indicates that energy transfer is the most important (if not the unique) quenching mechanism⁴⁷.

(b) From reference 47.

energy transfer efficiency equals or is near one, while if one of the species involved is a transition metal complex then α_{et} can be as low as 10^{-3} , and even lower when both the donor and the acceptor are transition metal complexes, as shown in Table 1.1⁴⁵. In these cases there are various factors which reduce the quenching efficiency, including the nature of the metal, the ionic charge, the orbital nature of the excited states involved, the nature of the solvent, and the geometry of the complex³⁹.

1.5 BIMOLECULAR ELECTRON-TRANSFER REACTIONS OF EXCITED STATES OF TRANSITION METAL COMPLEXES

An electronically excited state is virtually a new chemical species with its own chemical and physical properties. The main features of electronically excited states are: (i) they are transient species with lifetimes ranging from 10^{-12} - 10^{-3} s in fluid solution; (ii) an excited state always has a higher electronic affinity and a lower ionisation potential compared with the ground state molecule (and thus it is both a better oxidant and a better reductant than the ground state); (iii) the equilibrium nuclear geometry of the excited state may be more or less different from that of the ground state; (iv) formation of an excited state usually involves population of high energy molecular orbitals which may well occupy greater space or even be highly delocalised.

Outer-sphere electron transfer reactions can be very fast (even diffusion controlled) and can occur within the excited state lifetime of several transition

metal complexes. As a consequence, one of the most important pathways for the electronic deactivation of such complexes under suitable conditions is the intermolecular oxidation or reduction of a convenient substrate. The lowest spin-allowed excited state usually has a lifetime shorter than 10^{-10} s owing to interaction with its immediate environment and fast inter-system crossing to the lowest spin-forbidden excited state⁴⁷. Thus, only those excited states having lifetimes longer than 10^{-10} - 10^{-9} s can be involved in a bimolecular electron transfer, which usually means the lowest spin-forbidden excited state.

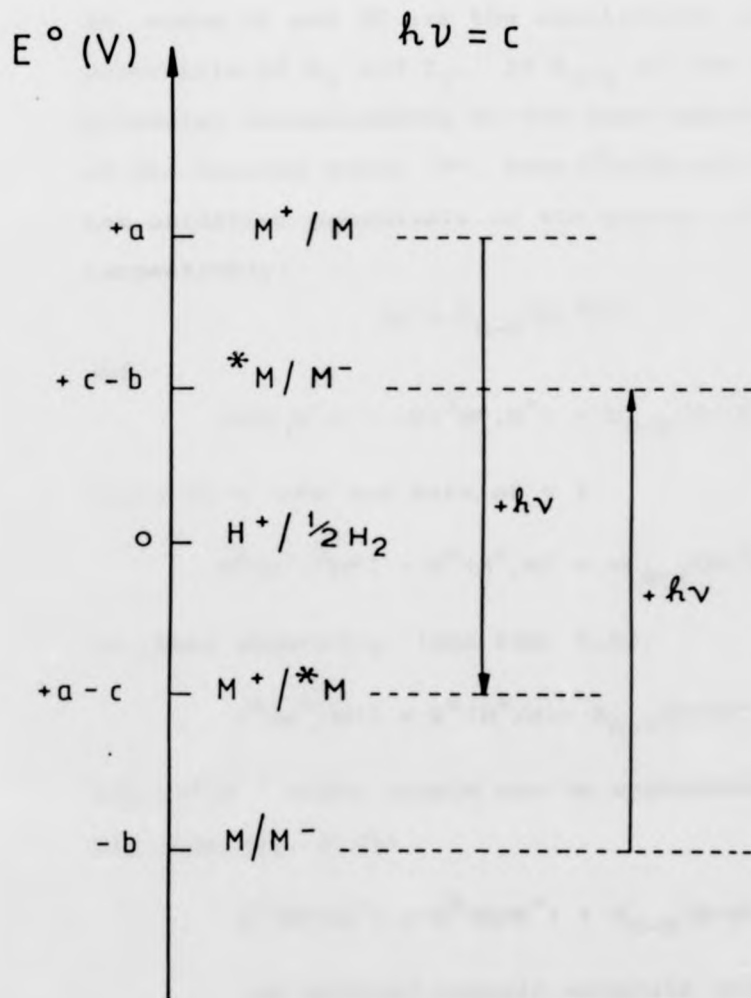
We have stated that an electronically excited state of a molecule is expected to be both a better oxidant and a better reductant than the corresponding ground state. If we consider the values of the redox potentials M/M^+ and M^*/M^+ (or \bar{M}/M and \bar{M}^*/M) where M is the ground state and M^* is the lowest excited state, then Fig. 1.5⁴⁸ represents the situation for oxidation of a molecule with a singlet ground state and singlet and triplet excited states ($^1M^*$ and $^3M^*$). The electrochemical redox potentials of the couples M/M^+ , $^3M^*/M^+$ and $^1M^*/M^+$ versus a reference couple Q/Q^- are related to the free energy changes

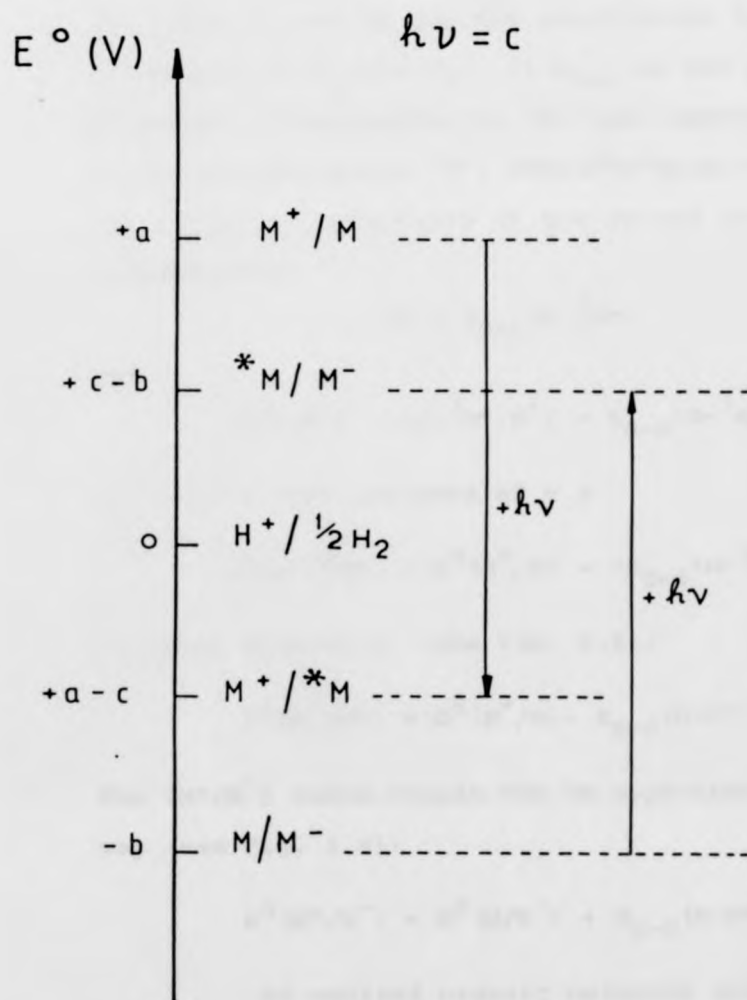
$$\Delta G = \Delta H - T\Delta S \quad (1.11)$$

When the Stokes shift is small, (which is the shift between absorption and emission, caused by the change in size, shape and solvation of an excited state versus the ground state), the difference between the entropies of the excited and ground states may reasonably be



Figure 1.5 Schematic representation of the energy change for the excitation and ionisation processes of a molecule (from reference 48).





neglected, ($\Delta S = 0$ and therefore $\Delta G = \Delta H$) so that:

$$\Delta G[M, M^+] - \Delta G[{}^3M^*, M^+] = \Delta H[M, M^+] - \Delta H[{}^3M^*, M^+] \quad (1.12)$$

The right hand side of equation 1.12 represents $AE - BE = AB$, where AE and BE are the equilibrium ionisation potentials of S_0 and T_1 . If E_{0-0} is the one-electron potential corresponding to the zero spectroscopic energy of the excited state ${}^3M^*$, then $E^0(M^+/M)$ and $E^0(M^+/{ }^3M^*)$ are the oxidation potentials of the ground and excited states, respectively:

$$AB = E_{0-0}(M-{}^3M^*)$$

and

$$\Delta G[M, M^+] - \Delta G[{}^3M^*, M^+] = E_{0-0}(M-{}^3M^*) \quad (1.13)$$

since $\Delta G = -nFE$ and here $nF = 1$

$$E^0(M^+, {}^3M^*) - E^0(M^+, M) = -E_{0-0}(M-{}^3M^*) \quad (1.14)$$

or, more generally, (see Fig. 1.6):

$$E^0(M^+/M^*) = E^0(M^+/M) - E_{0-0}(M-M^*) \quad (1.15)$$

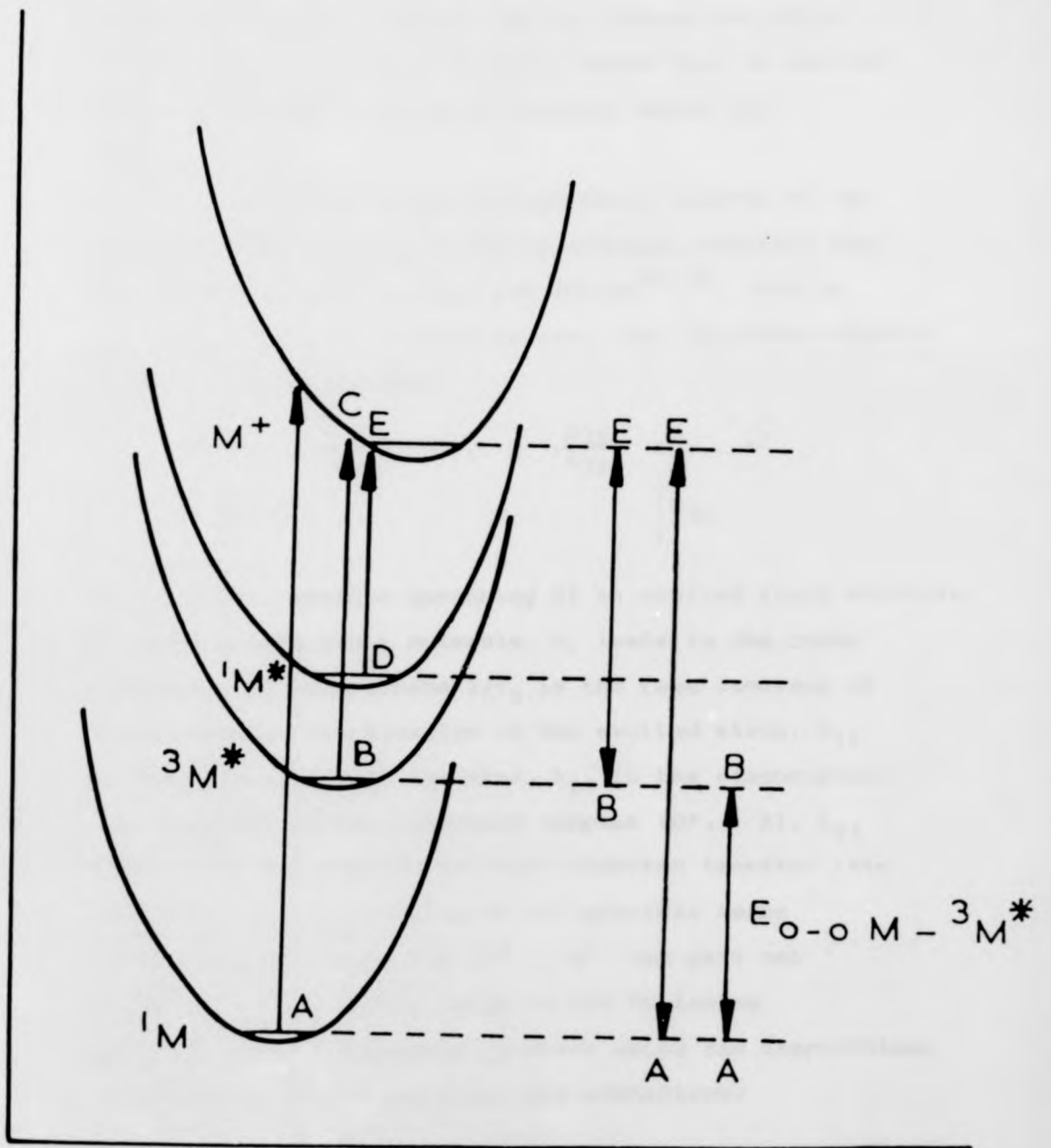
The (M^*/M^-) redox couple can be approximated in the same way (see Fig. 1.6):

$$E^0(M^*/M^-) = E^0(M/M^-) + E_{0-0}(M-M^*) \quad (1.16)$$

An excited organic molecule can usually serve as either an electron donor or acceptor (but rarely both); this situation is related to the considerable energy separation between oxidation states. In transition metal complexes⁴⁸ the presence of redox sites on both metal and ligand offers additional possibilities not

Figure 1.6 Schematic diagram showing the difference in the redox potentials of the lowest excited state and the ground state of a molecule according to equations 1.15 and 1.16; c is the one-electron potential corresponding to the zero-zero spectroscopic energy of the excited state.

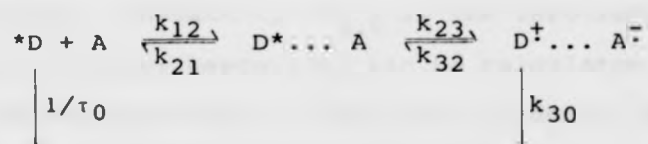
Potential Energy



Nuclear Configuration

normally available to either simple metal ions or organic molecules. These oxidation states are often closely spaced, so it is commonly found that an excited state can be used both as an electron donor and acceptor.

The kinetic and thermodynamic aspects of the quenching of an excited state by electron transfer were discussed in detail by Rehm and Weller^{49,50}. For an electron-transfer quenching process, the following kinetic scheme can be envisaged:



The electron transfer quenching of an excited state molecule, D^* , by a ground state molecule, A , leads to the redox products. In this scheme $1/\tau_0$ is the rate constant of intramolecular deactivation of the excited state, k_{12} is the diffusion rate constant, k_{21} is the dissociation rate constant of the encounter complex ($D^* \dots A$), k_{23} and k_{32} are the forward and back electron transfer rate constants, and k_{30} represents all possible modes (except k_{32}) by which the ($D^{\ddagger} \dots A^{\bar{}}$) ion pair can disappear. This scheme leads to the following equation for the quenching constant using the Stern-Volmer relationship and steady-state approximations:

$$k_q = \frac{k_{12}}{1 + \frac{k_{21}}{k_{23}} + \frac{k_{21}}{k_{30}} \cdot \frac{1}{K_{23}}} \quad (1.17)$$

with

$$K_{23} = \frac{k_{23}}{k_{32}} = \exp\left(-\frac{\Delta G_{23}}{RT}\right) \quad (1.18)$$

where ΔG_{23} is the free energy change involved in the actual electron transfer process (see Fig. 1.7), which can be calculated from:

$$\Delta G_{23} = 23.06[E(D/D^+) - E(A^-/A) - \frac{e_0^2}{\epsilon_a}] - \Delta E_{0,0} \quad (1.19)$$

where e_0^2/ϵ_a is the free energy, gained by bringing the two radical ions to encounter distance a in a solvent of dielectric constant ϵ , $\Delta E_{0,0}$ is the zero-zero transition energy; hence ΔG_{23} can be calculated from the oxidation potential of the electron donor (D), and the reduction potential of the acceptor (A).

Generally the rate constants of all three electron-transfer processes (k_{23}, k_{32}, k_{30}) are assumed to occur by the same outer-sphere type mechanism, viz.

$$k_{ij} = k^0 \exp\left[-\frac{\Delta G_{ij}^\ddagger}{RT}\right] \quad (1.20)$$

where ΔG_{ij}^\ddagger is the activation free energy, and k^0 is the frequency factor. As the free energy gained in the final electron transfer, k_{30} , leading to the ground state is exceedingly large, ΔG_{30}^\ddagger can be assumed to be close to zero, so that $k_{30} \approx k^0$ and

$$k_{23} = k_{30} \exp\left[-\frac{\Delta G_{23}^\ddagger}{RT}\right] \quad (1.21)$$

Rehm and Weller^{49,50} evaluated the rate constants of equation 1.17 and gave a simplified form, viz.

$$k_q = \frac{20 \times 10^9 \text{ M}^{-1} \text{ sec}^{-1}}{1 + 0.25 \left[\exp \left(\frac{\Delta G_{23}^\ddagger}{RT} \right) + \exp \left(\frac{\Delta G_{23}}{RT} \right) \right]} \quad (1.22)$$

The free energy of activation can be related to the free energy change of the electron transfer process as for ground state reactions. Equation 1.23 appeared to be

$$\Delta G_{23}^\ddagger = \left[\left(\frac{\Delta G_{23}}{2} \right)^2 + (\Delta G_{23}^\ddagger(0))^2 \right]^{1/2} + \frac{\Delta G_{23}}{2} \quad (1.23)$$

the most reasonable function of this type and it was found experimentally that $\Delta G_{23}^\ddagger(0)$, the activation free energy at $\Delta G_{23} = 0$, was $10.04 \text{ kJ mol}^{-1}$, which is related to the changes in the nuclear positions that must occur prior to electron transfer. $\Delta G_{23}^\ddagger(0)$ is referred to as the reorganisational intrinsic barrier.

The correlation between k_q and ΔG_{23} which should exist if quenching occurs by electron transfer, according to equations 1.22 and 1.23, is demonstrated in Fig. 1.8 where $\log k_q$ is plotted against ΔG_{23} . When ΔG_{23} is large and negative, the quenching rate constant reaches the diffusion-controlled limit, while when ΔG_{23} is positive, k_q decreases sharply and the slope of the linear portion is $-1/2.30 RT$. According to another relationship proposed by Marcus^{51,52} to calculate ΔG_{23}^\ddagger ,

$$\Delta G_{23}^\ddagger = \Delta G_{23}^\ddagger(0) \left[1 + \frac{\Delta G_{23}}{4\Delta G_{23}^\ddagger(0)} \right]^2 \quad (1.24)$$

the broken line in Fig. 1.8 is obtained, which is in good

Figure 1.7 Schematic diagram of the energy profiles for the electron-transfer processes.

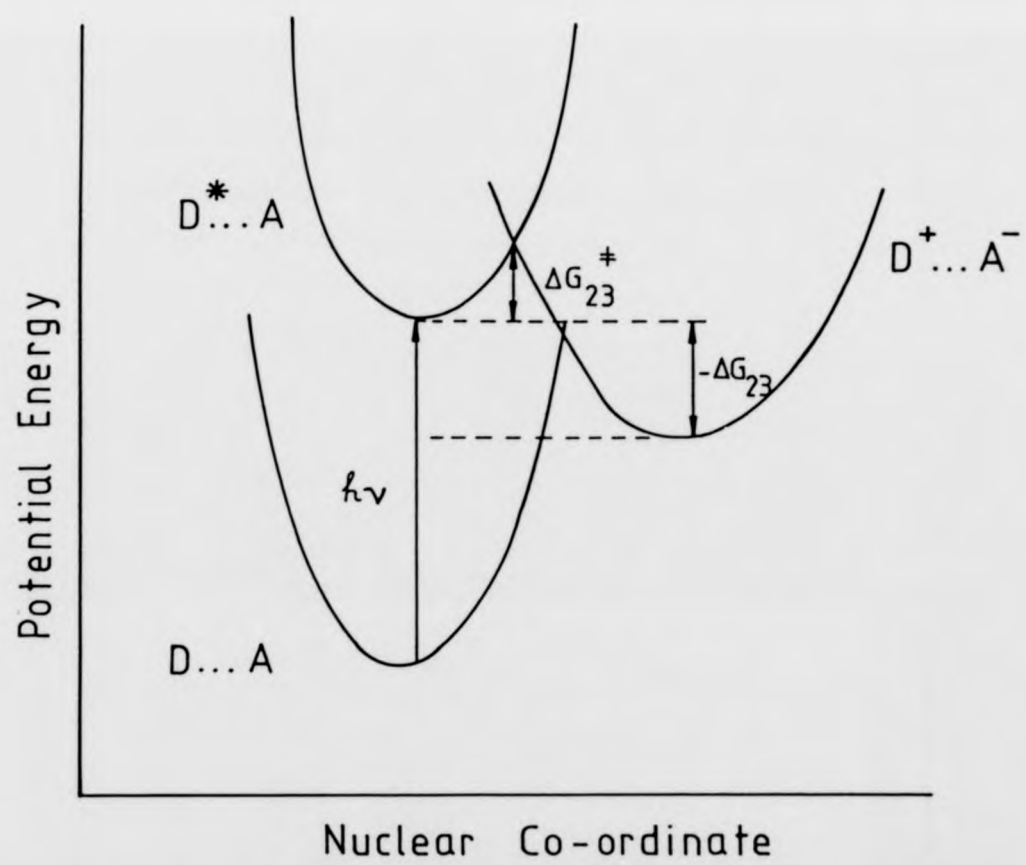
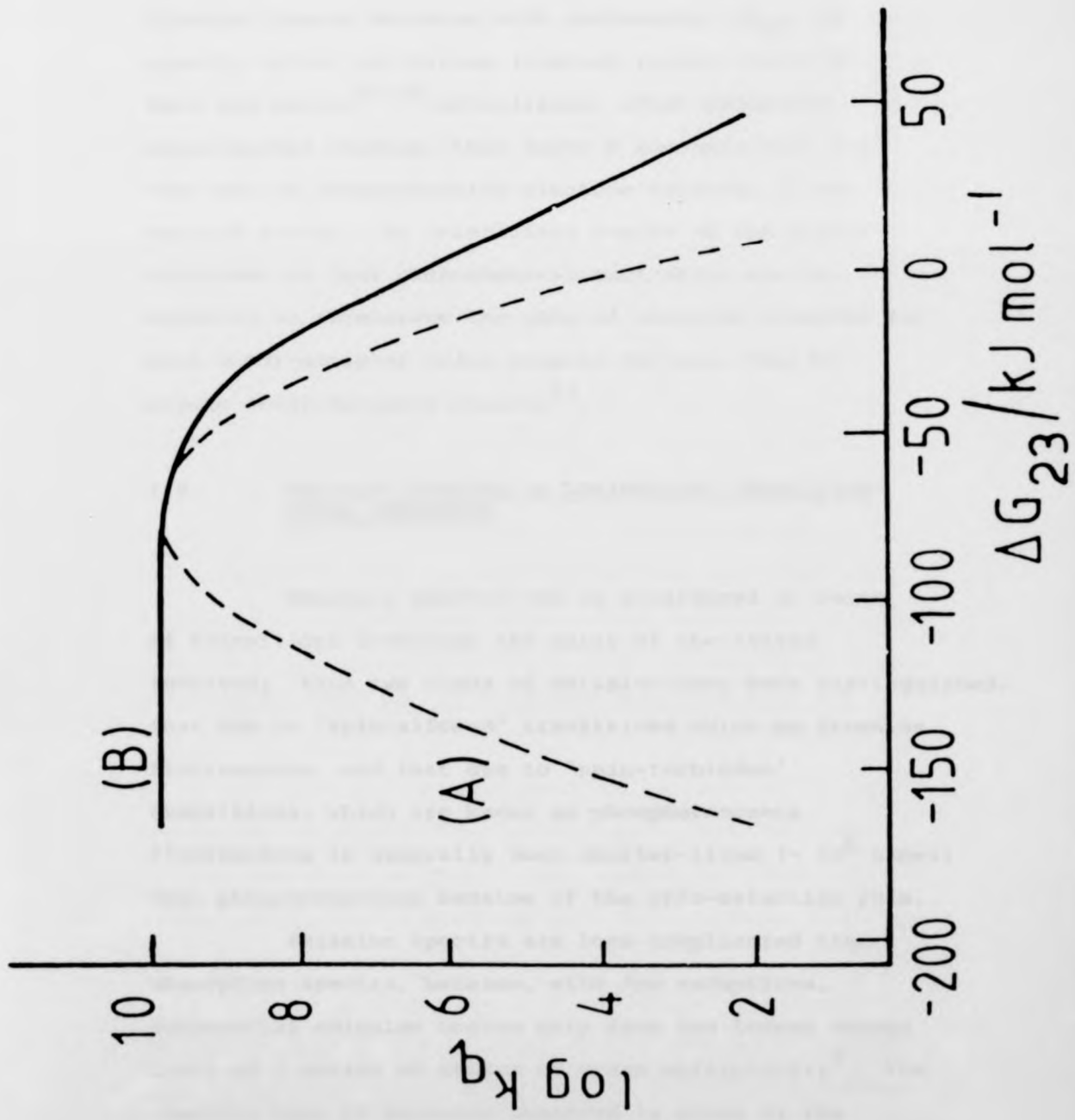


Figure 1.8 Plot of the logarithm of the quenching rate constant *versus* the free energy change for the electron-transfer process for $[\text{Cr}(\text{bpy})_3]^{3+}$ complex; (---) Marcus, (—) Weller (from reference 48).



agreement with the experimental results when $\Delta G_{23} = -62.76 \text{ kJ mol}^{-1}$, and shows strong deviations for more negative values of ΔG_{23} . The region, in which the rate constant should decrease with increasing $-\Delta G_{23}$, is usually called the Marcus-inverted region (curve A). Rehm and Weller^{49,50} established, after extensive experimental studies, that curve B accounts best for the rate of intermolecular electron transfer of the excited states. An interesting result of the Weller treatment is that photochemical excitation can be expected to accelerate the rate of electron transfer for weak donor-acceptor redox couples far more than for strong donor-acceptor couples⁵³.

1.6 EMISSION SPECTRA OF LUMINESCENT TRANSITION-METAL COMPLEXES

Emission spectra can be considered in terms of transitions involving the spins of the states involved; thus two kinds of emission have been distinguished, that due to "spin-allowed" transitions which are known as fluorescence, and that due to "spin-forbidden" transitions, which are known as phosphorescence. Fluorescence is generally much shorter-lived ($\sim 10^6$ times) than phosphorescence because of the spin-selection rule.

Emission spectra are less complicated than absorption spectra, because, with few exceptions, substantial emission occurs only from the lowest energy level of a series of states of given multiplicity³. The specific type of emission observed is given by the rule proposed by Demas and Crosby⁵⁴:

"In the absence of photochemistry from upper excited states, emission from a transition metal complex with an unfilled d shell will occur from the lowest electronic state in the molecule or from those states which can achieve a significant population relative to the lowest excited state."

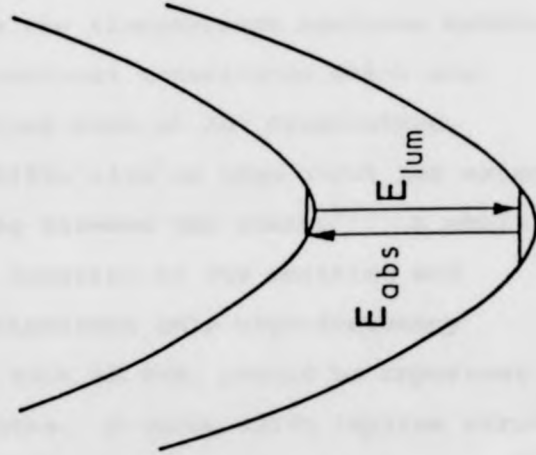
This rule covers all of the data so far collected for d^3 and d^6 complexes. These are the only two systems for which extensive studies have been undertaken, probably because they are thermally and photochemically stable and frequently emit strongly in an accessible region (300-1100 nm). Emission has been reported for complexes of Pt(II)⁵⁵ and Pt(0)⁵⁶, which promises to extend these studies to d^8 and d^{10} systems respectively.

The relation between the absorption and emission spectra for transitions between two electronic states is that the ground and excited state equilibrium geometries are either different from, or identical to, each other. The splitting between the emission and absorption maxima is called the "Stokes shift" (Fig. 1.9). It is apparent that a negligible shift implies little change in the geometry of the excited state from that of the ground state (Fig. 1.9a), whereas a large Stokes shift implies considerable distortion of the molecular moiety (Fig. 1.9b).

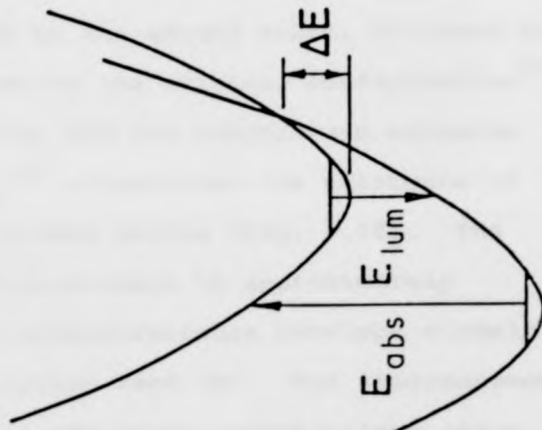
The distortion can be explained in terms of the changes in the position of the potential energy curves for the system, which represent the total energy

Figure 1.9 Potential energy diagram illustrating
the significance of a Stokes shift.

(a) weak coupling limit



(b) strong coupling limit



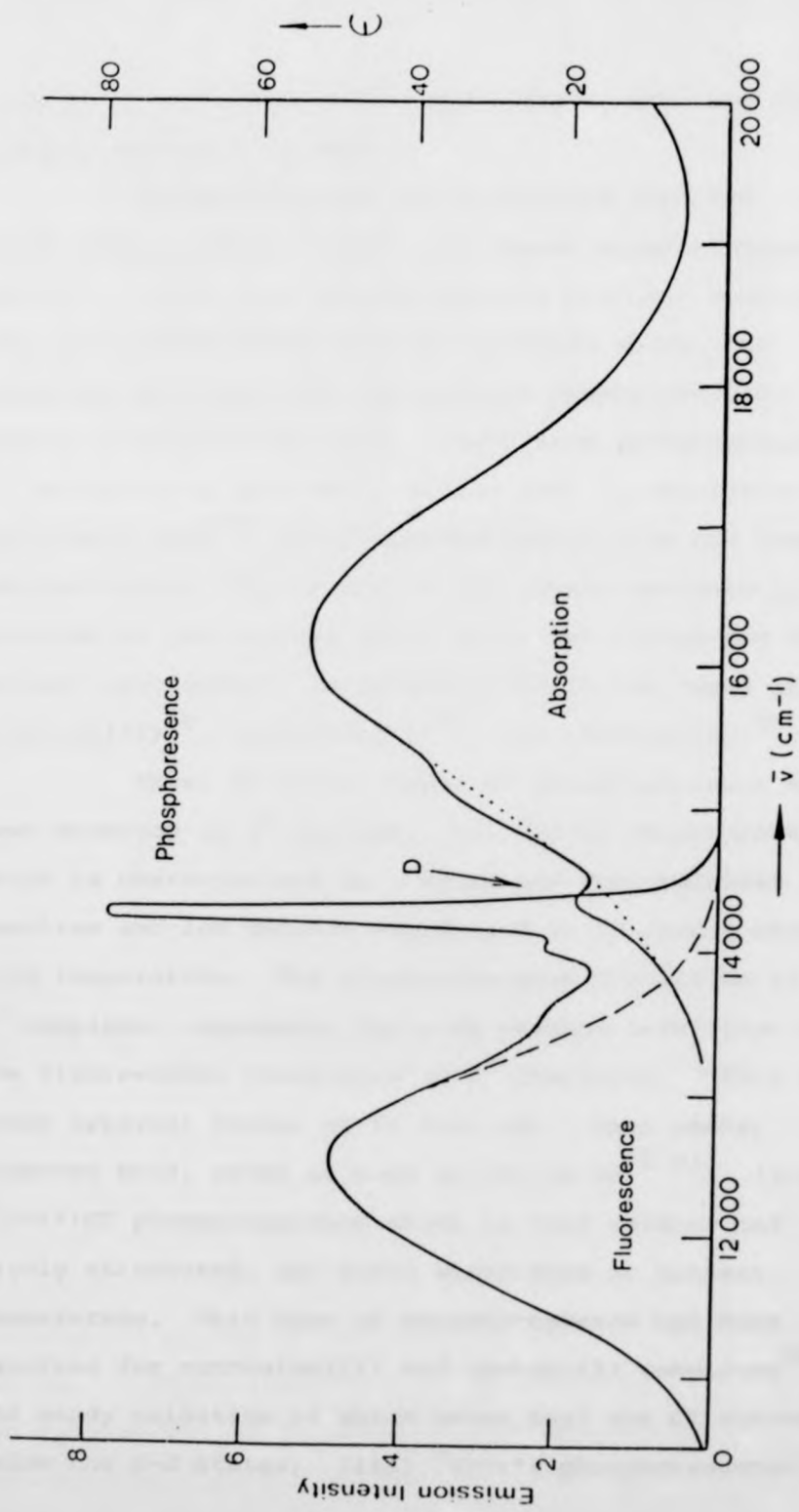
of a molecule in solution, and therefore include a contribution from its solvent environment. Excitation of a molecule causes a change in the molecular geometry, and is followed by the slower process of solvent relaxation to accommodate the new geometry. Deactivation of this state then occurs back to the ground state, followed by solvent relaxation back to the original configuration⁴⁶.

The absorption and low temperature emission spectra of $[\text{Cr}(\text{urea})_6]^{3+}$ illustrates the existence of both large and small Stokes shifts (Fig. 1.10). The Stokes shift of the fluorescence is approximately $3,700 \text{ cm}^{-1}$, while the phosphorescence overlaps closely the weak doublet absorption band (D). The fluorescence spectrum also resembles the broad structureless shape of the absorption band. The sharp, undistorted phosphorescence spectrum contains few vibrational components, whereas the fluorescence spectrum envelops a multitude of vibrational transitions which are evidently not resolved even at low temperature.

Stokes shifts give an idea about the extent of vibronic coupling between two states⁵⁷. A small shift implies weak coupling of the emitting and ground state, and therefore only high-frequency vibrational modes, such as O-H, should be important as deactivation routes. A large shift implies strong coupling of the states, and low-frequency heavy-atom vibrational modes may facilitate deactivation.

Fluorescence is very rare in transition metal complexes, and has been observed so far only for d^3

Figure 1.10 Absorption (298 K) and emission (78 K) spectra of 0.03 M $[\text{Cr}(\text{urea})_6](\text{ClO}_4)_3$; D - quartet-doublet absorption (from reference 26).



systems at low temperature, particularly when the singlet-triplet splitting is small.

Phosphorescence can be divided into two broad types, namely "light" and "heavy atom" phosphorescence. Light atom phosphorescence has been observed only for chromium(III) and is typically sharp, the excellent matching with the doublet absorption band making identification easy. Heavy atom phosphorescence is dominated by spin-orbit states and, in accordance with the Crosby rule⁵⁴, occurs predominantly from the lowest excited state. The nature of the lowest manifold is dictated by the central metal atom, the ligand and the solvent environment, as demonstrated in the cases of iridium(III)⁵⁸, ruthenium(II)⁵⁹, and rhodium(III)⁶⁰.

Three different types of phosphorescence have been observed in d^6 systems; (i) $^3(d-d)$ phosphorescence which is characterised by a broad and structureless spectrum and low quantum yield, and it is rarely seen at room temperature. The phosphorescence transition in these d^6 complexes represents the same orbital transition as the fluorescence transition in d^3 complexes. There is a large apparent Stokes shift from the lowest energy observed band, often as much as $16,000 \text{ cm}^{-1}$ ⁶¹; (ii) $^3(d-\pi^*)CT$ phosphorescence which is very intense and highly structured, and still observable at ambient temperature. This type of phosphorescence has been reported for ruthenium(II) and osmium(II) complexes²⁸, the ready oxidation of which means that the CT states lie below the $d-d$ states; (iii) $^3(\pi-\pi^*)$ phosphorescence

which is observed from a complex such as $[\text{Rh}(\text{phen})_3]^{3+}$ ⁶⁰, which fulfils the requirements of a large LF splitting and a metal ion which is difficult to oxidise. This situation pushes the d-d and CT states above the ligand states, causing ligand phosphorescence, which resembles that of the free ligand.

The latter investigation⁶⁰ revealed that complexes can be engineered to display a predetermined sequence of excited states of known types by careful choice of the central metal ion, the ligand and the environment in which the complex is placed. Fine alterations can be effected by means of ligand substitution and environmental modification, while coarse tuning involves changes in the central metal ions.

1.7 THEORY OF NON-RADIATIVE PROCESSES

A radiationless transition is a unimolecular process in which the energy difference between the initial and final states appears as heat in the surrounding medium. This process essentially consists of an isoenergetic conversion of the electronic energy of an upper state into vibrational energy of a lower state of the same molecule (intramolecular energy transfer), followed by the dissipation of the excess vibrational energy of the lower state into the surrounding medium. A distinction must be made between intramolecular and intermolecular relaxation; the latter consists of quenching by a second species, with or without electronic energy transfer.

Intramolecular non-radiative relaxation processes can be classified as:

- (i) Vibrational relaxation of an excited species within one electronic state by collisional interaction with the medium.
- (ii) Internal conversion (IC) from one electronic state to another state of the same multiplicity.
- (iii) Intersystem crossing (ISC) between states of different multiplicity.

Although the first process is not strictly intramolecular, the intimate contact of a complex with its environment qualifies it for inclusion in this category. Vibrational relaxation is assumed to be rapid compared with the other two processes, and occurs within approximately 10^{-12} s while ISC is considered to take place with a rate constant greater than 10^{10} s⁻¹.

The other two processes (IC and ISC) take place between isoenergetic vibronic levels of the two states, followed by vibrational relaxation removing excess vibrational energy. Englman and Jortner⁶² described the theory concerning rate constants of non-radiative processes. The rate constant of crossing from state *i* to state *j* is the sum over all levels of the individual transition probabilities, k_{ij} , each determined by matrix elements for the coupling of the states, which include both electronic factors, *C*, and Franck-Condon factors, S_{ij} :

$$k_{ij} = \langle \psi_j / V_{ij} / \psi_i \rangle \quad (1.25)$$

$$V_{ij} = C S_{ij} \quad (1.26)$$

Vibronic coupling largely determines C when the states involved have the same multiplicity (i.e. IC), but for states of different multiplicity (i.e. ISC), spin-orbit coupling must be included. The values of k_{ij} are dependent upon (i) ΔE , the difference in the zero point energies of i and j and (ii) ΔQ , the displacement of one potential minimum relative to the other along an appropriate co-ordinate, both in a complex fashion, although two limiting cases are envisaged, (i) weak coupling, when ΔQ is small, and (ii) strong coupling, when ΔQ is large. These conditions are analogous to the small and large Stokes shifts, E_S , and this fact is used to define the conditions for the two cases. Strong coupling implies

$$E_S \gg 2 \langle \bar{\nu} \rangle \tanh \langle \bar{\nu} \rangle / 2kT \quad (1.27)$$

where $\langle \bar{\nu} \rangle$ is the mean vibrational energy in the molecule, k is the Boltzmann constant, and T is the temperature, implying a strong temperature dependence which is related to the energy difference between crossing point and the minimum of the state i . The strong coupling limit applies for $E_S > 10,000 \text{ cm}^{-1}$ and is expected only to apply to relaxation *via* photochemical rearrangements. The weak coupling case ($E_S < 4,000 \text{ cm}^{-1}$) is given by $E_S = 2 \langle \bar{\nu} \rangle$, and is expected to apply for interstate crossing. At low temperatures, the transition probability for weak coupling case becomes:

$$k_{ij} = \frac{C^2 (2\pi)^{\frac{1}{2}}}{h(\bar{\nu}_M \Delta E)^{\frac{1}{2}}} \exp \frac{-\gamma \Delta E}{\bar{\nu}_M} \quad (1.28)$$

where $\bar{\nu}_M$ is the energy of the highest frequency vibrational modes and γ is given by:

$$\gamma = \log \frac{\Delta E}{\bar{\nu}_M \Delta_M} - 1 \quad (1.29)$$

where Δ_M corresponds to ΔQ .

The rate constants in equation (1.28) are temperature-insensitive and include a deuterium effect, qualitatively predicted earlier, since $\bar{\nu}_M$ incorporates high frequency vibrational modes such as O-H and C-H.

Spectral data and emission yields give only restricted information about non-radiative processes, but when complemented with lifetime measurements, a far greater insight ensues. The distinction between the emission lifetime, τ , and quantum yield, ϕ , is indicated by the definitive equations

$$\phi = k_r [M] / I \quad (1.30)$$

$$\tau = 1 / (k_r + k_{nr})$$

where k_r represents the radiative rate constant of the emitting level, $[M]$ the population, k_{nr} the sum of non-radiative rate constants for the emitting level, and I is the intensity of the excitation under which the quantum yield measurements are performed.

The emission lifetime and yield may be affected by ligand or solvent or both, which can act as "acceptor" modes of the vibronic energy. These pathways are distinguished by environmental modification. Changes in lifetime with solvent suggest a solvent contribution as an acceptor of

vibronic energy, whereas participation of metal-ligand vibrations as acceptors leads to an increase in lifetime.

1.8 KINETIC SCHEMES FOR LUMINESCENCE

In the analysis of the various interstate processes occurring subsequent to absorption of light, a visual display of the distribution in energy of the excited electronic states relative to the ground state is especially instructive. A general energy level scheme is represented by a Jablonski diagram in Fig. 1.11. The model assumes that vibrational relaxation and internal conversion are fast compared with the other deactivation rates, so that only the lowest excited states need be considered. Neglecting back-ISC, k_{-4} , the kinetic processes under these conditions are:

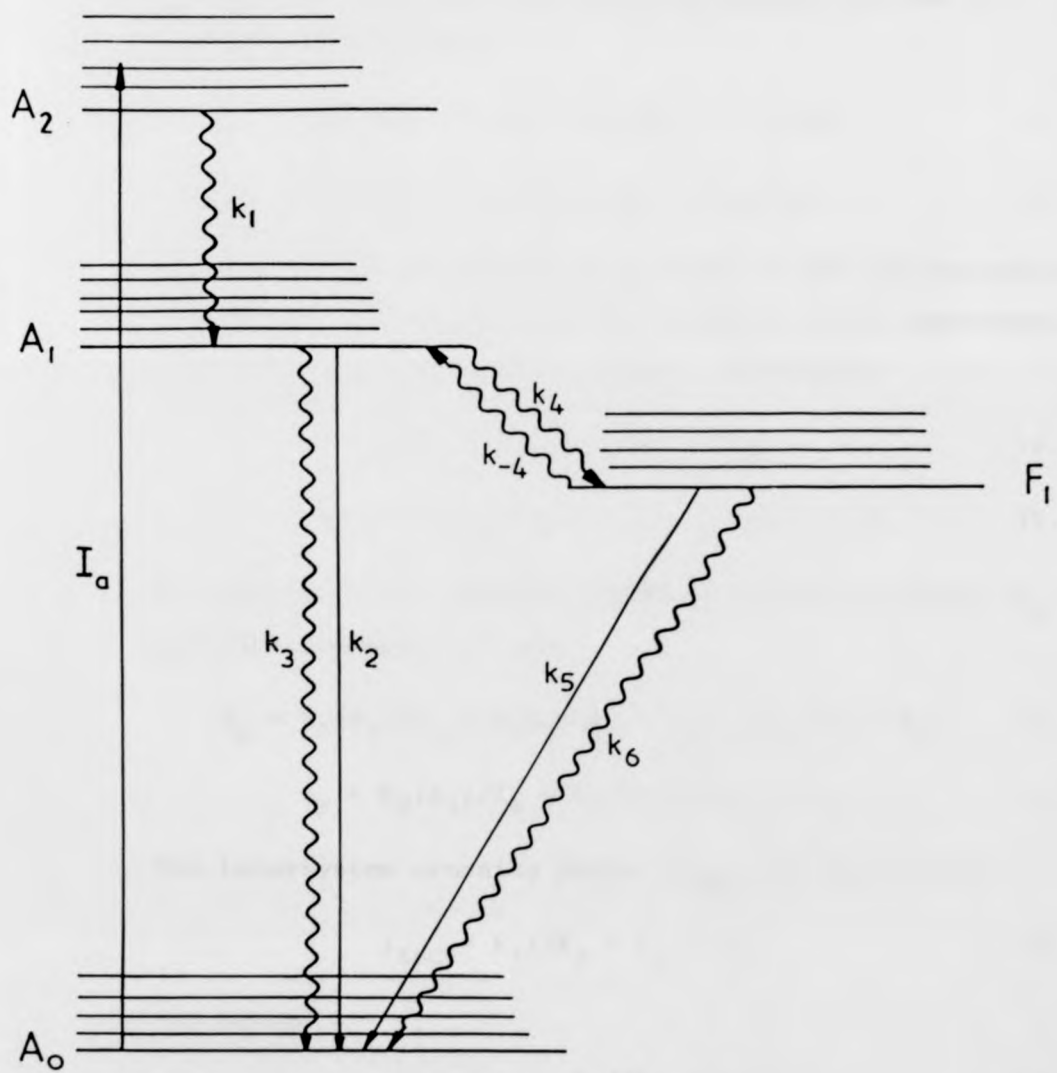
<u>Pathway</u>	<u>Rate</u>
$A_0 + h\nu \rightarrow A_2$	I_a
$A_2 \rightarrow A_1$	$k_1[A_2]$
$A_1 \rightarrow A_0 + h\nu_F$	$k_2[A_1]$
$A_1 \rightarrow A_0 + \text{heat}$	$k_3[A_1]$
$A_1 \rightarrow F_1$	$k_4[A_1]$
$F_1 \rightarrow A_0 + h\nu_P$	$k_5[F_1]$
$F_1 \rightarrow A_0 + \text{heat}$	$k_6[F_1]$

where k_2 and k_5 represent fluorescence and phosphorescence, respectively, whilst k_3 and k_6 are the sum of the intramolecular non-radiative rates for the two levels, and

Figure 1.11 Jablonski diagram depicting a general energy-level scheme for luminescence.

~~~~~ non-radiative transitions

— radiative transitions



Spin - allowed states

Spin - forbidden states

$k_4$  depicts ISC between the two levels. Combination of appropriate formation and decay processes for the  $F_1$  and  $A_1$  states yields:

$$d[F_1]/dt = -(k_5 + k_6)[F_1] + k_4[A_1] \quad (1.31)$$

$$d[A_1]/dt = I_a - (k_2 + k_3 + k_4)[A_1] \quad (1.32)$$

For continuous illumination, as used in the spectroscopic measurement of quantum yields, a steady state approximation  $d[F_1]/dt = d[A_1]/dt = 0$  is valid. Therefore,

$$[A_1] = I_a / (k_2 + k_3 + k_4) \quad (1.33)$$

$$[F_1] = k_4 I_a / (k_2 + k_3 + k_4)(k_5 + k_6) \quad (1.34)$$

By definition the quantum yields of phosphorescence ( $\phi_p$ ) and fluorescence ( $\phi_F$ ) are:

$$\phi_p = k_5[F_1]/I_a = k_4 k_5 / (k_2 + k_3 + k_4)(k_5 + k_6) \quad (1.35)$$

$$\phi_F = k_2[A_1]/I_a = k_2 / (k_2 + k_3 + k_4) \quad (1.36)$$

The intersystem crossing yield ( $\phi_{ISC}$ ) is defined as:

$$\phi_{ISC} = k_4 / (k_2 + k_3 + k_4) \quad (1.37)$$

and hence

$$\phi_p = \phi_{ISC} k_5 / (k_5 + k_6) \quad (1.38)$$

$$\phi_F = k_2 \phi_{ISC} / k_4 \quad (1.39)$$

Unfortunately, this treatment cannot be extended to define equations for the measured luminescence lifetimes, which are measured using a high energy pulse of negligible

duration and results in the following modification of equation 1.32

$$d[A_1]/dt = -(k_2 + k_3 + k_4)[A_1] \quad (1.40)$$

The two differential equations 1.31 and 1.40 can be solved completely, using the assumption  $[F_1] = 0$  and  $[A_1] = [A_1]_0$  at  $t = 0$ .

$$[F_1] = \{k_4[A_1]_0/(k_A - k_F)\}[e^{-k_F t} - e^{-k_A t}] \quad (1.41)$$

where  $k_A = k_2 + k_3 + k_4$ ,  $k_F = k_5 + k_6$ . The second term of equation 1.41 represents the "grow-in" of the phosphorescence, whilst the first term gives its decay, and

$$[A_1] = [A_1]_0 e^{-k_A t} \quad (1.42)$$

since  $k_A \gg k_F$ , at  $t > 1/k_A$ , then equation 1.41 reduces to

$$F_1 = (k_4[A_1]_0 e^{-k_F t})/k_A = [F_1]_0 e^{-k_F t} \quad (1.43)$$

where  $[F_1]_0 = \phi_{ISC}[A_1]_0 =$  initial population of  $F_1$ . The lifetime of  $F_1$  ( $\tau_p$ ) is defined in the expression  $F_1 = [F_1]_0 e^{-t/\tau_p}$ . By analogy

$$\tau_p = 1/k_F = 1/(k_5 + k_6) \quad (1.44)$$

While for fluorescence

$$\tau_F = 1/k_A = 1/(k_2 + k_3 + k_4) \quad (1.45)$$

Combining equations 1.44 and 1.38 gives

$$\phi_p/\tau_p = \phi_{ISC} k_5 \quad (1.46)$$

i.e. the ratio of the measured values of  $\phi_p$  and  $\tau_p$  should

be constant in the absence of back-intersystem crossing.

The inclusion of back-intersystem crossing into the rate equations introduces some complexity:

$$d[F_1]/dt = -(k_5 + k_6 + k_{-4})[F_1] + k_4[A_1] \quad (1.47)$$

$$d[A_1]/dt = I_a - (k_2 + k_3 + k_4)[A_1] + k_{-4}[F_1] \quad (1.48)$$

Applying the steady state approximation,

$$[F_1] = k_4 I_a / (k_T \cdot k_S - k_{-4} k_4) \quad (1.49)$$

$$[A_1] = I_a k_T / (k_T \cdot k_S - k_{-4} k_4) \quad (1.50)$$

where  $k_T = k_5 + k_6 + k_{-4}$ ,  $k_S = k_2 + k_3 + k_4$  and  $\phi_P$  and  $\phi_F$  are now given:

$$\phi_P = k_5 [F_1] / I_a = k_4 k_5 / (k_T \cdot k_S - k_{-4} k_4) \quad (1.51)$$

$$\phi_F = k_2 [A_1] / I_a = k_2 k_T / (k_T \cdot k_S - k_{-4} k_4) \quad (1.52)$$

The rate equations for flash techniques become:

$$d[F_1]/dt = -k_T [F_1] + k_4 [A_1] \quad (1.53)$$

$$d[A_1]/dt = -k_S [A_1] + k_{-4} [F_1] \quad (1.54)$$

which on differentiation give

$$d^2[F_1]/dt^2 = -k_T d[F_1]/dt + k_4 d[A_1]/dt \quad (1.55)$$

$$d^2[A_1]/dt^2 = -k_S d[A_1]/dt + k_{-4} d[F_1]/dt \quad (1.56)$$

By substitution of equations 1.53 and 1.54 into 1.55 and 1.56, two simultaneous differential equations are obtained, which can be solved to give the following expressions:

$$[F_1] = k_4[A_1]_0 (e^{-\lambda_1 t} - e^{-\lambda_2 t})/(\lambda_2 - \lambda_1) \quad (1.57)$$

$$[A_1] = [A_1]_0 \{ (\lambda_2 - k_S)e^{-\lambda_1 t} + (k_S - \lambda_1)e^{-\lambda_2 t} \} / (\lambda_2 - \lambda_1) \quad (1.58)$$

By analogy with equation 1.41

$$\lambda_1 = (\tau_p)^{-1} = \frac{1}{2}[(k_T + k_S) - \sqrt{(k_S - k_T)^2 + 4k_4k_{-4}}] \quad (1.59)$$

Although this equation appears rather complex, there are two limiting conditions which may be considered<sup>63</sup>:

- (i) The steady state limit, which becomes valid for  $A_1$  (after the decay of the exciting pulse) i.e.,  $k_4 \gg k_5 + k_6$  which results in the assumption  $4k_4k_{-4} \ll (k_S - k_T)^2$ . Equation 1.59 becomes:

$$(\tau_p)^{-1} \sim k_T - (k_4k_{-4}/(k_S - k_T)) \sim k_5 + k_6 + (1 - \phi_{ISC})k_{-4} \quad (1.60)$$

Equation 1.46 is still valid, and  $\phi_{ISC}$  is given by equation 1.37.

- (ii) Thermal equilibration, in which it is assumed that the two states are in thermal equilibrium with each other, i.e.,  $k_4 \gg k_2 + k_3$  and  $k_{-4} \gg k_5 + k_6$ . Equation 1.59 now becomes

$$(\tau_p)^{-1} \sim (k_F + k_A K)/(1 + K) \quad (1.61)$$

$$\text{Similarly, } \phi_p = k_5/(k_F + k_A K) \quad (1.62)$$

$$\text{therefore } \phi_p/\tau_p = k_5/(1 + K) \quad (1.63)$$

where  $K$  represents the inter-state equilibrium constant. By comparison of equations 1.46 and 1.63,  $(1 + K)^{-1}$  has become the equivalent of

$\phi_{ISC}$ . Knowing that

$$\phi_{ISC} = k_4/(k_2 + k_3 + k_4) \quad (1.37)$$

$$\text{and } (1 + K)^{-1} = k_4/(k_{-4} + k_4) \quad (1.64)$$

$k_{-4}$  has replaced  $(k_2 + k_3)$  as the competitive process to ISC. This highlights the difference between the two treatments. The steady-state limit assumes  $k_{-4}$  to be an inefficient pathway, which occurs in competition with  $k_5$  and  $k_6$  after ISC is complete. The equilibrium limit assumes  $k_{-4}$  to be directly competitive with  $k_4$  and precedes deactivation by  $k_5$  and  $k_6$ .

$k_{-4}$  and  $K$  both show a similar Boltzmann dependence on temperature, with  $K$  containing a degeneracy term:

$$K = (g_{A_1}/g_{F_1}) e^{-\Delta\epsilon/kT} \quad (1.65)$$

$$k_{-4} = k'_{-4} e^{-\Delta\epsilon/kT} \quad (1.66)$$

where  $g_{A_1}$  and  $g_{F_1}$  are the degeneracies of  $A_1$  and  $F_1$  respectively, and  $k'_{-4}$  is the limiting back-ISC rate.  $\Delta\epsilon$  is the energy level gap between the two levels,  $k$  is the Boltzmann factor and  $T$  is the temperature.

Crosby<sup>64</sup> has used the equilibrium limit to define the splittings of the emitting manifold  $[\text{Ru}(\text{bipy})_3]^{2+}$  between 0 and 100 K ( $\Delta\epsilon \leq 60 \text{ cm}^{-1}$ ), whereas Van Houten and Watts<sup>65</sup> have used the steady state limit to cover the luminescence behaviour between 273 and 380 K ( $\Delta\epsilon \sim 3,500 \text{ cm}^{-1}$ ), the finer splittings being indistinguishable.

Crosby<sup>66</sup> has used a generalised form of equation 1.61 to include the case for a set of  $n$  thermally equilibrated levels:

$$(\tau_p)^{-1} = \sum k_i g_i e^{-\Delta\epsilon_i/kT} / \sum g_i e^{-\Delta\epsilon_i/kT} \quad (1.67)$$

$k_{-4}$  has replaced  $(k_2 + k_3)$  as the competitive process to ISC. This highlights the difference between the two treatments. The steady-state limit assumes  $k_{-4}$  to be an inefficient pathway, which occurs in competition with  $k_5$  and  $k_6$  after ISC is complete. The equilibrium limit assumes  $k_{-4}$  to be directly competitive with  $k_4$  and precedes deactivation by  $k_5$  and  $k_6$ .

$k_{-4}$  and  $K$  both show a similar Boltzmann dependence on temperature, with  $K$  containing a degeneracy term:

$$K = (g_{A_1}/g_{F_1}) e^{-\Delta\epsilon/kT} \quad (1.65)$$

$$k_{-4} = k'_{-4} e^{-\Delta\epsilon/kT} \quad (1.66)$$

where  $g_{A_1}$  and  $g_{F_1}$  are the degeneracies of  $A_1$  and  $F_1$  respectively, and  $k'_{-4}$  is the limiting back-ISC rate.  $\Delta\epsilon$  is the energy level gap between the two levels,  $k$  is the Boltzmann factor and  $T$  is the temperature.

Crosby<sup>64</sup> has used the equilibrium limit to define the splittings of the emitting manifold  $[\text{Ru}(\text{bipy})_3]^{2+}$  between 0 and 100 K ( $\Delta\epsilon < 60 \text{ cm}^{-1}$ ), whereas Van Houten and Watts<sup>65</sup> have used the steady state limit to cover the luminescence behaviour between 273 and 380 K ( $\Delta\epsilon \sim 3,500 \text{ cm}^{-1}$ ), the finer splittings being indistinguishable.

Crosby<sup>66</sup> has used a generalised form of equation 1.61 to include the case for a set of  $n$  thermally equilibrated levels:

$$(\tau_p)^{-1} = \sum k_i g_i e^{-\Delta\epsilon_i/kT} / \sum g_i e^{-\Delta\epsilon_i/kT} \quad (1.67)$$

where  $k_i$  is the sum of the radiative and non-radiative rate constants for the  $i$ th level of degeneracy,  $g_i$ , excluding back-intersystem crossing.

Temperature dependence (Arrhenius) measurements are only one method of obtaining information about non-radiative rates, and give insight into individual temperature-independent pathways. The advent of picosecond lasers<sup>67</sup> enables measurements of the risetime of the luminescence to be made, and hence to gain information about  $\phi_{ISC}$ . Low temperature studies<sup>63</sup> have the advantage of "freezing out" diffusional and, in some cases, temperature-dependent deactivation pathways, which simplifies equation 1.60:

$$(\tau_p)^{-1} = k_5 + k_6 \quad (1.68)$$

but makes correlation with the ambient temperature situation dubious.

Intermolecular energy transfer techniques, which have been discussed in the context of photochemistry, apply equally well to  $\phi_p$  and  $\tau_p$ , and can yield invaluable information about the emitting level and the intramolecular processes.

CHAPTER 2  
SELECTED SYSTEMS

## 2.1 COBALT(III) - A 3d<sup>6</sup> SYSTEM

In its solution chemistry, cobalt has two important oxidation states, namely II(3d<sup>7</sup>) and III(3d<sup>6</sup>). Divalent cobalt complexes have been rather neglected from the photochemical point of view, while extensive photochemical studies have been carried out on cobalt(III) complexes. On the other hand, Co(III) complexes have received very little attention from the point of view of their luminescent properties, mainly because only a few cobalt(III) complexes have been reported to emit, such as  $K_3[Co(CN)_6]$ <sup>68,69</sup> and  $Na_5[Co(CN)_4(SO_3)_2]$ <sup>70</sup> on u.v. excitation.

The photochemical behaviour of Co(III) complexes is characterised by the simultaneous occurrence of photoaquation and photo-oxidation-reduction reactions. The quantum yields for photoaquation are often very low, and the possibility of relating the nature and quantum yield of photoaquation to intrinsic properties of the complexes is very limited. The occurrence of photoaquation is not generally related to the type of irradiation employed (ligand field or charge transfer). However, in cases of photo-oxidation-reduction reactions, charge transfer excitation is that responsible for this type of process.

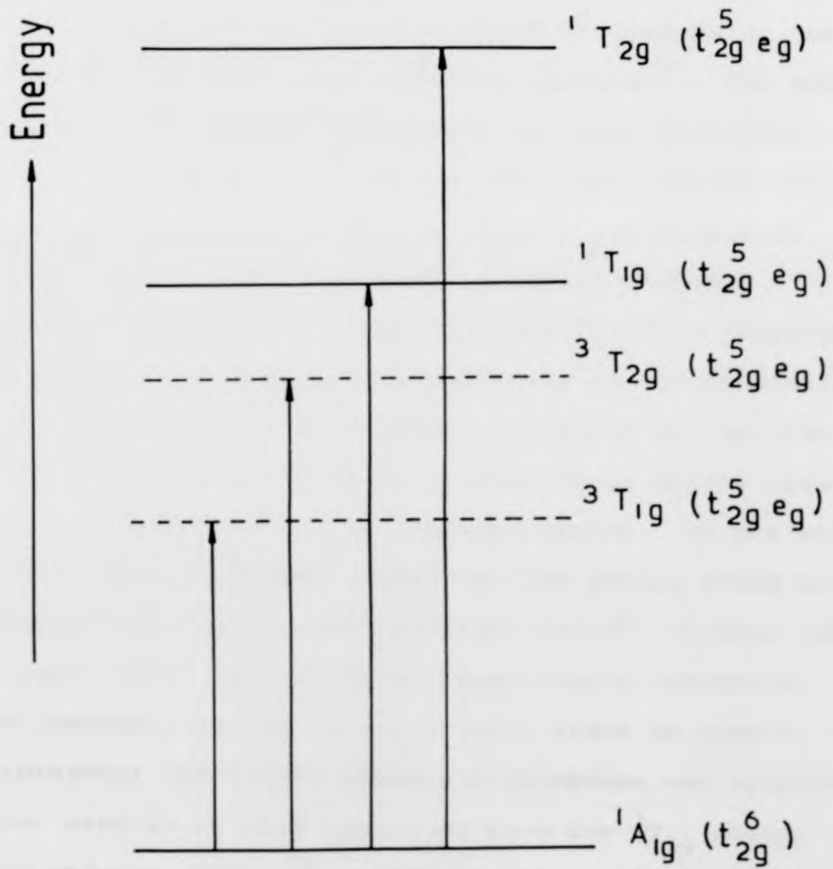
### 2.1.1 Absorption Spectra and some Photochemical Aspects of Co(III) Complexes

In octahedral symmetry, the ground state for low-spin systems is  ${}^1A_{1g}$  which has the  $t_{2g}^6$  configuration. The lowest-energy excited configuration,  $t_{2g}^5 e_g$ , gives rise to two spin-allowed levels,  ${}^1T_{1g}$  and  ${}^1T_{2g}$ , and to the corresponding spin-forbidden  ${}^3T_{1g}$  and  ${}^3T_{2g}$  levels (Figure 2.1). It is interesting to note that, unlike the corresponding Cr(III) complexes, the low-lying spin-forbidden states have a different electronic configuration with respect to the ground state. The two low-intensity bands which appear in the visible or near-u.v. regions (see Figure 1.3), being located, for example, at 472 and 338 nm for  $[\text{Co}(\text{NH}_3)_6]^{3+}$ , are identified with the spin-allowed ligand field transitions  ${}^1A_{1g} \rightarrow {}^1T_{1g}$  and  ${}^1A_{1g} \rightarrow {}^1T_{2g}$ . The corresponding spin-forbidden bands are usually undetectable, since they are overlapped to a large extent by spin-allowed bands. The intense bands at higher energies are due to LMCT transitions and occur at longer wavelengths than for the analogous Cr(III) complexes, in agreement with the higher reducibility of Co(III). The assignment is consistent with the progressive red shift of this band in complexes of the type  $[\text{Co}(\text{NH}_3)_5\text{X}]^{2+}$ , as the ionisation potential of X decreases<sup>71</sup>.

The lack of information about the luminescent behaviour of Co(III) complexes contrasts strongly with the comprehensive studies concerning the analogous Cr(III) complexes<sup>12</sup>. In theory, the ligand field

Figure 2.1 Schematic energy level diagram for the ligand field states of Co(III) complexes in octahedral symmetry (from reference 12).

es

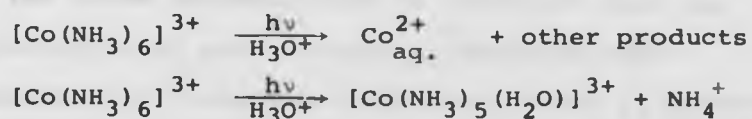


states of Co(III), which have a  $d^6$  configuration, should not offer a favourable situation for phosphorescent emission, in contrast to the Cr(III) systems which have a  $d^3$  configuration. The close similarity observed for the absorption spectra of the  $d^3$  and  $d^6$  systems is not expected to extend to the emission spectra<sup>72</sup>. For both  $d^6$  and  $d^3$  configurations, we have the spin-forbidden levels lying below the first excited spin-allowed state, but for  $d^6$  we have the same electronic configuration ( $t_{2g}^5 e_g$ ) for both spin-allowed and spin-forbidden excited states, which is not the case for  $d^3$ . Therefore, the equilibrium internuclear distances of the spin-allowed  $d^6$  states are likely to be equal or nearly so, and the potential energy surfaces are likely to be nearly parallel, with a low probability for interconversion. On the other hand, the spin-forbidden levels and the ground state have different electronic configurations for  $d^6$ , so that they are expected to have different equilibrium distances. This implies that the lowest triplet state is likely to intersect the ground state and therefore the triplet state, even if it were populated from the  $^1T_{1g}$  state, would undergo rapid radiationless deactivation rather than phosphorescent emission. Thus, all circumstances which act favourably for the phosphorescent d-d emission in  $d^3$ -systems become unfavourable for  $d^6$ -systems<sup>72</sup>. In the cases of the only two cobalt(III) complexes for which phosphorescence has been reported ( $[\text{Co}(\text{CN})_6]^{3-}$  and  $[\text{Co}(\text{CN})_4(\text{SO}_3)_2]^{5-}$ ), the energy splitting between the lowest triplet and the ground state is expected to be

rather high because of the strong ligand field and thus the intersystem crossing  ${}^3T_{1g} \rightsquigarrow {}^1A_{1g}$  should be rather improbable.

The photochemistry of Co(III) complexes requires the presence of at least two photoreactive states<sup>73</sup>, namely the charge-transfer excited state, which is responsible for the oxidation-reduction reactions, and the ligand field excited state, which is responsible for photo-substitution. The charge transfer states in most of these complexes have higher energies than the ligand field states, so that they cannot be the proverbial 'lowest states of any multiplicity'. It is assumed for oxidation-reduction reactions that the homolytic bond fission in the reactive charge transfer state must be unusually rapid to compete with the deactivating transitions. Probably, a necessary condition for such a high rate of bond fission is that the potential energy surface of the reactive CT excited state is unstable with respect to a vibrational coordinate along which the molecule is dissociated.

When  $[\text{Co}(\text{NH}_3)_6]^{3+}$  is irradiated in solution, two processes may occur, redox decomposition yielding  $\text{Co}^{2+}$  and an aquation reaction:

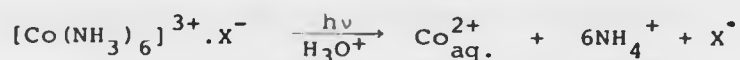


In the case of aquation, a heterolytic bond fission occurs due to ligand field excitation. The redox decomposition may occur in three possible ways<sup>74</sup>;

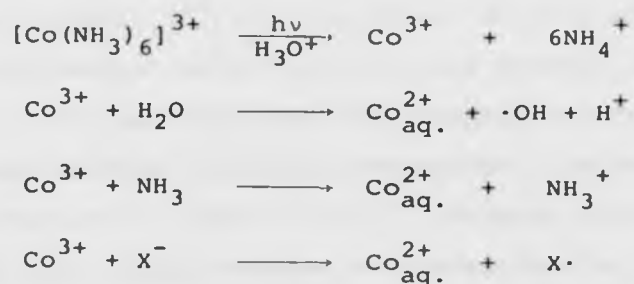
(i) an intramolecular oxidation-reduction reaction between the metal atom and one of the ligands:



(ii) an intermolecular oxidation-reduction reaction between the metal atom and the negative ion partner in the ion pair:



(iii) a heterolytic splitting of all the coordinated Co-NH<sub>3</sub> bonds, followed by the thermal reduction of the Co<sup>3+</sup> ion by water, ammonia or X<sup>-</sup>:



It is found that the redox reactions take place upon excitation in the CT region with high quantum yield, whereas practically no redox reaction occurs upon irradiation in the ligand field bands. This indicates that the redox decomposition is connected with the population of CT excited states, implying that mechanism (iii) cannot be important, since it involves heterolytic splitting of Co-NH<sub>3</sub> bonds originating from ligand field excited states, in which no charge redistribution between metal atom and ligands has

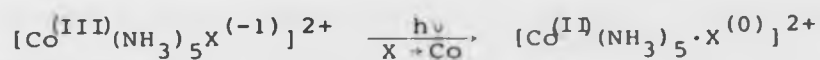
occurred. When  $X^- = \text{ClO}_4^-$ , there are no changes in either the absorption spectrum or the quantum yield of the redox reaction when the anion concentration is increased to  $\sim 1 \text{ M}$ , while in the case of  $X^- = \text{Cl}^-$ , there are changes in both the absorption spectrum and the quantum yield upon increasing the concentration of  $\text{Cl}^-$ . This indicates that when the anion is  $\text{ClO}_4^-$ , both light absorption and its chemical consequences concern only the complex cation, which implies an intramolecular process for the redox decomposition (mechanism (i)) proceeding from a LMCT excited state. On the other hand, when  $X^- = \text{Cl}^-$ , most of the light is absorbed by  $[\text{Co}(\text{NH}_3)_6]^{3+} \cdot \text{Cl}^-$  ion-pairs, which display greater photochemical efficiency (at the irradiation wavelength of 254 nm) than the free complex cation. It seems that another photoredox mechanism intervenes besides mechanism (i) when  $X^- = \text{Cl}^-$ . Evidently the light absorbed by the ion-pair causes an intermolecular CT transition from the anion to the empty d-orbitals of the metal (mechanism (ii)).

The occurrence of photoaquation is not solely connected with ligand field excitation<sup>12</sup>. Reactions have been observed upon charge transfer irradiation such as:



One might note that the quantum yield of aquation is higher when a simultaneous photoredox decomposition also takes place. Excitation of the lowest spin-allowed ligand field band does not lead to appreciable photo-

aquation. Moreover, an aquation reaction does not necessarily require a heterolytic metal-ligand bond fission, for it can also occur as a consequence of a primary homolytic bond fission followed by a rapid thermal reaction leading to the observed substitution product. The mechanism of simultaneous redox decomposition and  $\text{NH}_3$  substitution upon excitation to a LMCT excited state is as follows: the LMCT transition causes a reduction in the oxidation state of the metal atom:



The radical-pair is expected to release rapidly those ligands easily replaced by water, because Co(II) complexes are very labile systems<sup>75</sup>. In the meantime, the X radical will either escape from the solvent cage or undergo recombination with the central metal. In the first case, excitation causes complete photodecomposition:



while in the second case, the net reaction may be the substitution of one (or more) ammonia molecule(s):

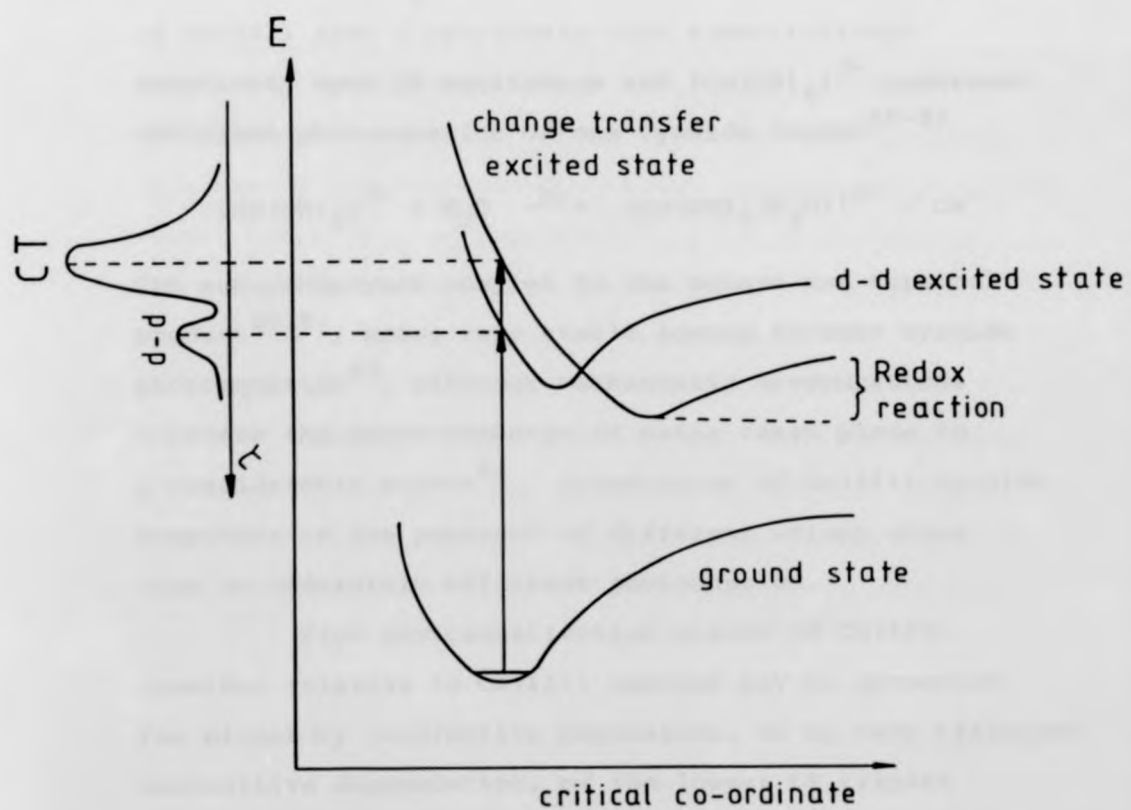


Thus, the charge transfer excited states play the dominant role in determining the photochemical behaviour of Co(III) complexes. Usually, the spin-allowed LMCT state appears at shorter wavelength than the LF band, but it must be remembered that the energies taken from band maxima in the absorption spectra generally

represent vibrational as well as electronic energy. The greater the antibonding character of an excited state, the more it will be distorted, and the more its pure electronic energy will differ from that given by the band maximum. If two excited states are distorted to a different extent, it could be that the state absorbing at shorter wavelengths has actually the lower pure electronic energy. Thus, the occurrence of a redox decomposition (which is expected to originate from a LMCT excited state) upon ligand field excitation may be easily explained by assuming that a charge transfer state, which lies 'spectroscopically' above the ligand field excited state, could extend downwards in energy below the ligand field state, so that radiationless conversion from the latter to the former would be possible. In terms of potential energy curves, such a situation is shown in Figure 2.2. In fact, since the reducing power of the ligands has the effect of lowering the energy of the CT states with respect to the LF states, it appears that the more reducing are the ligands, the more a situation like that of Figure 2.2 is probable.

For cobalt(III) amines, excitation to LF states can be achieved only with a small number of these compounds, that is, with those having the intense CT absorption band at sufficiently short wavelengths. When 'pure' LF excited states are produced, ligand photoaquation takes place, although with very low efficiency. In acidoamine complexes, both

Figure 2.2 Schematic representation of a possible situation of ligand field and charge transfer excited states in cobalt(III) complexes (from reference 9).



ammonia and acido groups may be released, giving rise to antithermal labilisation paths. Thermal aquation of all  $[\text{Co}(\text{NH}_3)_5\text{X}]^{2+}$ -type ions involves replacement of the  $\text{X}^-$  ligand<sup>75</sup>; when  $\text{X} = \text{F}, \text{Cl}$  and  $\text{CN}$ , it has been found<sup>77</sup> that these complexes undergo simultaneous  $\text{X}^-$  and  $\text{NH}_3$  photoaquation. The only photoreaction mode reported to occur for the  $\text{X} = \text{OCOCH}_3$ <sup>78</sup> and  $\text{X} = \text{N}_3$ <sup>79</sup> systems is aquation of  $\text{NH}_3$ . On the other hand, cyano complexes of Co(III) show a relatively high substitutional reactivity upon LF excitation and  $[\text{Co}(\text{CN})_6]^{3-}$  undergoes efficient photoaquation of one cyanide ligand<sup>80-82</sup>.



The aquapentacyano complex is the unique and terminal product<sup>80,81</sup>, being very stable toward further cyanide photoaquation<sup>83</sup>, although mechanistic investigations indicate that photo-exchange of water takes place to a considerable extent<sup>82</sup>. Irradiation of Co(III) cyanide complexes in the presence of different anions gives rise to moderately efficient photoaquation.

High photosubstitution yields of Co(III) cyanides relative to Co(III) amines may be accounted for either by ineffective population, or by very efficient competitive depopulation, of the lowest LF triplet state. Energy-transfer studies show that the substitutional reactivity of the lowest triplet state is high; the differences observed in direct photolysis are ascribed to a greater, or lesser, extent of intersystem crossing<sup>3</sup>. In the case of Co(III) amines there is inefficient

intersystem crossing which may be explained by a relatively rapid internal conversion from the lowest excited singlet to the ground state. This may be understood<sup>12</sup> as the same  $t_{2g}^5 e_g$ , one-electron configuration is associated with both  ${}^1T_{1g}$  and  ${}^3T_{1g}$  excited states, while the ground state ( ${}^1A_{1g}$ ) has the  $t_{2g}^6$  configuration. In both excited states, the same degree of metal-ligand repulsion, and hence of distortion with respect to the ground state, is expected. The result is that intersystem crossing between the  ${}^1T_{1g}$  and  ${}^3T_{1g}$  states is much less probable than the  ${}^1T_{1g} \rightarrow {}^1A_{1g}$  and  ${}^3T_{1g} \rightarrow {}^1A_{1g}$  relaxation processes. Strong-field ligands such as  $CN^-$  increase the energy difference between the ground and the excited state, decreasing the possibility of radiationless deactivation.

Another reason for the high photosubstitution yields of  $[Co(CN)_6]^{3-}$  may be found in the stability of the photo-produced  $[Co(CN)_5]^{2-}$  intermediate, which survives long enough to be able to react either within the solvent cage, or even after escaping from it<sup>82,84,85</sup>.

#### 2.1.2 Photosensitised Reactions of Co(III) Complexes

The quenching of the triplet states of various organic donors by coordination compounds has been established for a long time, but the use of organic donor molecules as sensitizers for photochemical reactions has been reported only relatively recently<sup>12</sup>.

Vogler and Adamson<sup>86</sup> published the first study on photosensitised reactions of Co(III) complexes in 1968, noting that the redox decomposition of  $[\text{Co}(\text{NH}_3)_6]^{3+}$  and  $[\text{Co}(\text{NH}_3)_5(\text{H}_2\text{O})]^{3+}$  in aqueous or aqueous-alcoholic solutions is photosensitised efficiently by organic compounds, most of which were standard carbonyl donors with relatively stable triplet excited states. They observed upon irradiation, the production of Co(II) with relatively high efficiency in the presence of the sensitiser, and not at all in its absence. Since the sensitised photoreduction of  $[\text{Co}(\text{NH}_3)_6]^{3+}$  caused the quenching of biacetyl phosphorescence, they proposed that the observed reaction was the consequence of an energy-transfer process from the lowest triplet state of the donor to a charge-transfer triplet state of the complex. However, caution must be exercised in accepting observations of this kind as proof of energy-transfer between the organic donor and the complex. In fact, photoexcited carbonyl compounds are known to be voracious hydrogen atom abstractors<sup>87</sup>, and in the case of Co(III) ammine complexes, the coordinated ammonia molecules have loosely bound hydrogen atoms. Therefore, a chemical quenching of the carbonyl donor triplets could be expected, so the redox decomposition of the complexes might be due to hydrogen atom abstraction rather than energy-transfer<sup>88</sup>.

Photosensitisation of hexacyanocobaltate(III) ions gives rise to aquation. The most thoroughly investigated system is the sensitisation of  $[\text{Co}(\text{CN})_6]^{3-}$

photoaquation by biacetyl<sup>89,90</sup>. The complex quenches biacetyl phosphorescence without affecting its fluorescence in deoxygenated solutions, showing that the donor triplet is implicated in the energy-transfer process. On the basis of the excited-state energies, the  ${}^3T_{1g}$  state of  $[\text{Co}(\text{CN})_6]^{3-}$  is indicated to be the acceptor level. The quantum yield for sensitised cyanide aquation, which is 0.8<sup>90</sup>, is much higher than that due to direct photolysis, which is 0.31<sup>81</sup>. Table 2.1 summarises some photosensitised reactions of Co(III) complexes.

A number of successful intermolecular, sensitised redox decomposition reactions of Co(III) complexes and other donors have been reported<sup>12,42,85,86,92-95</sup>. The most interesting of these have employed donor molecules, D, with relatively long-lived triplet states. Co(III) complexes quench the donor triplets to form  $\text{Co}^{2+}$ . These reported studies revealed that the Co(II) products are formed in a triplet-to-triplet energy-transfer process and that the charge-transfer triplet state of the Co(III) complex is the photoactive state in both the photosensitised and the directly excited redox decompositions. The mechanism for the sensitisation process is represented as follows:

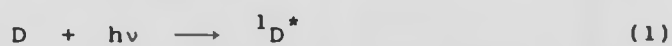


Table 2.1 Systems Showing Photosensitised Reactions of Co(III) Complexes <sup>12</sup>

| Complex                                                               | Sensitiser   | Type of Reaction | Remarks                   | Ref.       |
|-----------------------------------------------------------------------|--------------|------------------|---------------------------|------------|
| [Co(NH <sub>3</sub> ) <sub>6</sub> ] <sup>3+</sup>                    | Biacetyl     | Redox            | Phosphorescence quenching | 86         |
|                                                                       | Benzophenone | Redox            |                           | 86, 88, 90 |
|                                                                       | Benzaldehyde | Redox            |                           | 90         |
|                                                                       | HTSC (a)     | Redox            |                           | 86         |
|                                                                       | Naphthalene  | Redox            | Fluorescence quenching    | 91         |
| [Co(NH <sub>3</sub> ) <sub>5</sub> (H <sub>2</sub> O)] <sup>3+</sup>  | Benzophenone | Redox            |                           | 86         |
|                                                                       | Benzil       | Redox            |                           | 86         |
|                                                                       | HTSC (a)     | Redox            |                           | 86         |
| [Co(NH <sub>3</sub> ) <sub>5</sub> (NO <sub>2</sub> )] <sup>2+</sup>  | Biacetyl     | Redox            |                           | 90         |
|                                                                       | Benzophenone | Redox            |                           | 90         |
|                                                                       | Benzaldehyde | Redox            |                           | 90         |
| [Co(NH <sub>3</sub> ) <sub>5</sub> (HCO <sub>2</sub> )] <sup>2+</sup> | Benzophenone | Redox            |                           | 88         |
|                                                                       | Biacetyl     | Aquation         | Phosphorescence quenching | 89         |
| [Co(CN) <sub>6</sub> ] <sup>3-</sup>                                  |              |                  |                           |            |

(a) *Trans*-stilbene-4-carboxylic acid



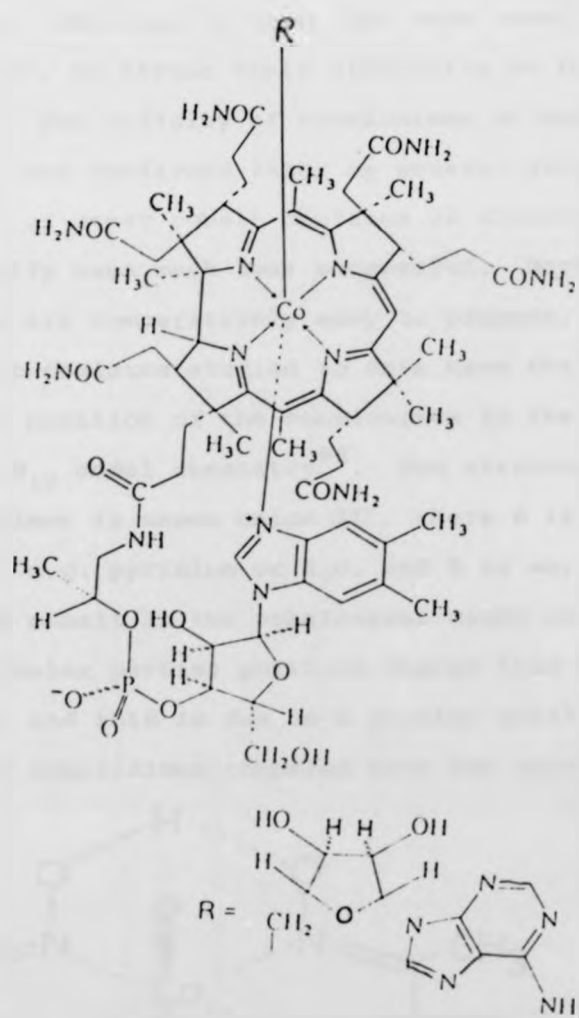
Actually, these systems are very difficult to characterise fully, and the literature contains many errors. Sensitisation reactions of Co(III) complexes, using biacetyl as a sensitiser, were found to proceed by means of a chemical mechanism<sup>92,93</sup> rather than triplet-to-triplet energy-transfer as reported earlier<sup>86</sup>. Gafney and Adamson<sup>42</sup> have hypothesised that the  $[\text{Ru}(\text{bpy})_3]^{2+}$ -sensitised redox decomposition of Co(III) complexes may occur by means of an electron-transfer reaction from the charge-transfer triplet excited state of  $[\text{Ru}(\text{bpy})_3]^{2+}$ . Natarajan and Endicott<sup>94</sup> reported later that the sensitised redox decomposition of Co(III) complexes, using  $[\text{Ru}(\text{bpy})_3]^{2+}$  as a sensitiser, occurs via triplet-to-triplet energy transfer and that there is no evidence for electron transfer from the triplet excited state of the sensitiser.

Recently Reed<sup>96</sup> reported that  $[\text{Co}(\text{acac})_2\text{N}_3(\text{NH}_3)]$  is decomposed on photolysis to yield  $\text{Co}(\text{acac})_2$  and azide radicals due to a triplet charge-transfer photoreactive state. The quantum efficiency of the sensitised decomposition of  $[\text{Co}(\text{acac})_2\text{N}_3(\text{NH}_3)]$  with benzil, benzophenone and phenanthrene to yield Co(II) is comparable to, but somewhat smaller than, that observed in direct photolysis.  $[\text{Co}(\text{acac})_2\text{N}_3(\text{NH}_3)]$  quenches the phosphorescence of both biacetyl and benzophenone but it does not affect the fluorescence of biacetyl and

zinc tetraphenylporphyrin. In an attempt to investigate the redox properties of coordination compounds with macromolecular-ligands, Arunachalam and Natarajan<sup>97</sup> reported that the quantum yield for the redox decomposition of *cis*-[Co(en)<sub>2</sub>(pvp)X]<sup>2+</sup> (en = ethylenediamine; pvp = poly(vinylpyridine) and X = Cl or Br) are affected by the presence of the macromolecular ligand.

### 2.1.3 Cobaloximes as Models for Vitamin B<sub>12</sub>

Studies with cobaloximes, which are regarded as models for Vitamin B<sub>12</sub>, provide a basis for the understanding of the mode of action of corrinoid coenzymes in enzymatic reactions. Moreover, they give a clearer picture about the general properties and reactions of organo-cobalt compounds<sup>98</sup>. In 1961, Hodgkin and Lenhert<sup>99</sup> demonstrated that coenzyme B<sub>12</sub> (5'-deoxy-5'-adenosylcobalamin) contains a direct cobalt-carbon bond (I). This indicated for the first time that organometallic reactions occur in biological systems. In the case of vitamin B<sub>12</sub>, which has a complicated structure, it is assumed that the macrocyclic ligand system modifies the properties of cobalt significantly, enabling it to form stable Co-C bonds, whereas only a few unstable compounds were known to contain Co-C  $\sigma$  bonds. It was reported in 1964<sup>100</sup> that the reactions of the cobalt atom in vitamin B<sub>12</sub> can be simulated with much simpler complexes. Thus, *bis*(dimethylglyoximate)cobalt(III) complexes, which were first prepared by Tshugaev in 1907, show many



(I)

reaction, typical of the cobalt atom in the corrins. These complexes resemble vitamin B<sub>12</sub> so closely in their chemical properties that they were introduced as coordination-chemical models of vitamin B<sub>12</sub> and for convenience, complexes of this type were named "cobaloximes", to stress their similarity to the cobalamins. The validity of cobaloximes as models for vitamin B<sub>12</sub> was confirmed later by several groups. Suggestions of other cobalt chelates as alternative models have generally been much less successful. Moreover, cobaloximes are comparatively easy to prepare, so no other cobalt chelates studied to date have challenged the leading position of the cobaloximes in the field of vitamin B<sub>12</sub> model chemistry<sup>98</sup>. The structure of the cobaloximes is shown below (II), where B is any Lewis base, e.g. pyridine or H<sub>2</sub>O, and R is any alkyl group. The cobalt in the cobaloximes might carry a slightly greater partial positive charge than in the cobalamins, and this is due to a shorter axial Co-B bond in the cobaloximes compared with the cobalamins<sup>103</sup>.

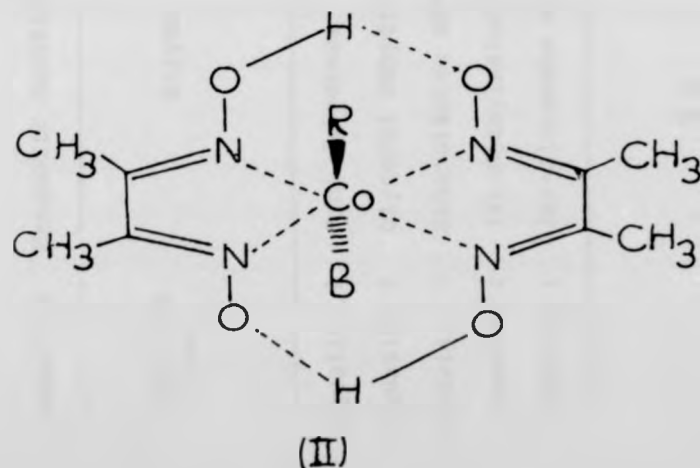
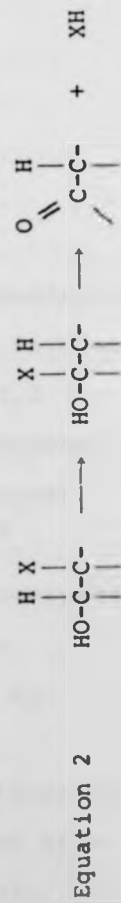
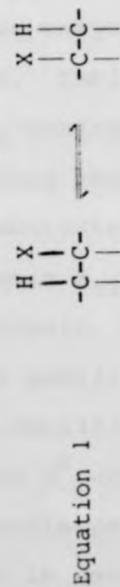
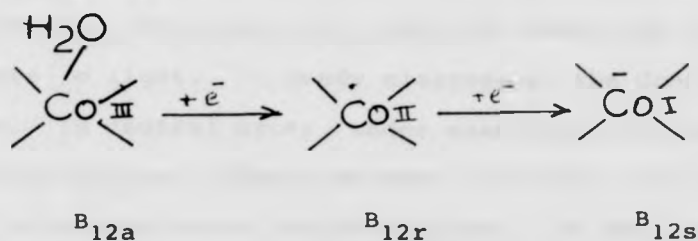


Table 2.2 Enzymatic Reactions Catalysed by Adenosylcobalamin 129

| Reaction Type | Enzyme                       | $\begin{array}{c} \text{H X} \\     \\ \text{a-C-C-d} \\     \\ \text{b c} \end{array}$ | $\begin{array}{c} \text{X H} \\     \\ \text{a-C-C-d} \\     \\ \text{b c} \end{array}$ | X                         |                                                |
|---------------|------------------------------|-----------------------------------------------------------------------------------------|-----------------------------------------------------------------------------------------|---------------------------|------------------------------------------------|
| Equation 2    | Diol dehydrase               | OH                                                                                      | H                                                                                       | e.g. H or CH <sub>3</sub> | OH                                             |
| Equation 2    | Glycerol dehydrase           | OH                                                                                      | H                                                                                       | CH <sub>2</sub> OH        | OH                                             |
| Equation 2    | Ethanolamine ammonia-lyase   | OH                                                                                      | H                                                                                       | H or CH <sub>3</sub>      | NH <sub>2</sub>                                |
| Equation 1    | (R)-Methylmalonyl-CoA mutase | H or CH <sub>3</sub>                                                                    | H                                                                                       | CO <sub>2</sub> H         | COSCoA                                         |
| Equation 1    | (S)-Glutamate mutase         | H                                                                                       | H                                                                                       | CO <sub>2</sub> H         | CHNH <sub>3</sub> CO <sub>2</sub> <sup>-</sup> |



The structure of vitamin B<sub>12</sub><sup>101</sup> features a central cobalt atom surrounded by a corrin ring, which is not fully conjugated. When the lower axial ligand is α-5,6-dimethylbenzimidazole nucleotide, the system is called cobalamin. The upper axial ligand R is variable and can be CH<sub>3</sub> (methylcobalamin), H<sub>2</sub>O, OH<sup>-</sup>, CN<sup>-</sup> (vitamin B<sub>12</sub>), or 5'-deoxyadenosine, (known as coenzyme B<sub>12</sub>). The cobalt atom is normally in oxidation state III (B<sub>12a</sub>) but can be reduced to oxidation state II (B<sub>12r</sub>) or I (B<sub>12s</sub>)<sup>102</sup>:



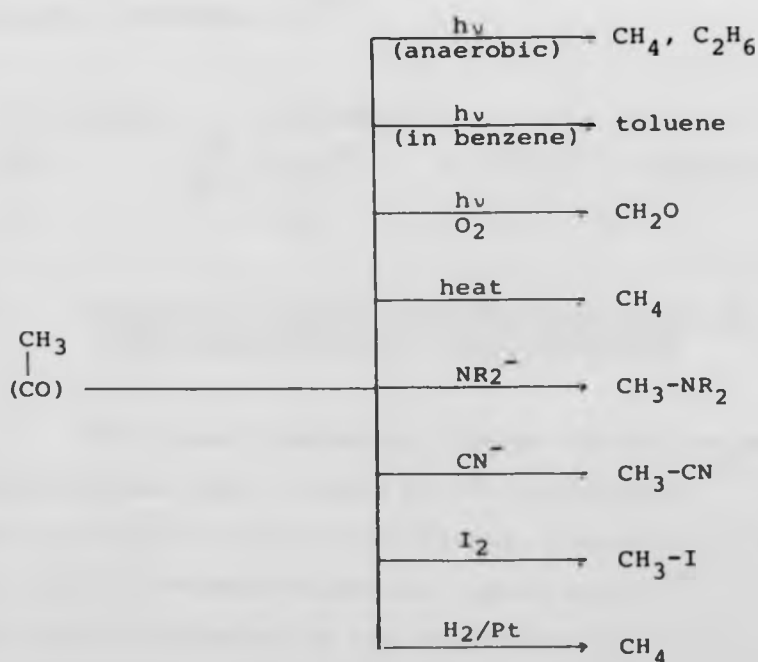
Whereas coenzyme B<sub>12</sub> is a cofactor for hydrogen-transferring enzymes, methylcobalamin is a cofactor for enzymes involved in the metabolism of one-carbon fragments. Table 2.2 summarises the 1,2-shifts executed by B<sub>12</sub>-centred enzymes. These have been successfully modelled during photolysis of alkylcobaloximes in the presence of substrate<sup>129</sup>.

The biological activity of vitamin B<sub>12</sub> coenzymes must be associated with the presence of cobalt, the oxidation reduction potential of which is modified by incorporation into the corrin system. In cobalt(I) derivatives, the metal is in a spin-paired d<sup>8</sup> configuration, and these are some of the most powerful nucleophiles known<sup>104,105</sup>. Vitamin B<sub>12s</sub> and cobaloximes(I) decompose in neutral

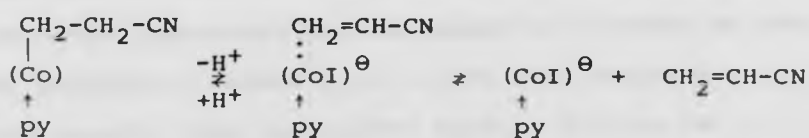
or weakly alkaline solution, but the rates are comparatively slow. Cobalt ion in vitamin B<sub>12r</sub> and the cobalt(II) derivatives of the cobaloximes is in a d<sup>7</sup> configuration. Cobaloximes(II) form 1:1 and 1:2 adducts with a variety of bases<sup>106</sup>, while vitamin B<sub>12r</sub> shows no tendency to dimerise, possibly due to steric factors, nor does it form adducts with two molecules of base.

Simple alkylcobaloximes are regarded as the most stable transition metal organic compounds<sup>107</sup>. They remain unchanged up to 200°C, and show resistance to concentrated non-oxidising acids and bases, but upon exposure to light, ready cleavage of the Co-C bond occurs. In neutral water, under anaerobic conditions, methylcobaloxime yields a mixture of methane and ethane, while ethylcobaloxime yields ethylene. In the presence of oxygen, formaldehyde is the main product of methylcobaloxime photodecomposition. In benzene, the photodecomposition of methylcobaloxime yields toluene, and this is due to combination of the generated methyl radical with the solvent<sup>108</sup>. Thermolysis of methylcobaloxime produces methane and very little ethane, while higher alkylcobaloximes yield mainly alkenes. On the other hand, cobaloximes with bulky alkyl groups attached to the cobalt are thermally less stable. Aquamethylcobaloxime can be dehydrated to a red, air-stable, and weakly hygroscopic anhydride which is insoluble in all non-coordinating solvents and is probably associated in the solid state. This indicates that the axial base component is not essential for Co-C bond stabilisation<sup>108</sup>. Carbon-cobalt bond cleavage in alkylcobaloximes can be effected by a number of nucleophiles,

such as  $\text{CN}^-$  and  $\text{SR}^-$ . During the substitution, the base component in the sixth coordination position is displaced by the nucleophile, but this does not seem to produce an accelerating effect on the bond cleavage reaction. The reaction with  $\text{CN}^-$  is very slow, and large excess of  $\text{CN}^-$  is required for exchange, while weaker nucleophiles (e.g.  $\text{NCS}^-$  and  $\text{I}^-$ ), and also methyl-lithium, fail to cleave the Co-C bond in alkylcobaloximes. The cleavage of the Co-C bond occurs under reducing conditions in the presence of a catalyst. It was reported<sup>108</sup> that the first reduction step is irreversible, presumably due to the Co-C bond cleavage which occurs at this point. The reactions of methylcobaloxime, which involve the cleavage of the Co-C bond, are summarised below:



Higher alkylcobalt derivatives react with some of the nucleophiles as well, but frequently by way of  $\beta$ -elimination rather than nucleophilic substitution. Isopropyl(pyridine)cobaloxime reacts with tri-*n*-butylphosphine rapidly at 50°C to yield propylene and hydrido(tri-*n*-butylphosphine)cobaloxime. Neopentyl(pyridine)-cobaloxime, which is a compound with no hydrogen atom in the  $\beta$ -position, does not undergo Co-C bond cleavage, even on heating with tributylphosphine to 100°C, but it undergoes only displacement of the axially bound pyridine by the phosphine<sup>109</sup>. In organocobalt complexes, electron-attracting substituents at the  $\beta$ -position increase the tendency to undergo elimination reactions.  $\beta$ -Cyanocobaloxime<sup>110</sup> is base-sensitive, and decomposes reversibly according to<sup>111</sup>:



#### 2.1.4 Electronic Spectra and Photochemistry of Alkylcobaloximes and Alkylcobalamins

The great similarity between cobalamins and cobaloximes has been related to the fortuitous identity of the in-plane coordinating strengths of the corrin and *bis*-dimethylglyoxime ligand system<sup>107</sup>. This view is supported by the results of an x-ray structural analysis<sup>103</sup> of a cobaloxime as well as by

polarographic<sup>112</sup> and e.s.r.<sup>113</sup> data. These results suggest that the properties of the cobalt atom are not specifically dependent on the  $\pi$ -electron system of the in-plane ligands.

It is known that the electronic spectra of the transition metal complexes of conjugated ligands fall into three limiting categories; (i) transitions localised on the metal atoms and involving d-d and sp electrons, (ii) transitions largely localised on the ligand, i.e. as  $\pi\text{-}\pi^*$  or  $n\text{-}\pi^*$ , (iii) charge-transfer transitions from metal to ligand, or *vice versa*.

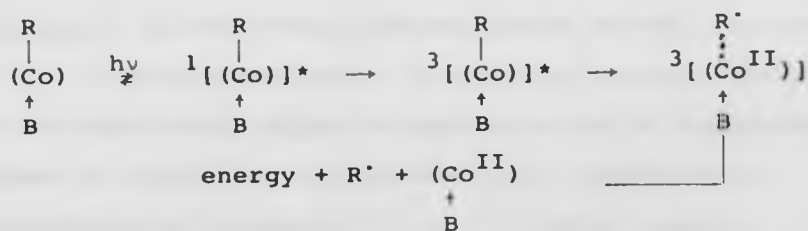
The absorption spectra of Co(II) corrinoids have their main bands at  $\lambda > 300$  nm, and these bands are attributed to  $\pi\text{-}\pi^*$  transitions. On the other hand, the spectra of the cobalamins are also dominated by transitions associated with the corrin ring and such  $\pi$  transitions appearing in the region of 400-600 nm have been designated commonly as  $\alpha$  (590 nm), while the vibrationally fine structured band at 550 nm is designated  $\beta$ . The intense transitions between 350-420 nm are designated  $\gamma$ . The cobalt corrinoids are expected to have absorption spectra due to: (i) d-d transitions, (ii) internal transitions corresponding to the equatorial corrin ligand, (iii) internal transitions of the axial ligand, (iv) charge-transfer transitions from the corrin ring to cobalt, or *vice-versa*, and (v) charge-transfer transitions from an axial ligand to cobalt, or *vice-versa*. At low temperature, the absorption bands become sharper and easier to resolve<sup>114</sup>.

It is believed that the major bands beyond 300 nm correspond to  $\pi-\pi^*$  transitions of the corrin ring. The numbers and intensities of these bands are variable, and they are very sensitive to changes in the numbers and nature of the substituents in the conjugated chain and are also slightly affected by changes in the side chains, in the solvent and in temperature.

The absence of extensive conjugation in the cobaloxime ligand  $\pi$ -electron system causes the energy of the  $\pi-\pi^*$  transition to be at much higher energy (240 nm) than in the corrin system<sup>115</sup>. Between 400-250 nm there are several bands with  $\epsilon$  between  $10^3$  and  $10^4$ , which are not well-assigned although the axial bases may absorb in this region, but the important low-energy absorption of organocobaloximes occurs between 400 and 500 nm and is believed to be indicative of the presence of covalent axial bonds in view of the  $\epsilon$  of about  $10^3$ ; more specifically this band has been assigned to a charge-transfer band (Co-C CT). Its energy is very sensitive to the axial base and also to some extent on inductive effects and the 2s-character of the axial carbon residue attached to the cobalt atom. The Co-C CT transition is shifted to higher energy on changing the hybridisation of the carbon residue and also on varying the axial base.

The homolytic Co-R bond cleavage results from the excitation to a  $R \rightarrow Co$  CT state. The corresponding transition has been localised in cobaloximes in the 400-450 nm area with  $\epsilon$  of 1000-2000<sup>115</sup>, while in the case

of cobalamins this CT transition is hidden underneath the strong intraligand  $\pi-\pi^*$  transition of the corrin  $\pi$ -system. The quantum yields for Co-R cleavage under aerobic conditions are smaller by a factor of 10 for the cobaloximes, and this is due to the lower strength of the Co-C bond in cobalamins than in the cobaloximes in which a slightly greater partial positive charge resides on the cobalt atom. In the photodealkylation of cobaloximes, and during the excitation process, intermediate states of the complexes are formed which ultimately decompose into the free radical  $R^\cdot$  and cobaloxime(II) fragments<sup>98</sup>:



Methyl radicals recombine with the cobalt(II) fragments with high efficiency if the photolysis is performed under strictly anaerobic conditions in water. Some of the methyl radicals diffuse out of the coordination sphere of cobalt and terminate either by dimerisation to ethane, or by hydrogen abstraction to methane. Photolysis in alcoholic media, particularly isopropanol, favours hydrogen abstraction reactions and methane is formed virtually exclusively<sup>116</sup>.

The photolysis of trideuteriomethyl-cobalamin

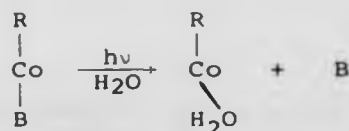
and cobaloxime in aqueous media, produces  $C_2D_6$  (89%) and  $CH_3CD_3$  (11%), which proves that ligand-methyl groups are detached during photolysis.

Ethylcobalamin and ethylcobaloxime undergo photolysis to yield ethylene, while the cobalt(II) fragments produced are reduced to cobalt(I) derivatives, which in turn decompose with the release of hydrogen<sup>116-118</sup>. The overall process can be expressed as:



In alcoholic solvents, the photolysis of the higher alkylcobalt derivatives produces alkane as well as alkenes<sup>116</sup>.

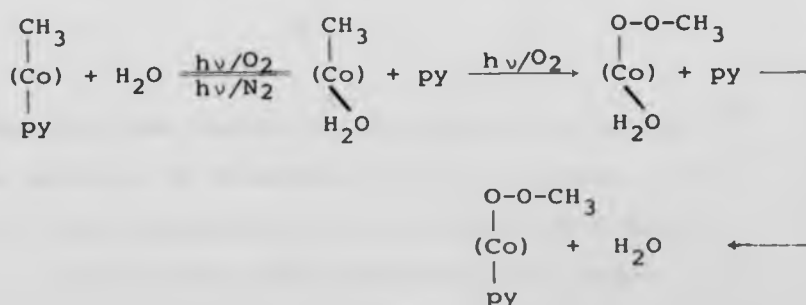
Photodissociation of the bond between cobalt and the lower axial ligand B appears to be an important process in cobaloxime photochemistry, according to observations by Giannotti *et al.*<sup>119</sup> (under aerobic conditions):



Another explanation for the differing quantum yields could be different ratios of photodealkylation and cleavage of the Co-B bond in cobaloximes and cobalamins, due to different rates of internal conversion. An e.s.r.<sup>120</sup> study in anaerobic conditions of cobaloximes, all of

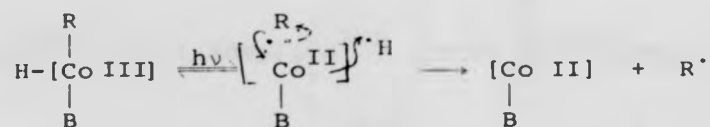
which contained pyridine as the axial ligand B, indicated that compounds with R as methyl and benzyl abstract an electron from the solvent ( $\text{CHCl}_3$  > 0.75%  $\text{C}_2\text{H}_5\text{OH}$  at  $-20^\circ\text{C}$ ) in the primary photochemical process, leading to Co(II) species still containing both axial ligands (however, see below). By contrast cobaloximes with R as isopropyl, isobutyl, n-pentyl, and cyclohexyl at  $-160^\circ\text{C}$  gave the corresponding radicals R and the dealkylated Co(II) species. On warming up the samples to  $-100^\circ\text{C}$  further changes occurred, which were ascribed to loss of pyridine ligand or substitution of a solvent molecule in the alkyl position. This work provides the first direct evidence for the production of Co(II) species as the primary product of anaerobic cobaloxime photochemistry.

Peroxy compounds could play a role in the aerobic photolysis of cobalamins, particularly in view of the established insertion of  $\text{O}_2$  into alkylcobaloximes on photolysis<sup>119</sup>.



The first detectable photochemical process of alkylcobaloximes (in alcoholic solution) in the presence of water generally appears to be the expulsion of the lower axial ligand B and the rapid formation of the alkyl(aquo)cobaloxime<sup>119</sup>. The insertion of O<sub>2</sub> into the Co-R bond of the aquo-complex needs another light quantum. The reactivity of the aquo-complex in this second step parallels the general enhancement of relative aerobic photolysis rates of alkylcobaloximes on decreasing the basicity of B, rendering the aquo-complexes the most photo-reactive system<sup>115</sup>.

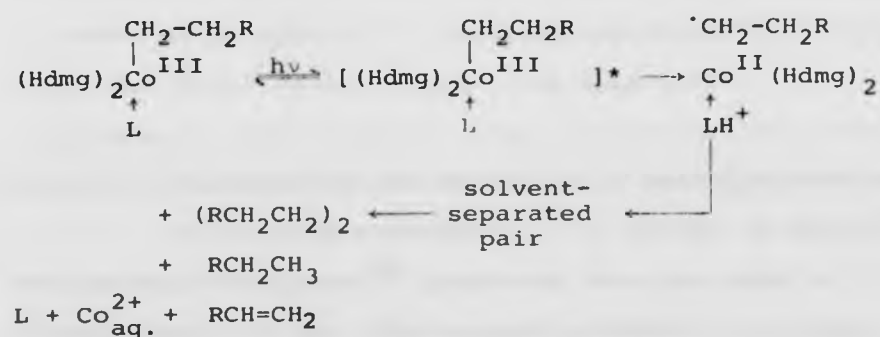
Giannotti<sup>121</sup> reported that the photolysis of any alkylcobaloxime with visible light proceeds through a mechanism involving an initial electron transfer reaction from an equatorial ligand to the central metal atom which leads to the production of cobalt(II) species, retaining both original axial ligands. The suggested mechanism is:



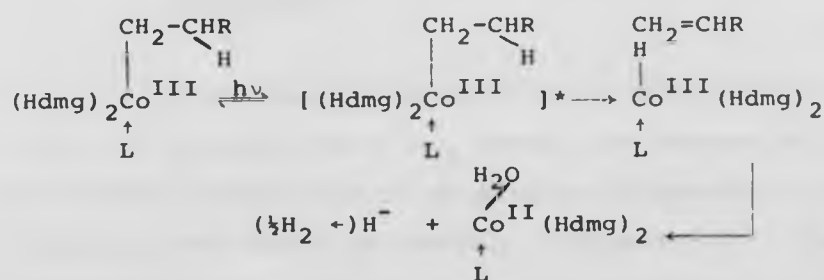
but this has been emphatically rejected by Symons<sup>128</sup> who is critical of Giannotti's e.s.r. results, and prefers simple photolysis of the Co(III)-C bond.

It has also been reported that, under anaerobic conditions, the photochemical decomposition of alkylaquocobaloximes in aqueous solution depends

on pH<sup>122</sup>. At pH 2, photoreaction is fast ( $\Phi \approx 0.1$  for several alkyl substituents), and wavelength-independent and involves the productions of  $\text{Co}^{2+}$  aq. and radical intermediates which yield products typical of abstraction and dimerisation reactions:



On the other hand, at pH 7, photoreaction is about ten-fold less efficient to yield  $[\text{Co}^{\text{II}}(\text{dmgH})_2(\text{OH}_2)_2]$  together with an alk-1-ene derived from the axial alkyl ligand:



In a flash photolysis study of methylcobalamin, Endicott and Ferraudi<sup>123</sup> observed the efficient generation of  $\text{B}_{12\text{r}}$  during the flash, and the amount of  $\text{B}_{12\text{r}}$  generated was independent of the medium. The generation

of  $B_{12r}$  was accompanied by a decrease in concentration of methyl-cobalamin. In deaerated aqueous solution, the initial generation of  $B_{12r}$  was followed by a rapid partial decay which also corresponded to a rapid partial regeneration of the methyl-cobalamin absorbance. Thus, the back-reaction to form methyl-cobalamin is believed to occur very rapidly. In aerated solutions the initial  $B_{12r}$  absorbance decays rapidly and apparently completely in what appears to be a second-order process. This is attributed to the formation of methylperoxo-cobalamin.

Picosecond excitation ( $\lambda = 527$  nm) of methyl- and adenosylcobalamin<sup>124</sup> indicates that the rate of disappearance of the cage-trapped products is probably similar for both materials, although one might expect the larger adenosyl radicals to diffuse more slowly than methyl radicals into the bulk solution.

#### 2.1.5 The Photochemistry of *Tris*(acetylacetonato)-cobalt(III)

Since the ground state of Co(III) low-spin  $d^6$  ion is an uncomplicated  $^1A_{1g}$  state, the absorption spectra of Co(III) systems should be simpler compared to Cr(III) chelates, and should be readily interpretable<sup>3</sup>. The absorption maxima for  $Co(acac)_3$  in chloroform and ethanol were reported by Barnum<sup>125,126</sup> as given in Table 2.3. The assignment of an intense band in the near-u.v.-to-visible region creates some difficulties. In  $Co(acac)_3$ , the assignment of this band at 25.0 kK to the second spin-allowed d-d transition is not entirely reasonable,

firstly because of simple ligand-field predictions and secondly because of its intensity. One interpretation of the 25.0 kK band is that it is a combination of  ${}^1T_{2g} \leftarrow \pi$  and  ${}^1T_{2g} \leftarrow {}^1A_{1g}$ , in which the calculated energies for the 'pure' transition are 27.0 kK for  ${}^1T_{2g} \leftarrow \pi$  and 23.8 kK for  ${}^1T_{2g} \leftarrow {}^1A_{1g}$ .

There are few data in literature about the photochemistry of Co(III) complexes in organic solvents, and most of the studies have been reported in aqueous media<sup>12</sup>. The photoredox reactions of  $\text{Co}(\text{acac})_3$  were examined by Filipescu and Way<sup>127</sup>. The Co(II) chelate and biacetyl were believed to be the major products from the photolysis. The organic products depend on the presence or absence of oxygen.

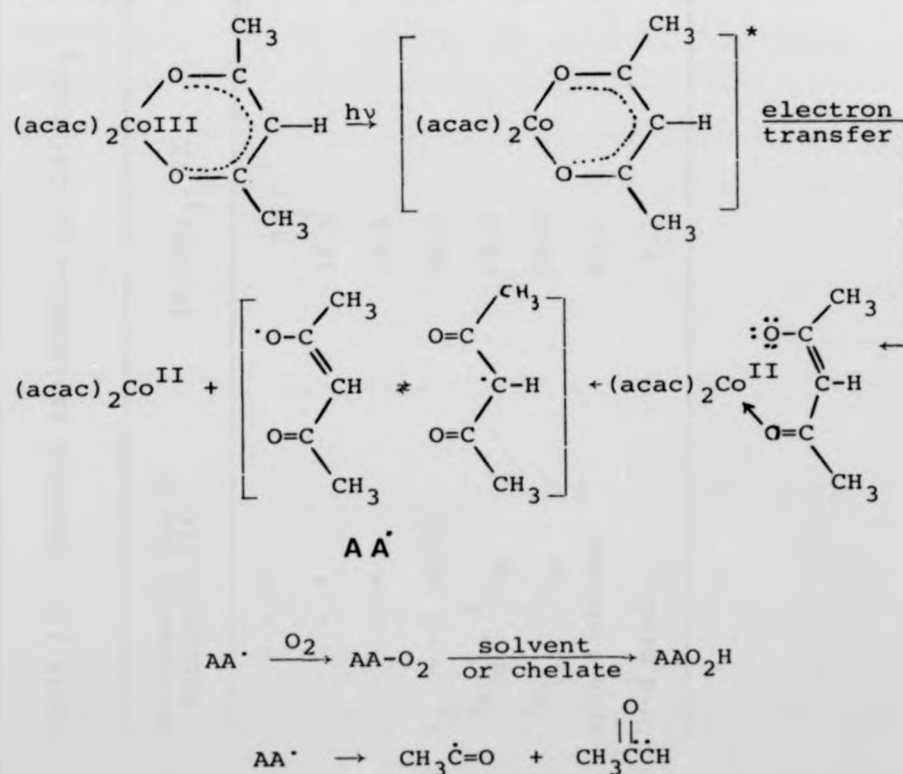


Table 2.3 Spectral Assignments for  $\text{Co}(\text{acac})_3$

| Assignments due to<br>Barnum 125, 126 | in $\text{CHCl}_3$ , kK | $\log \epsilon$ | in $\text{C}_2\text{H}_5\text{OH}$ , kK | $\log \epsilon$ |
|---------------------------------------|-------------------------|-----------------|-----------------------------------------|-----------------|
| $\pi \rightarrow \pi^*$               | -                       | -               | 43.8                                    | 4.6             |
| $\pi \rightarrow \pi^*$               | 39.3                    | 4.54            | 39.3                                    | 4.53            |
| $\pi \rightarrow \pi^*$               | 33.9                    | 4.0             | 33.9                                    | 4.0             |
| $t_{2g} \rightarrow \pi^*$ (MLCT)     | 30.9                    | 3.9             | 30.9                                    | 3.9             |
| ${}^1A_{1g} \rightarrow {}^1T_{2g}$   | 25.0                    | 2.5             | 25.0                                    | 2.5             |
| ${}^1A_{1g} \rightarrow {}^1T_{1g}$   | 16.8                    | 2.10            | 16.8                                    | 2.10            |
| spin forbidden                        | 12.5                    | 0.5             | -                                       | -               |
| d-d bands                             | 9.1                     | 0.28            | -                                       | -               |

The quantum yield for the production of Co(II) is independent of the presence of oxygen, while it is dependent on the wavelength. The values are about 0.5 for irradiation in the region of the strong intraligand  $\pi^* \leftarrow \pi$  transition (265 nm), but fall to about 0.14 in the charge transfer region (325), and then decline further to  $2 \times 10^{-3}$  for irradiation in the d-d band (590 nm). These results indicate that the photoreduction takes place from relatively high-energy charge-transfer bands, presumably of the LMCT type. The quantum yield dependence on wavelength indicates that one of the intense bands occurring at 295 and 325 nm is a LMCT transition. However, the 295 nm band occurs in  $\text{acac}^-$  itself, and, therefore, is almost certainly due to the  $\pi^* \leftarrow \pi$  transition. The 325 nm band was originally assigned by Barnum<sup>125,126</sup> to a  $\pi^* \leftarrow t_{2g}$  transition, that is MLCT, but, in view of the photochemical results, it is more logical to assign it to  ${}^1T_{2g} \leftarrow \pi$ , which is LMCT<sup>3</sup>.

The assignment of the 400 nm band, that is the combination of  $\pi^* \leftarrow {}^1A_{1g}$  and  ${}^1T_{2g} \leftarrow {}^1A_{1g}$  (MLCT type), may well explain the sharp decrease in Co(II) formation at longer wavelength irradiations.

## 2.2 RUTHENIUM(II); A SYSTEM EXHIBITING 'HEAVY-ATOM' LUMINESCENCE

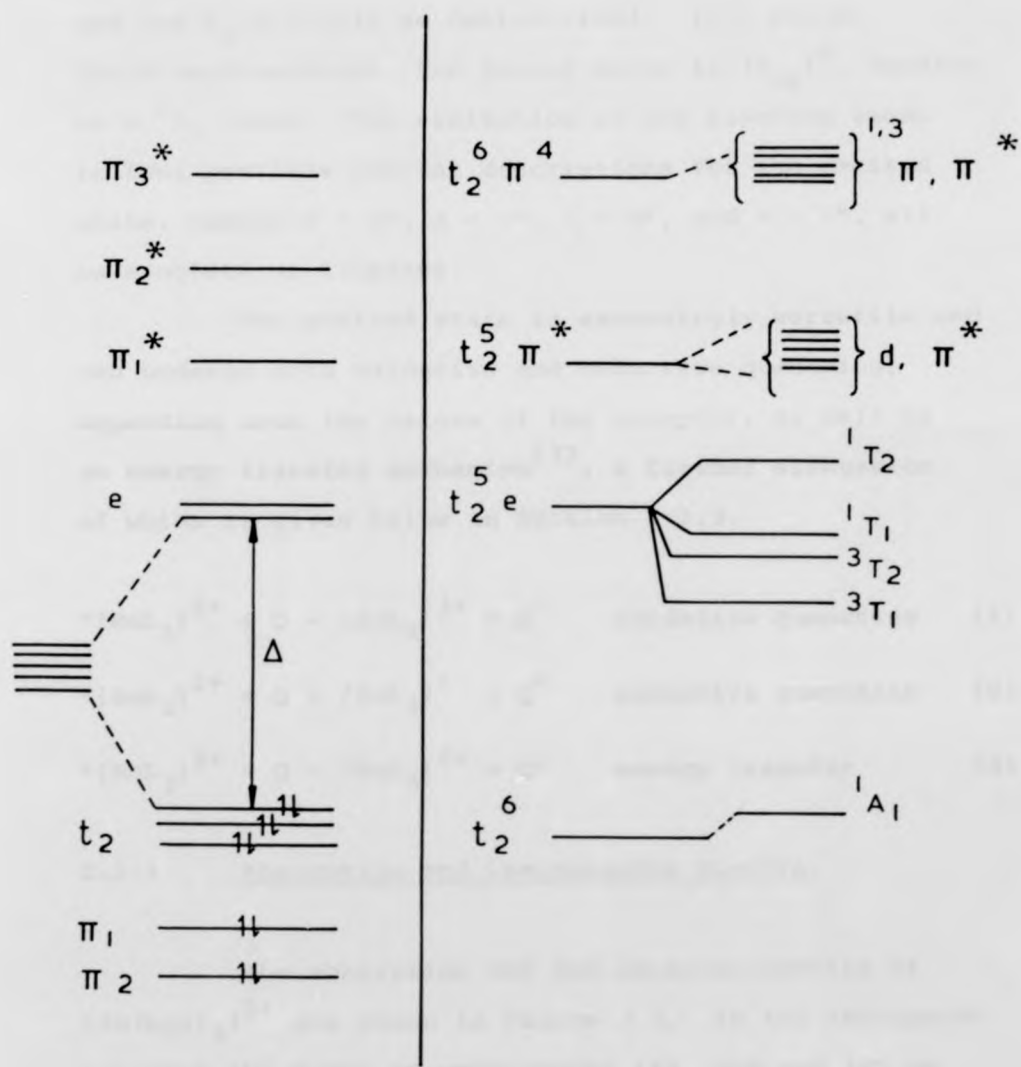
The excited state chemistry of Ru(II) complexes, particularly with polypyridyl ligands, has attracted intense interest since the discovery of strong emission

from  $[\text{Ru}(\text{bpy})_3]^{2+}$  by Paris and Brandt in 1959<sup>130</sup>.

The properties of luminescent polypyridyl complexes of Ru(II) such as  $[\text{Ru}(\text{bpy})_3]^{2+}$  and  $[\text{Ru}(\text{phen})_3]^{2+}$  have resulted in these complexes and their analogues being the recipients of particular attention with reference to solar energy conversion schemes and their use as versatile and powerful sensitizers. The relevant properties are<sup>131</sup>: (i) their solubility in aqueous solutions; (ii) their strong absorption in the visible region; (iii) their photostability at room temperature; (iv) their luminescence in an experimentally very accessible region ( $\sim 580$  nm) while remaining reasonably energetic; (v) their strong luminescence at room temperature with a lifetime of  $\sim 0.7$   $\mu\text{s}$  for  $[\text{Ru}(\text{bpy})_3]^{2+}$ ; and (vi) their unique photoelectrochemical properties (being both powerful photo-oxidants and photo-reductants towards the water molecule). Taking  $[\text{Ru}(\text{bpy})_3]^{2+}$  as typical, it represents one of the few transition metal complexes that exhibits powerful photosensitisation capacity for electron- and energy-transfer processes, and so it has generated lively debate on the fundamental questions concerning the factors that govern the excited state processes.

The electronic situation for a  $d^6$ -complex (such as Ru(II) in octahedral symmetry) is shown in Figure 2.3. The ground and the low-lying excited states can be discussed in terms of the  $t_{2g}$  and  $e_g$  d-orbitals of the metal ion and the  $\pi$ -bonding and  $\pi^*$ -antibonding orbitals of the ligand. The  $t_{2g}$  d-orbitals are referred to as stabilised,

Figure 2.3 Simplified representation of the  
electronic states for a  $d^6$ -complex  
(from reference 133).



Orbitals

States

and the  $e_g$  orbitals as destabilised. In a strong field configuration, the ground state is  $(t_{2g})^6$ , leading to a  $^1A_1$  label. The excitation of one electron leads to four possible orbital descriptions for the excited state, namely  $d \rightarrow d^*$ ,  $d \rightarrow \pi^*$ ,  $\pi \rightarrow d^*$ , and  $\pi \rightarrow \pi^*$ , all as singlets or triplets.

The excited state is exceedingly versatile and can undergo both oxidative and reductive quenching, depending upon the nature of the acceptor, as well as an energy transfer mechanism<sup>132</sup>, a further discussion of which is given below in Section 2.2.3.

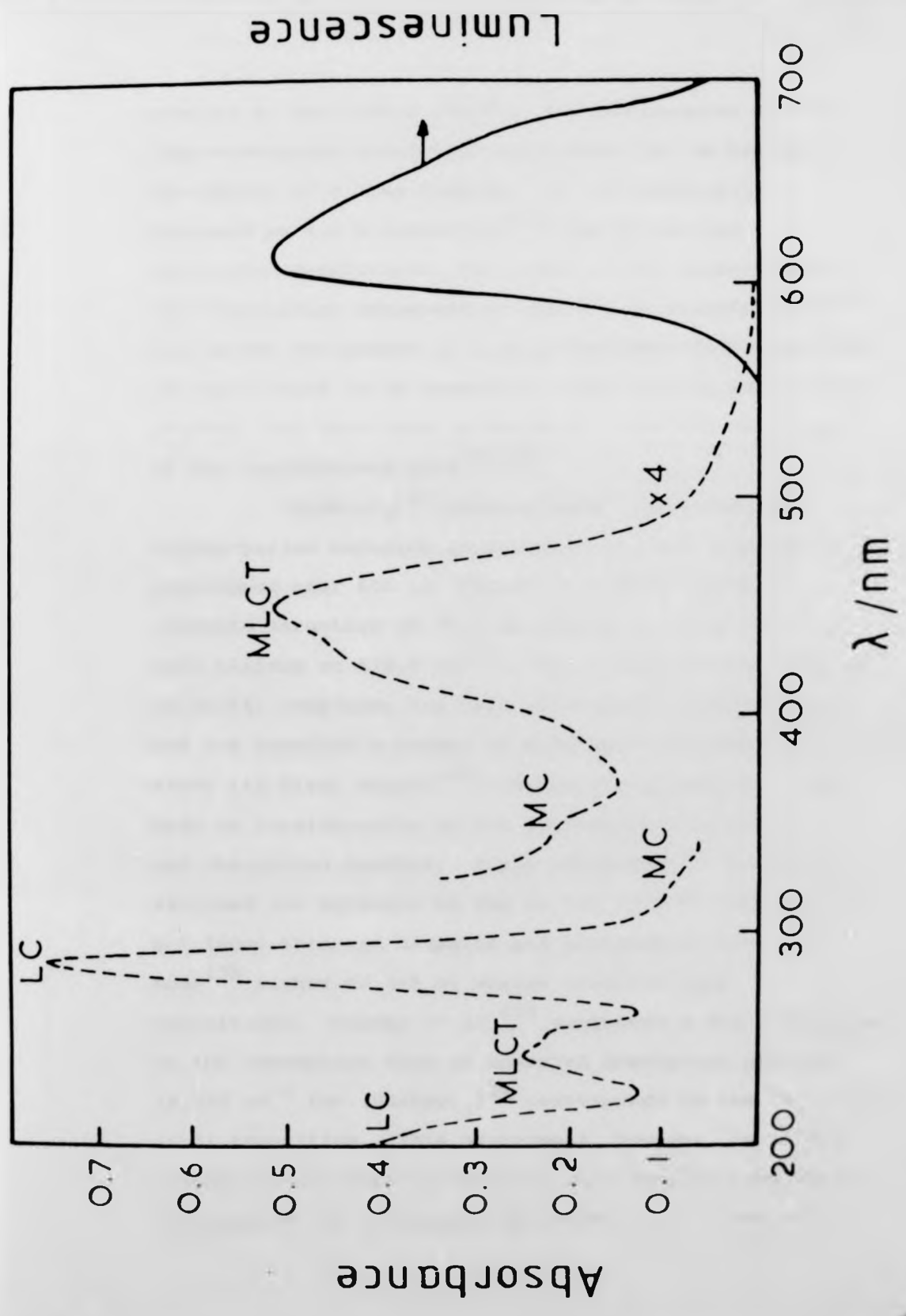


### 2.2.1 Absorption and Luminescence Spectra

The absorption and the emission spectra of  $[\text{Ru}(\text{bpy})_3]^{2+}$  are shown in Figure 2.4. In the absorption spectrum the bands at wavelengths 185, 208 and 285 nm have been assigned as ligand-centred  $\pi-\pi^*$  transitions by comparison with the spectrum of protonated bipyridine<sup>134-136</sup>. The weak shoulders at 323 and at 345 nm, as well as the peak at 250 nm, are assigned as metal-centred d-d transitions. The two remaining intense absorption bands at 240 and 452 nm have been assigned to a CT transition in which an electron is promoted from the metal  $t_2$

Figure 2.4 Absorption and emission spectra for  
 $[\text{Ru}(\text{bpy})_3]^{2+}$  in aqueous solution at  
room temperature (from reference 133).

LC



orbital to the ligand (MLCT). The assignments of the long-wavelength absorption tail above 500 nm has been the object of a long dispute. It was originally assigned as a d-d transition<sup>137</sup> due to its low extinction coefficient, but later it was reassigned to the vibrational component of the charge transfer band<sup>138</sup>. Its recent assignment to a spin-forbidden MLCT transition has been found to be consistent with various experimental results, and this band is believed to be the counterpart of the luminescence band<sup>70,134</sup>.

$[\text{Ru}(\text{bpy})_3]^{2+}$  shows a broad, structureless orange-yellow emission in solution at room temperature positioned near 600 nm (Figure 2.4) which exhibits vibronic structure at 77 K in glassy solution with a band maximum at 579.9 nm<sup>133</sup>. The nature of the emission of Ru(II) complexes has been extensively investigated and has received a number of different assignments<sup>130,134,137,139</sup> since its first report<sup>130</sup>. These assignments have been made on consideration of the low-temperature emission and absorption spectra. Paris and Brandt<sup>130</sup> initially assigned the emission as due to the  $\pi^*$ -d CT fluorescence, but later this was disputed and assignments have been made<sup>139</sup> either to d-d or charge transfer type transitions. Crosby *et al.*<sup>137</sup> suggested a d-d transition on the assumption that an observed absorption peak at  $18,550 \text{ cm}^{-1}$  for  $[\text{Ru}(\text{bpy})_3]^{2+}$  corresponds to the  ${}^1\text{A}_1 \rightarrow {}^1\text{T}_1$  (d-d) transition. This assignment, however, is in disagreement with other studies of this complex from which estimates of the octahedral splitting of  $> 21,000 \text{ cm}^{-1}$

were predicted<sup>24,155</sup>, putting this d-d transition closer to the u.v. region, and Crosby later reassigned the luminescence to a CT type transition. Further evidence for this assignment comes from a study of a series of substituted complexes of the type  $[\text{Ru}(\text{bpy})_2\text{X}]^{2+}$ <sup>138</sup> when it was found that there exists a good correlation between the shift of the CT band and the luminescence spectrum, but the shifts are not large, as would be expected from the large changes in LF strength employed if these were d-d bands. The band is assigned as  $d \rightarrow \pi^*$  due to the ease with which ruthenium(II) is oxidised, the possibility of  $\pi^* \rightarrow d$  being dismissed on the grounds that the transition would be of higher energy due to the low oxidation state of the ruthenium core<sup>138</sup>. The assignment of the luminescence as fluorescence or phosphorescence should be made on the basis of the emission lifetime, as the emission intensity may lead to incorrect assignments<sup>130,137</sup>. Demas and Crosby<sup>156</sup> found the lifetimes of a series of Ru(II) complexes containing polypyridyl ligands at 77 K to be between 0.5 and 10  $\mu\text{s}$ , which is longer than expected for fluorescence, but not long enough for phosphorescence. Demas and Crosby reported later in 1971<sup>28</sup> that the luminescence from  $[\text{RuL}_3]^{2+}$  type complexes is essentially of charge transfer type, spin-forbidden in character at least at 77 K.

The charge transfer emission in  $[\text{Ru}(\text{bpy})_3]^{2+}$  and  $[\text{Ru}(\text{phen})_3]^{2+}$  occurs at lower energy than does  $\pi - \pi^*$  ligand phosphorescence in the free ligand<sup>133</sup>. This, in

conjunction with the intense CT absorption bands, implies a substantial metal d-ligand  $\pi$  interaction. The large d-orbital contribution, and the spin-orbit coupling associated with this system will mix singlets and triplets so that the spin quantum number  $S$  for these systems is not well-defined. Consequently, the emission is better defined as occurring from a manifold of spin-orbit states rather than from a spin-triplet electronic state.

Other Ru(II) polypyridyl complexes displaying analogous luminescence are the 'mixed-ligand chelates', i.e.  $[\text{Ru}(\text{bpy})_m(\text{phen})_n]^{2+}$ , for which it was found  $\nu_0$  (the highest-frequency vibrational component in the luminescence),  $\phi_p$  (77 K) and  $^1T \rightarrow 0$  for the mixed-ligand complexes are weighted averages of the corresponding values of the pure-ligand complexes, indicating strong ligand-ligand interaction<sup>140</sup>.  $[\text{Ru}(\text{phen})_2(\text{CN})_2]$  which luminesces at 635 nm has attracted attention as an electrically neutral analogue of  $[\text{Ru}(\text{bpy})_3]^{2+}$ <sup>141,142</sup>.

### 2.2.2 The Crosby Model for Low Temperature Luminescence of Ruthenium(II) Complexes

Temperature studies on ruthenium(II) complexes between 77 K and 4 K<sup>143,144</sup> have indicated that luminescence occurs from a set of thermally equilibrated excited levels at 77 K, and it is suggested that the emitting CT triplet label merely indicates that there are three emitting levels of CT origin, each spin-orbit level coupled to the perturbing singlet state. The temperature dependence between 77 and 4.2 K of luminescence decay

times for ruthenium(II)<sup>145,146</sup> gives the unexpected result that the measured lifetime at 4.2 K exceeds the intrinsic lifetime calculated at 77 K by factors of between 4 and 15, while the quantum yield decreases<sup>64</sup>, suggesting a manifold of emitting levels. Crosby<sup>64</sup> has used the general equation 1.67 to fit these data, assuming that (i) thermal equilibration is fast compared with depopulating processes, (ii) each of the levels is capable of coupling with the ground state either radiatively or radiationlessly, and these pathways are controlled by first-order kinetics with temperature-independent rate constants, (iii) the manifold of luminescing states is populated from higher excited states with near-unit efficiency at all temperatures, and this efficiency is independent of excitation wavelength. A minimum of three levels are needed to produce a good fit to the experimental data and the observed lifetime,  $\tau$ , is given by the equation:

$$\tau = (1 + 2e^{-\Delta\epsilon_1/KT} + e^{-\Delta\epsilon_2/KT}) / (k_1 + 2k_2e^{-\Delta\epsilon_1/KT} + k_3e^{-\Delta\epsilon_2/KT}) \quad (2.1)$$

where  $k_i$  represents the sum of radiative and non-radiative processes for the  $i$ th level, and  $\Delta\epsilon_i$  is the energy gap between  $(i + 1)$ th and first levels. The second level has been given a two-fold degeneracy on the basis of the theoretical model which has been proposed to allow symmetry labels to be attached to these levels. The values of these parameters are tabulated in Table 2.3 for a number of ruthenium(II) systems<sup>144</sup>.

Table 2.4 Energy Gaps, Rate Constants and Exchange Integrals for the lowest Excited States of Ruthenium(II) Complexes in Polymethylmethacrylate Film for the Range 4-80 K

| Complex                                                      | $\Delta\epsilon_1$ (cm <sup>-1</sup> ) | $\Delta\epsilon_2$ (cm <sup>-1</sup> ) | $\tau_1 = \frac{1}{k_1}$ (μs) | $\tau_2 = \frac{1}{k_2}$ (μs) | $\tau_3 = \frac{1}{k_3}$ (μs) | $K(a_1, a_2)$ | $K(e^+, a_2)$ | $\frac{K(a_1 a_2)}{K(e^+, a_2)}$ | References |
|--------------------------------------------------------------|----------------------------------------|----------------------------------------|-------------------------------|-------------------------------|-------------------------------|---------------|---------------|----------------------------------|------------|
| [Ru(bpy) <sub>3</sub> ]SO <sub>4</sub>                       | 10                                     | 80                                     | 220                           | 19                            | 0.5                           | 47            | 67            | 0.70                             | 146        |
| [Ru(bpy) <sub>3</sub> ]Cl <sub>2</sub>                       | 10.1                                   | 61.2                                   | 183.1                         | 18.8                          | 0.58                          | 36            | 63            | 0.57                             | 64         |
| [Ru(4,4'-Ph <sub>2</sub> bpy) <sub>3</sub> ]Cl <sub>2</sub>  | 9.5                                    | 60.1                                   | 165                           | 18                            | 0.7                           | 36            | 59            | 0.61                             | 146        |
| [Ru(4,4'-Me <sub>2</sub> (bpy) <sub>3</sub> ]Cl <sub>2</sub> | 9.2                                    | 64.2                                   | 152                           | 18.8                          | 0.58                          | 38            | 57            | 0.66                             | 64         |
| <i>cis</i> -[Ru(CN) <sub>2</sub> (bpy) <sub>2</sub> ]        | 11.2                                   | 32.5                                   | 62.5                          | 9.7                           | 1.8                           | 19            | 75            | 0.25                             | 146        |
| [Ru(phen) <sub>3</sub> ]I <sub>2</sub>                       | 8.9                                    | 53                                     | 380                           | 41                            | 12                            | 31            | 56            | 0.55                             | 153        |
| [Ru(4,7-Me <sub>2</sub> phen) <sub>3</sub> ]Cl <sub>2</sub>  | 8.5                                    | 30.4                                   | 271.2                         | 43.7                          | 3.06                          | 18            | 53            | 0.33                             | 147        |
| [Ru(4,7-Ph <sub>2</sub> phen) <sub>3</sub> ]Cl <sub>2</sub>  | 8.6                                    | 30.1                                   | 230                           | 22.9                          | 2.56                          | 18            | 53            | 0.33                             | 147        |
| [Ru(5,6-Me <sub>2</sub> phen) <sub>3</sub> ]Cl <sub>2</sub>  | 8.5                                    | 53.1                                   | 377                           | 45.0                          | 1.13                          | 32            | 53            | 0.6                              | 147        |

All the complexes studied show a similar splitting pattern in that  $\Delta_1$  is small ( $\approx 10 \text{ cm}^{-1}$ ) and almost constant for a given ligand system, whereas  $\Delta_2$  is larger (30 to  $100 \text{ cm}^{-1}$ ) and more susceptible to change in both ligand substituent and counter ion. The levels are ordered in decreasing lifetime, with the longer lived level lying lowest (15 to 300  $\mu\text{s}$ ), the second level being 5 to 10 times shorter-lived, and the highest level having a lifetime of the order of a microsecond.

These results have been used to develop an electron coupling model for CT transitions of these  $d^6$  complexes<sup>64,146-148</sup>, in which the lowest excited state produced by promotion of an electron from the  $d^6$  core to a  $\pi^*$ -antibonding orbital of the ligand system is split by weak electrostatic coupling to the strongly spin-orbit coupled ground state of the resultant  $d^5$  core. This model is in contrast to that employed by Fujita and Kobayashi<sup>149</sup> in which SOC causes finer splitting of the gross splittings produced by electrostatic forces.

For  $(nd)^6$  systems with  $D_3$ -symmetry<sup>148</sup>, CT transitions from the ground state ( $^1A_1$ ) to the  $\pi^*(a_2)$  or  $\pi^*(e)$  antibonding orbitals of the ligands leave the oxidised metal core in one of several possible states, the energies of which can be calculated by treating the system as a  $d^5$  LF problem. The final CT states are then calculated by introducing the perturbation of the optical electron in one of the  $\pi^*$  ligand orbitals into the Hamiltonian of the system. Consideration of the electrostatic interaction between the core and the excited electron produces

the final splitting of the CT state functions and energies of the excited  $d^6$  complex ion. The case of  $[\text{Ru}(\text{bpy})_3]^{2+}$  produces typical results for this treatment<sup>146</sup>. The promotion of the optical electron to the ligand system produces a  $d^5$  ruthenium(III) core, the ground state of which is the strongly spin-orbit coupled  $E'$  in the  $D_3^*$  double group. The optical electron with spin  $E'$  interacts with the lowest unoccupied orbitals of the ligand system, which transform as either  $a_2$  or  $e$  in  $D_3$ -symmetry, through their direct product. The final symmetries of the microstates are found by allowing these states to interact with the metal core by the direct product of the two systems. Reduction of this product in the  $D_3^*$ -symmetry group produces the final set of states  $\Gamma d\pi^*$ . The two possibilities are either

$$\Gamma d\pi^* = (E')_{\text{core}} \times (E' \times a_2)_{\text{ligand}} = A_1 + E + A_2$$

or

$$\Gamma d\pi^* = (E')_{\text{core}} \times (E' \times e)_{\text{ligand}} = A_1 + A_2 + E + E + E$$

The temperature data suggest that a three-level manifold is lowest, and this is assumed to be  $d + \pi^*(a_2)$ , so that the three emitting levels are  $A_1$  (forbidden),  $A_2$  ( $z$  allowed), and  $E$  ( $x, y$  allowed). The ordering of these levels is assumed to be  $A_1$  lowest, then  $E$ , then  $A_2$ , superficially, by comparison with the calculated lifetimes of the three states and, more rigorously, from a full mathematical treatment of the system<sup>148</sup>.

The splittings of these three states, which are dependent both on SOC and electrostatic interactions of

the optical electron on the ligand system with the  $d^5$  core, are given by the exchange interactions  $K(e^+, a_2)(1 - k_1^2)$  for the  $A_1 - E$  splitting and  $2k_1^2 K(a_1, a_2)$  for the  $A_1 - A_2$  splitting where  $k_1^2$  is related to spin-orbit coupling,  $K(e^+, a_2)$  is the exchange integral representing the non-classical electrostatic interaction between the promoted electron residing in the  $\pi^*(a_2)$  ligand orbital and an electron in a d-orbital of e symmetry and  $K(a_1, a_2)$  is the exchange interaction between the promoted electron and one occupying the d-orbital extending along the principal symmetry axis of the complex. Assuming a value of 0.85 for  $k_1^2$  <sup>148</sup> in both  $[\text{Ru}(\text{phen})_3]^{2+}$  and  $[\text{Ru}(\text{bpy})_3]^{2+}$  systems, the experimental splitting (Table 2.4) can be rationalised in terms of the two exchange integrals, which can be calculated from these splittings. The smaller splittings, and hence the exchange integrals, for the phenanthroline series can be attributed to greater delocalisation of the promoted electron by the larger  $\pi$ -structure of this ligand. It also seems reasonable that  $K(e^+, a_2)$  should be greater than  $K(a_1, a_2)$  since the e orbital of the metal core is in the x,y plane of the ligands whereas the  $a_1$  orbital is directed along the z-axis. The case of 4,7-substitution on the phenanthroline ring produces a remarkable effect, while 5,6-substitution gives no appreciable change (Table 2.4). This is explained by the  $\pi^*(a_2)$  being more sensitive to 4,7- than to 5,6-substitution, a result indicated by studies of the analogous iron(II) system <sup>150</sup>.

However, this study would also predict a marked effect for 4,4'-substitution into the bipyridyl ring, which is not observed. This implies that  $k_1^2$  may also vary as well as the two exchange integrals, which restricts the validity of the treatment to systems for which  $k_1^2$  has been determined experimentally from e.p.r. data for the oxidised complex. It is, however, apparent from the rate constants that the phenanthroline system is less susceptible to quenching, reflecting the enhanced rigidity of this ligand.

The excitation of the optical electron to produce a ruthenium(III) core might be thought to involve geometrical change, but only a small Stokes shift is observed for the luminescence, and the report of little change in bond lengths on complete oxidation of the ruthenium(II) system<sup>151</sup> indicates this not to be so.

Further experimental tests of this model have been hindered by the diffuseness of the peaks of the emission spectra even at 4.2 K ( $\approx 3,000 \text{ cm}^{-1}$ )<sup>147</sup>, but the doubly degenerate E(x,y) level should be split by the application of an external magnetic field along the principal symmetry axis. The application of a 75 kG field to  $[\text{Ru}(\text{bpy})_3]^{2+}$  in this direction at 1.65 K<sup>152</sup> produces a distinct change in the emission band shape with a concomitant decrease in the measured luminescence lifetime. The result is explained by the splitting of the E state into two components, which reduces the gap between the  $A_1$  and E levels so decreasing the lifetime. The study of circularly polarised luminescence

induced by an external magnetic field can also be explained by similar reasoning within the context of this model. Further evidence for this three-level model comes from a study of the lower-temperature luminescence spectra of  $[\text{Ru}(\text{bpy})_3]\text{SO}_4$  between 10 and 1.65 K<sup>152</sup> which shows the 'grow-in' of a new spectrum, red shifted by  $400\text{ cm}^{-1}$  at 1.65 K which is attributed to the  $A_1$  state, while analysis of the temperature dependence of the spectra yield an  $A_1$ -E splitting of  $10.2\text{ cm}^{-1}$  in good agreement with that obtained from lifetime measurements (Table 2.4).

This model, therefore, offers an excellent interpretation of the low-temperature luminescence properties of these ruthenium(II) systems. Crosby<sup>153</sup> further suggests that the variation of the splittings of these levels, and hence the measured lifetime of the complex, with ligand substitution as well as a total shift of the manifold to produce a shift in the emission spectrum, can be utilised to produce fine tuning of the emission properties of the system to specified requirements, coarse tuning being provided by total change of the ligand or central metal ion.

Recently, it was reported<sup>154</sup> that the deactivation of the luminescent state of  $[\text{Ru}(\text{bpy})_3]^{2+}$  and  $[\text{Ru}(\text{phen})_3]^{2+}$  proceeds through two energy-controlled pathways. For  $[\text{Ru}(\text{bpy})_3]^{2+}$  one of these is characterised by a relatively large activation energy ( $\sim 48\text{ kJ mol}^{-1}$ ) which dominates at  $T > 270\text{ K}$ , while the other route, which dominates at  $T < 130\text{ K}$  has an activation energy ( $\sim 2\text{ kJ mol}^{-1}$ ) in fluid media. This study provides

a link between  $100 \text{ cm}^{-1}$  splittings of the levels at 4 K and the room-temperature situation encountered by the solution photochemist.

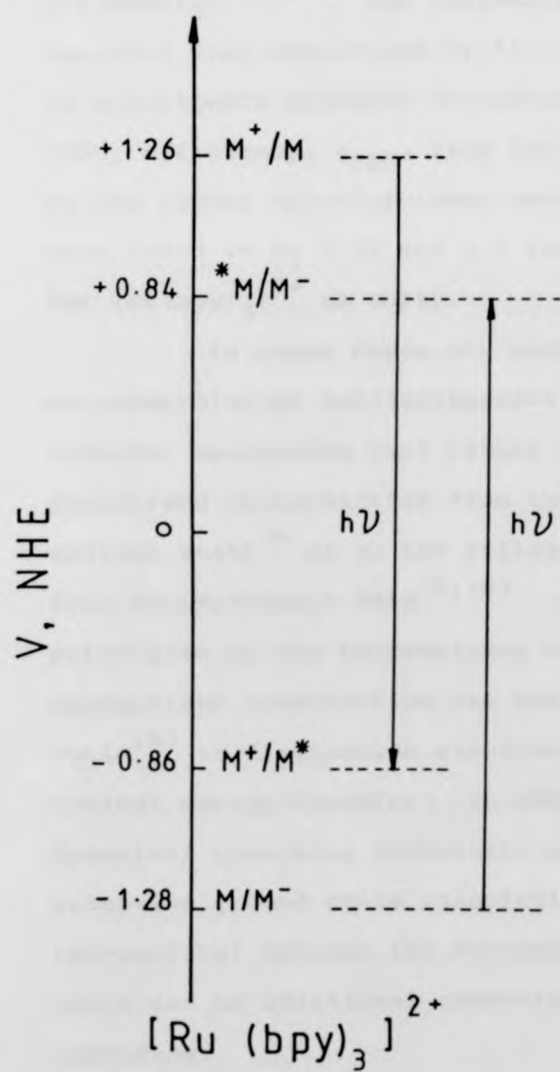
### 2.2.3 Photoredox Reactions and Quenching Mechanisms

The most interesting chemical aspect of excited  $[\text{Ru}(\text{bpy})_3]^{2+}$  is its rich photoredox chemistry. The excited state redox potentials estimated from corresponding ground state values and the excited state energy indicate that the luminescent excited state is a strong reductant as well as a good oxidant as illustrated in Figure 2.5<sup>48</sup>. This is due to an electron deficient  $d^5$  metal centre and an excess electron located in the ligand in the excited state. Studies have shown that  $*[\text{Ru}(\text{bpy})_3]^{2+}$  sensitises formation of triplet excited states in both inorganic and organic molecules by energy-transfer processes. As mentioned before, the electron-transfer quenching can be either oxidative or reductive. Thermodynamically, the ability of an excited state to be involved in energy-transfer processes is related to the 0-0 spectroscopic energy levels of the donor-acceptor pair; and the ability to be involved in electron-transfer processes is related to the excited state reduction and oxidation potentials.

In the case of the energy-transfer mechanism, the growth of transient luminescence corresponding to the acceptor excited state on a time scale concurrent with the decay of the Ru-complex excited state is

Figure 2.5 Oxidation-reduction potentials in  
aqueous solution of  $^*[\text{Ru}(\text{bpy})_3]^{2+}$   
(from reference 48).

$$E_{o-o} (M^* - M) = 2.12 \text{ eV}$$



valuable supporting evidence for this type of mechanism. This has been achieved for certain Cr(III) complexes, e.g.  $[\text{Cr}(\text{CN})_6]^{3-}$  43, 157-161,  $[\text{Cr}(\text{NCS})_6]^{3-}$  159, and  $[\text{Cr}(\text{phen})_3]^{3+}$  162. The luminescence of Cr(III) complexes has also been sensitised by  $*[\text{Ru}(\text{phen})_3]^{2+}$  and  $*[\text{Ru}(\text{bpy})_2(\text{CN})_2]$  160, in experiments designed to measure the inter-system crossing (ISC) efficiency,  $\phi_{\text{ISC}}$ , from the lowest spin-allowed to the lowest spin-forbidden excited states; the figures were found to be 0.65 and 1.0 respectively, taking  $\phi_{\text{ISC}}$  for  $[\text{Ru}(\text{bpy})_3]^{2+}$  as unity.

In cases where the quencher excited states are non-absorbing or non-luminescent, assignments to energy-transfer mechanisms rest either on the observation of sensitised photoreaction from the appropriate acceptor excited state<sup>39</sup> or on the ruling out of electron-transfer from thermodynamic data<sup>39,163</sup>. The fact that the redox potentials of the Ru-complexes can be 'tuned' by appropriate substitution has been exploited by Lin and Sutin<sup>164</sup> to distinguish electron-transfer processes as against energy-transfer. In addition to the above dynamical quenching processes, provided there is extensive ground state association (complexing or ion-pairing) between the Ru-complex and the quencher, there can be additional quenching modes *via* static quenching.

Demas and Adamson<sup>165</sup> reported sensitised photoaquation of  $[\text{PtCl}_4]^{2-}$  to occur by energy-transfer. In the absence of direct observation of emission from acceptor excited states, sensitised photodecomposition

valuable supporting evidence for this type of mechanism. This has been achieved for certain Cr(III) complexes, e.g.  $[\text{Cr}(\text{CN})_6]^{3-}$ <sup>43,157-161</sup>,  $[\text{Cr}(\text{NCS})_6]^{3-}$ <sup>159</sup>, and  $[\text{Cr}(\text{phen})_3]^{3+}$ <sup>162</sup>. The luminescence of Cr(III) complexes has also been sensitised by  $^*[\text{Ru}(\text{phen})_3]^{2+}$  and  $^*[\text{Ru}(\text{bpy})_2(\text{CN})_2]$ <sup>160</sup> in experiments designed to measure the inter-system crossing (ISC) efficiency,  $\phi_{\text{ISC}}$ , from the lowest spin-allowed to the lowest spin-forbidden excited states; the figures were found to be 0.65 and 1.0 respectively, taking  $\phi_{\text{ISC}}$  for  $[\text{Ru}(\text{bpy})_3]^{2+}$  as unity.

In cases where the quencher excited states are non-absorbing or non-luminescent, assignments to energy-transfer mechanisms rest either on the observation of sensitised photoreaction from the appropriate acceptor excited state<sup>39</sup> or on the ruling out of electron-transfer from thermodynamic data<sup>39,163</sup>. The fact that the redox potentials of the Ru-complexes can be 'tuned' by appropriate substitution has been exploited by Lin and Sutin<sup>164</sup> to distinguish electron-transfer processes as against energy-transfer. In addition to the above dynamical quenching processes, provided there is extensive ground state association (complexing or ion-pairing) between the Ru-complex and the quencher, there can be additional quenching modes *via* static quenching.

Demas and Adamson<sup>165</sup> reported sensitised photoaquation of  $[\text{PtCl}_4]^{2-}$  to occur by energy-transfer. In the absence of direct observation of emission from acceptor excited states, sensitised photodecomposition

or photoaquation is often taken as adequate evidence that the occurrence of the energy-transfer  $[\text{Cr}(\text{CN})_6]^{3-}$  quenching of  $^*[\text{Ru}(\text{bpy})_3]^{2+}$  is clearly due to direct energy-transfer, as has been demonstrated by the observation of sensitised phosphorescence from the chromium complex<sup>157,158,160,161,166</sup>. Sensitisation by the Ru-complex leads to populating of the lowest doublet state ( $^2E_g$ ). Luminescence quenching of  $^*[\text{Ru}(\text{bpy})_3]^{2+}$  by a number of organic molecules with established triplet-state energies, and the sensitisation of *cis-trans*-isomerisation of stilbene strongly indicates a simple triplet-triplet energy-transfer<sup>167</sup>.

Verification of the electron-transfer mechanism depends on wide systematic variation of the half-wave or redox potentials of one of the participants, as illustrated by the Rehm-Weller dependance<sup>50</sup> (Figure 2.6) for the reductive quenching of  $^*[\text{Ru}(\text{bpy})_3]^{2+}$  by aromatic amines and ethers<sup>168</sup>. In contrast, quenching of  $^*[\text{Ru}(\text{bpy})_3]^{2+}$  and  $^*[\text{Ru}(4,4\text{-dimethylbpy})]^{2+}$  by other *tris*-(bipyridyl)metal complexes features a perceptible Marcus-inverted region<sup>169</sup>, also suggestive of electron-transfer quenching. Ballardini *et al.*<sup>168</sup> have shown that the reorganisational parameter for quenching of  $^*[\text{Cr}(\text{bpy})_3]^{3+}$ ,  $^*[\text{Ru}(\text{bpy})_3]^{2+}$  and  $^*[\text{Ir}(5,6\text{-Me}_2\text{phen})_2\text{Cl}_2]^+$  by aromatic quenchers is small, suggesting that the self-exchange electron-transfer reactions of these excited states are as fast as the ground state self-exchange reactions<sup>169,177,178</sup>. This is in agreement with the small Stokes shift values<sup>28,58,59,179,180</sup>, which indicate

Figure 2.6 Plot of  $\log k_Q$  versus  $\Delta G^\circ$  for the electron-transfer quenching of  $^*[\text{Cr}(\text{bpy})_3]^{3+}$  ( $\blacktriangle, \triangle$ ),  $^*[\text{Ru}(\text{bpy})_3]^{2+}$  ( $\blacksquare$ ), and  $^*[\text{Ir}(5,6\text{-Me}_2\text{phen})_2\text{Cl}_2]^+$  ( $\bullet, \circ$ ) by aromatic quenchers (full points) and aliphatic amines (open points) (from reference 168).



that the excited states are quite similar in size, shape and solvation to the ground states.

Oxidative quenching has been established in a number of cases, e.g.  $[\text{Fe}(\text{H}_2\text{O})_6]^{3+}$ <sup>48</sup>,  $[\text{Cu}(\text{H}_2\text{O})_6]^{2+}$ <sup>170</sup>,  $[\text{Ru}(\text{NH}_3)_6]^{3+}$ <sup>171</sup>, paraquat<sup>172</sup>, and  $[\text{Fe}(\text{CN})_6]^{3-}$ <sup>173</sup>. Very typical of the kind of correlation found in these series is that between  $\log k_2$  and the (oxidative) quencher half-wave potential for (neutral) nitroaromatic quenchers shown in Figure 2.7<sup>174</sup>. The plot is linear at low  $E_{1/2}(\text{Q}/\text{Q}^-)$  values with a slope of  $-1/2.303 \text{ RT}$  and it approaches a plateau at higher  $E_{1/2}(\text{Q}/\text{Q}^-)$  according to the Rehm-Weller<sup>50</sup> approach. Analogous treatments of electron-transfer mechanisms by Marcus<sup>51,52</sup> and Hush<sup>175</sup>, however, predict that plots of  $\log k_q$  versus  $E_{1/2}$  should be parabolic with  $\log k_q$  decreasing as  $\Delta G$  becomes more negative (the so-called inverted Marcus region). No absolutely unequivocal evidence for a 'Marcus inverted' region has been adduced, and it has recently been found<sup>167</sup> that there is no fall-off even when  $\Delta G_{23}$  approaches 2.0 V, and only a plateau region is reached.

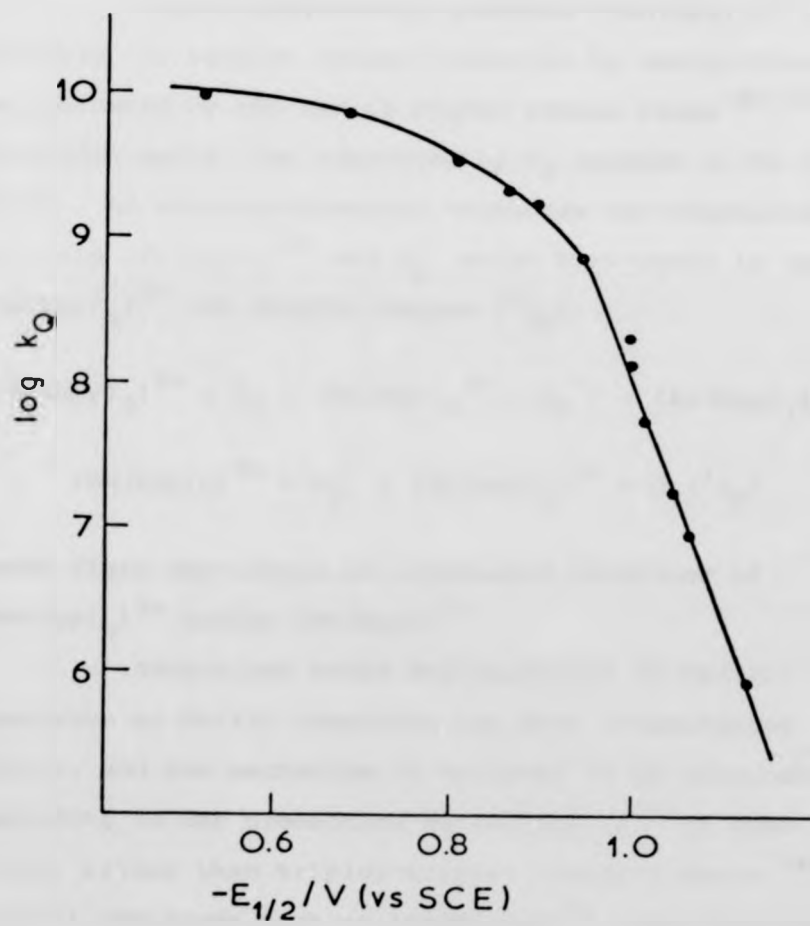
Quenching by ions such as  $\text{Tl}^{3+}$  and  $\text{S}_2\text{O}_8^{2-}$  leads to irreversible formation of  $[\text{Ru}(\text{bpy})_3]^{3+}$  with a quantum yield of 2.0<sup>177-179</sup>.



Overall:

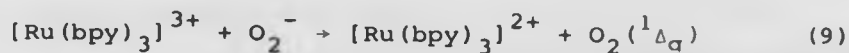


Figure 2.7 Plot of  $\log k_Q$  versus half-wave reduction potential of a series of nitroaromatic quenchers in the quenching of  $^*[\text{Ru}(\text{bpy})_3]^{2+}$  (from reference 174).



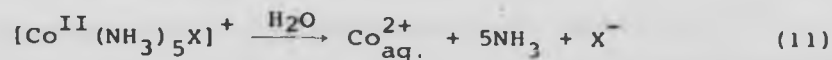
The higher quantum yield arises from thermal oxidation of a second molecule of  $[\text{Ru}(\text{bpy})_3]^{2+}$  by the photoreduced quencher molecule.

Oxygen effectively quenches  $^*[\text{Ru}(\text{bpy})_3]^{2+}$ , probably *via* singlet oxygen formation by energy-transfer, as indicated by the use of singlet oxygen traps<sup>180-182</sup>. In acidic media, the quenching by  $\text{O}_2$  appears to be complicated. An electron-transfer mechanism was suggested<sup>183</sup> to yield  $[\text{Ru}(\text{bpy})_3]^{3+}$  and  $\text{O}_2^-$  which back-react to give  $[\text{Ru}(\text{bpy})_3]^{2+}$  and singlet oxygen ( $^1\Delta_g$ ).



Laser flash photolysis of oxygenated solutions of  $[\text{Ru}(\text{bpy})_3]^{2+}$  yields  $[\text{Ru}(\text{bpy})_3]^{3+}$ .

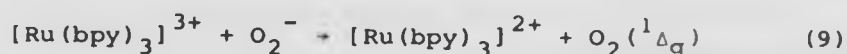
Sensitised redox decomposition of Co(III) complexes by Ru(II) complexes has been investigated in detail, and the mechanism is believed to be electron-transfer<sup>240</sup> according to the production of  $[\text{Ru}(\text{bpy})_3]^{3+}$  in good yield, rather than triplet-triplet energy-transfer<sup>94,95,184,185</sup>. Co(III) complexes such as  $[\text{Co}(\text{NH}_3)_5\text{X}]^{2+}$  upon photoreduction to the Co(II) state, readily decompose yielding the aquo complex ( $\text{X} = \text{Cl}^-$ ,  $\text{Br}^-$  or  $\text{I}^-$ ).



Reductive quenching of the luminescent excited

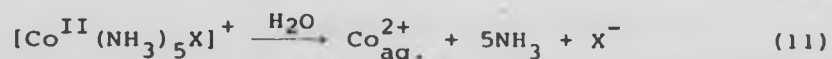
The higher quantum yield arises from thermal oxidation of a second molecule of  $[\text{Ru}(\text{bpy})_3]^{2+}$  by the photoreduced quencher molecule.

Oxygen effectively quenches  $^*[\text{Ru}(\text{bpy})_3]^{2+}$ , probably *via* singlet oxygen formation by energy-transfer, as indicated by the use of singlet oxygen traps<sup>180-182</sup>. In acidic media, the quenching by  $\text{O}_2$  appears to be complicated. An electron-transfer mechanism was suggested<sup>183</sup> to yield  $[\text{Ru}(\text{bpy})_3]^{3+}$  and  $\text{O}_2^-$  which back-react to give  $[\text{Ru}(\text{bpy})_3]^{2+}$  and singlet oxygen ( $^1\Delta_g$ ).



Laser flash photolysis of oxygenated solutions of  $[\text{Ru}(\text{bpy})_3]^{2+}$  yields  $[\text{Ru}(\text{bpy})_3]^{3+}$ .

Sensitised redox decomposition of Co(III) complexes by Ru(II) complexes has been investigated in detail, and the mechanism is believed to be electron-transfer<sup>240</sup> according to the production of  $[\text{Ru}(\text{bpy})_3]^{3+}$  in good yield, rather than triplet-triplet energy-transfer<sup>94,95,184,185</sup>. Co(III) complexes such as  $[\text{Co}(\text{NH}_3)_5\text{X}]^{2+}$  upon photoreduction to the Co(II) state, readily decompose yielding the aquo complex ( $\text{X} = \text{Cl}^-$ ,  $\text{Br}^-$  or  $\text{I}^-$ ).



Reductive quenching of the luminescent excited

state of  $[\text{Ru}(\text{bpy})_3]^{2+}$  by numerous organic molecules has been reported, including detailed studies of aromatic amines<sup>186,187</sup> and dithioanions<sup>188</sup>.



These reactions are carried out in non-aqueous media, because  $[\text{Ru}(\text{bpy})_3]^+$  is a strong reductant and reacts with various substances including water. Deronzier and Meyer<sup>188</sup> have attempted to build up  $[\text{Ru}(\text{bpy})_3]^+$  as a stable species during continuous photolysis without success, using irreversible reductants such as dithioanions. The slow back reaction between the disulphides and the reduced Ru(II) complex returns the system to its initial state. However, they have shown that by using multicomponent systems containing  $[\text{Ru}(\text{bpy})_3]^{2+}$ , dithiocarbonate and weak electron acceptors, it is possible to build up sufficient quantities of radical anions of these acceptors for spectroscopic analysis.

Recently Balzani *et al.*<sup>193</sup> reported the first example of ligand-centred luminescence from a Ru(II) complex. They found strong luminescence from  $[\text{Ru}(\text{i-biq})_3]^{2+}$ , where i-biq is 2,2'-bis-isoquinoline, at liquid nitrogen temperature which is characterised as a triplet state ligand-centred emission. Elfring and Crosby<sup>194</sup> studied the photoluminescence of a series of mixed-ligand chelates of Ru(II) of general formula  $[\text{Ru}(\text{bpy})_n(\text{NN})_{3-n}]^{2+}$ , where NN represents either 1,10-phenanthroline (phen) or substituted phen or substituted bpy; these showed a prominent visible luminescence and a strong temperature dependence of the lifetimes, which are in the range of few microseconds

state of  $[\text{Ru}(\text{bpy})_3]^{2+}$  by numerous organic molecules has been reported, including detailed studies of aromatic amines<sup>186,187</sup> and dithioanions<sup>188</sup>.



These reactions are carried out in non-aqueous media, because  $[\text{Ru}(\text{bpy})_3]^+$  is a strong reductant and reacts with various substances including water. Deronzier and Meyer<sup>188</sup> have attempted to build up  $[\text{Ru}(\text{bpy})_3]^+$  as a stable species during continuous photolysis without success, using irreversible reductants such as dithioanions. The slow back reaction between the disulphides and the reduced Ru(II) complex returns the system to its initial state. However, they have shown that by using multicomponent systems containing  $[\text{Ru}(\text{bpy})_3]^{2+}$ , dithiocarbonate and weak electron acceptors, it is possible to build up sufficient quantities of radical anions of these acceptors for spectroscopic analysis.

Recently Balzani *et al.*<sup>193</sup> reported the first example of ligand-centred luminescence from a Ru(II) complex. They found strong luminescence from  $[\text{Ru}(\text{i-biq})_3]^{2+}$ , where i-biq is 2,2'-bis-isoquinoline, at liquid nitrogen temperature which is characterised as a triplet state ligand-centred emission. Elfring and Crosby<sup>194</sup> studied the photoluminescence of a series of mixed-ligand chelates of Ru(II) of general formula  $[\text{Ru}(\text{bpy})_n(\text{NN})_{3-n}]^{2+}$ , where NN represents either 1,10-phenanthroline (phen) or substituted phen or substituted bpy; these showed a prominent visible luminescence and a strong temperature dependence of the lifetimes, which are in the range of few microseconds

at 77 K, but up to over 100 microseconds as the temperature lowered to 4.2 K. Emission spectra and luminescence lifetimes have also been reported for the mixed-ligand 1,10-phenanthroline/2-(2-pyridyl)quinoline complexes of ruthenium(II)<sup>195</sup>. Charge-transfer absorption and emission states appear to be located on the individual ligands and there is evidence that energy-transfer occurs from the initially excited phenanthroline centred state to the emitting pyridylquinoline-centred state. Kinnaird and Whitten<sup>196</sup> reported that there are ground-state complexes between  $[\text{Ru}(\text{bpy})_2(\text{CN})_2]$  and Ag(I); one of these complexes is strongly luminescent which indicates that intramolecular redox reactions are not an important route for non-radiative decay.

CHAPTER 3  
EXPERIMENTAL

### 3.1 INSTRUMENTATION

#### 3.1.1 Luminescence Intensities and Spectra

The measurements were carried out with a Perkin Elmer MPF-3 spectrofluorimeter, fitted with a Hamamatsu R666S photomultiplier tube for  $\lambda$  between 500-1000 nm but with a RCA IP28 photomultiplier tube for  $\lambda$  up to 600 nm. The dark current produced by the red-sensitive photomultiplier was not excessive, and cooling was not considered necessary. This model, which uses right-angle illumination, is a double-beam instrument and consequently the spectra are automatically corrected for lamp intensity fluctuation by feeding the reference lamp signal to the sliding contact (pen) so that the voltage changed caused by lamp fluctuation on both the slide wire and contact are balanced, which results in a constant pen position, as the pen servo-control monitoring the difference between these two voltages will sense no voltage difference. The spectra were not corrected, either for photomultiplier wavelength-response or the transmittance and bandwidth of the analysing monochromator, although a reasonably 'flat' photomultiplier response was ensured throughout the relevant region of the emission spectra.

The instrument employs a 150 W xenon lamp as the excitation source, the emitted light from which is passed through an excitation monochromator, allowing an excitation wavelength of between 220 and 800 nm to be chosen with a bandwidth of between 1 and 40 nm. The analysing monochromator is

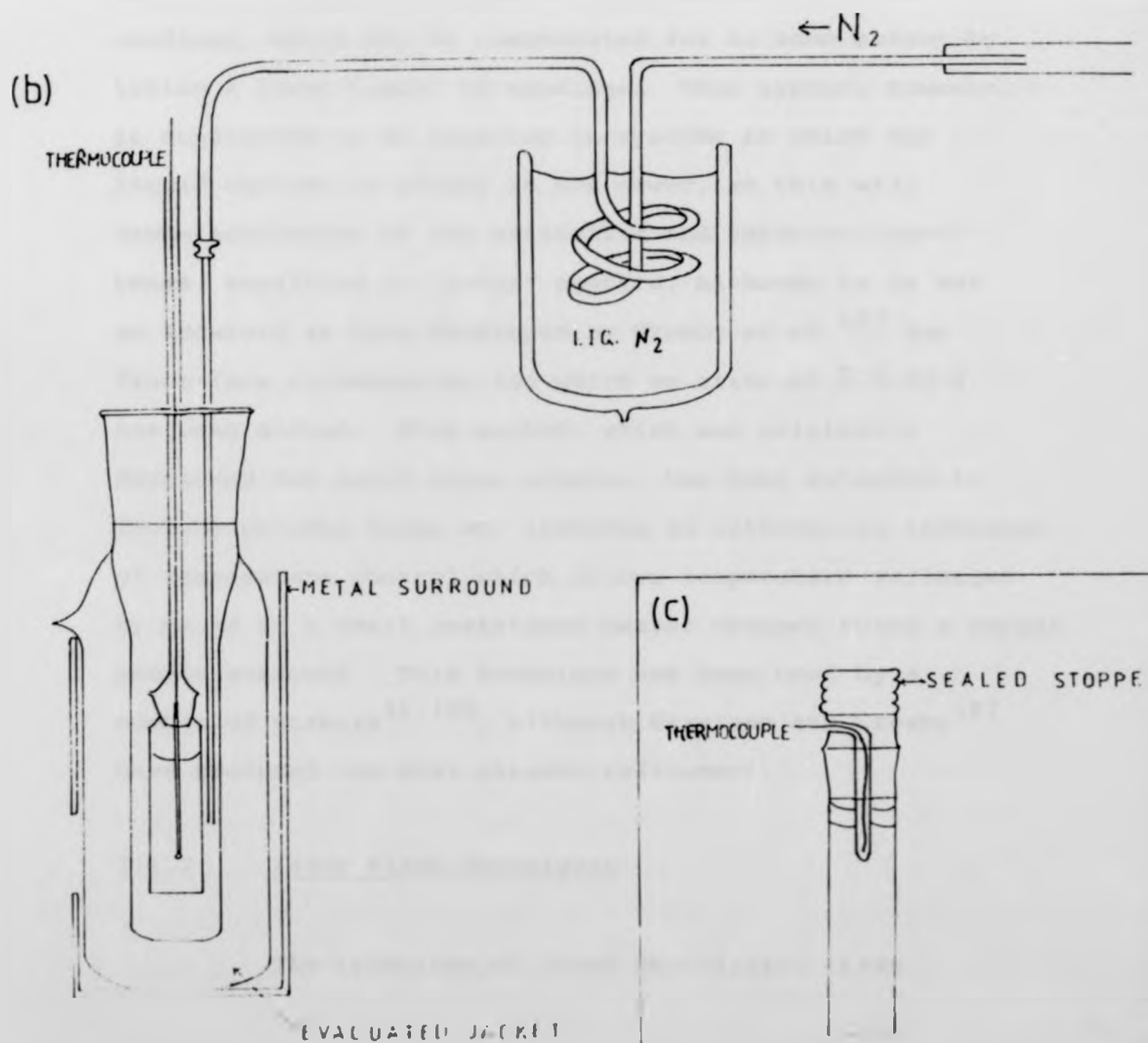
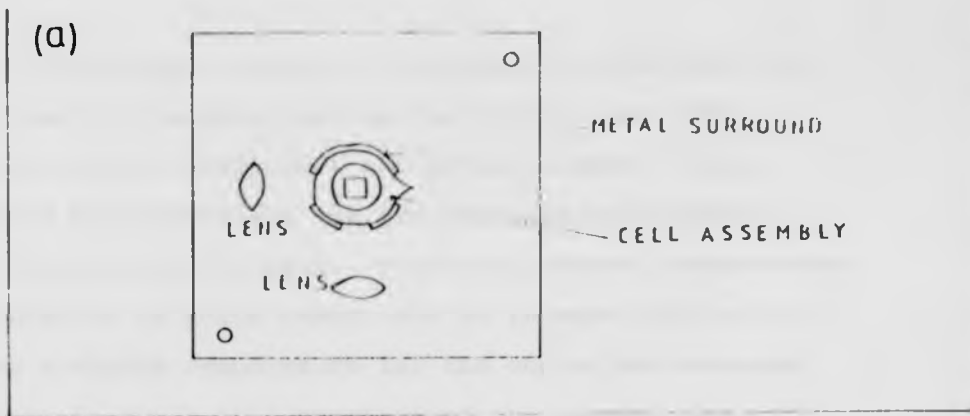
identical to its excitation counterpart, and activates a photomultiplier whose amplified signal is fed to a chart recorder to give the luminescence spectrum, as described above. The emission or excitation wavelengths can be scanned at preset speeds by means of a motor to give either emission or excitation spectra, depending upon whether the emission or excitation wavelength control is engaged. The right angle-illumination mode of the instrument reduces effects from scattered light, sample cell luminescence and the portion of the excitation beam which is transmitted, and gives most accurate measurements when weakly-absorbing solutions are used which reduce inner filter effects caused by re-absorption of the luminescence to give 'front-facing'. For the luminescence spectra in polymer films, the films were mounted across the diagonal of the sample cell to give effectively front-face illumination.

A low-temperature cell compartment has been designed to replace the existing cell compartment of the spectrofluorimeter, and is shown in Figure 3.1. The sample cell is placed in an unsilvered quartz dewar which is surrounded by a metal shroud, with appropriate spaces to allow entry of the excitation beam and exit of the emission, which acts as a safeguard against implosion of the dewar, which is cooled by passage of nitrogen through a stainless steel coil immersed in liquid nitrogen, and heated by placing a water bath underneath the coil. Stainless steel tubing was chosen in preference to copper as the latter was found to produce contamination of the



Figure 3.1 Sample cell arrangements used for ambient and low-temperature luminescence measurements.

- (a) Aerial view of low-temperature sample cell holder insert for the Perkin-Elmer MPF-3 spectrofluorimeter.
- (b) Low-temperature sample cell and cooling arrangement.
- (c) Room-temperature sample cell.

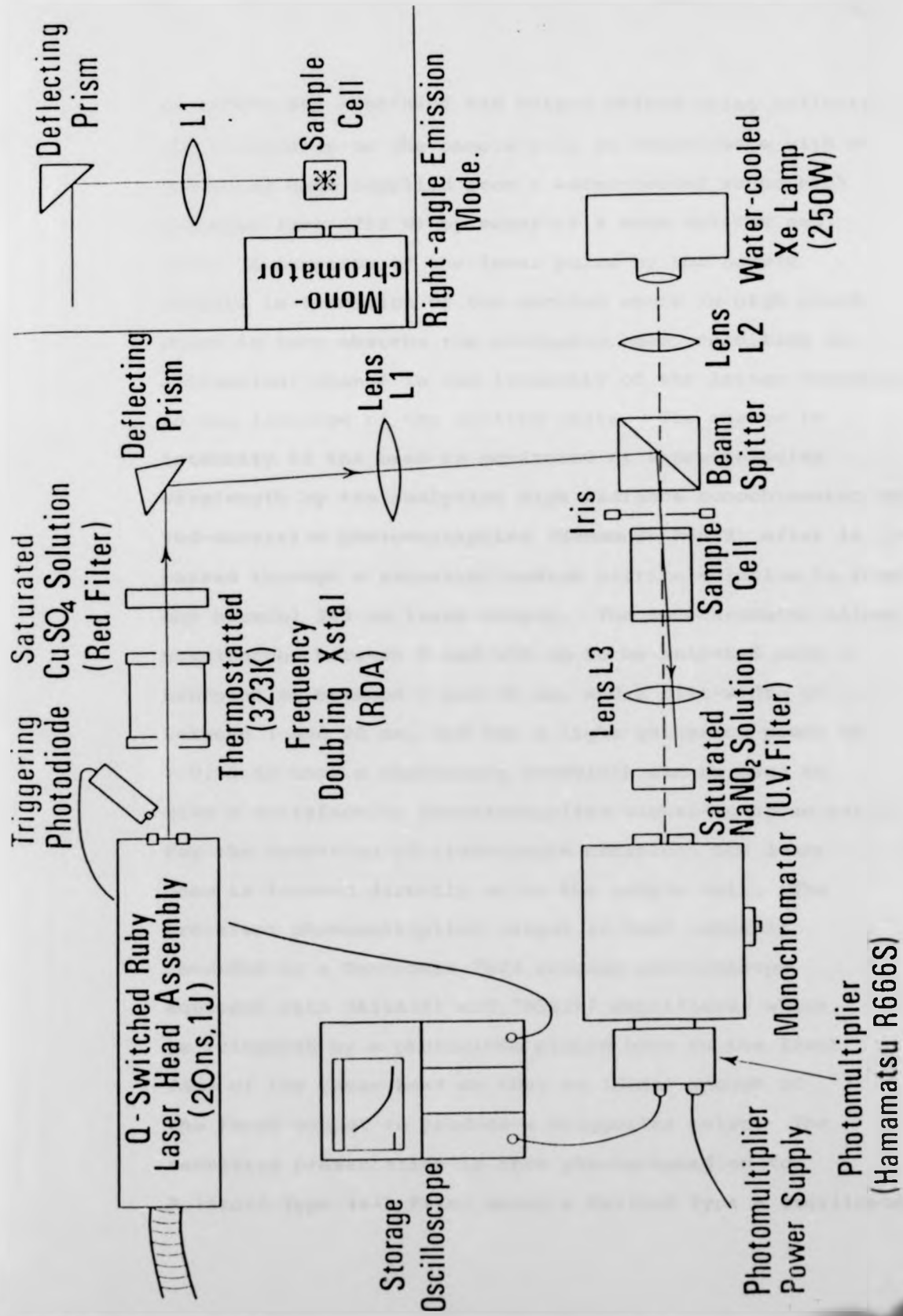


dewar on prolonged heating. A previous version had two coils, one for heating and one for cooling, but this was found to be inefficient and better control could be gained by controlling the gas pressure and position of the dewar over the coil. With this system, temperature equilibration is quite rapid, but it is more difficult to keep a stable temperature for the one or two minutes necessary to run a full spectrum of the sample, and an error of up to  $\pm 2$  K has to be tolerated for some readings, which may be compensated for to some extent by taking a large number of readings. This system, however, is considered to be superior to systems in which the liquid coolant is placed in the dewar, as this will cause scattering of the excitation and emission light beams, resulting in 'noisy' spectra, although it is not as accurate as that developed by Crosby *et al.*<sup>197</sup> for front-face illumination for which an error of  $\pm 0.02$  K has been quoted. This method, which was originally developed for solid state samples, has been extended to include polymer films and involves an alternative technique of temperature control which allows temperature variation by means of a small resistance heater wrapped round a copper sample surround. This technique has been used by a number of workers<sup>46,198</sup>, although Harrigan and Crosby<sup>197</sup> have produced the most elegant refinement.

### 3.1.2 Laser Flash Photolysis

The technique of flash photolysis, first

reported by Norrish and Porter in 1949<sup>199</sup>, has had a profound effect on the study of fast reactions. The technique, which is not limited to luminescent compounds, but can be applied to any molecule which absorbs light and is therefore almost universal in its application, is essentially a relaxation method in which an initial high energy pulse of light produces a momentarily large number of molecules in their excited state which absorb a following analysing pulse or 'spectroflash' to give an excited state absorption (ESA) spectrum which can either be recorded on a spectrograph or as time-dependent kinetics at a pre-selected monitoring wavelength by attaching the photomultiplier detector output to an oscilloscope (spectrophotometric method). In this original form, the main limitation of the technique is the duration of the high energy lamp pulse, which was overcome by the production of a laser flash photolysis assembly in 1967<sup>200</sup> allowing the possibility of studying events in the nanosecond time domain. Further techniques were later devised in order to monitor rate processes with a time resolution of the order of picoseconds<sup>201</sup>. The original assembly for the nanosecond set-up was essentially the same as the apparatus used for this work (supplied by Applied Photophysics Ltd.), and is depicted in Figure 3.2. The red output (694.3 nm, ~ 1 J/pulse) of the Q-switched ruby laser pulse is frequency doubled by an RDA (rubidium dihydrogen arsenate) crystal, thermostated at 323 K, to give an ~ 75 mJ ultraviolet (347.1 nm) output which is first passed through a saturated copper sulphate solution



LASER FLASH PHOTOLYSIS ASSEMBLY

to remove any remaining red output before being deflected and focused on to the sample cell in coincidence with an analysing beam supplied from a water-cooled xenon high pressure lamp (250 W) by means of a beam splitter and iris. Absorption of the laser pulse by the sample results in formation of the excited state in high yield which in turn absorbs the analysing beam, resulting in a transient change in the intensity of the latter corresponding to the lifetime of the excited state. The change in intensity of the beam is monitored at a pre-selected wavelength by the analysing high radiance monochromator and red-sensitive photomultiplier (Hamamatsu R666S) after it has passed through a saturated sodium nitrite solution to remove any harmful 347 nm laser output. The monochromator allows wavelengths between 0 and 999 nm to be selected with a bandpass of between 1 and 20 nm, and a slit-width of between 1 and 20 nm, and has a light gathering power of  $> 0.25$  so that a reasonable bandwidth can be used to give a satisfactory photomultiplier signal-to-noise ratio. For the detection of right-angle emission, the laser beam is focused directly on to the sample cell. The transient photomultiplier output in both cases is recorded on a Tektronix 7623 storage oscilloscope, equipped with 7A15A(Y) and 7B50(X) amplifiers, which is triggered by a photodiode placed near to the front face of the laser head so that it 'sees' enough of the laser output to produce a triggering pulse. The resulting presentation is then photographed on to Polaroid Type 46-L Film, using a Telford Type A oscilloscope

camera, ready for analysis after enlargement and digitising.

This technique, therefore, has essentially replaced the conventional lamp source with a laser to give a high-intensity coherent pulse of very short duration. It should be noted, however, that it is not the laser itself, which can be simply viewed as an optical amplifier inside a conventional Fabry-Perot etalon, which is responsible for this property, but the Q-switching of the laser action which results in the 'giant' pulse. This statement can be understood by considering the nature of the laser action. The laser head consists of a partially reflecting sapphire front window and a rear total internally reflecting prism which acts as an optical resonator (Fabry-Perot etalon). In between these is placed a reflecting cavity containing a ruby rod (6" x  $\frac{1}{2}$ ") which is in line with these mirrors and a Wingent (or more recently, Nobelight) F<sub>12-120</sub> flash tube lying in parallel above the rod. The whole cavity is flooded with circulating water refrigerated at 288 K to allow for good laser action. When the flash-lamp is fired by discharging a bank of capacitors (680  $\mu$ F) through it (2 kV plus an initial 5 kV triggering pulse), the resultant light is absorbed by chromium ions in the rod to excite a large number of molecules into the <sup>4</sup>F states from which they spontaneously decay into the <sup>2</sup>E state and thence gradually phosphoresce back to the ground state. The component of this phosphorescence, travelling normal to the mirrors of the optical resonator, is reflected between the two mirrors and amplified by stimulated emission from the <sup>2</sup>E state on each passage

through the laser rod, losing a fraction  $(1-R)$  where  $R$  is the reflectivity of the front face mirror, during each oscillation. Laser action occurs when amplification and feedback are greater than the light losses within the cavity and a series of high intensity spikes of random intensity and separation are produced, lasting almost the duration of the flash ( $\sim 1.5$  ms) caused by the continuous feedback to the  ${}^2E$  state throughout the lifetime of the flashlamp. There is, therefore, an obvious need to reduce the number of pulses to make the laser useful, and this is achieved by using a Q-switch where Q refers to the quality factor of the optical resonator. The purpose of the Q-switch is to lower this factor so that no oscillation occurs during the pumping of the rod so that the gain (population inversion) builds up to a very high value. Once this reaches its peak, the Q-switch is opened and the gain per pass in the laser rod is now extremely high, resulting in a rapid build-up of the oscillation with a simultaneous rapid exhaustion of the population inversion to produce the required high-intensity, sharp 'spike' which releases a  $(1-R)$  fraction of intensity on each oscillation to give a lifetime of  $\sim 20$  ns.

In this work a chemical Q-switch, consisting of a 1 cm cylindrical cell containing a reversibly bleachable dye (vanadyl phthalocyanine) in nitrobenzene, is placed between the reflector cavity and the rear mirror which is misaligned with the reflector cavity to reduce oscillation caused by reflection from the front face of the Q-switch. The concentration of the

Q-switch is varied until an optimum pulse is produced (usually  $\sim 0.3$  optical density at 694 nm), a weak solution producing 'double pulsing' and an over-concentrated solution resulting in reduced efficiency and eventually loss of laser action.

Frequency doubling, as mentioned earlier, was produced by an RDA (rubidium dihydrogen arsenate) crystal thermostatted at 323 K and supplied by JK Lasers Ltd. This replaced the original ADP (ammonium dihydrogen phosphate) crystal, and gives a ten-fold improvement in ultra-violet output as well as the need for less critical adjustment, although the hygroscopic nature of the crystal makes it more susceptible to damage. Further changes to the original system have included the replacement of the deflecting mirror by a deflecting prism, which avoids the degradation of the mirror coating by the laser pulse and the change of the 347.1 nm filter in front of the monochromator which was found to luminesce by a saturated sodium nitrite solution in a 1 cm cylindrical cell which filters 347.1 nm light. As indicated previously, the apparatus can be used to give either ESA or emission measurements, and the method used for each case is given below. Very recently the output of the triggering photodiode has been split between the Tektronix oscilloscope and a second oscilloscope (Iwatsu Model DMS-510) which exhibits a profile of the structure and intensity of the laser pulse, enabling correction for fluctuations in pulse amplitude or giving warning of multiple pulsing.

(i) ESA Measurements

As mentioned before, the transient absorption is detected by change in the analysing beam intensity. It is, therefore, imperative to ensure a stable power supply (in this case an iREM E<sub>2</sub>-X20P) so that fluctuations do not occur over the lifetime of the transient. Similarly, to observe weak, short-lived transients, an intense beam will be needed to reduce the effects of scattered light and provide an adequate photocathode current, and to facilitate this, a pulsing unit is connected to the xenon arc lamp which increases the lamp intensity up to a hundred-fold, depending on the wavelength, for approximately 1.5 ms. The pulse is flat to within 5% for 400  $\mu$ s, and is better than 1% over 100  $\mu$ s. To ensure that the transient absorption is recorded over the flat part of the pulse, the triggering of the pulsing unit and laser are synchronised.

A further restriction on the measurement of weakly absorbing transients is the need to restrict  $I_0$  (initial intensity of the analysing light) so that it produces a full-scale deflection on the oscilloscope screen in order that the value of  $I_0$  can be measured in terms of applied photomultiplier voltage. As the transient intensity is a constant percentage of  $I_0$  for a given time, then one way of enlarging the transient signal to allow more accurate measurements would be to increase  $I_0$ . This has been achieved by off-setting the zero-light level off the 'top' of the oscilloscope screen, which means that the 'light off'

trace will no longer appear on the screen. However, using an 'off-set box' which gives a precalibrated output voltage which when applied to the Y amplifier of the oscilloscope, in place of the photomultiplier output, allows the 'light-off' level to be brought back on to the screen. This value can now be used to give the 'apparent'  $I_0$  value and by addition of the applied voltage from the 'off-set box', the true value of  $I_0$  in mV can be calculated. The circuit diagram of the 'off-set box' is shown in Figure 3.2.

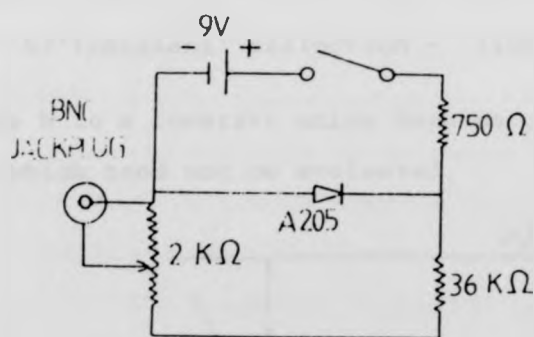


Fig. 3.2 Circuit diagram for 'off-set box' used in recording weak transient absorptions.

Transient absorption spectra were recorded by measuring the initial intensity as a function of monitoring wavelength, each reading being taken several times to allow for fluctuation in the intensity of the laser pulse. For kinetic studies it is further assumed that Beer's law is obeyed. Under these conditions the

optical density at an instant  $t$ , O.D., can be calculated from the transient absorption decay curve (see Figure 3.3) as

$$\text{O.D.} = \log I_0/I_t = \log X_0/X = \epsilon_{\lambda} c_t l \quad (3.1)$$

so that relative or absolute concentrations can be determined as a function of time, and the order and rate of the transient reactions determined. In equation 3.1  $I_0$  and  $I_t$  (transmitted intensity at time  $t$ ) are related to the oscilloscope deflections through

$$I_0 = k(\text{'light-on' deflection} - \text{'light-off' deflection}) = kX_0$$

$$I_t = k(\text{'transient' deflection} - \text{'light-off' deflection}) = kX_t$$

where  $k$  is a constant which depends on detector sensitivity and which need not be evaluated.

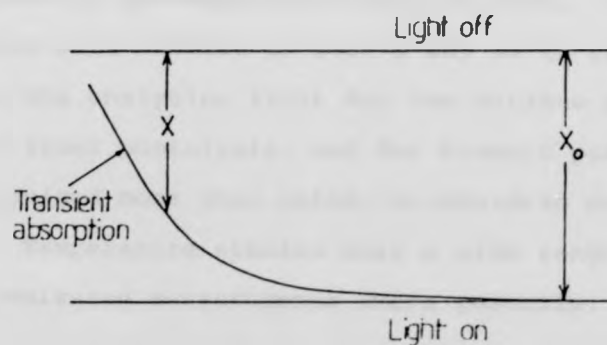


Fig. 3.3 Representation of a transient absorption decay curve.

Frequent checks for photodecomposition were made by determining the lifetime and intensity of the transient absorption at a wavelength chosen at the beginning of the experiment, and when photodecomposition

was suspected, the ground state absorption spectrum was recorded to see whether any change had occurred. This was done automatically at the end of the experiment to confirm no change in the spectrum. Photodecomposition of the sample is always a danger when using high-intensity light sources, and checks were made in all experiments both in emission and absorption modes of the reproducibility of the results and, where anomalies were found, absorption spectra were run in order to test for photodecomposition.

The sample cell used for normal room temperature work consisted of a 2 cm cylindrical cell ( $5 \text{ cm}^3$  volume) with optical faces at each end. All samples were prepared immediately before use and deoxygenated by bubbling the solution with high purity argon (B.O.C. 99.999%) for 20 minutes, special care being taken to avoid evaporation of the solvent by pre-saturation with solvent. On the other hand, samples were handled in such a way as to restrict exposure to the analysing light for the minimum possible time before laser photolysis, and for kinetic purposes were never pulsed more than twice, to minimise secondary reactions. Temperature studies over a wide range were done using emission measurements where possible.

(ii) Emission Measurements

These measurements are easier to make than the ESA measurements, requiring minimal critical 'tuning', and optically pure glasses are unnecessary.

The sample cells used for room-temperature measurement were ordinary quartz fluorimetry cells,

and an analogous arrangement to that used for the spectrofluorimeter being adopted for low-temperature work. However, the dewar was constructed of 'pyrex' rather than quartz as the latter was found to luminesce and was inessential for this work as 'pyrex' gives good transmission at 347 nm and above (> 80%). Similarly, the quartz cell insert was replaced by cheaper pyrex cylinder tubes of  $\sim 1$  cm diameter which reduced the probability of the cell shattering when using solvents which give poor glasses and which expand on freezing. The same cooling system was adopted as used for the spectrofluorimeter. As emission (and ESA) measurements are taken over a very short time period (usually < 1 ms) then a greater accuracy in the measured temperature ( $\pm 0.2$  K) should be gained compared with the fluorimeter.

As indicated, the results of all the laser experiments were photographed on to Polaroid film which records the results as transparencies, which are then fixed using a 'Polaroid dippit' containing a fixing solution of  $\text{SnCl}_4$  ( $0.03 \text{ mol dm}^{-3}$ ) in isopropanol. The negatives were then enlarged ( $\times 2$ ) on to graph paper, and the transient curves digitised by hand ready for analysis.

### 3.1.3 The Optical Bench

The optical bench (Figure 3.4) consisted of a suitably housed high-pressure mercury vapour lamp, Wotan type HBO 200 W, connected to a power supply unit type S.C.T. 104 (supplied by K.S.M. Electronics Ltd., Potters Bar, Hertfordshire), giving a stabilised current to within  $\pm 0.1\%$ . Two quartz plano-convex lenses were positioned directly in front of the lamp to give a parallel light beam which was focused by a third quartz lens. Narrow band Balzer metal interference filters were used to obtain monochromatic light of an appropriate wavelength. Solutions were photolysed in a cylindrical quartz cell which measured 5 cm (depth) by 2.5 cm (diameter) and to its sidearm (at  $90^\circ$ ) was glass-blown a 1 cm quartz spectrophotometer cell, enabling absorbance and spectral measurements to be performed easily as photolysis proceeded. The sidearm terminated in a Teflon tap of 1 mm bore enabling the insertion of  $< 1$  mm diameter Teflon tubing for argon bubbling of the solution prior to photolysis. The cell was placed in the water bath through which tap water was continually circulated to maintain a constant temperature.

Quantum yields are given in terms of reactant disappearance which may be defined as:

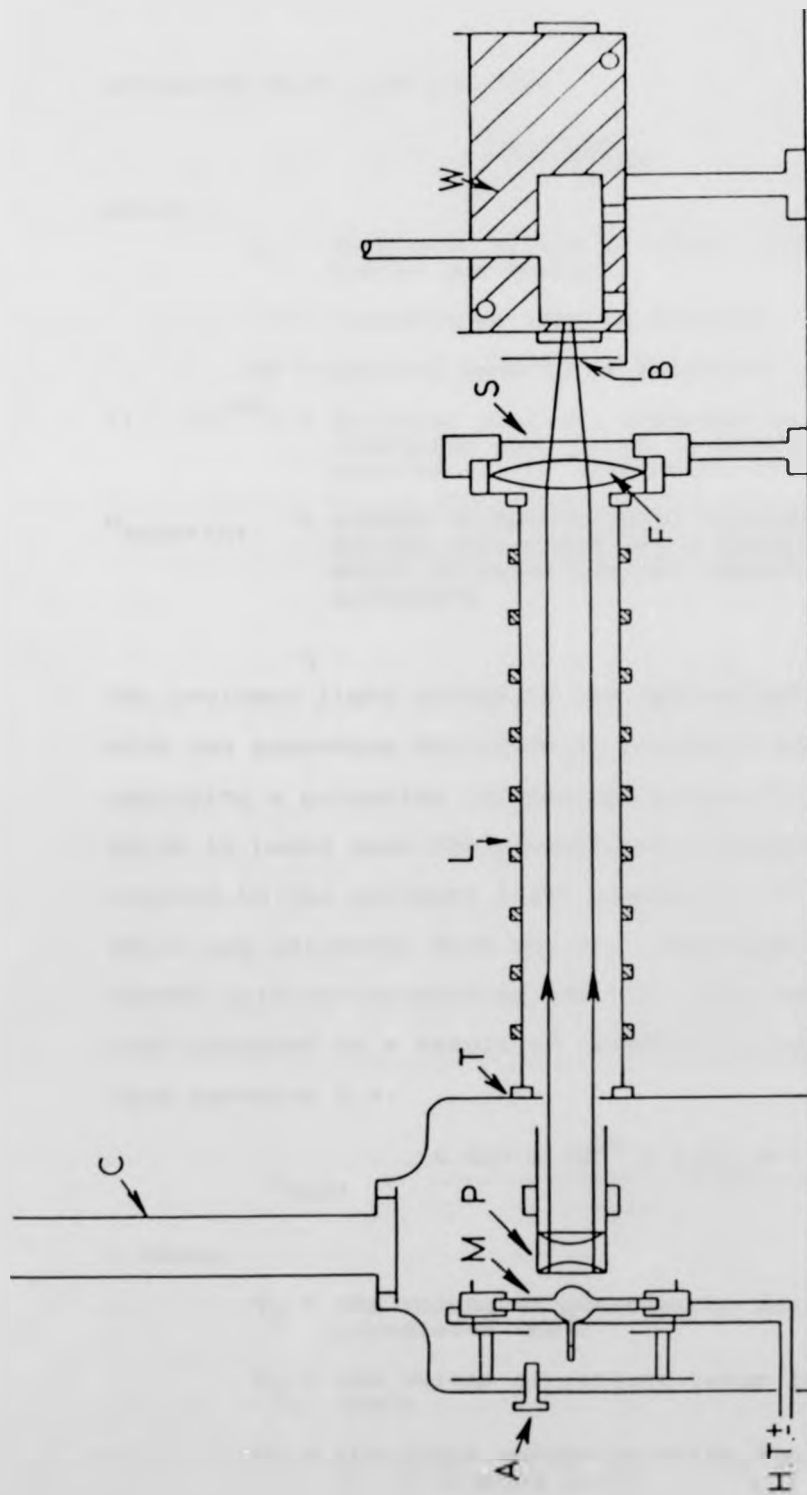
$$\phi = \frac{\text{number of molecules undergoing the particular process concerned}}{\text{number of quanta absorbed}} \quad (3.2)$$

If the number of molecules,  $n$ , undergoing a particular process is known, then the quantum yield can be

Figure 3.4 The optical bench.

Key:

- (C) Cooling tower
- (M) Mercury vapour lamp
- (A) Adjustment screws (for aligning lamp)
- (P) Quartz plano-convex lenses
- (F) Quartz focusing lenses
- (S) Shutter
- (B) Balzer filter
- (W) Water bath
- (L) Light shield
- (T) Teflon seals



estimated from equation 3.3.

$$\phi = \frac{n_{\text{reactant}}}{I_0 t (1 - 10^{-OD})} \quad (3.3)$$

where

$I_0$  = intensity of the incident light, in quanta per second

$t$  = irradiation time in seconds

OD = optical density of solution

$(1 - 10^{-OD})$  = fraction of light absorbed by the reactant (assuming that there is only one absorbing species at the wavelength of investigation)

$n_{\text{reactant}}$  = number of molecules of reactant destroyed during photolysis for a period sufficiently short to leave the net absorbance virtually unchanged

The incident light intensity was determined in accordance with the procedure described by Hatchard and Parker<sup>202</sup> employing a potassium trisoxalatoferate(III) actinometer, which is based upon the proportional release (with respect to the incident light intensity) of  $\text{Fe}^{2+}$  ions, which are estimated from the high absorbance of the easily formed 1,10-phenanthroline complex. The number of  $\text{Fe}^{2+}$  ions produced as a result of irradiation may be calculated from equation 3.4.

$$n_{\text{Fe}^{2+}} = \frac{6.023 \times 10^{20} \times V_1 V_3 \times \text{O.D.}}{V_2 l \epsilon} \quad (3.4)$$

where

$V_1$  = the volume of actinometer solution irradiated ( $\text{cm}^3$ )

$V_2$  = the volume of aliquot taken for analysis ( $\text{cm}^3$ )

$V_3$  = the final volume to which the aliquot  $V_2$  is diluted ( $\text{cm}^3$ )

O.D. = the measured optical density of the solution at 510 nm after addition of 0.1% 1,10-phenanthroline and buffer.

$\epsilon$  = the experimental value of the molar extinction coefficient of the  $\text{Fe}^{2+}$  complex as determined from the slope of a calibration plot (i.e.  $1 \times 10^4 \text{ M}^{-1} \text{ cm}^{-1}$ )

#### 3.1.4 Other Instrumentation Used

Visible and ultraviolet absorption measurements were made on Perkin-Elmer 552 and Shimadzu 365 spectrophotometers, and optical measurements in single wavelength work were performed mostly on a Unicam SP500 spectrophotometer.  $^1\text{H}$  n.m.r. spectra were taken on a Perkin-Elmer model R-34 220 MHz spectrometer. The small amount of pulse radiolysis work was carried out at the Cookridge Radiation Research Centre, Leeds University, using the systems of pulsed electron irradiation, sample preparation and data analysis described previously<sup>212</sup>. The lifetime measurements for  $[\text{Ru}(\text{bpy})_2\text{acac}]^+$  and  $[\text{Ru}(\text{bpy})_2\text{Cl}_2]$  complexes were performed at Preston Polytechnic by means of time-correlated single photon counting with special detectors for red emission. The potentials for the Ru(II)/Ru(III) couples were measured by Dr. N. G. Connelly at the University of Bristol. All potentials were measured *versus* the saturated calomel electrode using  $[\text{NBu}^n_4][\text{PF}_6]$  as base electrolyte. The measurements were carried by cyclic voltammetry at a platinum wire electrode, and were checked after every experiment against a ferrocene/ferricinium ion secondary electrode.

### 3.2 SAMPLE PREPARATION

For work over a wide temperature range, a good glassing solvent is required. A number of these are known, and the most commonly used are organic glasses of ethanol:methanol mixtures, EPA (ethanol:isopentane:ether 2:5:5) and methanol:water:ethylene glycol mixtures, a comprehensive list being given in the excellent monograph by Murov<sup>203</sup>. However, for this work a single solvent medium is preferred as this is more meaningful in discussing environmental effects, removing the complicating possibility of preferential solvation by one component of the mixed solvent medium. Relatively few of these are known, and aqueous 9 M lithium chloride has been the one extensively used in this work to give an extended temperature range to the aqueous environment while MTHF (2-methyltetrahydrofuran) has been used as a good organic glass, although the selective use of solvents obviously depends upon the solubility of the sample.

Most of the samples used were sensitive to oxygen quenching and required deoxygenation before use. This was achieved by passing high purity argon gas (B.O.C. 99.999%) through them for 15-20 minutes, special care being taken to avoid evaporation of the solvent by pre-saturation with the solvent. This method of 'degassing' was used because of the ease with which it can be implemented, and it was found to be just as effective as the other popular freeze-pump-thaw method in which the sample is placed on a

vacuum line, frozen, and pumped to remove the air from the line. The sample is then allowed to thaw and re-equilibrate its residual oxygen with the dead-space. The procedure is then repeated two or three times to ensure all the oxygen is removed. This method was used in the determination of luminescence lifetimes by time-correlated single photon counting (at Preston Polytechnic). To prevent oxygen re-dissolving into the solution during experiments, the samples were either sealed or a constant flow of argon was passed over the top of the sample.

A more recent innovation has been the use of polymer matrices<sup>204</sup> which give the distinct advantages of (i) optical clarity, (ii) the possibility of investigation of the luminescence over a much wider temperature range, (iii) frequent absence of the complications caused by transition through the glassing point of the solvent, (iv) strengthening of the luminescence intensity in many cases due to restriction of diffusional deactivation modes, giving better resolution of the luminescence spectra at ambient temperatures, (v) in the case of luminescence spectra, removal of the perturbing influence of peaks from the vibrational Raman spectrum of the solvent. (The Raman spectrum can be distinguished from the luminescence spectrum by changing the excitation wavelength which will cause a parallel shift in the Raman spectrum), and (vi) relatively easy preparation.

It is necessary for the polymer to have a negligible absorption in the excitation region and little, or preferably no, luminescence. The polymer which has been

most widely used is poly(methylmethacrylate) (PMM), which is transparent to well below 330 nm, although early reports of no luminescence<sup>205</sup> have been contradicted by more recent studies<sup>206</sup> which show a luminescence spectrum between 400 and 500 nm with an excitation maximum at  $\sim 360$  nm. However, for strongly luminescent complexes, the effect is considered negligible, and PMM matrices have been used by Crosby *et al.*<sup>64</sup> for low-temperature studies of ruthenium(II) complexes and by Forster<sup>63</sup> for thermal quenching studies of chromium(III) luminescence. In this work, however, cellulose acetate has been used as the polymer film for which no luminescence could be detected even at excitation wavelengths of  $\sim 240$  nm; it is also transparent at 347 nm and below. The films were mounted at an angle of  $45^\circ$  to both the excitation and detection system to allow front-face illumination in the case of both emission spectra and lifetime measurements. For low-temperature work, the acetate film was placed in a cell containing 9 M LiCl which afforded good thermal equilibration with the surrounding dewar with no leaching of the film by the soliton being apparent. Unfortunately, polymer matrices can only be used when a common solvent, in this case acetone, for both polymer and compound can be found, although a small addition of water (1 to 2%) can be tolerated without significant 'clouding' of the film, and care must be taken not to allow crystallisation of the sample in the matrix. The films were made by adding AnalaR acetone to a small amount of cellulose acetate powder with stirring, until a solution with

the consistency of treacle was obtained (2 to 3 hours). A solution of the sample in acetone ( $\sim 20 \text{ cm}^3$ ) is then added, and the doped solution stirred to give a homogeneous distribution of the sample until it becomes treacle-like again. The doped solution is then poured into a crystallising dish until there is a 3-5 mm thick layer, and the solvent is allowed to evaporate overnight. The resultant very thin film (0.1 mm) is then cut into 1 cm strips ready for use, and pumped on a vacuum line for twenty-four hours, both to 'degas' the film and remove any excess solvent trapped in the film.

The optical density of the sample used was varied, depending on the nature of the experiment. For fluorimetry, a weakly absorbing solution ( $< 0.01$ ) is preferred, as this eliminates 'inner filter' effects caused either by total absorption of the exciting light at the front of the cell or re-absorption of the luminescence, which can result in distortion of the luminescence spectrum<sup>46</sup>, although this is sometimes not possible when the luminescence is weak. In contrast, laser measurements require a good optical density (between 0.5 to 1.0) at 347 nm to ensure substantial absorption of the laser pulse.

The luminescence of most of the compounds used in this work is extremely sensitive to impurities, and special precautions were taken, including the frequent cleaning of the sample cell, and also volumetric flasks used in sample preparation, in chromic acid to remove trace organic impurities.

### 3.3 PURITY OF CHEMICALS

All organic solvents used were either of spectroscopic grade, which were used without further purification, or AnalaR grade, in which case some of them were subject to further purification. Acetone (AnalaR grade) was refluxed over  $\text{KMnO}_4$  for two weeks, and then fractionally distilled. The lifetime of the excited uranyl ion ( $0.2 \text{ mol dm}^{-3}$ ) in this solvent was then measured. The distillation was then repeated until a constant lifetime was recorded ( $1.37 \mu\text{s}$  at 298 K). Doubly distilled water was also further purified by refluxing over alkaline  $\text{KMnO}_4$  for 24 hours and then distilled repeatedly to constant emission lifetime of dissolved uranyl ion ( $1.9 \mu\text{s}$  for  $0.2 \text{ mol dm}^{-3} [\text{UO}_2]^{2+}$  solution at 298 K).

All deuterated solvents were used without further purification and were of 'Gold Label' standard (e.g.  $> 99.79\%$  D for  $\text{D}_2\text{O}$ ).

Lithium chloride (BDH grade) was twice recrystallised from distilled water and dried in a vacuum oven (393 K) to remove water of crystallisation, and cooled in a vacuum desiccator over  $\text{P}_2\text{O}_5$  before use. The organic sensitisers were purchased as AnalaR or scintillation grade materials where possible, otherwise purification was by recrystallisation.

3.4 SAMPLE SYNTHESSES

Ethyl(aquo)cobaloxime,  $C_2H_5Co(DH)_2OH_2$ , where DH = monoanion of dimethylglyoxime, was prepared by the same procedure as for methyl(aquo)cobaloxime,  $CH_3Co(DH)OH_2$ , but using ethyl iodide as alkylating agent. Ethyl(aquo)-cobaloxime was best prepared from ethyl(dimethyl sulphide)cobaloxime,  $C_2H_5Co(DH)_2S(CH_3)_2$ , according to Schrauzer<sup>207</sup>. The ethyl(dimethyl sulphide)cobaloxime was boiled in water for 15 minutes and then cooled to 0°C for 24 hours to give dark orange crystals of ethyl(aquo)cobaloxime. The recrystallisation of ethyl(aquo)cobaloxime was from a mixed solvent of water, methanol and dichloromethane (1:8:10 respectively). The purity of this compound was checked by <sup>1</sup>H n.m.r., and the absorption spectrum in aqueous buffer at pH 5 featured bands at 390 ( $\epsilon$   $1.36 \times 10^3 \text{ dm}^3 \text{ mol}^{-1} \text{ cm}^{-1}$ ) and 456 nm ( $1.24 \times 10^3$ ; cf.  $1.38 \times 10^3$  in alcohol-water<sup>115</sup>).

Tris(acetylacetonato)cobalt(III) was prepared according to the principle of Bryant and Fernelins<sup>208</sup> by addition of acetylacetone and hydrogen peroxide to cobalt(II) carbonate. This was recrystallised from benzene-petroleum ether (60-80°C) giving very dark green crystals (m.p. 213-214°C). Analysis calculated for  $Co(C_5H_7O_2)_3$ : C, 50.57; H, 5.94; found C, 50.45; H, 6.02.

Ruthenium complexes,  $[Ru(bpy)_2Cl_2]$ ,  $[Ru(bpy)_2(acac)]ClO_4$ ,  $[Ru(bpy)_2(NH_3)_2](ClO_4)_2$ ,  $[Ru(phen)_2Cl_2]$ ,  $[Ru(phen)_2(acac)]ClO_4$ , and  $[Ru(phen)_2(en)]I_2$  were prepared according to the general procedures of the literature<sup>209-211</sup>. A useful starting

material for bis(bipyridine) and bis(phenanthroline) ruthenium(II) compounds are the complexes  $[\text{Ru}(\text{bpy})_2\text{Cl}_2]$  and  $[\text{Ru}(\text{phen})_2\text{Cl}_2]$ . These two complexes were prepared by reduction of,  $(\text{bpy-H})[\text{RuCl}_4(\text{bpy})]$  with zinc in hydrochloric acid, and  $(\text{phen-H})[\text{RuCl}_4(\text{phen})]$  using dimethylformamide. The complexes  $[\text{Ru}(\text{bpy})_2\text{X}_2]^{n+}$  and  $[\text{Ru}(\text{phen})_2\text{X}_2]^{n+}$  were obtained by treating an aqueous alcohol solution of the bis-dichloro complex with the appropriate ligands such as ammonia, ethylenediamine, or acetylacetone. The purity of these complexes was checked by u.v. absorption and elemental analysis.

$[\text{Ru}(\text{bpy})_2(\text{en})](\text{ClO}_4)_2$  was prepared by Dr. N. Winterton, methylcobalamin was a gift from Dr. B. T. Golding, and  $[\text{Pt}(\text{PPh}_3)_2]_2$  complex was prepared by Professor O. Traverso of the University of Ferrara, Italy.

### 3.5 ANALYSIS OF RESULTS

#### 3.5.1 ESA and Emission Lifetime Measurements

The digitised form of the traces, obtained from the graphical enlargement of the traces (X2) were analysed by computer techniques for normal first-order kinetics (ESA) according to the equation

$$I_t = I_0 \exp(-k_{\text{obs}} t) \quad (3.5)$$

where  $k_{\text{obs}}$  is the first order rate constant in  $\text{s}^{-1}$ ,

$I$  is the transmitted intensity of the analysing beam measured in terms of the photomultiplier voltage. The pertinent computer program (V1EØX) utilised a subroutine (VBØ1A) which involves a least-squares approximation to the relevant function. Initial estimates for  $k_{\text{obs}}$  were obtained by inspection of the transient decay, and  $I_0$  was calculated accurately and fed into the program. For second-order decay curves, a plot of  $1/O.D.$  versus  $t$  is undertaken, and by a linear least-squares procedure a slope is obtained which is equal to  $k_2/\epsilon_\lambda l$ ,  $k_2$  being the second-order rate constant and  $\epsilon_\lambda$  and  $l$  are the decadic extinction coefficient, at the monitoring wavelength  $\lambda$ , and the sample thickness. In the case of emission lifetime measurements the linear least-squares program was used according to the linear relationship between the logarithm of  $I_T$  (which is the intensity of emitted light at time  $t$ ) and the time  $t$  in seconds, which gives a slope of  $-k_{\text{obs}}$ .

### 3.5.2 Analysis of Arrhenius-type Data

The results in the form of  $k_{\text{obs}}$  and  $T(K)$  are collected on to data files ready for analysis by one of two methods, depending on the form of Arrhenius plot.

(i) A simple linear Arrhenius plot, i.e.

$$k_{\text{obs}} = A \exp(-E_A/RT) \quad (3.6)$$

For this case, the data can be analysed by a simple linear least-squares method.

(ii) An Arrhenius plot of the form

$$k = A\exp(-E_A/RT) + B\exp(-E_B/RT) \quad (3.7)$$

This type of plot is easily recognisable by the presence of two distinct regions with different slopes, usually apparent over a large temperature range. The data are fitted using another modified form of VBO1A (DOUBEXP) and A and B are estimated from the intercepts of the two regions, whereas  $E_A$  and  $E_B$  are given by the slopes of these regions.

CHAPTER 4

QUENCHING AND SENSITISATION PROCESSES  
OF ALKYLCOBALT(III) COMPOUNDS

4.1 QUENCHING OF ORGANIC TRIPLET STATES  
BY ETHYL(AQUO)COBALOXIME

The quenching of a wide variety of organic triplet donors, having different values of  $E_T$  (the triplet energy), with ethyl(aquo)cobaloxime has been investigated, using the laser flash photolysis method previously described (Section 3.12). The range of triplet energies covered was from that of benzophenone ( $E_T = 289.5 \text{ kJ mol}^{-1}$ )<sup>203</sup> down to that for  $\beta$ -carotene ( $E_T = 75 \text{ kJ mol}^{-1}$ )<sup>213</sup>. All the organic donors gave absorption transients readily assigned from comparison with the literature to donor triplet states, and in most cases with an absorbance at  $\lambda_{\text{max}}$  enabling quenching experiments to be performed. The absorption maxima for the triplet-triplet absorptions for all the donors are listed in Table 4.1 and agree well with literature data. Typical T-T absorption spectra are illustrated in Figures 4.1 and 4.2 for naphthacene and 2,5-diphenyloxazole. The quenching rates of organic donors by ethyl(aquo)-cobaloxime are presented in the form of the dependence of the first-order decay constants of the organic excited states upon concentration of ethyl(aquo)cobaloxime as in Figures 4.3, 4.4 and 4.5. Some of the organic donors presented problems of solubility. The low solubility of naphthacene, for example, suppresses the ground-state quenching term ( $k[{}^3\text{N}][\text{N}]$ ), which results in approximation to second-order, rather than first-order kinetics, even in the presence of the quencher.

Table 4.1 Quenching of the Absorption Organic Triplet States by Ethyl (aquo)cobaloxime

| Donors                      | Solvent         | Triplet energy<br>/kJ mol <sup>-1</sup> | Analysing<br>Wavelength<br>/nm | 10 <sup>-9</sup> k <sub>q</sub> /dm <sup>3</sup> mol <sup>-1</sup> s <sup>-1</sup> | (a) (b) |
|-----------------------------|-----------------|-----------------------------------------|--------------------------------|------------------------------------------------------------------------------------|---------|
| Benzophenone (1)            | Acetone         | 289.5 <sup>203</sup>                    | 535                            | 3.76 ± 0.07                                                                        | (9) (b) |
| 2,5-Diphenyloxazole (2)     | Methanol        | (c)                                     | 500                            | 1.84 ± 0.08                                                                        | (10)    |
| Riboflavin (3)              | Water           | 196.1 <sup>214</sup>                    | 650                            | 1.44 ± 0.12                                                                        | (9)     |
| 1-Chloroanthracene (4)      | Methanol        | 176.3 <sup>203</sup>                    | 430                            | 0.94 ± 0.03                                                                        | (8)     |
| Eosin (5)                   | Water           | 171.5 <sup>215</sup>                    | 570                            | 1.13 ± 0.09                                                                        | (8)     |
| Erythrosin (6)              | Water           | 171.0 <sup>216</sup>                    | 570                            | 1.41 ± 0.06                                                                        | (8)     |
| 9,10-Dichloroanthracene (7) | Dioxan          | 169.2 <sup>203</sup>                    | 420                            | 0.312 ± 0.019                                                                      | (9)     |
| Naphthacene (8)             | Dichloromethane | 122.6 <sup>217</sup>                    | 495                            | 0.236 ± 0.036                                                                      | (7)     |
| Rubrene (9)                 | Benzene         | 110.0 <sup>218</sup>                    | 475                            | < 0.01                                                                             | (2) (d) |
| 8-Carotene (10)             | Acetone         | 75.0 <sup>213</sup>                     | 520                            | < 0.01                                                                             | (7)     |

(a) Numbering in Figure 4.7

(b) Number of concentrations of quencher employed

(c) Unlisted in J. B. Birks, "Photolysis of Aromatic Molecules", Wiley, New York, 1970, Vol. 1, or any other reference

(d) Three determinations were made at each concentration

In this particular case we used the method of initial rates to calculate the quenching rates, which gave in the case of the quenching of naphthacene by ethyl(aquo)cobaloxime a figure of  $(2.36 \pm 0.36) \times 10^8 \text{ dm}^3 \text{ mol}^{-1} \text{ s}^{-1}$  (Table 4.1).

The absorption transient for  $\beta$ -carotene in acetone produced by direct laser flash photolysis was prohibitively weak for carrying out quenching experiments, and accordingly a triplet sensitiser<sup>219</sup> was used to produce a workable triplet state absorption; the triplet sensitiser selected was 1-chloroanthracene. Under these conditions, the kinetics of triplet formation were on a similar timescale to those of triplet decay, requiring the use of a series-first-order computer program<sup>220</sup> to factorise the two rate constants. The quenching rate constant for the sensitised triplet  $\beta$ -carotene by ethyl(aquo)cobaloxime was rather insensitive to the presence of quencher, and the quenching rate constant  $k_q$  was estimated to be less than  $10^7 \text{ dm}^3 \text{ mol}^{-1} \text{ s}^{-1}$ .

In the case of rubrene, it was very difficult to obtain its triplet absorption in toluene by direct laser flash photolysis. While there was a small transient due to rubrene triplets after sensitisation with benzophenone in toluene, which was quenched by ethyl(aquo)cobaloxime, its weakness made it impossible to perform kinetic studies adequately. This persuaded us to generate rubrene triplet states by pulse radiolysis in benzene containing biphenyl as an energy transfer agent. Rubrene ( $10^{-4} \text{ mol dm}^{-3}$ ) in benzene containing biphenyl

Figure 4.1 Triplet-triplet absorption obtained  
on laser flash photolysis of  
naphthacene in dichloromethane  
solvent.

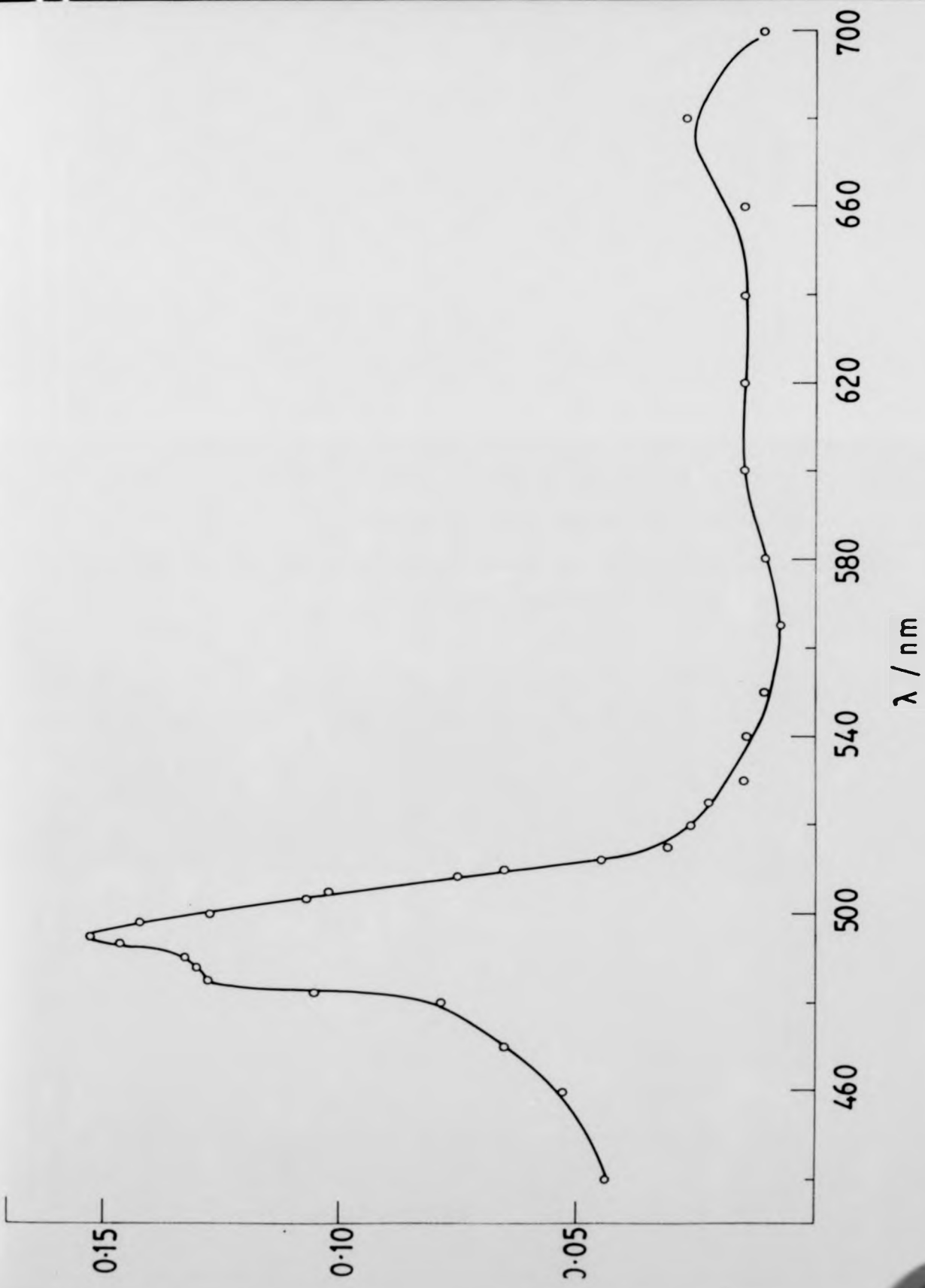


Figure 4.2 Triplet-triplet absorption obtained  
on laser flash photolysis of 2,5-  
diphenyloxazole in methanol  
solvent.

0.3

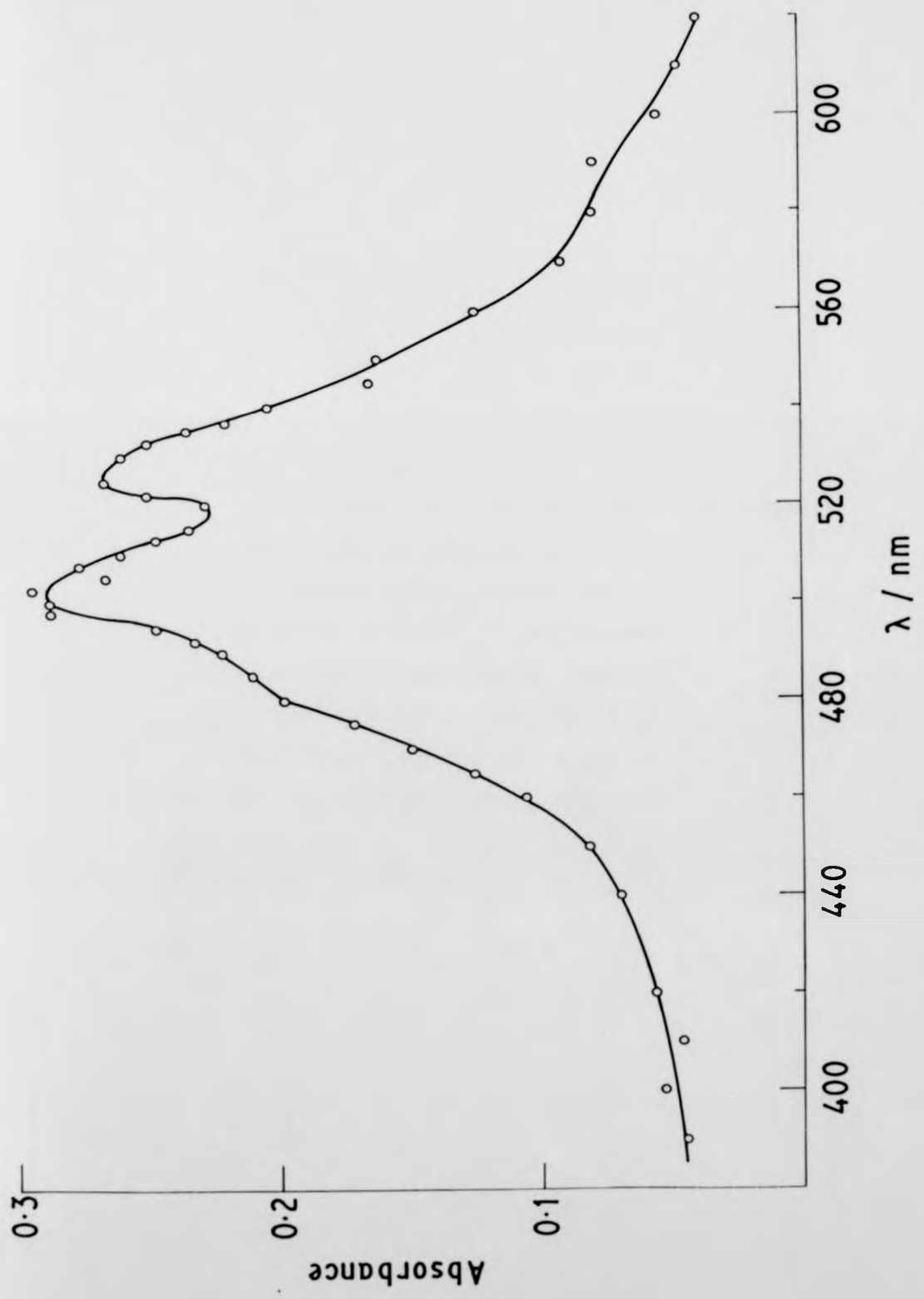


Figure 4.3 Dependence of first-order decay constants for excited states upon concentration of ethyl(aquo)-cobaloxime. ●, Triplet state of 2,5-diphenyloxazole in methanol. O, Triplet states of Riboflavin in water. (The straight lines refer to least-squares analysis of the data.)

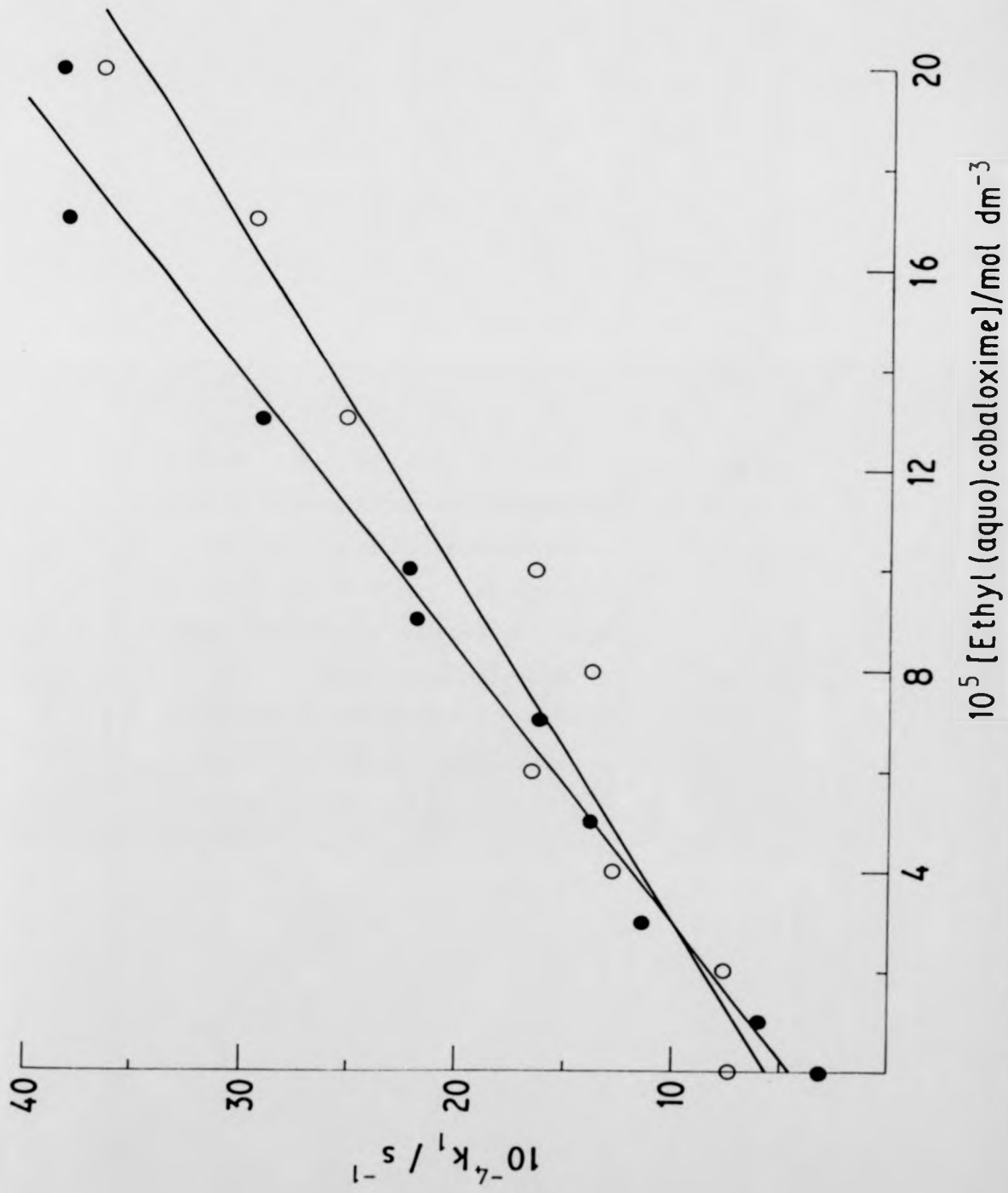


Figure 4.4 Dependence of first-order decay constants for excited states upon concentration of ethyl(aquo)-cobaloxime. ●, Triplet state of Eosin in Water. ○, Triplet state of Erythrosin in water. (The straight lines refer to least-squares analysis of the data.)

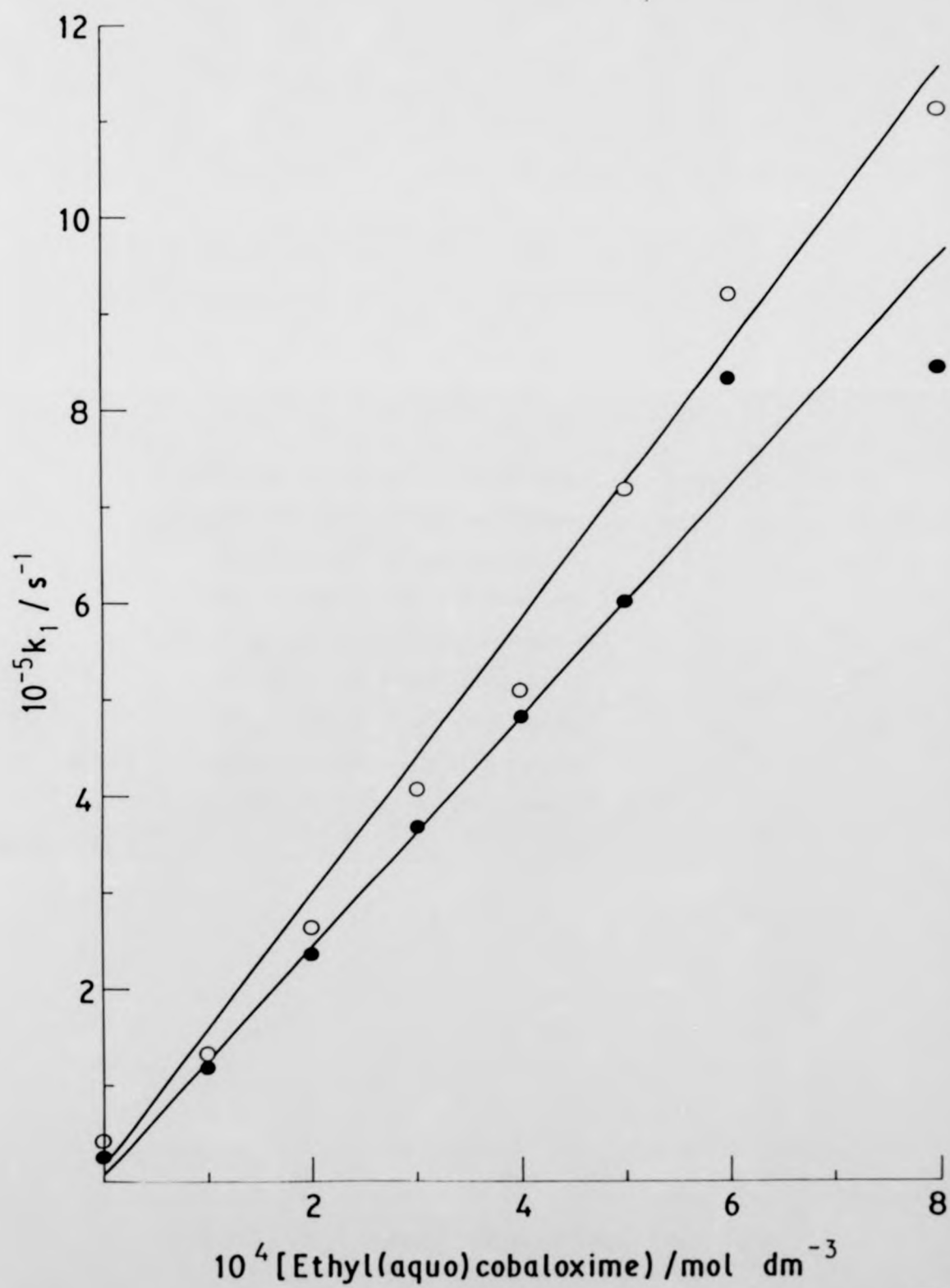
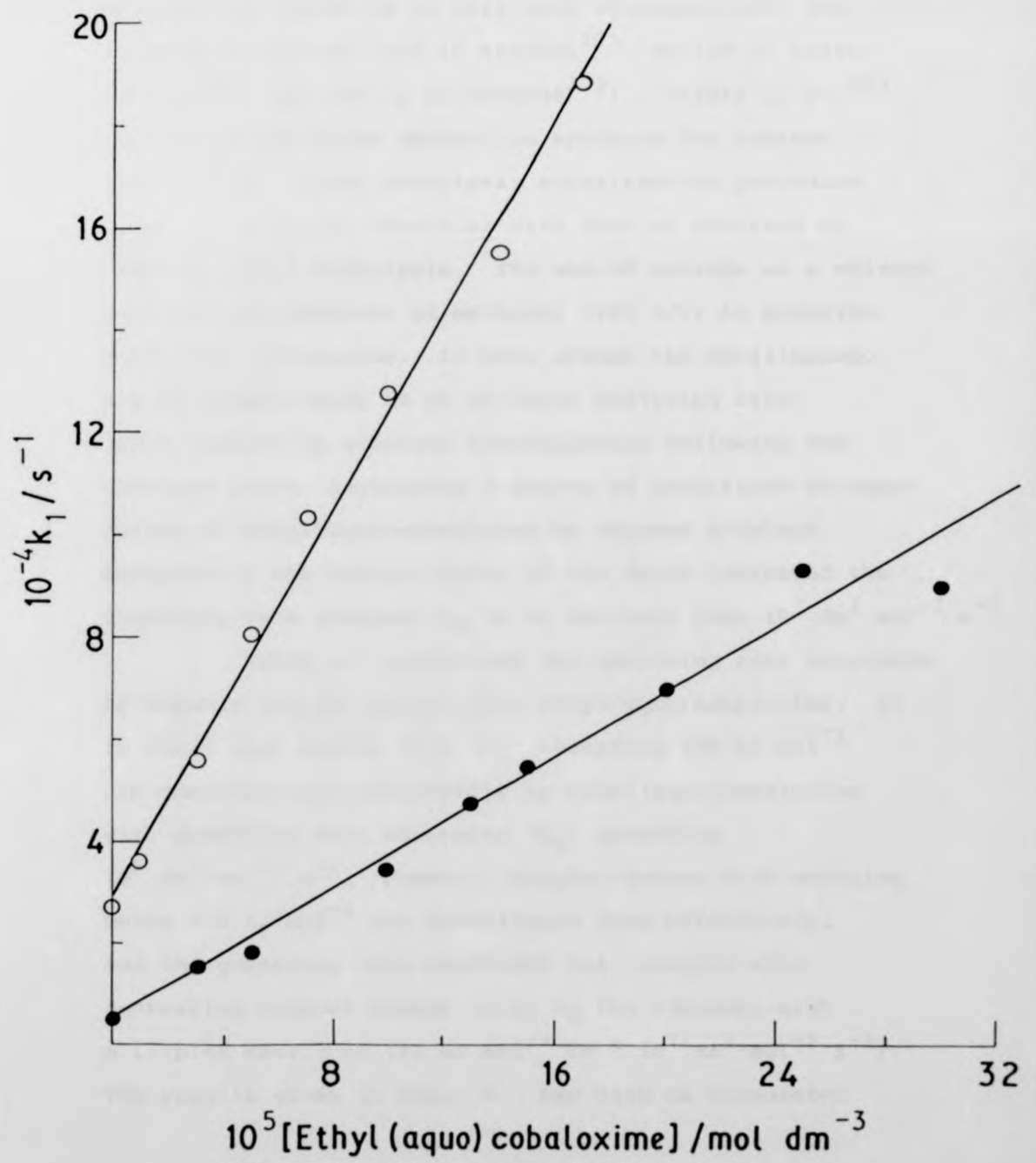


Figure 4.5 Dependence of first-order decay constants for excited states upon concentration of ethyl(aquo)-cobaloxime. ●, Triplet state of 9,10-dichloroanthracene in dioxane. ○, Triplet state of 1-chloroanthracene in methanal. (The straight lines refer to least-squares analysis of the data.)

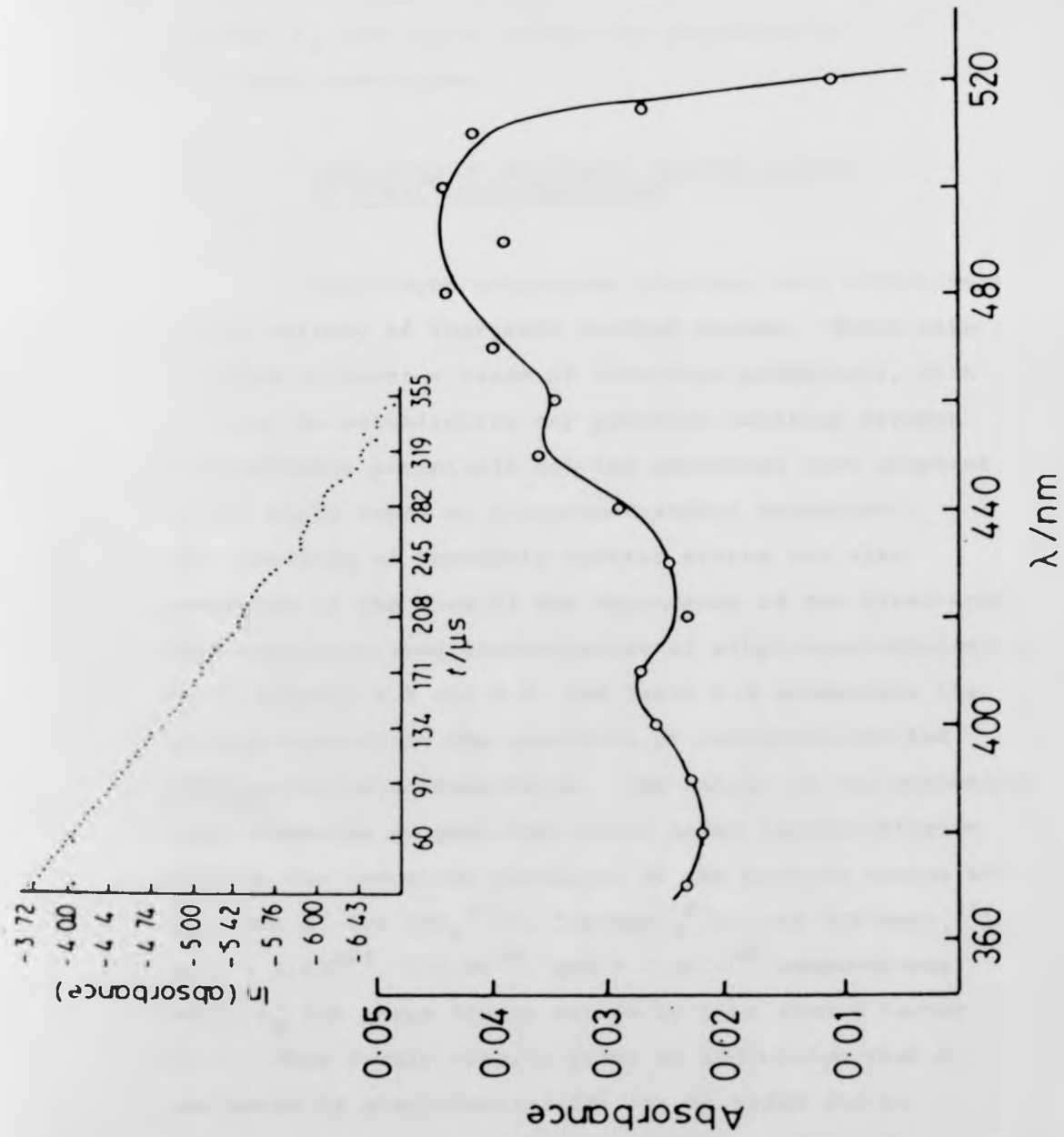


( $0.1 \text{ mol dm}^{-3}$ ) gave an intensely absorbing transient with  $\lambda_{\text{max}}$  of about 475 nm (Figure 4.6) by using this procedure. The measured lifetime of decay was 109  $\mu\text{s}$  (Figure 4.6) which is in very good agreement with the literature figures (125 in ethanol<sup>221</sup>, 80-120 in acetonitrile<sup>222</sup>, and 112  $\mu\text{s}$  in benzene<sup>223</sup>). Yildiz *et al.*<sup>223</sup> reported a transient absorption spectrum for rubrene obtained by a flash photolysis sensitisation procedure which is virtually identical with that we obtained by means of pulse radiolysis. The use of benzene as a solvent required the addition of methanol (10% v/v) to dissolve ethyl(aquo)cobaloxime. In this system the oscilloscope traces showed decay to an ultimate analysing light level indicating enhanced transmission following the electron pulse, suggesting a degree of sensitised decomposition of ethyl(aquo)cobaloxime by rubrene triplets. Analysis of the initial parts of the decay indicated the quenching rate constant  $k_{\text{q}}$  to be not more than  $10^7 \text{ dm}^3 \text{ mol}^{-1} \text{ s}^{-1}$ .

Table 4.1 summarises the quenching rate constants of organic triplet donors with ethyl(aquo)cobaloxime. It is clear that donors with  $E_{\text{T}}$  exceeding  $170 \text{ kJ mol}^{-1}$  are quenched very effectively by ethyl(aquo)cobaloxime with quenching rate constants ( $k_{\text{q}}$ ) exceeding  $10^9 \text{ dm}^3 \text{ mol}^{-1} \text{ s}^{-1}$ . However, triplet donors with energies below  $170 \text{ kJ mol}^{-1}$  are deactivated less effectively, and the quenching rate constants fall sharply with decreasing triplet energy (e.g.  $k_{\text{q}}$  for rubrene, with a triplet energy of  $110 \text{ kJ mol}^{-1}$  is  $\approx 10^7 \text{ dm}^3 \text{ mol}^{-1} \text{ s}^{-1}$ ). The results given in Table 4.1 may also be formulated

Figure 4.6 T-T absorption of rubrene ( $10^{-4}$  mol dm $^{-3}$ ) produced on pulse radiolysis of a deaerated solution in benzene containing biphenyl ( $0.1$  mol dm $^{-3}$ ). Inset, decay of rubrene triplet at absorption maximum of 475 nm.

-3.72  
-4.00



as a so-called Wilkinson<sup>219</sup> plot (Figure 4.7), which is a plot of the dependence of the second-order quenching constant  $k_q$  upon donor energy for quenching by ethyl(aquo)cobaloxime.

#### 4.2 QUENCHING OF INORGANIC EXCITED STATES BY ETHYL(AQUO)COBALOXIME

Ethyl(aquo)cobaloxime quenches very effectively a wide variety of inorganic excited states. These were selected to cover a range of reduction potentials, with the view to establishing any possible relation between the reduction potentials and the quenching rate constant, (which would imply an electron-transfer mechanism). The quenching of inorganic excited states are also presented in the form of the dependence of the first-order rate constants upon concentration of ethyl(aquo)cobaloxime, as in Figures 4.8 and 4.9, and Table 4.2 summarises the results concerning the quenching of inorganic excited states by ethyl(aquo)cobaloxime. The values of the quenching rate constants suggest that there seems little relation between the reduction potential of the excited states and  $k_q$ , thus  $E^0$  for  $[\text{UO}_2^{2+}]^*$ ,  $[\text{Ru}(\text{bpy})_3^{2+}]^*$  and  $[\text{Cr}(\text{bpy})_3^{3+}]^*$  are, + 2.60<sup>224</sup>, + 0.84<sup>48</sup>, and + 1.46 V<sup>48</sup> respectively, while  $k_q$  for these donors varies by less than a factor of 2. This result clearly gives an indication that a mechanism of electron-transfer can be ruled out in favour of one of simple energy-transfer, and the data in Section 4.3 below, which is concerned with the

Table 4.2 Quenching of Inorganic Excited States by Ethyl(aquo)cobaloxime

| Donors                                        | Solvent                        | Excited State Energy /kJ mol <sup>-1</sup> | Analysing Wavelength /nm | 10 <sup>-9</sup> k <sub>q</sub> /dm <sup>3</sup> mol <sup>-1</sup> s <sup>-1</sup> |
|-----------------------------------------------|--------------------------------|--------------------------------------------|--------------------------|------------------------------------------------------------------------------------|
| Uranyl nitrate (11) (a)                       | Aq. HClO <sub>4</sub> (0.01 M) | 245.2 <sup>225</sup>                       | 510                      | 1.18 ± 0.06 (9) (b)                                                                |
| [Ru(bpy) <sub>3</sub> ] <sup>2+</sup> (12)    | Water                          | 204.8 <sup>28</sup>                        | 580                      | 1.95 ± 0.04 (12)                                                                   |
| [Ru(phen) <sub>3</sub> ] <sup>2+</sup> (13)   | Water                          | 210.8 <sup>28</sup>                        | 580                      | 2.13 ± 0.34 (9)                                                                    |
| Bis-(8-hydroxyquinolino)Pt <sup>II</sup> (14) | Acetone                        | 185.6 <sup>226</sup>                       | 656                      | 3.58 ± 0.20 (9)                                                                    |
| [Cr(phen) <sub>3</sub> ] <sup>3+</sup> (15)   | Aq. HCl (0.01 M)               | 163.8 <sup>227</sup>                       | 730                      | 1.70 ± 0.06 (9)                                                                    |
| [Cr(bpy) <sub>3</sub> ] <sup>3+</sup> (16)    | Aq. HCl (0.01 M)               | 163.2 <sup>227</sup>                       | 733                      | 1.39 ± 0.10 (9)                                                                    |

(a) Numbering in Figure 4.7

(b) Number of concentrations of quencher employed

Figure 4.7 Plot of the logarithm of second-order constant  $\log k_q$  against donor energy for quenching by ethyl(aquo)-cobaloxime. Numbering key to quenchers as in Tables 4.1 and 4.2.

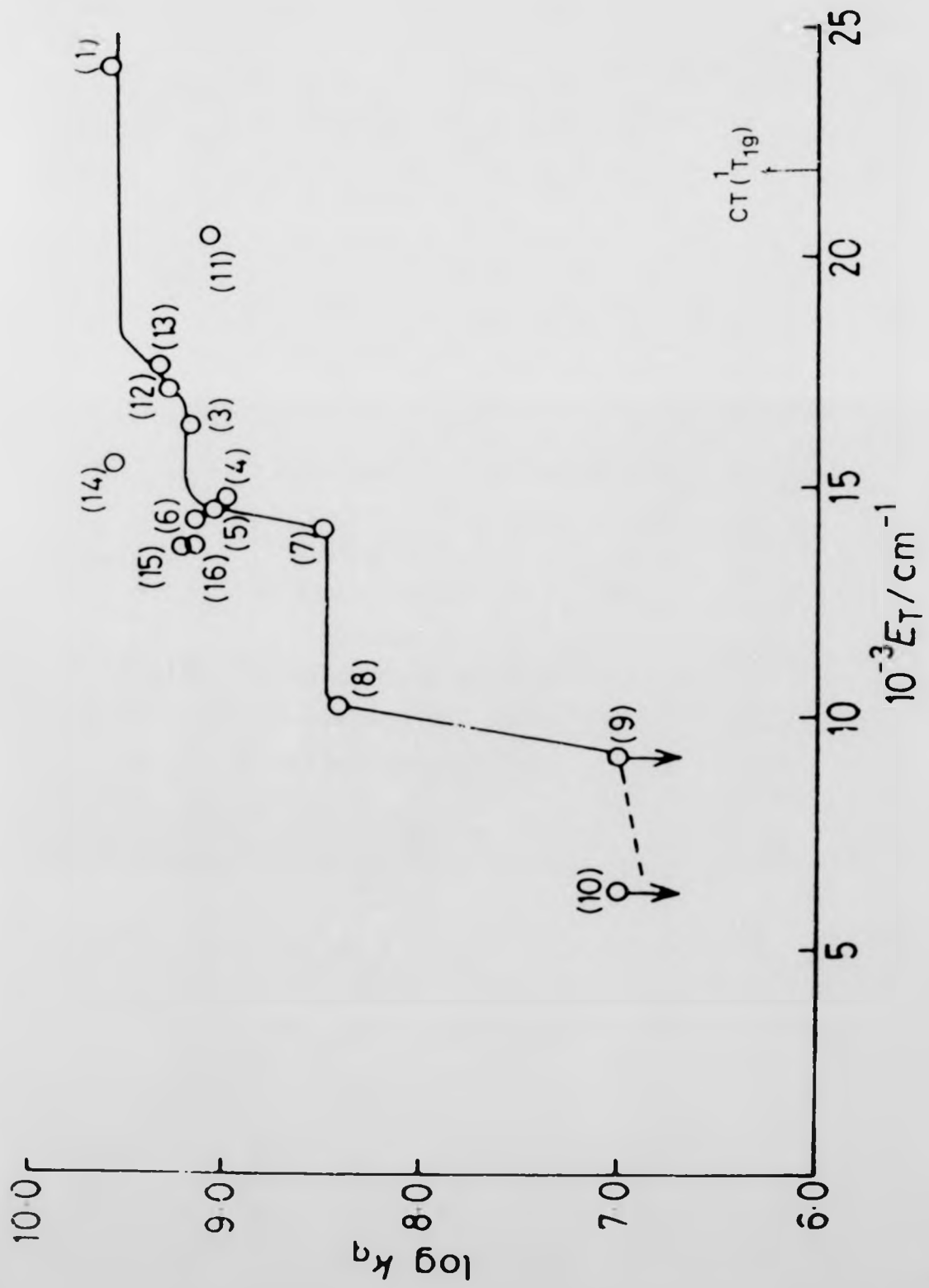


Figure 4.8 Dependence of first-order decay constants for excited states upon concentration of ethyl(aquo)-cobaloxime. ●, Excited state of  $[\text{Cr}(\text{bpy})_3]^{3+}$  in aqueous HCl. ○, Excited states of  $[\text{Cr}(\text{phen})_3]^{3+}$  in aqueous HCl. (The straight lines refer to least-squares analysis of the data.)

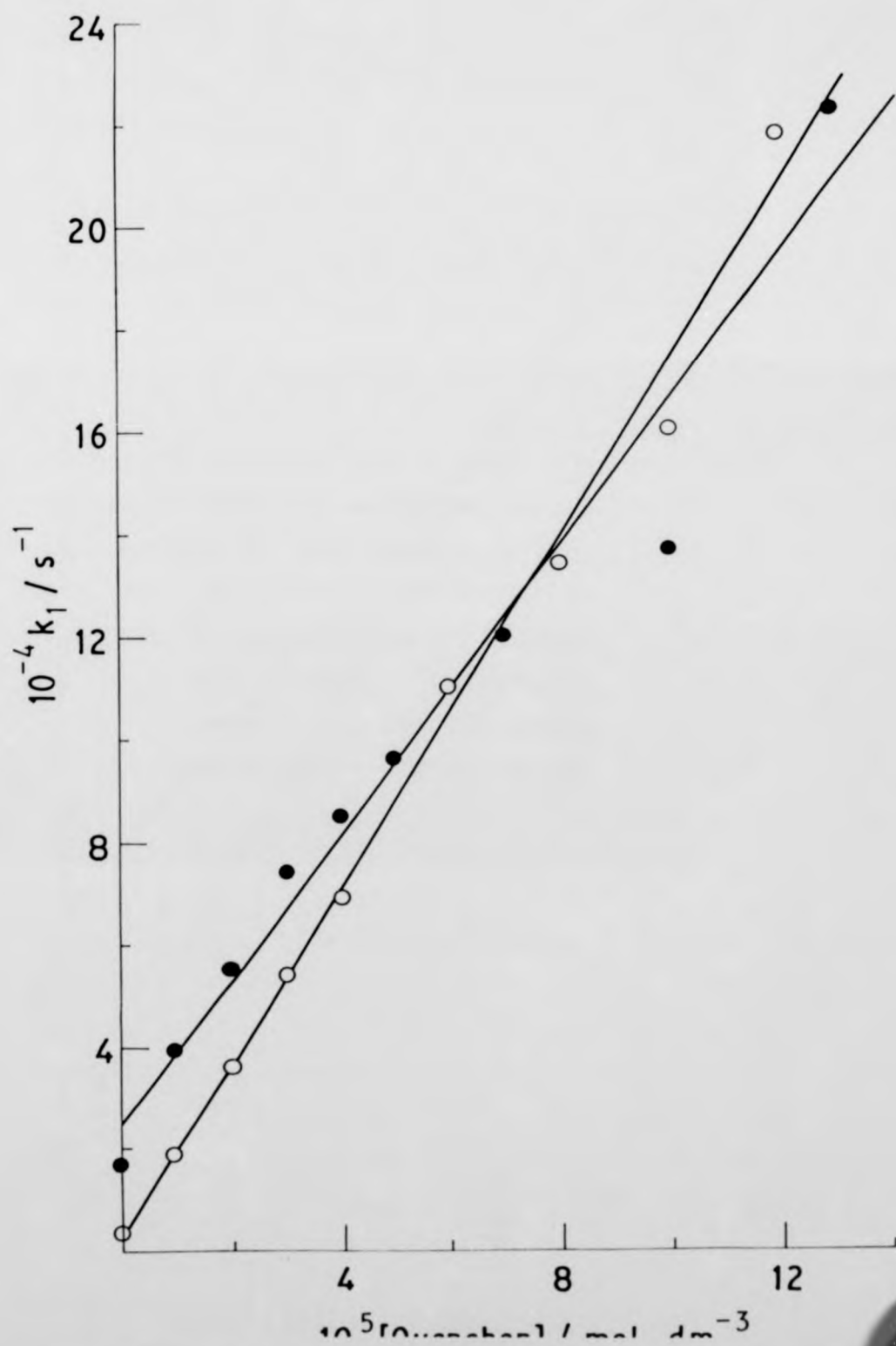
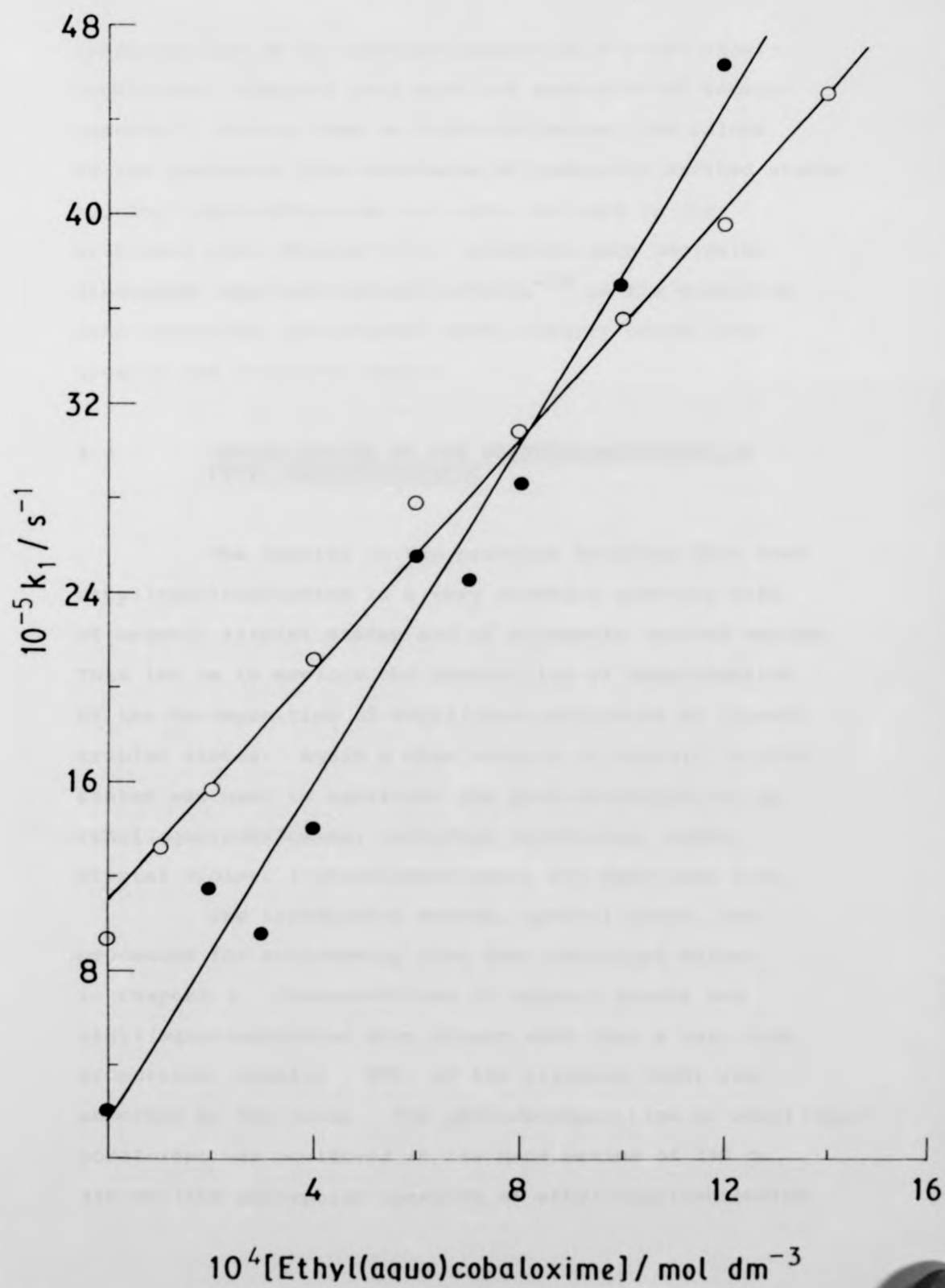


Figure 4.9 Dependence of first-order decay constants for excited states upon concentration of ethyl(aquo)cobaloxime. ●, Excited state of  $[\text{Pt}(8\text{-hydroxyquinolinato})_2]$  in acetone. ○, Excited state of  $[\text{Ru}(\text{phen})_3]^{2+}$  in water. (The straight lines refer to least-squares analysis of the data.)



sensitisation of the photodecomposition of ethyl(aquo)-cobaloxime, supports very much the mechanism of energy-transfer. Having come to this conclusion, the values of the quenching rate constants of inorganic excited states by ethyl(aquo)cobaloxime are also included in the Wilkinson plot (Figure 4.7); although such inclusion disregards spin-statistical effects<sup>219</sup> on the quenching rate constants, the overall trend clearly covers both organic and inorganic donors.

#### 4.3 SENSITISATION OF THE PHOTODECOMPOSITION OF ETHYL (AQUO) COBALOXIME

The results in the previous Sections show that ethyl(aquo)cobaloxime is a very powerful quencher both of organic triplet states and of inorganic excited states. This led us to explore the possibility of sensitisation of the decomposition of ethyl(aquo)cobaloxime by organic triplet states. Again a wide variety of organic triplet states was used to sensitise the photodecomposition of ethyl(aquo)cobaloxime, including erythrosin, eosin, Crystal Violet, 1-chloroanthracene, and Methylene Blue.

The irradiation source, optical bench, and procedure for actinometry have been described before in Chapter 3. Concentrations of organic donors and ethyl(aquo)cobaloxime were chosen such that a very high proportion, usually > 98%, of the filtered light was absorbed by the donor. The photodecomposition of ethyl(aquo)-cobaloxime was monitored at its band maxima of 390 or 456 nm (the absorption spectrum of ethyl(aquo)cobaloxime

is shown in Figure 4.10), depending on the absorption characteristics of the donor. It was necessary to select donors that did not absorb strongly at either of these two wavelengths but which absorbed very strongly elsewhere.

A typical example is provided by erythrosin which absorbs very strongly at 547 nm compared to ethyl(aquo)cobaloxime. When an aqueous buffered (pH 5.00  $\pm$  0.05) solution of ethyl(aquo)cobaloxime ( $2.0 \times 10^{-4}$  mol dm<sup>-3</sup>) was irradiated at 547 nm in a 5 cm cell (with O.D.<sub>547</sub><sup>\*</sup> = 0.050), the photodecomposition monitored at 390 nm, was quite rapid with an initial rate of  $-1.175 \times 10^{-4}$  O.D. units (390 nm) s<sup>-1</sup>; given the extinction coefficient of ethyl(aquo)cobaloxime at 390 nm, i.e.,  $1.36 \times 10^3$  dm<sup>3</sup> mol<sup>-1</sup> cm<sup>-1</sup>, the decomposition rate is  $8.64 \times 10^8$  mol dm<sup>-3</sup> s<sup>-1</sup> at the light intensity employed. Irradiation of a ( $2.0 \times 10^{-4}$  mol dm<sup>-3</sup>) solution of ethyl(aquo)cobaloxime under exactly the same conditions in the presence of erythrosin ( $4.0 \times 10^{-4}$  mol dm<sup>-3</sup>), with O.D.'s at 547 nm (5 cm cell) of 0.050 for ethyl(aquo)cobaloxime and 6.21 for erythrosin, gave an initial rate ( $\Delta$ O.D./ $\Delta$ t) at 390 nm of  $-1.210 \times 10^{-5}$  O.D. units s<sup>-1</sup> (Figure 4.11). Now since the inner filter effect of the erythrosin means that at 547 nm, the ratio of light absorbed by ethyl(aquo)cobaloxime is 0.0080 (or 0.8%), then direct photolysis of ethyl(aquo)cobaloxime is responsible for only 0.8% of  $-1.175 \times 10^{-4}$  O.D. units (390 nm) s<sup>-1</sup>, which is  $-9.4 \times 10^{-7}$  O.D. units (390 nm) s<sup>-1</sup>. Having values both

---

\*O.D. is the absorbance

Figure 4.10 Absorption spectrum of ethyl(aquo)-  
cobaloxime ( $2 \times 10^{-4} \text{ mol dm}^{-3}$ )  
in aqueous buffer pH  $5 \pm 0.05$ .

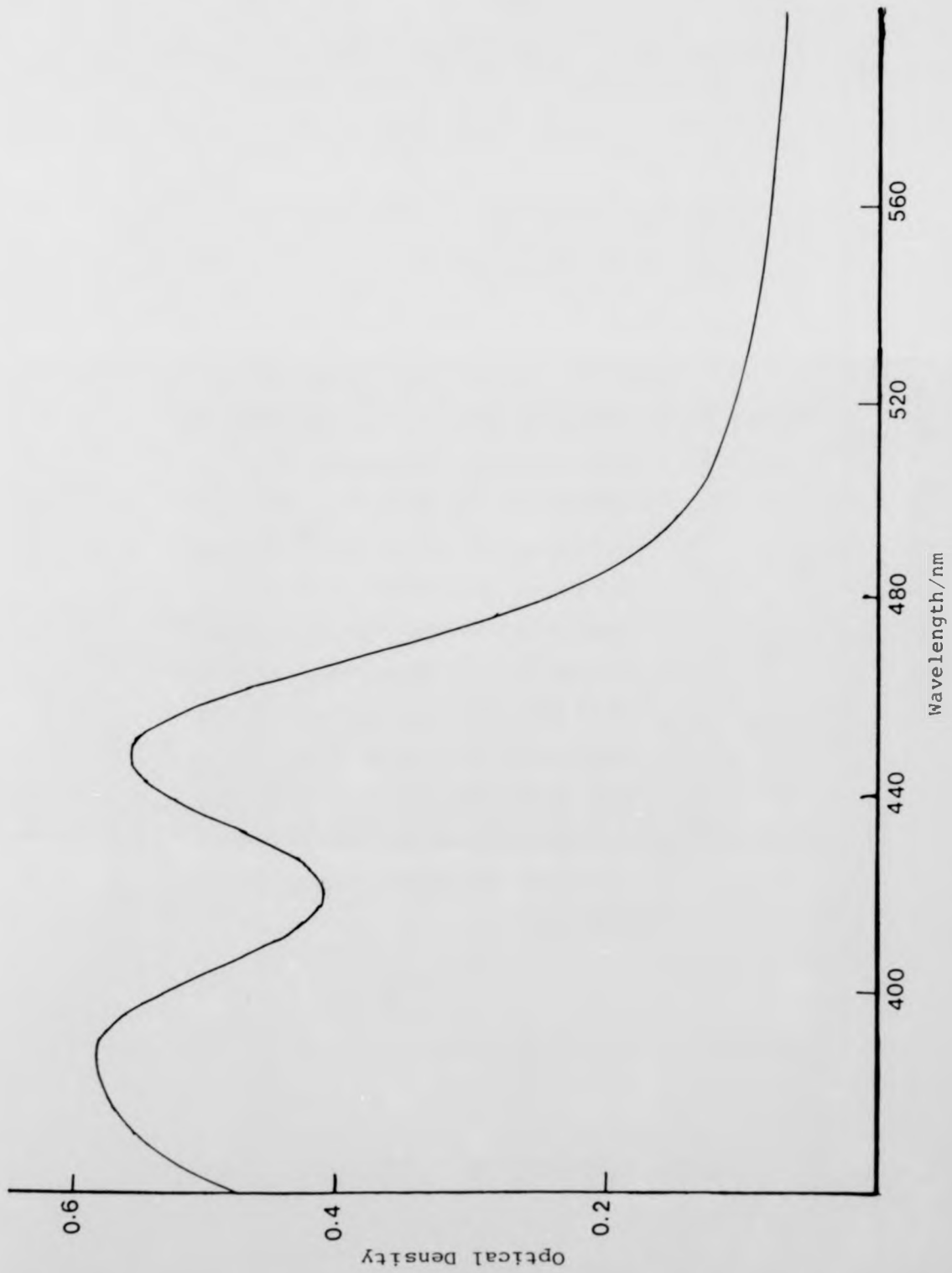
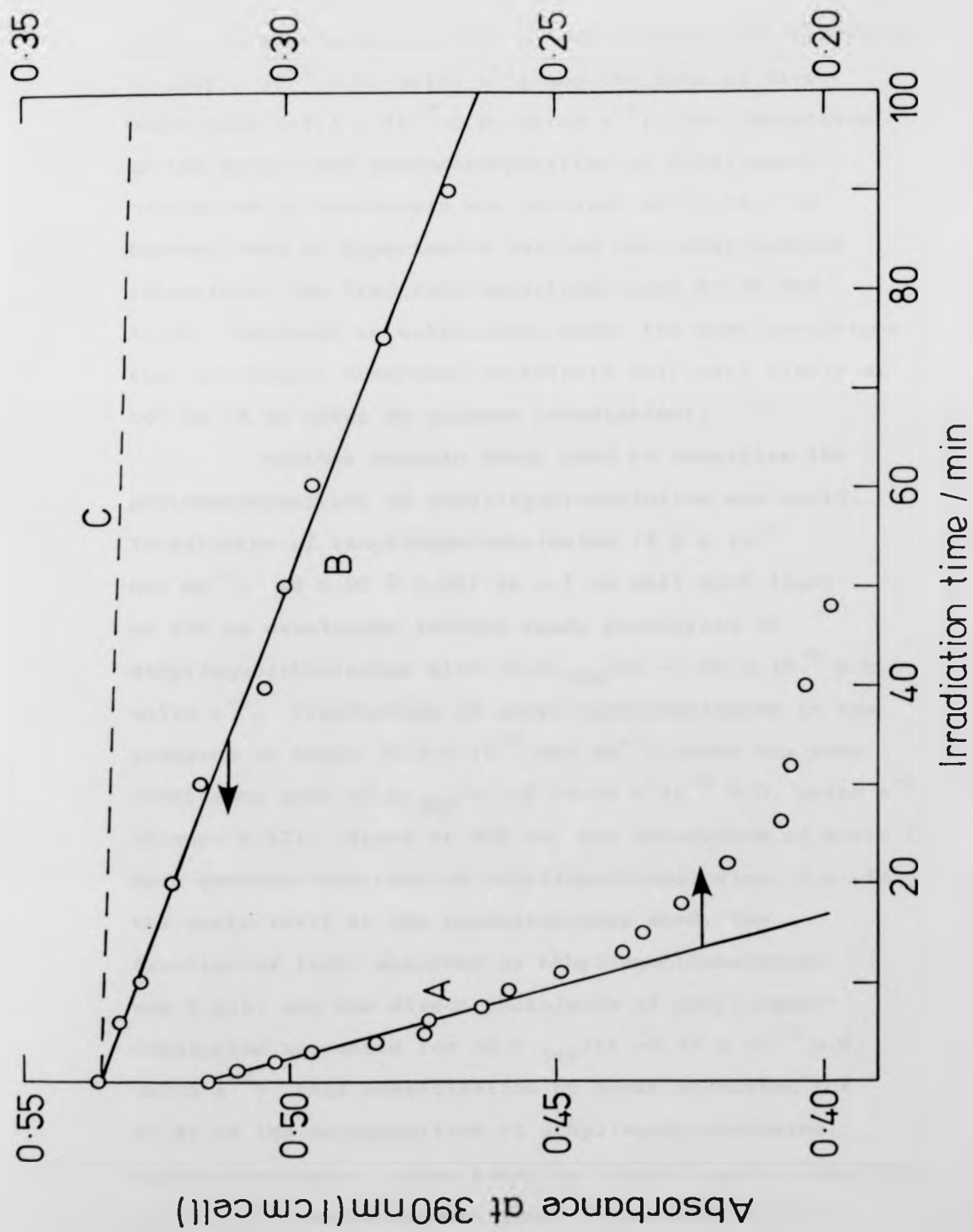


Figure 4.11 Sensitisation of the photodecomposition of ethyl(aquo)cobaloxime by erythrosin in aqueous buffer (pH  $5.00 \pm 0.05$ ) monitored at 390 nm. A, Direct photolysis (547 nm) of ethyl(aquo)cobaloxime ( $2.0 \times 10^{-4}$  mol dm $^{-3}$ ). B, Photolysis (547 nm) of a solution containing ethyl(aquo)cobaloxime ( $2.0 \times 10^{-4}$  mol dm $^{-3}$ ) and erythrosin ( $4.0 \times 10^{-4}$  mol dm $^{-3}$ ). C, Component of photolysis B attributed to direct photolysis of ethyl(aquo)cobaloxime.

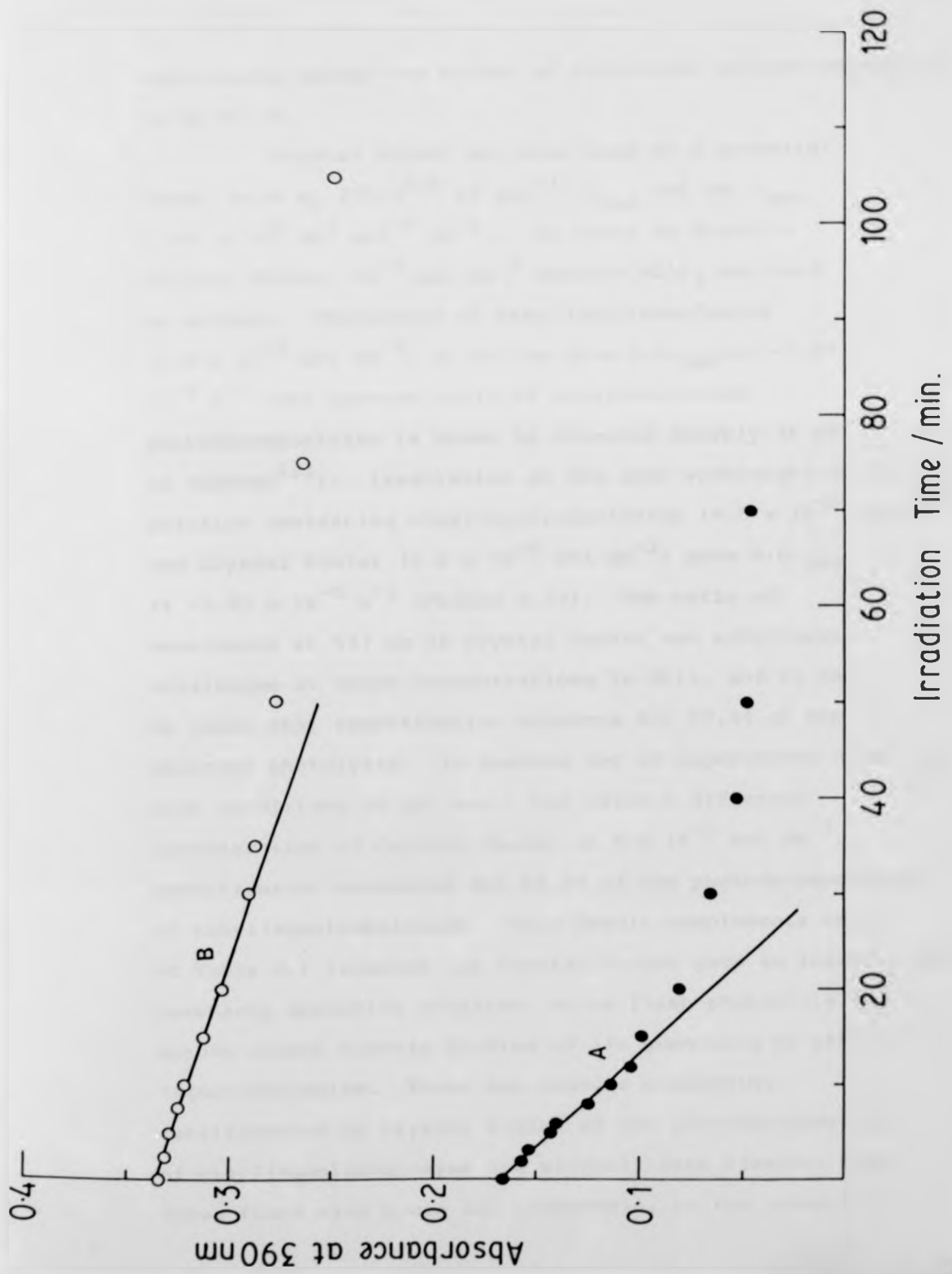


of the rate of decomposition in the presence of erythrosin ( $-1.210 \times 10^{-5}$  O.D. units  $s^{-1}$ ) and the rate of direct photolysis ( $-9.4 \times 10^{-7}$  O.D. units  $s^{-1}$ ), the percentage of the sensitised photodecomposition of ethyl(aquo)-cobaloxime by erythrosin was obtained as 92.2%. In further sets of experiments carried out under similar conditions, the fractions sensitised were 91.3% and 90.8%. Moreover we established under the same conditions that erythrosin underwent photolysis only very slowly at 547 nm (4.8% after 80 minutes irradiation).

Another organic donor used to sensitise the photodecomposition of ethyl(aquo)cobaloxime was eosin. Irradiation of ethyl(aquo)cobaloxime ( $2.0 \times 10^{-5}$  mol  $dm^{-3}$ ; pH  $5.00 \pm 0.05$ ) in a 5 cm cell with light of 498 nm wavelength induced ready photolysis of ethyl(aquo)cobaloxime with  $\Delta O.D._{390}/\Delta t$   $-7.83 \times 10^{-5}$  O.D. units  $s^{-1}$ . Irradiation of ethyl(aquo)cobaloxime in the presence of eosin ( $2.0 \times 10^{-5}$  mol  $dm^{-3}$ ) under the same conditions gave  $\Delta O.D._{390}/\Delta t$  of  $-2.18 \times 10^{-5}$  O.D. units  $s^{-1}$  (Figure 4.12). Since at 498 nm, the absorbance of eosin is much greater than that of ethyl(aquo)cobaloxime, i.e. in the ratio 164:1 at the concentrations used, the fraction of light absorbed by ethyl(aquo)cobaloxime was 0.61%, and the direct photolysis of ethyl(aquo)-cobaloxime accounted for  $\Delta O.D._{390}/\Delta t$   $-4.78 \times 10^{-7}$  O.D. units  $s^{-1}$ ; thus sensitisation by eosin accounted for 97.8% of the decomposition of ethyl(aquo)cobaloxime. Again irradiation under identical conditions of eosin gave only slight photodecomposition. A duplicate set of

Figure 4.12 Sensitisation of the photodecomposition of ethyl(aquo)cobaloxime by eosin in aqueous buffer (pH  $5.00 \pm 0.05$ ) monitored at 390 nm. A, Direct photolysis (498 nm) of ethyl(aquo)-cobaloxime ( $2.0 \times 10^{-5} \text{ mol dm}^{-3}$ ). B, Photolysis (498 nm) of a solution containing ethyl(aquo)cobaloxime ( $2.0 \times 10^{-5} \text{ mol dm}^{-3}$ ) and eosin ( $2.0 \times 10^{-5} \text{ mol dm}^{-3}$ ).

on



experiments showed the extent of sensitised photodecomposition to be 97.7%.

Crystal Violet was also used as a potential donor, with  $E_T$   $175.7^{215}$  kJ mol<sup>-1</sup> ( $\lambda_{max}$  586 nm,  $\epsilon_{max}$   $1.031 \times 10^5$  dm<sup>3</sup> mol<sup>-1</sup> cm<sup>-1</sup>). In order to dissolve Crystal Violet,  $10^{-2}$  mol dm<sup>-3</sup> aqueous HClO<sub>4</sub> was used as solvent. Photolysis of ethyl(aquo)cobaloxime ( $4.0 \times 10^{-5}$  mol dm<sup>-3</sup>) at 547 nm gave O.D.<sub>390</sub>/Δt  $-1.59 \times 10^{-4}$  s<sup>-1</sup> (the quantum yield of alkylcobaloxime photodecomposition is known to increase sharply as pH is reduced<sup>122</sup>). Irradiation at the same wavelength of a solution containing ethyl(aquo)cobaloxime ( $4.0 \times 10^{-5}$  mol dm<sup>-3</sup>) and Crystal Violet ( $6.0 \times 10^{-5}$  mol dm<sup>-3</sup>) gave O.D.<sub>390</sub>/Δt  $-6.92 \times 10^{-5}$  s<sup>-1</sup> (Figure 4.13). The ratio of absorbance at 547 nm of Crystal Violet and ethyl(aquo)-cobaloxime at these concentrations is 86:1, and it can be shown that sensitisation accounts for 97.4% of the observed photolysis. In another set of experiments under the same conditions of pH, etc., but using a different concentration of Crystal Violet ( $4.0 \times 10^{-5}$  mol dm<sup>-3</sup>), sensitisation accounted for 95.4% of the photodecomposition of ethyl(aquo)cobaloxime. This result complements those of Table 4.1 inasmuch as Crystal Violet gave an insufficiently intensely absorbing transient on ns flash photolysis to enable direct kinetic studies of its quenching by ethyl(aquo)cobaloxime. These two results concerning sensitisation by Crystal Violet of the photodecomposition of ethyl(aquo)cobaloxime are slightly less clearcut than those found with cosin and erythrosin, in the sense that

Figure 4.13 Sensitisation of the photodecomposition of ethyl(aquo)cobaloxime by Crystal Violet in aqueous  $\text{HClO}_4$  monitored at 390 nm. A, Direct photolysis (547 nm) of ethyl(aquo)cobaloxime ( $4.0 \times 10^{-5} \text{ mol dm}^{-3}$ ). B, Photolysis (547 nm) of a solution containing ethyl(aquo)-cobaloxime ( $4.0 \times 10^{-5} \text{ mol dm}^{-3}$ ) and Crystal Violet ( $6.0 \times 10^{-5} \text{ mol dm}^{-3}$ ).

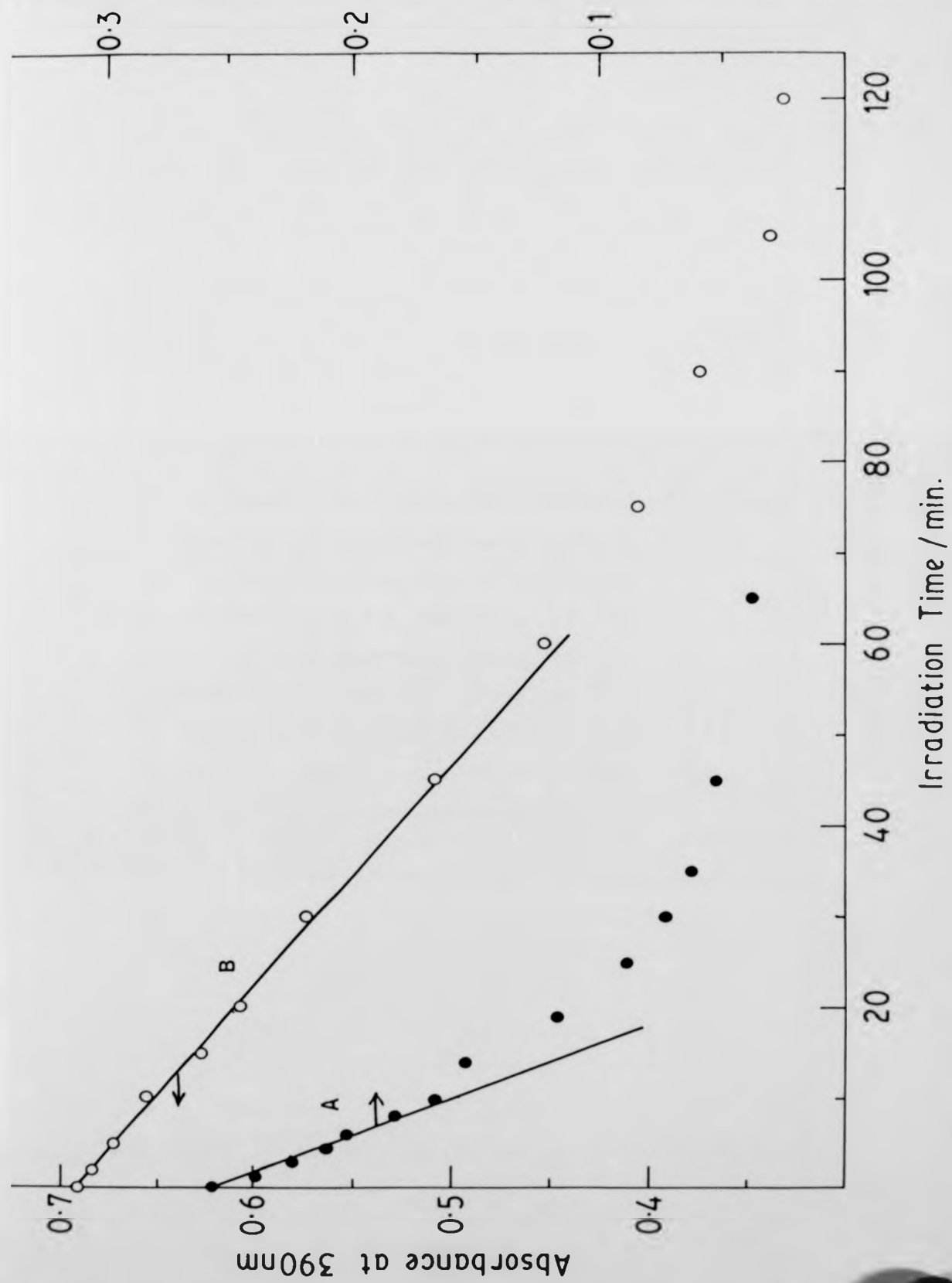


Figure 4.14 Sensitisation of the photodecomposition of ethyl(aquo)cobaloxime by 1-chloroanthracene in methanol monitored at 447 nm. A, Direct photolysis (363 nm) of ethyl(aquo)cobaloxime ( $2.0 \times 10^{-5} \text{ mol dm}^{-3}$ ). B, Photolysis (363 nm) of a solution containing ethyl(aquo)cobaloxime ( $2.0 \times 10^{-5} \text{ mol dm}^{-3}$ ) and 1-chloroanthracene ( $4.0 \times 10^{-5} \text{ mol dm}^{-3}$ ).

Absorbance at 447nm

0.15

0.10

0.05

B

A

100

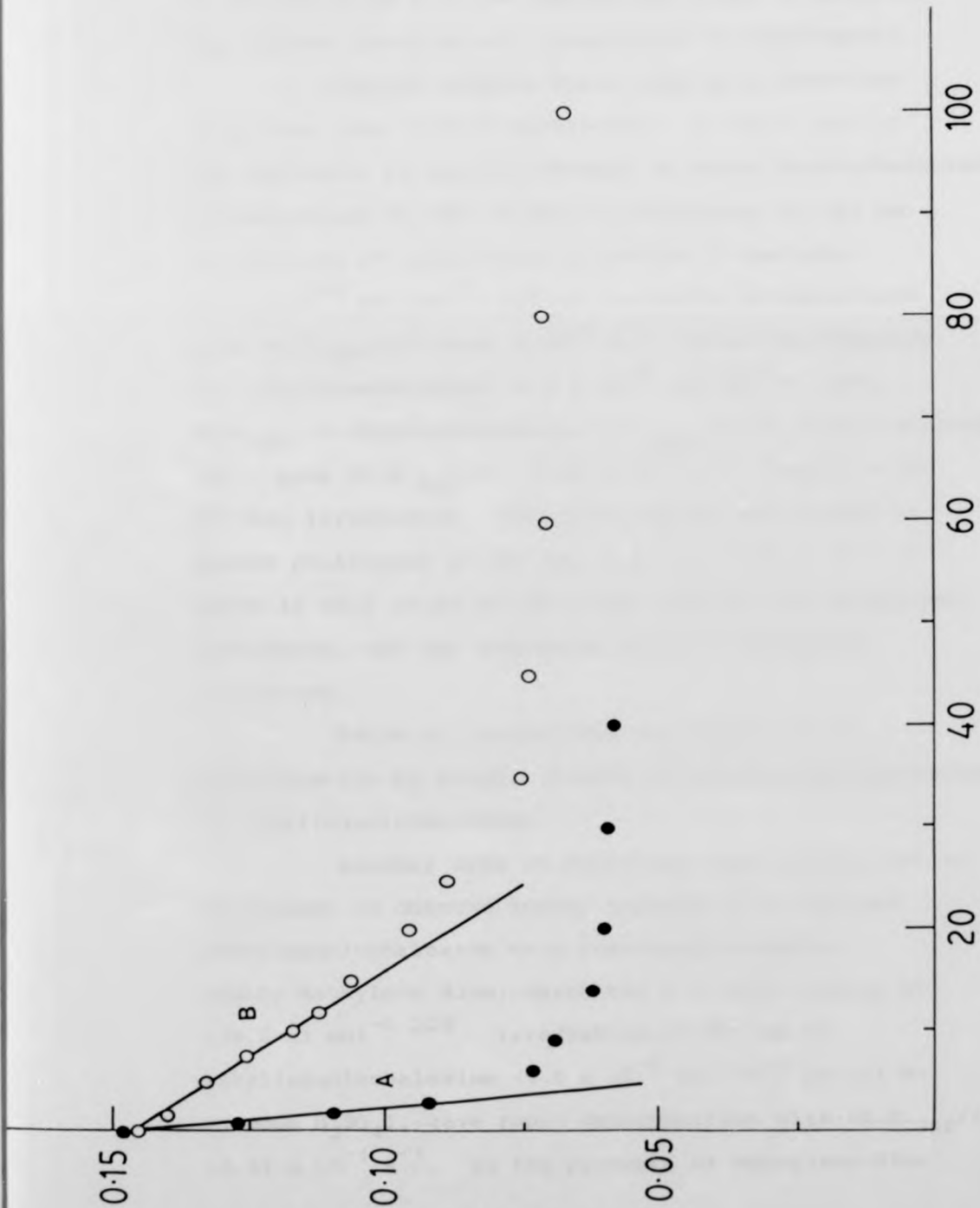
80

60

40

20

Irradiation Time / min.



the sensitising dye underwent appreciable photolysis at 547 nm at pH 2 (ca 10% during the first 12 minutes, the typical duration of a sensitisation experiment).

Another organic donor used as a potential sensitiser was 1-chloroanthracene. In this case it was necessary to monitor changes in ethyl(aquo)cobaloxime concentration at 447 nm while irradiating at 363 nm. Irradiation of ethyl(aquo)cobaloxime in methanol ( $2.0 \times 10^{-5} \text{ mol dm}^{-3}$ ) led to its ready decomposition with  $\Delta\text{O.D.}_{447}/\Delta t = 3.16 \times 10^{-4} \text{ s}^{-1}$ , while the presence of 1-chloroanthracene ( $4.0 \times 10^{-4} \text{ mol dm}^{-3}$ ), when  $\text{O.D.}_{363} (1\text{-chloroanthracene})/\text{O.D.}_{363} (\text{ethyl(aquo)cobaloxime}) = 54:1$ , gave  $\Delta\text{O.D.}_{447}/\Delta t = 3.96 \times 10^{-5} \text{ s}^{-1}$  (Figure 4.14). Of this irradiation, 1/55 parts may be attributed to direct photolysis at 363 nm, i.e. to  $-5.75 \times 10^{-6} \text{ s}^{-1}$ , which is only 14.5% of the total rate in the sensitised photolysis, and the remaining 85.5% is therefore sensitised.

Table 4.3 summarises the result of the sensitisation by organic donors of the photodecomposition of ethyl(aquo)cobaloxime.

Another type of experiment was carried out in an attempt to observe energy transfer *from* excited ethyl(aquo)cobaloxime to a low-energy acceptor, namely Methylene Blue, which has a triplet energy of  $139.2 \text{ kJ mol}^{-1}$  <sup>228</sup>. Irradiation at 401 nm of ethyl(aquo)cobaloxime ( $5.0 \times 10^{-5} \text{ mol dm}^{-3}$  in 0.1 M-aqueous  $\text{H}_2\text{SO}_4$ ), gave rapid decomposition with  $\Delta\text{O.D.}_{390}/\Delta t = 2.52 \times 10^{-4} \text{ s}^{-1}$ . In the presence of Methylene Blue

Table 4.3 Percentage of the Sensitised Photodecomposition of Ethyl(aquo)cobaloxime by Different Organic Donors

| Organic Donors     | Triplet Energy<br>/kJ mol <sup>-1</sup> | Irradiation<br>Wavelength<br>/nm | Monitored<br>Wavelength<br>/nm | Percentage of<br>Sensitised photo-<br>Decomposition |
|--------------------|-----------------------------------------|----------------------------------|--------------------------------|-----------------------------------------------------|
| Erythrosin         | 171.0                                   | 547                              | 390                            | 92.2<br>91.3<br>90.8                                |
| Eosin              | 171.5                                   | 498                              | 390                            | 97.8<br>97.7                                        |
| Crystal Violet     | 175.5                                   | 547                              | 390                            | 97.4<br>95.4                                        |
| 1-Chloroanthracene | 176.3                                   | 363                              | 447                            | 85.5                                                |

( $1.0 \times 10^{-5} \text{ mol dm}^{-3}$ ), the rate was  $-2.04 \times 10^{-4} \text{ s}^{-1}$ , but correction for the few percent of light internally filtered by the dye increases this to  $-2.20 \times 10^{-4} \text{ s}^{-1}$ . At a higher concentration of Methylene Blue ( $1.0 \times 10^{-4} \text{ mol dm}^{-3}$ ) the rate of photodecomposition of ethyl(aquo)cobaloxime was  $-1.05 \times 10^{-4} \text{ s}^{-1}$ , but the correction for the inner filtering by the dye (which is now larger) increases this figure to  $-2.29 \times 10^{-4} \text{ s}^{-1}$ . Considering the inherent errors in these experiments, we consider the results to indicate that  $10^{-4} \text{ mol dm}^{-3}$  Methylene Blue fails to protect excited ethyl(aquo)cobaloxime from decomposition by energy transfer.

#### 4.4 QUENCHING OF EXCITED STATES BY METHYLCOBALAMIN

As mentioned in Section 2.1.3, the behaviour of cobalamins is very similar to that of its models, the cobaloximes. As expected from the results of Section 4.1, methylcobalamin exhibited very powerful quenching of the lifetimes both of typical organic and inorganic donors, and typical quenching plots in the form of the dependence of the first-order decay constant for the excited states upon the concentration of methylcobalamin are given, (Figures 4.15 and 4.16). Table 4.4 summarises the results on the quenching of the donor excited states by methylcobalamin.

Table 4.4 Quenching of Excited States by Methylcobalamin (a)

| Donors                           | Solvent                      | $10^{-9} k_q / \text{dm}^3 \text{ mol}^{-1} \text{ s}^{-1}$ |
|----------------------------------|------------------------------|-------------------------------------------------------------|
| Uranyl nitrate                   | Aq. $\text{HClO}_4$ (0.01 M) | $3.02 \pm 0.11$ (8) (b)                                     |
| 1-Chloroanthracene               | Methanol                     | $0.327 \pm 0.017$ (9)                                       |
| Eosin                            | Methanol                     | $0.372 \pm 0.021$ (9)                                       |
| $[\text{Cr}(\text{bpy})_3]^{3+}$ | Aq. $\text{HCl}$ (0.01 M)    | $0.128 \pm 0.008$ (7)                                       |

(a) The donor excited state energy and analysing wavelength were listed in Tables 4.1 and 4.2

(b) Number of concentrations of quencher employed

Figure 4.15 Dependence of first-order decay constants for excited state of 1-chloroanthracene in methanol upon concentration of methylcobalamin. (The straight line refers to least-squares analysis of the data.)

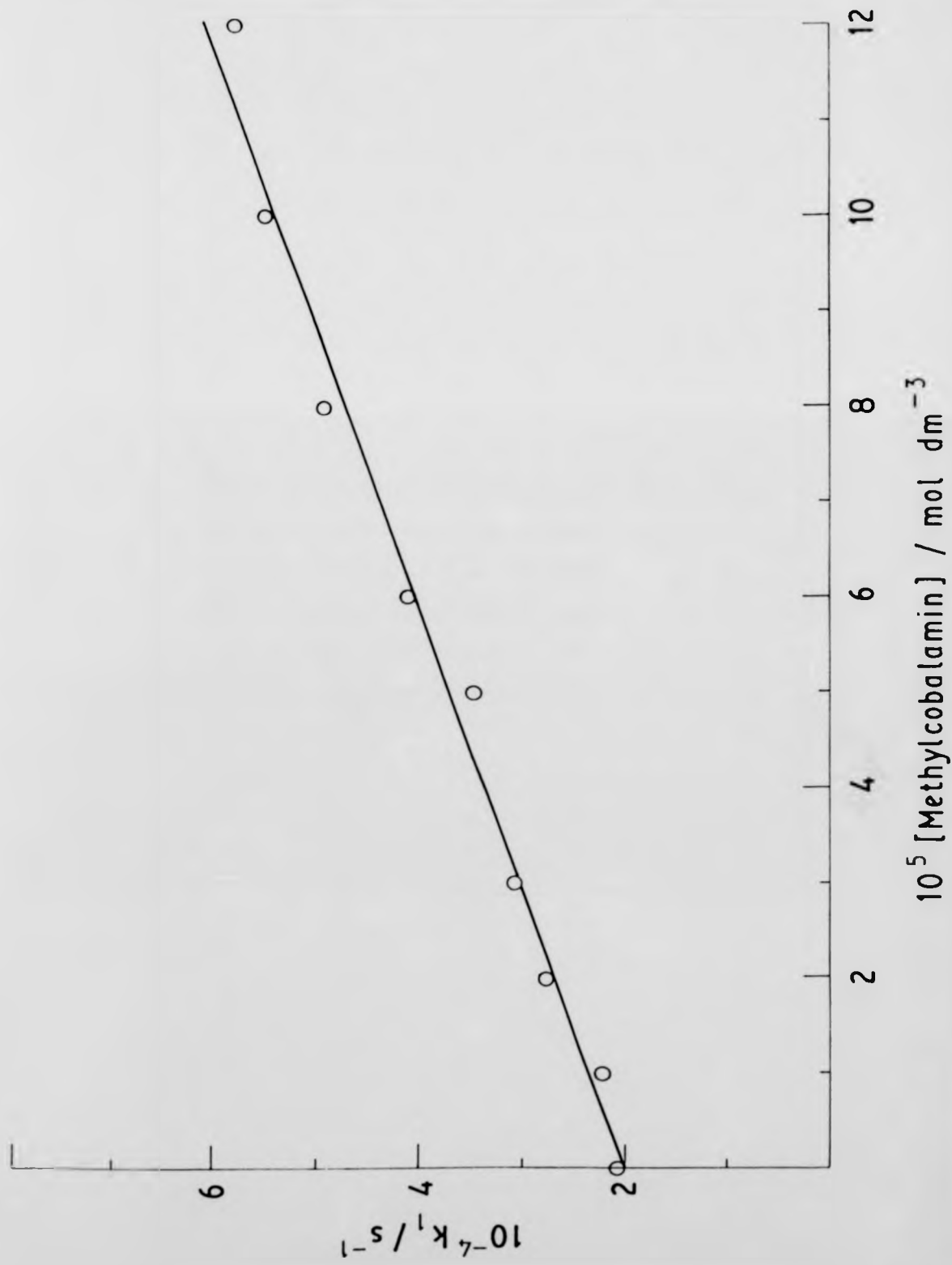
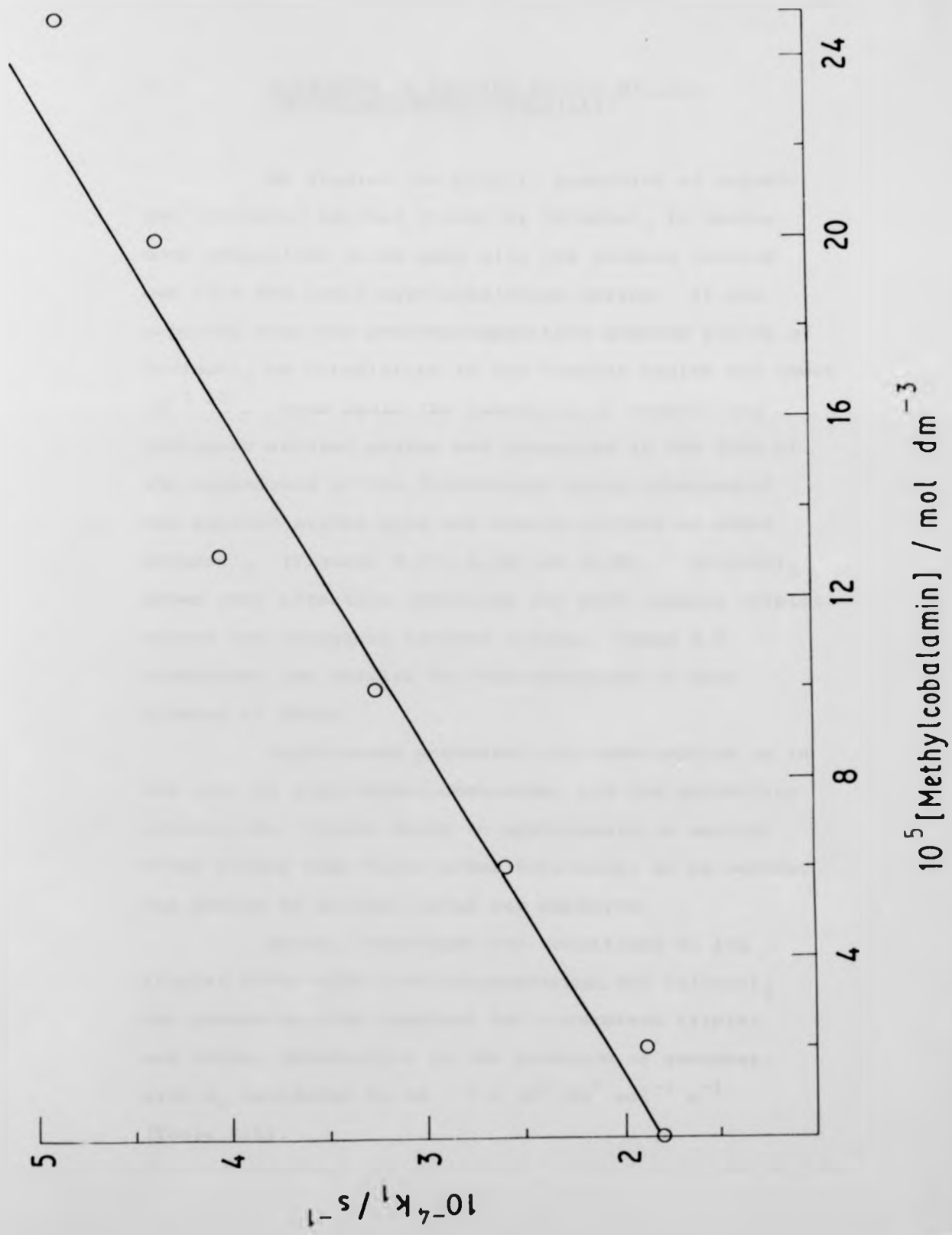


Figure 4.16 Dependence of first-order decay constants for excited state of  $[\text{Cr}(\text{bpy})_3]^{3+}$  in aqueous HCl upon concentration of methylcobalamin. (The straight line refers to least-squares analysis of the data.)



4.5 QUENCHING OF EXCITED STATES BY  $\gamma$ -Irradiation-  
(ACETYLACETONATO)COBALT (III)

We studied the kinetic quenching of organic and inorganic excited states by  $\text{Co}(\text{acac})_3$  to enable some comparison to be made with the studies carried out with the ethyl(aquo)cobaloxime system. It was reported that the photodecomposition quantum yields of  $\text{Co}(\text{acac})_3$  on irradiation in the visible region are about  $10^{-3}$  <sup>127</sup>. Once again the quenching of organic and inorganic excited states are presented in the form of the dependence of the first-order decay constants of the excited states upon the concentrations of added  $\text{Co}(\text{acac})_3$  (Figures 4.17, 4.18 and 4.19).  $\text{Co}(\text{acac})_3$  shows very effective quenching for both organic triplet states and inorganic excited states. Table 4.5 summarises the results for the quenching of both classes of donor.

Naphthacene presented the same problem as in the case of ethyl(aquo)cobaloxime, its low solubility causing the triplet decay to approximate to second-order rather than first-order behaviour, so as before, the method of initial rates was employed.

Again,  $\beta$ -carotene was sensitised to its triplet state with 1-chloroanthracene. For  $\text{Co}(\text{acac})_3$  the quenching rate constant for  $\beta$ -carotene triplet was rather insensitive to the presence of quencher, with  $k_q$  estimated to be  $> 2 \times 10^7 \text{ dm}^3 \text{ mol}^{-1} \text{ s}^{-1}$  (Table 4.5).

Figure 4.17 Dependence of first-order decay constants of excited states upon concentration of  $\text{Co}(\text{acac})_3$ .  
●, Triplet state of 1-chloroanthracene in methanol. O, Triplet state of erythrosin in methanol.

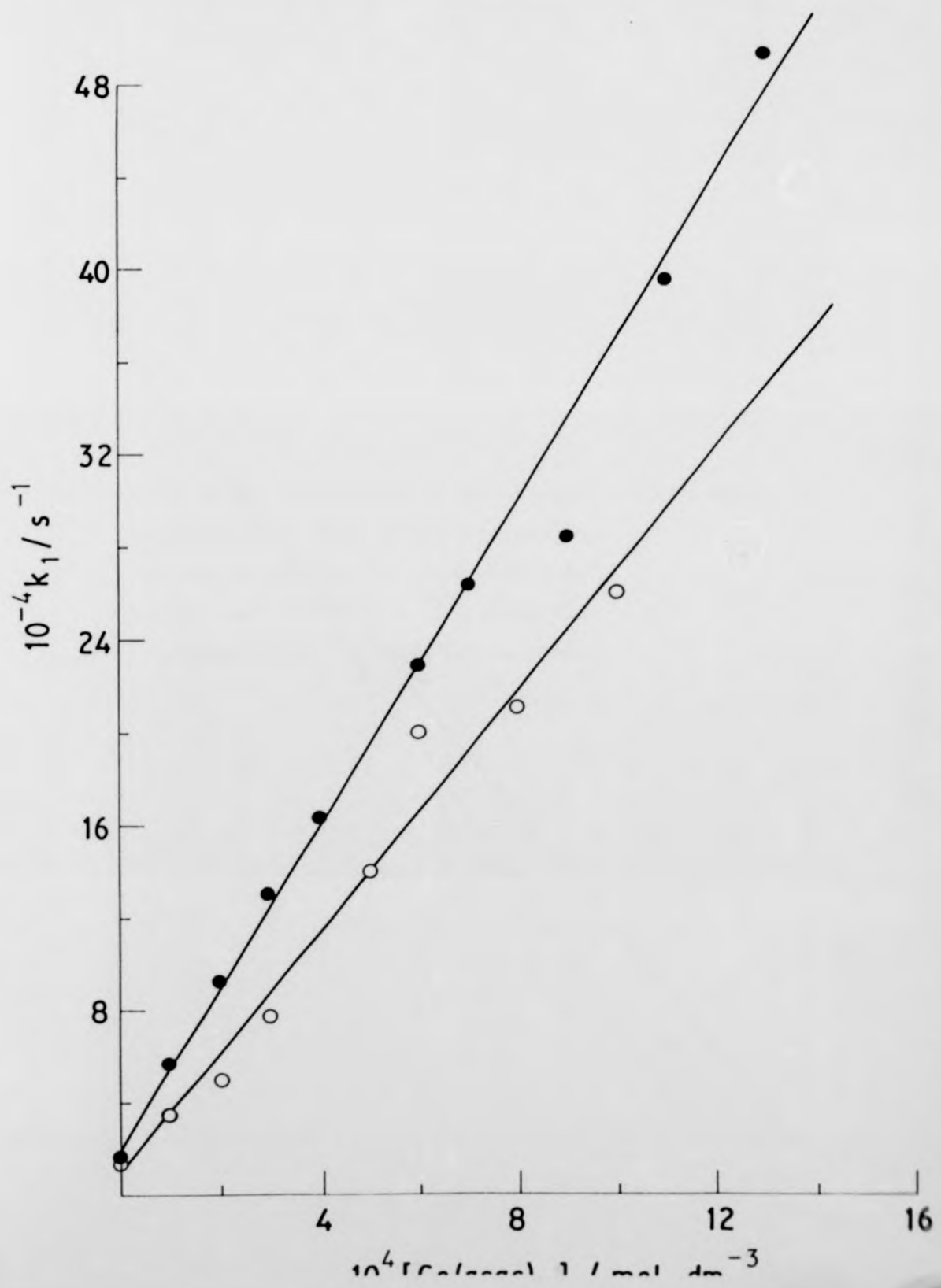


Figure 4.18 Dependence of first-order decay constants of excited states upon concentration of  $\text{Co}(\text{acac})_3$ . ●, Excited state of  $[\text{Cr}(\text{phen})_3]^{3+}$  in acetone. ○, Excited state of  $[\text{Cr}(\text{bpy})_3]^{3+}$  in acetone.

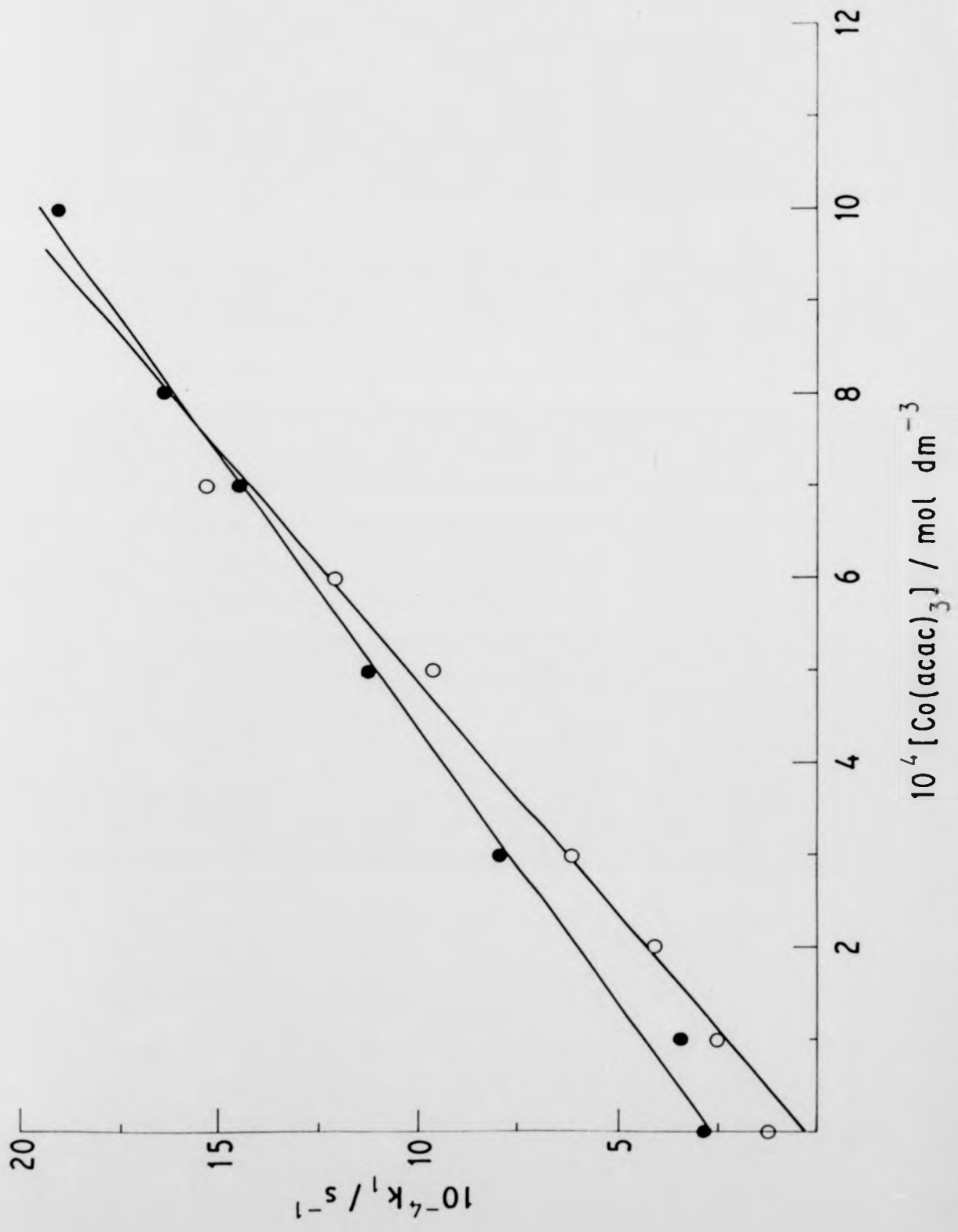


Figure 4.19 Dependence of first-order decay constants of excited states upon concentration of  $\text{Co}(\text{acac})_3$ . ●, Triplet state of eosin in methanol. ○, Triplet state of 9,10-dichloroanthracene in dioxane.

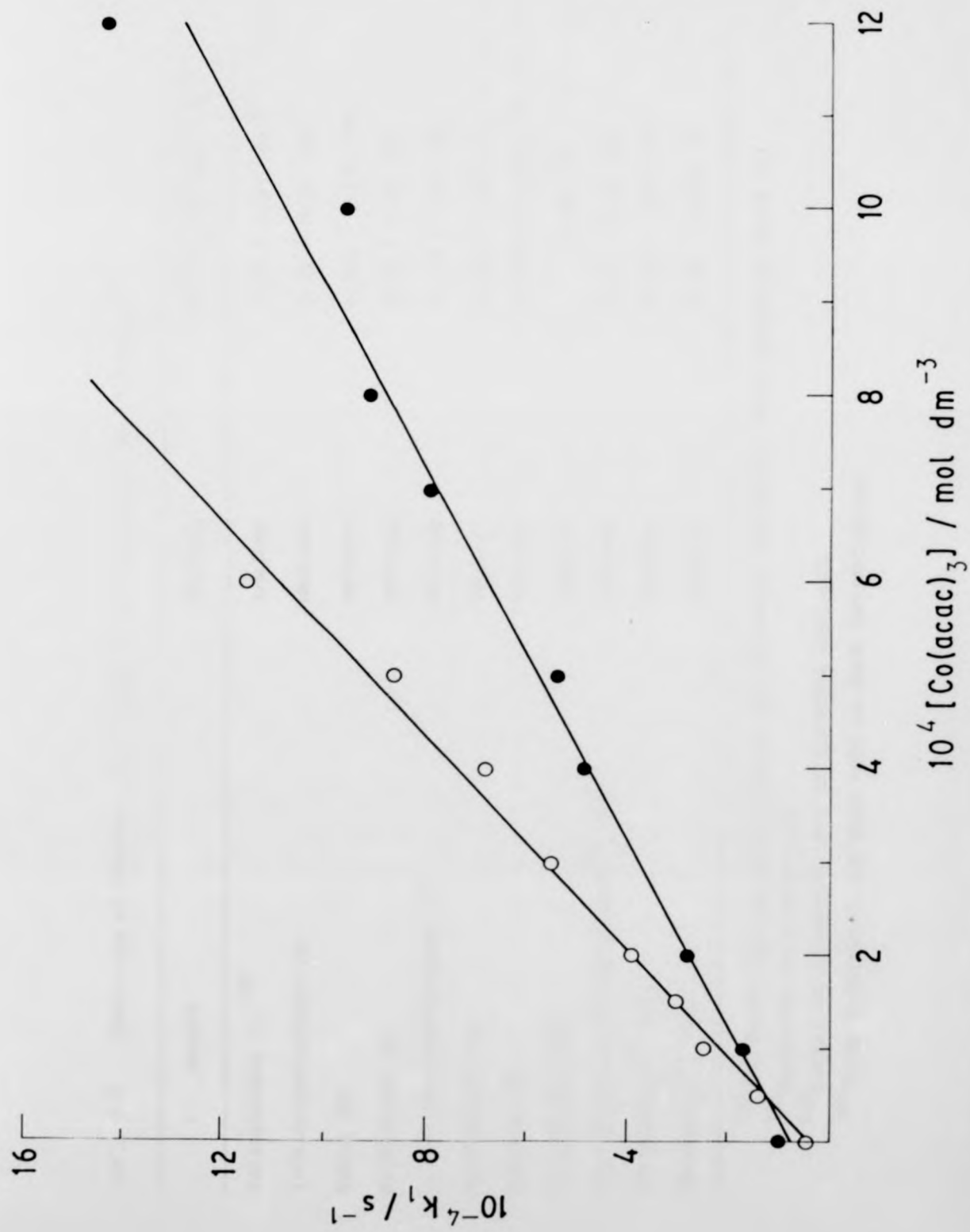


Table 4.5 Quenching of Organic and Inorganic Excited States by Co(acac)<sub>3</sub> (a)

| Donors                                        | Solvent                         | $10^{-9} k_q / \text{dm}^3 \text{ mol}^{-1} \text{ s}^{-1}$ |
|-----------------------------------------------|---------------------------------|-------------------------------------------------------------|
| Benzophenone (1) (b)                          | Acetone                         | $3.26 \pm 0.23$ (9) (c)                                     |
| 1-Chloroanthracene (4)                        | Methanol                        | $0.35 \pm 0.01$ (10)                                        |
| Eosin (5)                                     | Methanol                        | $0.103 \pm 0.006$ (9)                                       |
| Erythrosin (6)                                | Methanol                        | $0.26 \pm 0.02$ (6)                                         |
| 9,10-Dichloroanthracene (7)                   | Dioxane                         | $0.173 \pm 0.01$ (9)                                        |
| Naphthacene (8)                               | CH <sub>2</sub> Cl <sub>2</sub> | $0.195 \pm 0.02$ (7)                                        |
| Rubrene (9)                                   | Benzene                         | $0.0360 \pm 0.0031$ (d) (4)                                 |
| $\beta$ -Carotene (10)                        | Acetone                         | < 0.02 (7)                                                  |
| Bis-(8-hydroxyquinolato)Pt <sup>II</sup> (14) | Acetone                         | $0.89 \pm 0.05$ (9)                                         |
| [Cr(phen) <sub>3</sub> ] <sup>3+</sup> (15)   | Acetone                         | $0.167 \pm 0.01$ (7)                                        |
| [Cr(bpy) <sub>3</sub> ] <sup>3+</sup> (16)    | Acetone                         | $0.197 \pm 0.02$ (7)                                        |

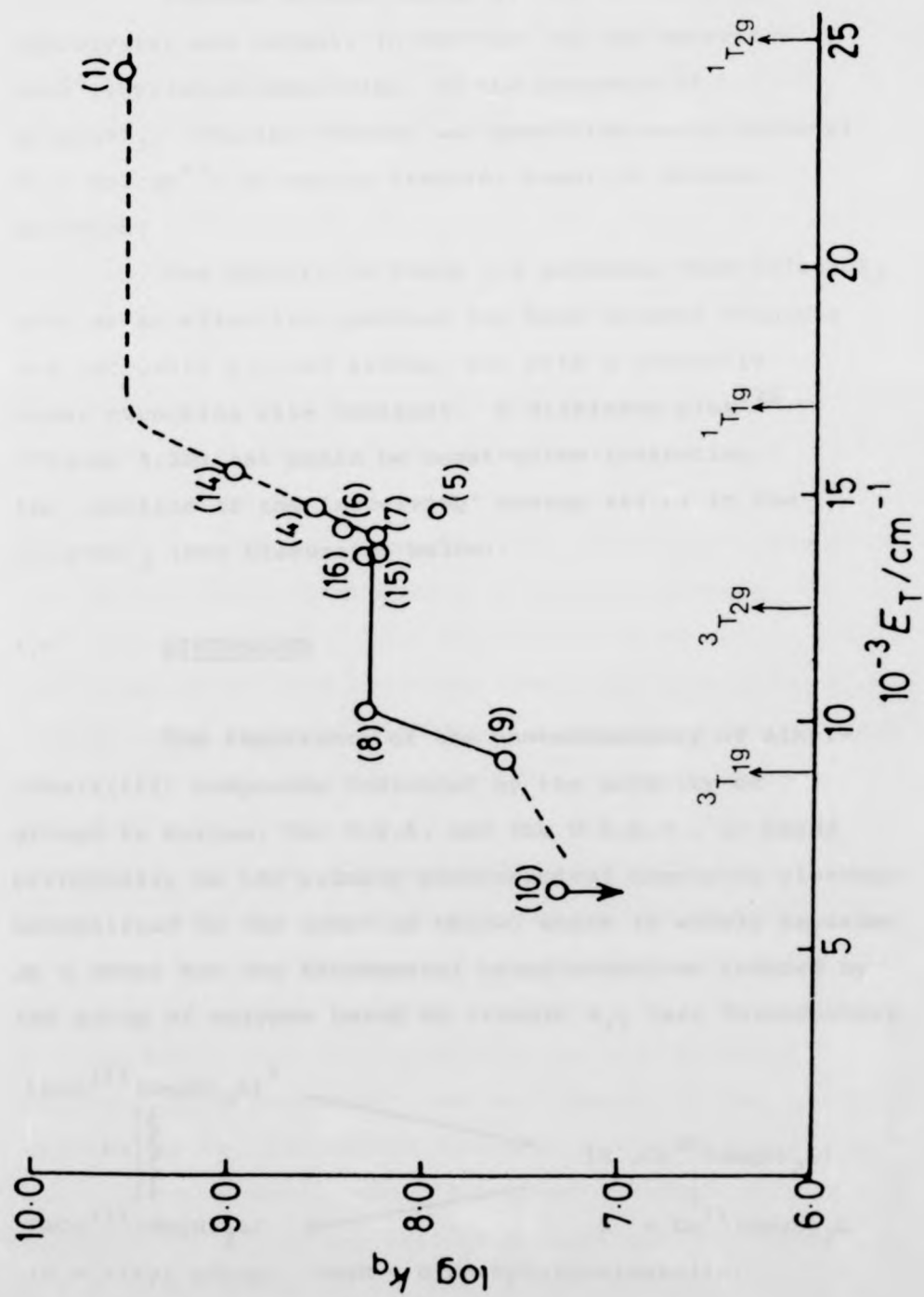
(a) The donor excited state energy and analysing wavelength were listed in Table 4.1

(b) Numbering in Figure 4.20

(c) Number of concentrations of quencher employed

(d) Three determinations were made at each concentration

Figure 4.20 Plot of the logarithm second-order quenching constant  $\log k_q$  against donor energy for quenching by  $\text{Co}(\text{acac})_3$ . Numbering key as in Table 4.5.

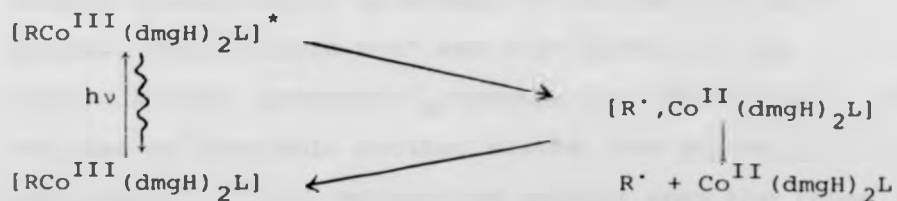


Rubrene triplet decay at 475 nm (by pulse radiolysis) was normal, in contrast to the behaviour with ethyl(aquo)cobaloxime, in the presence of  $\text{Co}(\text{acac})_3$ . Triplet rubrene was generated using biphenyl ( $0.1 \text{ mol dm}^{-3}$ ) as energy transfer agent in benzene solution.

The results in Table 4.5 indicate that  $\text{Co}(\text{acac})_3$  acts as an effective quencher for both organic triplets and inorganic excited states, but with a generally lower quenching rate constant. A Wilkinson plot<sup>219</sup> (Figure 4.20) can again be constructed indicating the location of the 'receiving' energy states in the  $\text{Co}(\text{acac})_3$  (see Discussion below).

#### 4.6 DISCUSSION

The importance of the photochemistry of alkylcobalt(III) compounds indicated by the activity of groups in Europe, the U.S.A. and the U.S.S.R., is based principally on the primary photochemical homolytic cleavage exemplified in the equation below, which is widely regarded as a model for the biochemical transformations induced by the group of enzymes based on vitamin  $\text{B}_{12}$  (see Introductory



(R = Alkyl group; dmgH = dimethylglyoximato(1-);

L = any Lewis base)

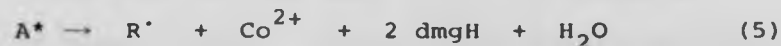
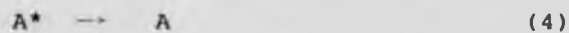
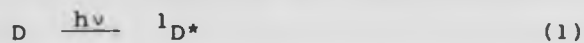
Section 2.1.3). This mechanism is now widely accepted as the main photoprocess for both alkylcobaloximes and alkylcobalamins, especially as a result of the spin-trapping of  $R^{\cdot}$  in solution<sup>229,230</sup>, and the detection by e.s.r. of an  $R^{\cdot}$ -Co<sup>II</sup> interaction in the solid state following photolysis<sup>231-234</sup>.

Because of the ready photodecomposition of alkylcobaloximes with light of rather low energy<sup>122</sup>, it seemed probable that these compounds would be very potent quenchers of triplet excited states of organic molecules and excited states of inorganic complexes, and furthermore, that their decomposition might be sensitised by energy-transfer, as are those for example, of hexammine and aquopentammine complexes of Co(III) by organic triplet states<sup>86,235</sup>. This is significant because sensitisation of (and by) transition metal complexes is a powerful means of studying the detailed photochemistry and spectroscopy of these compounds<sup>39</sup> because of the possibility of selecting individual states by energy transfer from donor of appropriate energy.

From the Tables and Figures in the previous Sections in this Chapter, it is clear that alkylcobalt(III) compounds are highly effective quenchers of both organic triplet states and of a variety of excited inorganic species. This covers  $n-\pi^*$  and  $\pi-\pi^*$  states in the organic series, provided  $E_T$  exceeds *ca.* 170 kJ mol<sup>-1</sup>. In the case of inorganic excited states, the reduction potentials<sup>48,224</sup> of the excited species span the range + 0.84 V for  $[\text{Ru}(\text{bpy})_3]^{2+}$ \* to + 2.60 V for  $[\text{UO}_2]^{2+}$ \*.

and the insensitivity of the quenching rate to these reduction potentials which differ by 1.8 V, indicates a quenching mechanism of energy-transfer rather than electron-transfer. Moreover, the very high values for  $k_q$  indicate the process to be one of energy-transfer throughout the series, and this view is supported by the much lower quenching efficiencies, both by ethyl(aquo)cobaloxime and  $\text{Co}(\text{acac})_3$ , towards naphthacene, rubrene, and  $\beta$ -carotene because of their lower triplet energies. The generally similar overall pattern of the Wilkinson plots (Figs. 4.7 and 4.20) of the two quenchers implies a common quenching mechanism, i.e. energy-transfer.

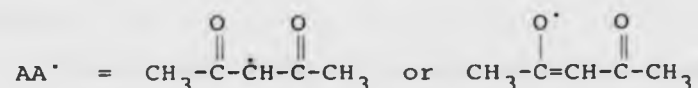
The role of energy-transfer is further supported by spectral measurements during photosensitisation experiments. In all cases, simple photodecomposition of ethyl(aquo)cobaloxime appeared to take place to give  $[\text{Co}(\text{H}_2\text{O})_6]^{2+}$ , free ligand, and alkyl ligand-derived products rather than the semi-reduced or semi-oxidised species:



where D = donor excited state, and A = ethyl(aquo)-cobaloxime. When A represents  $\text{Co}(\text{acac})_3$ , reaction (5) becomes:



where



(However, this will feature a very low quantum yield judging from photodecomposition quantum yields with visible irradiation<sup>3</sup>.) Although a number of organic triplet donors have been used to photodecompose  $\text{Co}(\text{III})$  complexes<sup>86,235</sup>, rather few attempts have been made to assess the exact energy requirements of the sensitisation process. Interestingly, while benzophenone and 2-acetophenone triplets sensitise the redox decomposition of  $\text{Co}(\text{dtp})_3$ , ( $\text{dtp}^- = \text{EtOPS}_2$ ), benzil triplet fails in this respect, indicating the dissociative level to lie at about  $247 \text{ kJ mol}^{-1}$ <sup>236</sup>.

The failure to protect the excited ethyl(aquo)-cobaloxime from decomposition by energy-transfer using a low-energy acceptor (Methylene Blue), simply reflects the extremely short life-time of the excited state of alkylcobalt(III) compounds which is on the ps time scale for methylcobalamin according to Endicott<sup>124</sup>.

Note that we have been unable to evaluate the role of donor *singlet* states in the sensitisation of

ethyl(aquo)cobaloxime (because of spectral overlap between donor and acceptor); however, we know that the donor triplet states interact strongly from the kinetic measurements, and thus the balance of probability favours these as the sensitising states. Again, erythrosin has a very high triplet quantum yield of practically unity (Bowers and Porter<sup>237</sup>), precluding any role for singlet erythrosin.

Sensitised chemical reactions of an acceptor may arise as a result of energy-transfer or chemical interaction, (such as electron transfer or hydrogen-atom abstraction) and it is only when the occurrence of the sensitised reactions of the acceptor is shown to be critically dependent on the energy of the excited state of the donor, and not on its chemical nature (e.g. reduction potential), that energy-transfer can be accepted as the most probable mechanism<sup>238</sup>.

The results depicted in Figures 4.7 and 4.20 demonstrate a strong relation between the rate constants for quenching and the energies of the excited states of the donors for both Co(III) complexes, which confirms that the mechanism of quenching is electronic energy-transfer. Hence if the mechanism of quenching is energy-transfer, it is not surprising that the quenching efficiencies of both complexes (ethyl(aquo)cobaloxime and Co(acac)<sub>3</sub>) drop off sharply for those triplet donors, such as rubrene and  $\beta$ -carotene, the triplet energies of which are estimated to lie below 120 kJ mol<sup>-1</sup>. The form of the triplet energy plots for ethyl(aquo)cobaloxime and Co(acac)<sub>3</sub> is just

what one might expect for quenching by energy transfer to several excited states within the complexes which have variable accepting probabilities. The discontinuities in the curves correlate very much with the spectroscopically determined energy levels. The quenching plateau in the region of  $\sim 3.5 \times 10^9 \text{ dm}^3 \text{ mol}^{-1} \text{ s}^{-1}$  for both complexes suggests diffusion-controlled energy-transfer where quenching is independent of the energy of the donor. The transitions within the complexes are shown above the abscissa in Figures 4.7 and 4.20. For  $\text{Co}(\text{acac})_3$  (Figure 4.20) the excited states labelled  ${}^3\text{T}_{1g}$  and  ${}^3\text{T}_{2g}$  at  $9,000$  and  $12,500 \text{ cm}^{-1}$  correspond to the spin-forbidden absorption maxima, while  ${}^1\text{T}_{1g}$  and  ${}^1\text{T}_{2g}$  to spin-allowed absorption maxima<sup>3</sup>. There is a fall-off in the quenching efficiency for donors with triplet energies much less than  $E({}^3\text{T}_{2g})$ , while triplet donors with energy more than  $E({}^1\text{T}_{1g})$  have high quenching efficiency following the plateau region. In the case of ethyl(aquo)cobaloxime, donor triplets with energies higher than  $15,000 \text{ cm}^{-1}$  have high quenching efficiency (Figure 4.7) leading to a plateau region. The spin-forbidden transitions in ethyl(aquo)cobaloxime are undetectable, and there is a noticeable fall-off in the quenching efficiency donors of triplet energy  $< 15,000 \text{ cm}^{-1}$  and an even sharper fall with donors of triplet energy  $< 10,000 \text{ cm}^{-1}$ , which indicates that there are more energy levels in this region. From the above-mentioned results we conclude that the mechanism of quenching of triplet organic donors

by  $\text{Co}(\text{acac})_3$  and ethyl(aquo)cobaloxime is electronic energy-transfer. As each level in the quencher becomes accessible for electronic energy-transfer, there is a marked rise in quenching ability with increasing triplet energy to a plateau value and no further increase in quenching rate constant is observed until a further excited state of the quencher is reached. This stepwise pattern follows that characterised by Wilkinson and co-workers and by others.<sup>213,219,239</sup>

CHAPTER 5

LUMINESCENCE KINETICS AND ELECTRON-TRANSFER  
QUENCHING OF BIS (POLYPYRIDYL) COMPLEXES OF  
RUTHENIUM(II)

5.1 INTRODUCTORY REMARKS

In recent years there has been an enormous growth in interest in the photophysics of transition metal complexes<sup>7,57,241,242</sup>. Most of the effort has been focused on the excited state chemistry of *tris*-chelated complexes of Ru(II)<sup>3</sup> with the ligands 2,2'-bipyridine (bpy) and 1,10-phenanthroline (phen). This is, firstly, because of the strong room temperature luminescence of these compounds<sup>130</sup>, which makes them easily monitored, secondly, because of their powerful photosensitising both of energy<sup>94,131,161,167</sup> and electron-transfer<sup>132,163,171,172</sup> processes of a wide range of both organic and inorganic acceptors, and thirdly, because of the potential of [Ru(bpy)<sub>3</sub>]<sup>2+</sup> as a component of a solar energy storage system<sup>243</sup>. Earlier, in this laboratory, it was examined how the excited state lifetimes ( $\tau$ ) of a variety of luminescent metal complexes, including those of Ru(II)<sup>154</sup>, Cr(III)<sup>245</sup>, Pt(II)<sup>226</sup>, Os(II)<sup>246</sup> and U(VI)<sup>244</sup>, were dependent strongly on temperature in the range 77 - ca. 370 K in LiCl-water (and D<sub>2</sub>O) glasses, organic solvents, and polymer film (cellulose acetate). The following effects were examined: (i) that of various solvent transitions such as the glass transition temperature ( $T_g$ ), and also freezing, in inducing sharp discontinuities in rate-temperature profiles; (ii) the effect on lifetimes of (a) gross change of solvent characteristics, and (b) deuteration of solvent O-H groups. These various observations indicated an important role of the solvent in the sum of non-radiative

decay processes, a view also supported by very detailed examination of the solvent-dependence of the lifetime of  $[\text{Cr}(\text{NH}_3)_4(\text{NCS})_2]^-$  ion which has featured in several recent review articles<sup>7,247,248</sup>. In general, the temperature dependence of  $\tau$  derives from two terms, equation 5.1,

$$k_{\text{obs}} = \tau^{-1} = A_1 \exp(-\Delta E_1/RT) + A_2 \exp(-\Delta E_2/RT) \quad (5.1)$$

namely (i), a term with a large energy component  $\Delta E_1$  combined with a large frequency factor  $A_1$  (this term dominates at  $T > ca. 250 \text{ K}$ ) and (ii), a term featuring a small energy component  $\Delta E_2$  of a few  $\text{kJ mol}^{-1}$ , or even zero, combined with a small frequency factor  $A_2$ ; the latter term dominates at  $T < 150 \text{ K}$ <sup>145,226,244-246</sup>.

In this part of the work we examined the dependence of the excited state lifetime on temperature for mixed-ligand complexes of Ru(II), having regard to understanding how the various components of  $\tau$  given in equation 5.1 are influenced by the nature of the ligands. We have also studied how the rates of electron-transfer quenching of these complexes depend on the chelating ligands, which greatly influence their excited state reduction potentials, analysing the results in terms of the Rehm-Weller treatment and making comparison with oxidative quenching of  $*[\text{Ru}(\text{bpy})_3]^{2+}$ <sup>174,249</sup>.

5.2 LUMINESCENCE SPECTRA AND LIFETIME MEASUREMENTS IN DIFFERENT SOLVENTS

The effects of temperature and solvent on both the luminescence lifetime and spectrum of different mixed-ligand complexes of Ru(II), of the type  $[\text{Ru}(\text{bpy})_2\text{X}]^{n+}$  or  $[\text{Ru}(\text{phen})_2\text{X}]^{n+}$  where X = an aliphatic chelate or a monodentate ion or molecule, have been investigated. The absorption spectra of the complexes,  $[\text{Ru}(\text{bpy})\text{en}]^{2+}$ ,  $[\text{Ru}(\text{bpy})_2\text{acac}]^+$ ,  $[\text{Ru}(\text{bpy})_2(\text{NH}_3)_2]^{2+}$ ,  $[\text{Ru}(\text{bpy})_2\text{Cl}_2]$ ,  $[\text{Ru}(\text{phen})_2\text{en}]^{2+}$ ,  $[\text{Ru}(\text{phen})_2\text{Cl}_2]$ , and  $[\text{Ru}(\text{phen})_2\text{acac}]^+$ , were identical to those reported in the literature<sup>208-211</sup>. These complexes exhibited quite strong luminescence at 77 K and, in some cases, reasonable luminescence at room temperature. The luminescence spectra of these complexes, both at room temperature and 77 K, are shown in Figures 5.1 to 5.7.  $[\text{Ru}(\text{bpy})_2\text{en}]^{2+}$ , which is fairly typical of the whole series in its spectral behaviour, shows two emission maxima at  $\sim 680$  and 725 nm (Figure 5.1) at room temperature, the position of which do not vary much with solvent. Using DMSO as a solvent, the 680 nm peak appears as a shoulder to the main peak centred at 725 nm. The emission peak at 680 nm shows a marked shift towards the blue (to about 660 nm) for  $[\text{Ru}(\text{bpy})_2\text{en}]^{2+}$  in aqueous LiCl at 77 K, but there is no change in the position of the peak at 725 nm (Figure 5.2). The emission intensity is barely affected by the presence of oxygen. The luminescence spectrum of  $[\text{Ru}(\text{bpy})_2(\text{NH}_3)_2]^{2+}$  is similar to that of  $[\text{Ru}(\text{bpy})_2\text{en}]^{2+}$ , while that of

Figure 5.1 Luminescence spectra of  $[\text{Ru}(\text{bpy})_2\text{en}]^{2+}$   
in different solvents.

- (a) MeOH
- (b)  $\text{H}_2\text{O}$
- (c)  $\text{Me}_2\text{CO}$
- (d) DMSO
- (e) MeCN

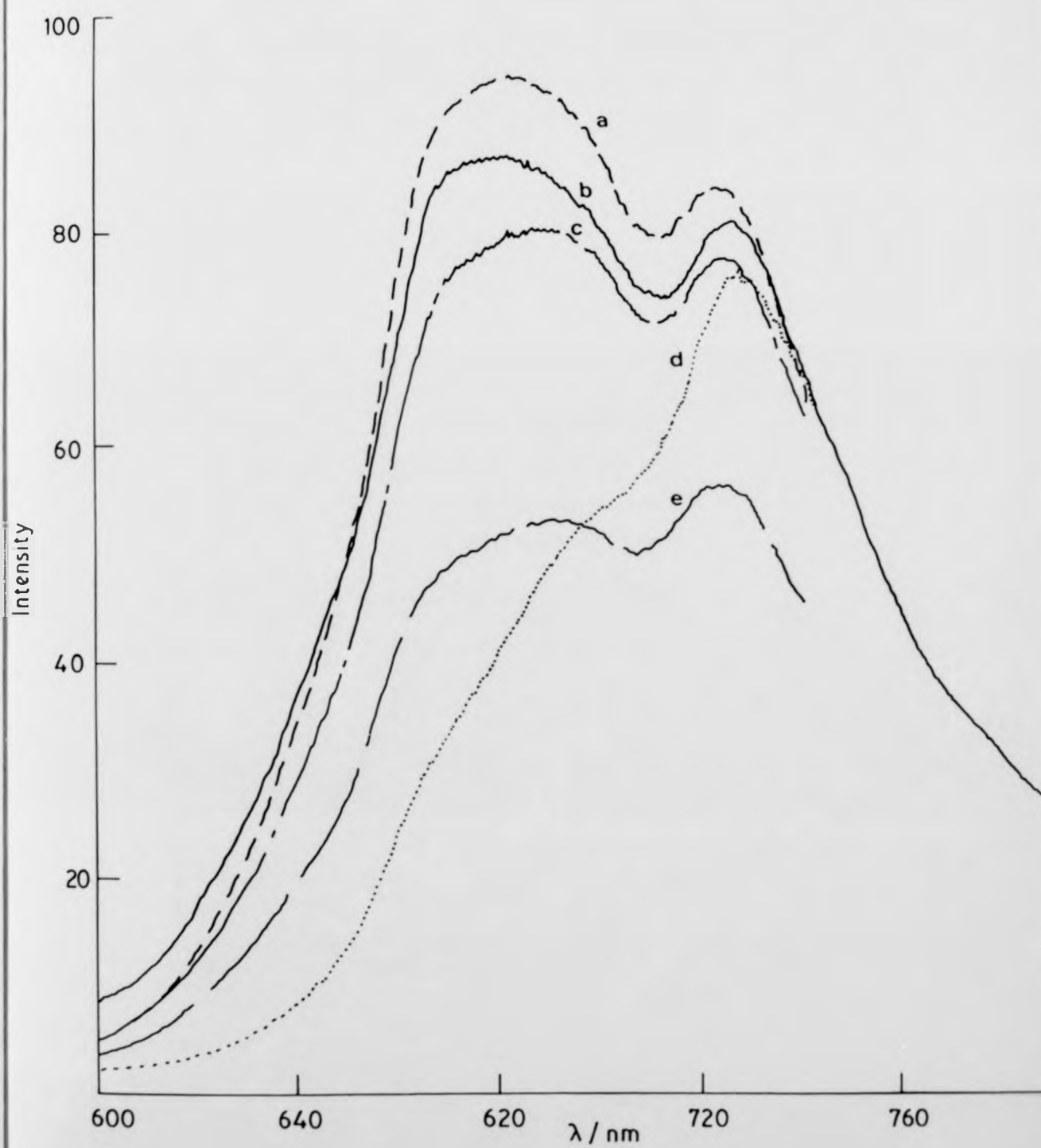


Figure 5.2 Luminescence spectra of  $[\text{Ru}(\text{bpy})_2\text{en}]^{2+}$   
in  $9 \text{ mol dm}^{-3}$   $\text{LiCl-H}_2\text{O}$  solvent at  
room temperature (full line) and at  
82 K (broken line).

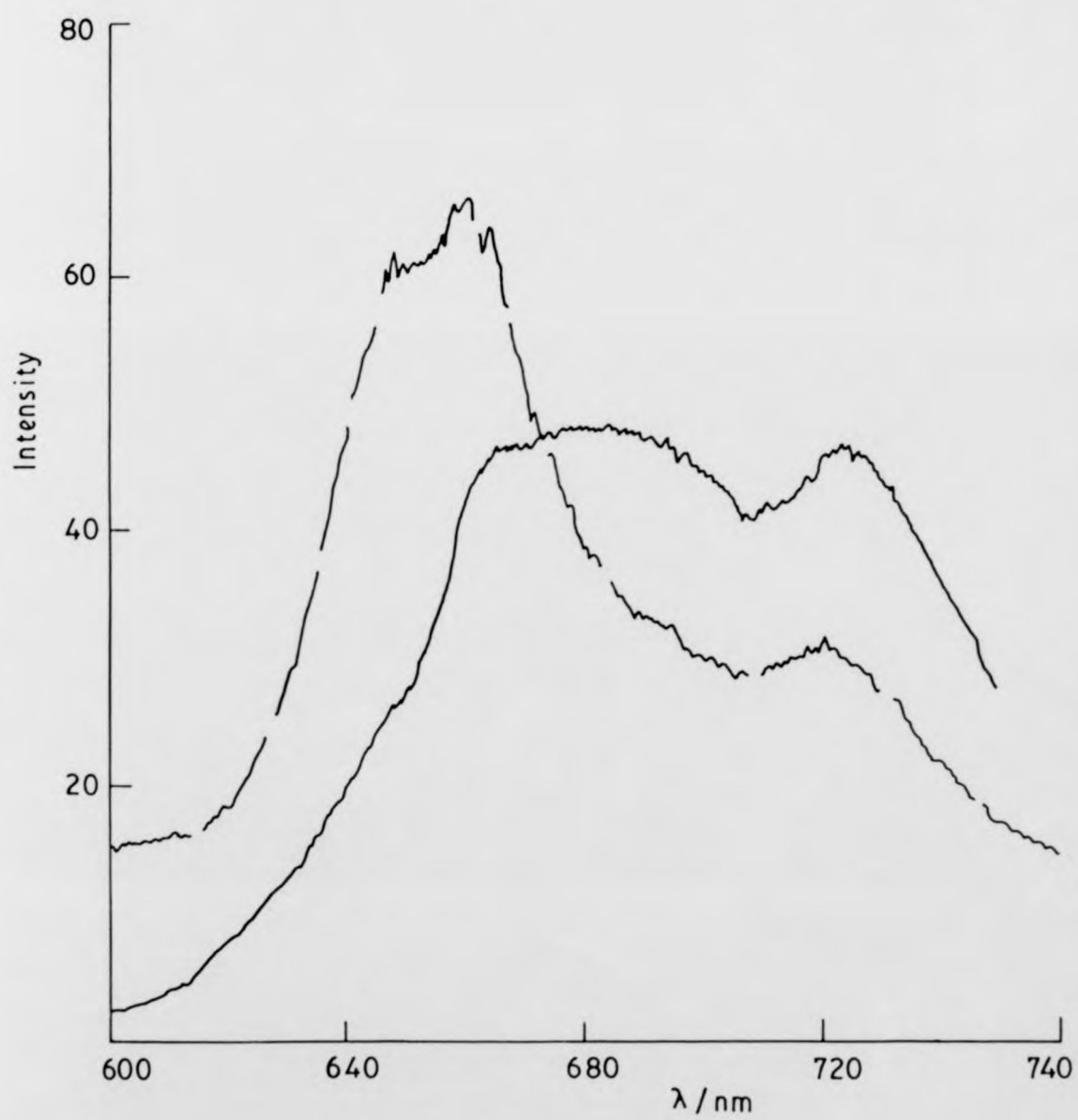


Figure 5.3 Luminescence spectra of  $[\text{Ru}(\text{bpy})_2(\text{NH}_3)_2]^{2+}$  in EtOH-MeOH (4:1) at 82 K (a) and  $[\text{Ru}(\text{bpy})_2\text{Cl}_2]$  in MeCN at room temperature (b).

10  
8  
Intensity  
6

2+

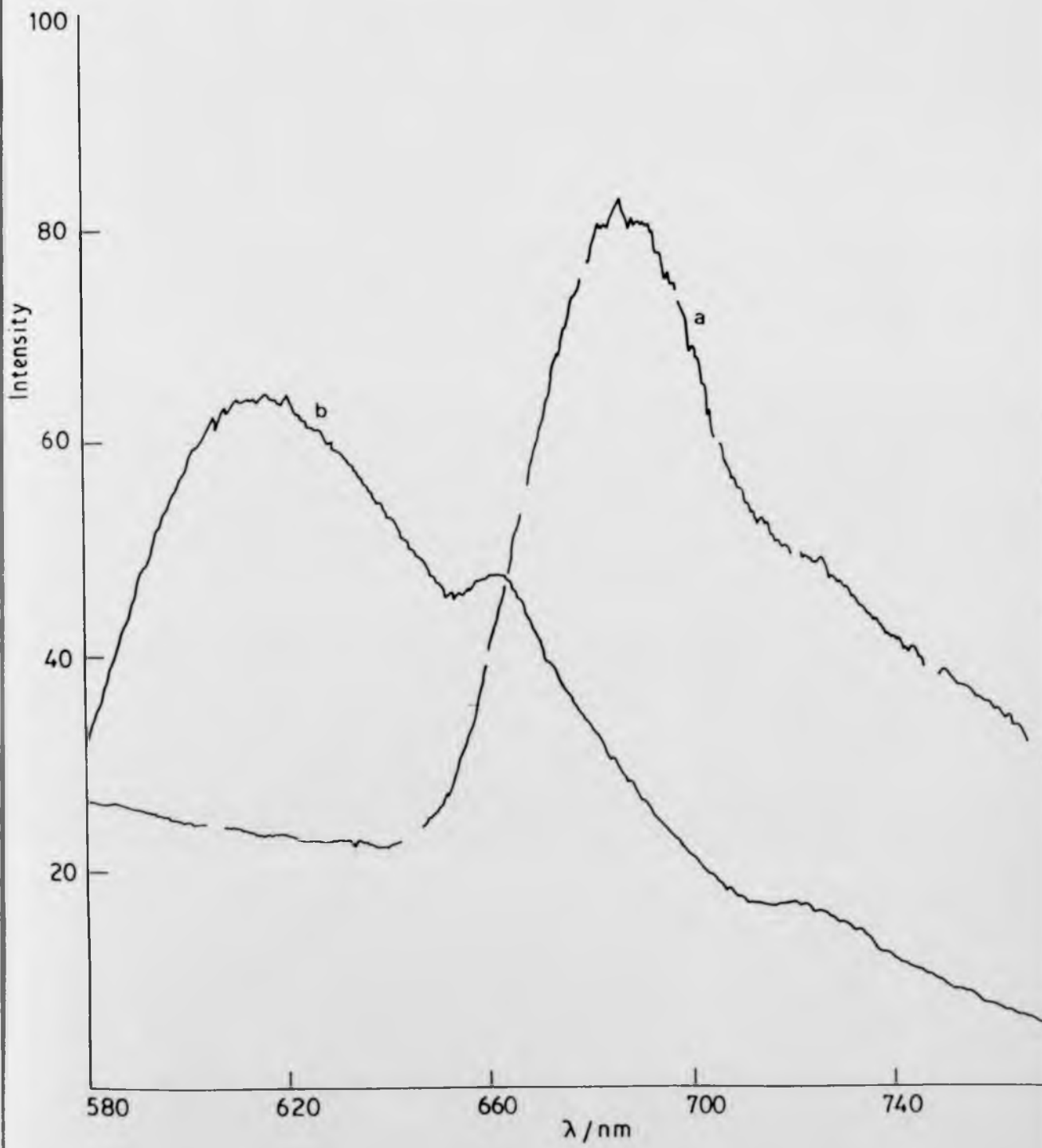


Figure 5.4 Luminescence spectra of  $[\text{Ru}(\text{bpy})_2\text{acac}]^+$  at room temperature in MeCN (a) and  $\text{Me}_2\text{CO}$  (b).

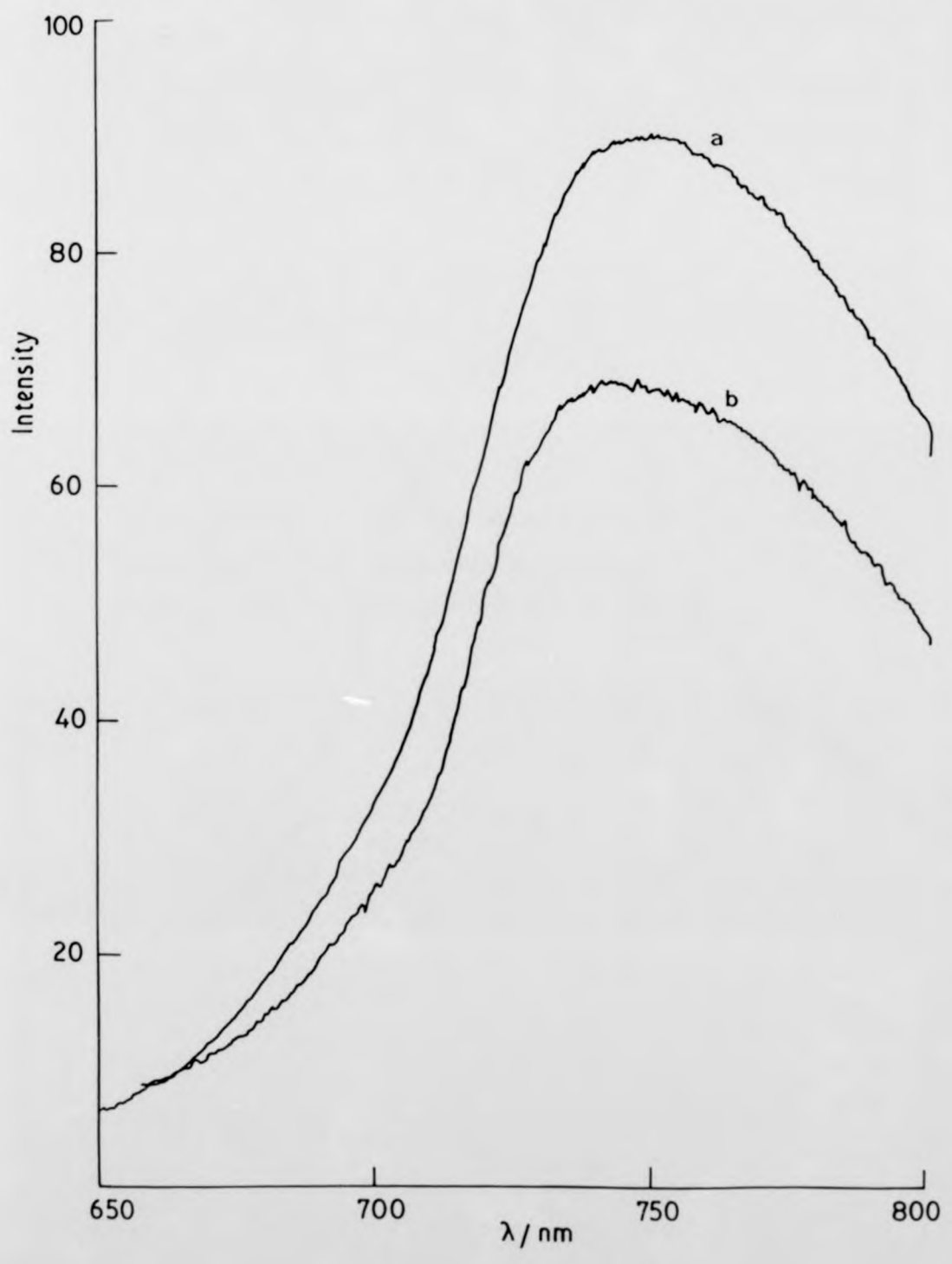


Figure 5.5 Luminescence spectra of  $[\text{Ru}(\text{bpy})\text{acac}]^+$   
at 82 K in EtOH-MeOH (4:1) (full line)  
and  $9 \text{ mol dm}^{-3}$  LiCl-H<sub>2</sub>O (broken line).

Intensity

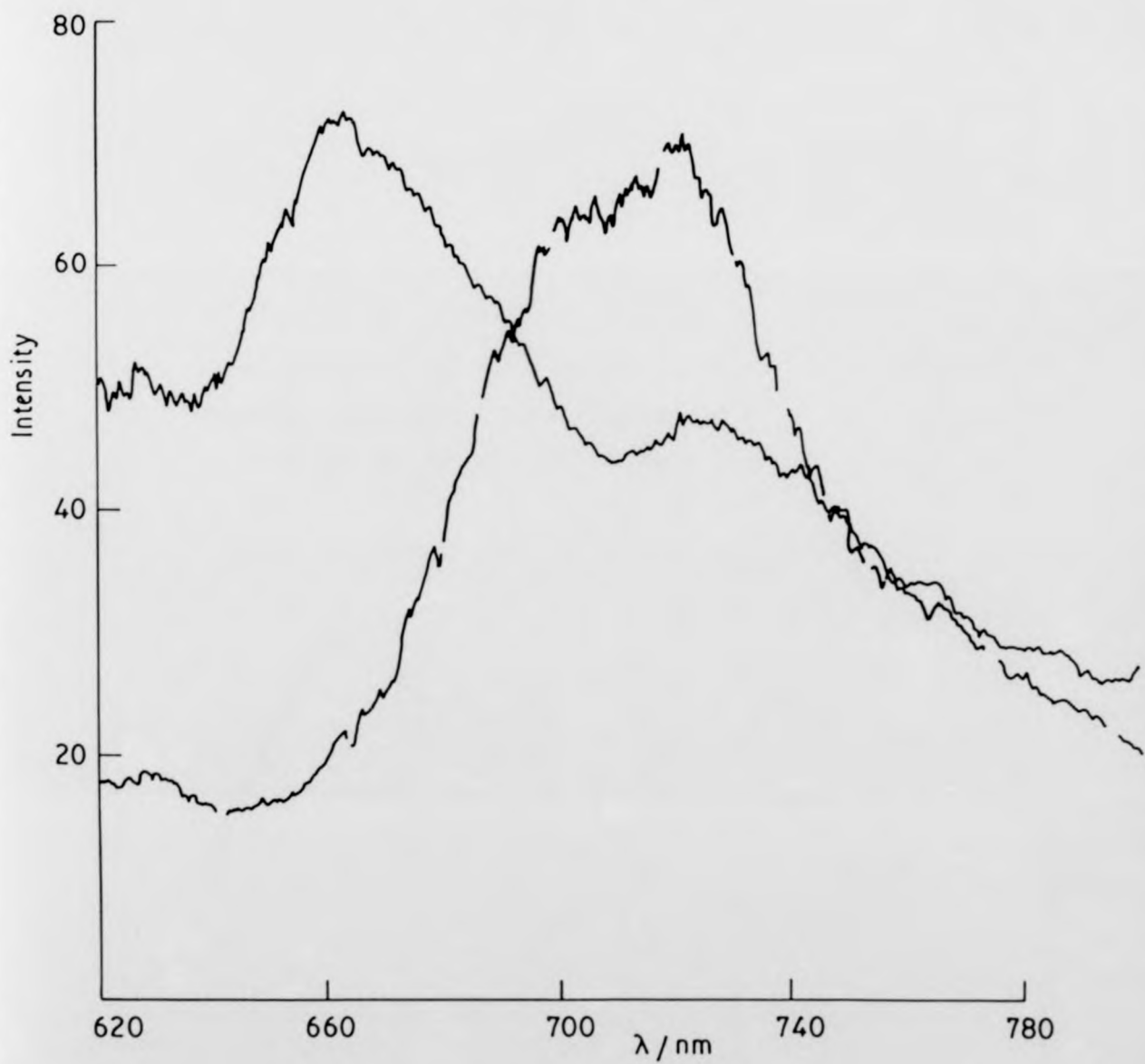


Figure 5.6 Luminescence spectra of  $[\text{Ru}(\text{phen})_2\text{en}]^{2+}$   
in  $9 \text{ mol dm}^{-3}$   $\text{LiCl-H}_2\text{O}$  solvent at room  
temperature (full line) and at 82 K  
(broken line).

Intensity

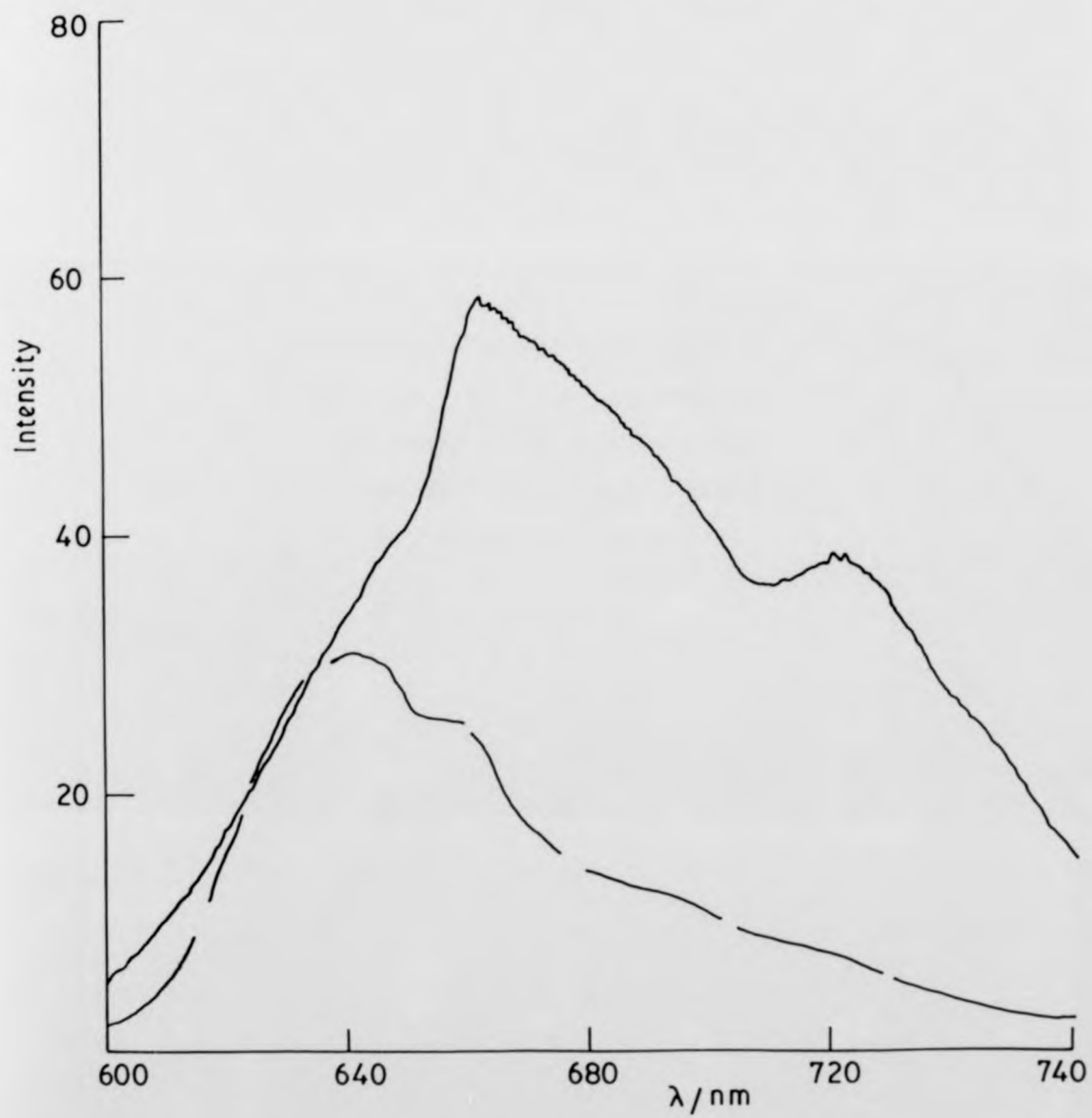


Figure 5.7 Luminescence spectra at 82 K of  
 $[\text{Ru}(\text{phen})_2\text{acac}]^+$  in cellulose  
acetate film (full line) and  
 $[\text{Ru}(\text{phen})_2\text{Cl}_2]$  in EtOH-MeOH  
(4:1) solvent (broken line).

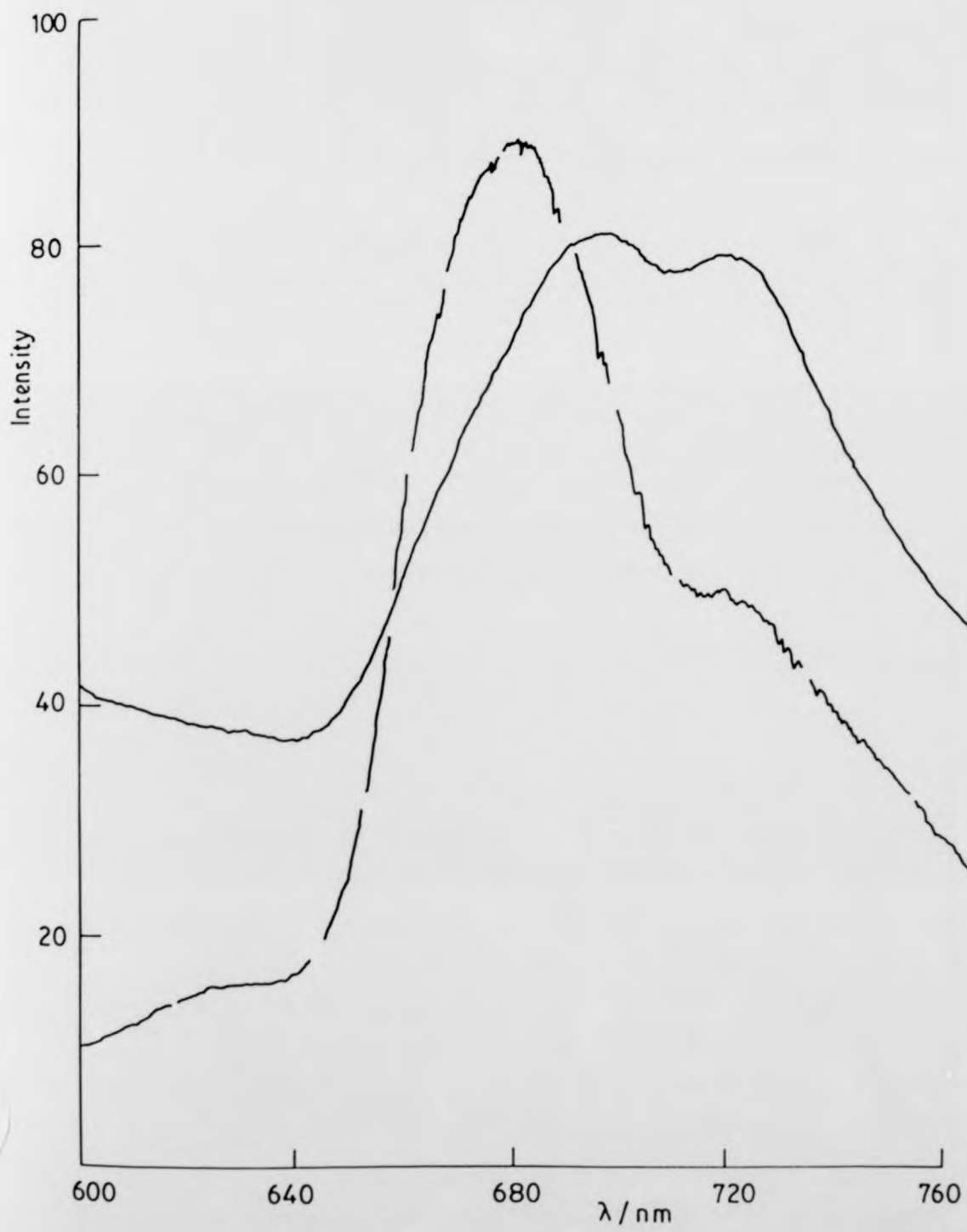
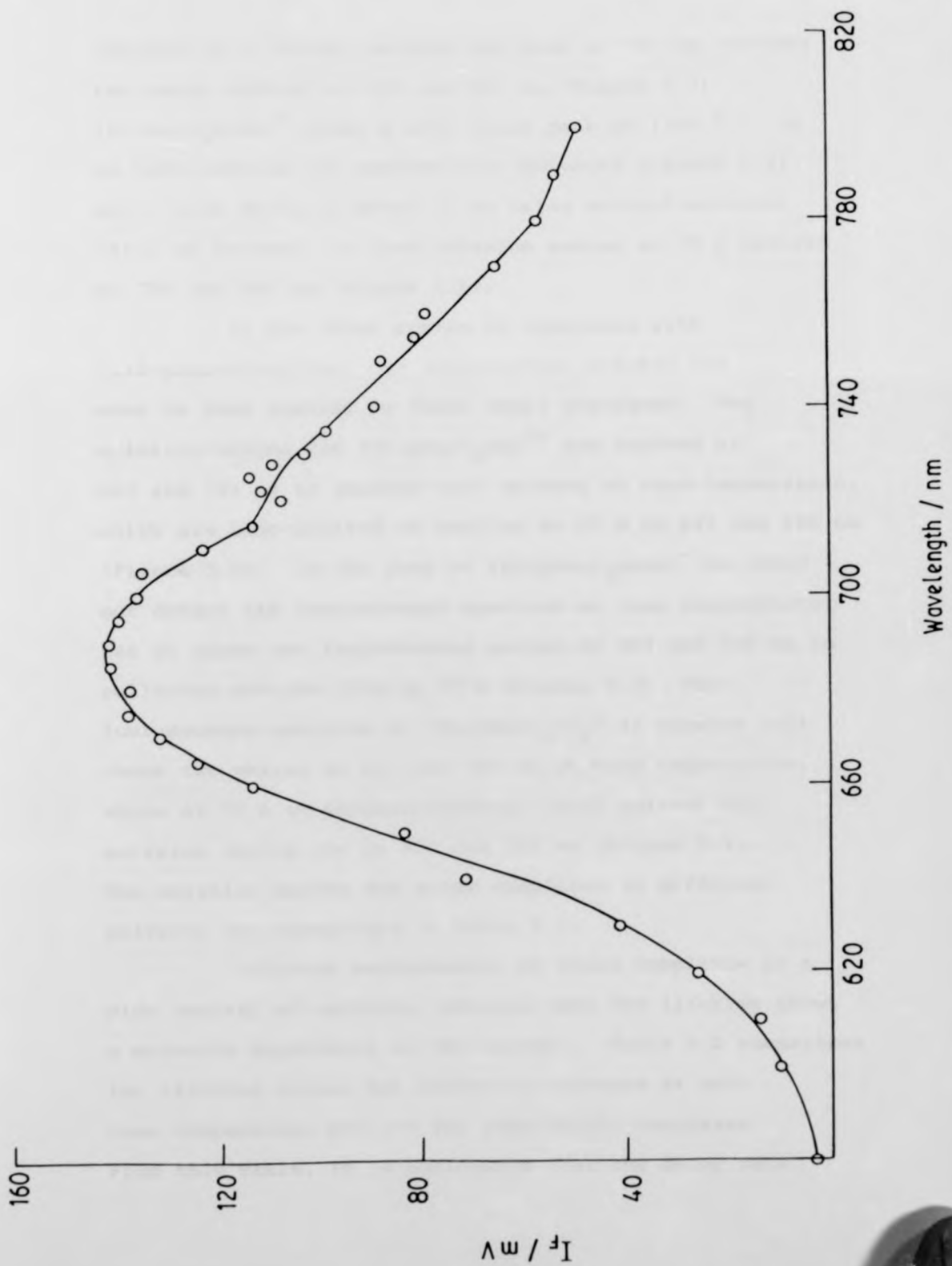


Figure 5.8 Luminescence spectra of  $[\text{Ru}(\text{bpy})_2\text{en}]^{2+}$   
in  $\text{H}_2\text{O}$  at room temperature obtained  
by laser flash photolysis.



[Ru(bpy)<sub>2</sub>Cl<sub>2</sub>] shows, besides the peak at 720 nm, another two peaks centred at 615 and 660 nm (Figure 5.3).

[Ru(bpy)<sub>2</sub>acac]<sup>+</sup> shows a very broad peak at (745 ± 2) nm in both acetone and acetonitrile solvents (Figure 5.4), and a blue shift of about 20 nm using ethanol-methanol (4:1) as solvent, to give emission maxima at 77 K centred at 700 and 720 nm (Figure 5.5).

In the other system of complexes with 1,10-phenanthroline, the luminescence spectra are more or less similar to their (bpy) analogues. The emission maxima for [Ru(phen)<sub>2</sub>en]<sup>2+</sup> are centred at 662 and 721 nm in aqueous LiCl solvent at room temperature, which are blue-shifted on cooling to 77 K to 642 and 656 nm (Figure 5.6). In the case of [Ru(phen)<sub>2</sub>acac]<sup>+</sup> we could not detect its luminescence spectrum at room temperature, but it shows two luminescence maxima at 697 and 720 nm in cellulose acetate film at 77 K (Figure 5.7). The luminescence spectrum of [Ru(phen)<sub>2</sub>Cl<sub>2</sub>] in aqueous LiCl shows two maxima at 667 and 720 nm at room temperature, while at 77 K in ethanol-methanol (4:1) solvent the emission maxima are at 680 and 720 nm (Figure 5.7). The emission maxima for these complexes in different solvents are summarised in Table 5.1.

Lifetime measurements of these complexes in a wide variety of solvents indicate that the lifetime shows a moderate dependence on the solvent. Table 5.2 summarises the lifetime values for different solvents at both room temperature and 77K for some Ru(II) complexes. From this table, it is noticeable that the decay rate

Table 5.1 Emission maxima in different solvents for *bis* (polypyridyl) complexes of Ru(II)

| Complex                                                               | Solvent                 | Temperature /K | Emission Maxima /nm |
|-----------------------------------------------------------------------|-------------------------|----------------|---------------------|
| [Ru(bpy) <sub>2</sub> en] <sup>2+</sup>                               | H <sub>2</sub> O        | 294            | 680,725             |
|                                                                       | MeOH                    | 294            | 682,724             |
|                                                                       | Me <sub>2</sub> CO      | 294            | 688,725             |
|                                                                       | MeCN                    | 294            | 690,725             |
|                                                                       | DMSO                    | 294            | 725                 |
|                                                                       | 9MLiCl/H <sub>2</sub> O | 82             | 660,720             |
| [Ru(bpy) <sub>2</sub> (NH <sub>3</sub> ) <sub>2</sub> ] <sup>2+</sup> | EtOH-MeOH (4:1)         | 82             | 685                 |
|                                                                       | MeCN                    | 294            | 682,725             |
| [Ru(bpy) <sub>2</sub> Cl <sub>2</sub> ]                               | MeCN                    | 294            | 615,660,720         |
| [Ru(bpy) <sub>2</sub> acac] <sup>+</sup>                              | Me <sub>2</sub> CO      | 294            | 745                 |
|                                                                       | MeCN                    | 294            | 748                 |
|                                                                       | EtOH-MeOH (4:1)         | 83             | 700,720             |
|                                                                       | 9MLiCl/H <sub>2</sub> O | 82             | 662,722             |
| [Ru(phen) <sub>2</sub> en] <sup>2+</sup>                              | 9MLiCl/H <sub>2</sub> O | 294            | 662,721             |
|                                                                       | 9MLiCl/H <sub>2</sub> O | 83             | 642,656,720         |
| [Ru(phen) <sub>2</sub> acac] <sup>+</sup>                             | Cellulose Acetate Film  | 82             | 697,720             |
| [Ru(phen) <sub>2</sub> Cl <sub>2</sub> ]                              | EtOH-MeOH (4:1)         | 82             | 680,720             |

Table 5.2 Decay Constants for Ru(II) Complexes

| Complex                                        | Solvent                                        | Temperature /K                                 | $\tau^*/\text{ns}$ |
|------------------------------------------------|------------------------------------------------|------------------------------------------------|--------------------|
| [Ru(bpy) <sub>2</sub> en] <sup>2+</sup>        | H <sub>2</sub> O                               | 298.2                                          | 81.5               |
|                                                | D <sub>2</sub> O                               | 297.1                                          | 140.3              |
|                                                | CH <sub>3</sub> OH                             | 296.7                                          | 129.1              |
|                                                |                                                | 78.9                                           | 722.5              |
|                                                | CH <sub>3</sub> OD                             | 297.3                                          | 168.9              |
|                                                |                                                | 78.8                                           | 565.3              |
|                                                | 9 mol dm <sup>-3</sup> LiCl + H <sub>2</sub> O | 296.8                                          | 85.5               |
|                                                |                                                | 79.2                                           | 876.4              |
|                                                | 9 mol dm <sup>-3</sup> LiCl + D <sub>2</sub> O | 79.1                                           | 1469.5             |
|                                                |                                                | CH <sub>3</sub> CN                             | 297.2              |
|                                                | DMF                                            | 296.6                                          | 74.5               |
|                                                | DMSO                                           | 297.8                                          | 80.5               |
|                                                | Cellulose Acetate Film                         | 297.7                                          | 226.8              |
|                                                |                                                | 82.7                                           | 1101.3             |
|                                                | [Ru(bpy) <sub>2</sub> acac] <sup>+</sup>       | CH <sub>3</sub> CN                             | 296.3              |
| 9 mol dm <sup>-3</sup> LiCl + H <sub>2</sub> O |                                                | 81.2                                           | 500.7              |
|                                                |                                                | 9 mol dm <sup>-3</sup> LiCl + D <sub>2</sub> O | 80.8               |
| CH <sub>3</sub> OH                             |                                                |                                                | 80.2               |
| CH <sub>3</sub> OD                             |                                                | 80.6                                           | 833.0              |
| CD <sub>3</sub> OD                             |                                                | 79.9                                           | 769.2              |
| DMF                                            |                                                | 80.5                                           | 709.2              |
| MTHF                                           |                                                | 80.2                                           | 961.5              |
| Cellulose Acetate Film                         |                                                | 297.1                                          | 92.8               |
|                                                |                                                | 82.7                                           | 1141.5             |

Table 5.2 Decay Constants for Ru(III) Complexes  
(Continued)

| Complex                                                               | Solvent                                                     | Temperature<br>/K | $\tau^*/\text{ns}$ |
|-----------------------------------------------------------------------|-------------------------------------------------------------|-------------------|--------------------|
| [Ru(bpy) <sub>2</sub> (NH <sub>3</sub> ) <sub>2</sub> ] <sup>2+</sup> | 9 mol dm <sup>-3</sup> LiCl + H <sub>2</sub> O              | 238.3             | 57.5               |
|                                                                       |                                                             | 81.3              | 507.6              |
| [Ru(bpy) <sub>2</sub> Cl <sub>2</sub> ]                               | CH <sub>3</sub> CN                                          | 297.5             | 3 ± 0.5            |
| [Ru(phen) <sub>2</sub> acac] <sup>+</sup>                             | 9 mol dm <sup>-3</sup> LiCl + H <sub>2</sub> O              | 80.7              | 2087.7             |
| [Ru(phen) <sub>2</sub> Cl <sub>2</sub> ]                              | CH <sub>3</sub> OH + C <sub>2</sub> H <sub>5</sub> OH (1:4) | 81.3              | 2127.6             |
|                                                                       |                                                             | 181.7             | 970.9              |
| [Ru(phen) <sub>2</sub> en] <sup>2+</sup>                              | 9 mol dm <sup>-3</sup> LiCl + H <sub>2</sub> O              | 80.3              | 3246.7             |
|                                                                       |                                                             | 296.3             | 355.8              |

\*An Average of Two Determinations

constant in  $9 \text{ mol dm}^{-3}$  aqueous LiCl is faster for  $[\text{Ru}(\text{bpy})_2\text{en}]^{2+}$  than its analogue,  $[\text{Ru}(\text{phen})_2\text{en}]^{2+}$  at both room temperature and 77 K. The same behaviour was noticed with  $[\text{Ru}(\text{bpy})_2\text{acac}]^+$  and  $[\text{Ru}(\text{phen})_2\text{acac}]^+$  in the above-mentioned solvent, where decay of the former complex is much faster than the latter. Deuteriation of the solvent always lengthens the lifetime at all temperatures.

### 5.3 TEMPERATURE-DEPENDENCE STUDIES OF EMISSION LIFETIME RESULTS

The temperature-dependence of the lifetime of the emission from several *bis*(polypyridyl) complexes of Ru(II) have been investigated in a variety of solvents, using the experimental method described in Sections 3.1.1 and 3.1.2. The temperature range covered was as wide as possible, with restrictions being imposed by poor transmission of the solvent glass. The emission was monitored at the relevant wavelength of maximum intensity (Table 5.1), determined either by fluorimetry or laser flash photolysis. Both the luminescence (excitation wavelength = 347 nm) and the ground state absorption spectra of all the ruthenium(II) samples used were recorded at room temperature and none of the complexes showed any significant change with solvent environment.

The resultant activation data have been computer-fitted to a double exponential expression (2EXP).

$$k_{\text{obs}} = A_1 \exp(-\Delta E_1/RT) + A_2 \exp(-\Delta E_2/RT) \quad (5.1)$$

Equation 5.1 has been used by Kemp *et al.*<sup>250</sup> to fit activation data for  $[\text{Ru}(\text{bpy})_3]^{2+}$  over a similar range, and was originally described by Lytle and Hercules<sup>134</sup> who generalised equations used to rationalise thermally-activated ISC in substituted anthracenes.

The iterated values of the Arrhenius parameters for the double exponential expression obtained from the computer routine are given in Table 5.3 together with those results reported in the literature for both  $[\text{Ru}(\text{bpy})_3]^{2+}$  and  $[\text{Ru}(\text{phen})_3]^{2+}$ .

In adopting this double exponential fit, it appears that  $k_r$  has been neglected; however, this simplification can be explained in terms of the Crosby<sup>64</sup> model according to which the low-temperature luminescence from ruthenium(II) complexes originates from a tightly-grouped three-level manifold of emitting states. At temperatures of 70 K and above, at least 90% of the observed luminescence originates from the (thermally activated) highest level of this manifold.

An alternative expression was used by Van Houten and Watts<sup>65</sup> to fit their emission lifetime data for aqueous  $[\text{Ru}(\text{bpy})_3]^{2+}$  systems between 273 and 373 K, based on a single exponential expression (VHW).

$$k_{\text{obs}} = k_r + k_{\text{nr}} + A_1 \exp(-\Delta E_1/RT) \quad (5.2)$$

Table 5.3 Computer-Fitted Arrhenius Parameters for the Temperature-dependent Luminescence of Ru(II) Complexes

| Complex                                                               | Medium                                                | $10^{-13} A_1/s^{-1}$     | $\Delta E_1/kJ mol^{-1}$ | $10^{-6} A_2/s^{-1}$ | $\Delta E_2/kJ mol^{-1}$ | Source of fitted data |
|-----------------------------------------------------------------------|-------------------------------------------------------|---------------------------|--------------------------|----------------------|--------------------------|-----------------------|
| [Ru(bpy) <sub>3</sub> ] <sup>2+</sup>                                 | H <sub>2</sub> O                                      | 4.00 (2.01) (a)           | 46.72 (1.60)             | 4.27 (2.29)          | 2.64 (1.25)              | Ref. 250              |
|                                                                       |                                                       | 91.8 (58.6)               | 56.05 (2.00)             | 7.95 (3.93)          | 4.12 (1.18)              | Ref. 65               |
|                                                                       | D <sub>2</sub> O                                      | 5.37 (3.41)               | 47.26 (1.98)             | 1.05 (1.33)          | 0.74 (2.94)              | Ref. 250              |
|                                                                       |                                                       | 217.4 (65.4)              | 58.40 (0.94)             | 11.68 (4.70)         | 6.52 (0.96)              | Ref. 65               |
|                                                                       | DMF                                                   | 8.04 (2.47)               | 47.64 (0.93)             | 1.42 (0.41)          | 1.25 (0.62)              | Ref. 250              |
| Cellulose Acetate Film                                                | 1.73 x 10 <sup>-6</sup><br>(0.78 x 15 <sup>6</sup> )  | 9.61 (1.12)               | 0.50 (0.04)              | 0.64 (0.07)          | Ref. 154                 |                       |
| [Ru(bpy) <sub>2</sub> en] <sup>2+</sup>                               | 9MLiCl in H <sub>2</sub> O (< 200 K)                  | 1.61 x 10 <sup>-3</sup>   | 13.55 (1.20)             | 1.68 (0.11)          | 0.388 (0.13)             | This work             |
|                                                                       |                                                       | (0.1 x 10 <sup>-3</sup> ) |                          |                      |                          |                       |
|                                                                       | T > 200 K                                             | 4.76 x 10 <sup>-6</sup>   | 3.91 (0.51)              | -                    | -                        | This work             |
|                                                                       | 9MLiCl in D <sub>2</sub> O                            | 3.44 x 10 <sup>-3</sup>   | 18.09 (0.58)             | 0.76 (0.05)          | 0.25 (0.06)              | This work             |
| (1.07 x 15 <sup>3</sup> )                                             |                                                       |                           |                          |                      |                          |                       |
| T > 220 K                                                             | 5.91 x 10 <sup>-6</sup>                               | 6.04 (0.34)               | -                        | -                    | This work                |                       |
| Cellulose Acetate Film                                                | 5.13 x 10 <sup>-6</sup><br>(2.31 x 10 <sup>-6</sup> ) | 6.53 (1.31)               | 0.59 (0.05)              | Essentially Zero     | This work                |                       |
| [Ru(bpy) <sub>2</sub> (NH <sub>2</sub> ) <sub>2</sub> ] <sup>2+</sup> | 9MLiCl in H <sub>2</sub> O                            | 0.20 (0.03)               | 19.72 (9.28)             | 2.67 (0.26)          | 0.16 (0.11)              | This work             |

Table 5.3 Computer-Fitted Arrhenius Parameters for the Temperature-dependent Luminescence of Ru(II) Complexes

| Complex              | Medium                     | $10^{-13} A_1/s^{-1}$                              | $\Delta E_1/kJ mol^{-1}$ | $10^{-6} A_2/s^{-1}$ | $\Delta E_2/kJ mol^{-1}$ | Source of fitted data |
|----------------------|----------------------------|----------------------------------------------------|--------------------------|----------------------|--------------------------|-----------------------|
| $[Ru(bpy)_3]^{2+}$   | $H_2O$                     | 4.00 (2.01) (a)                                    | 46.72 (1.60)             | 4.27 (2.29)          | 2.64 (1.25)              | Ref. 250              |
|                      |                            | 91.8 (58.6)                                        | 56.05 (2.00)             | 7.95 (3.93)          | 4.12 (1.18)              | Ref. 65               |
|                      | $D_2O$                     | 5.37 (3.41)                                        | 47.26 (1.98)             | 1.05 (1.33)          | 0.74 (2.94)              | Ref. 250              |
|                      |                            | 217.4 (65.4)                                       | 58.40 (0.94)             | 11.68 (4.70)         | 6.52 (0.96)              | Ref. 65               |
|                      | DMF                        | 8.04 (2.47)                                        | 47.64 (0.93)             | 1.42 (0.41)          | 1.25 (0.62)              | Ref. 250              |
|                      | Cellulose Acetate Film     | $1.73 \times 10^{-6}$<br>( $0.78 \times 10^{-6}$ ) | 9.61 (1.12)              | 0.50 (0.04)          | 0.64 (0.07)              | Ref. 154              |
| $[Ru(bpy)_2en]^{2+}$ | 9MLiCl in $H_2O$ (< 200 K) | $1.61 \times 10^{-3}$                              | 13.55 (1.20)             | 1.68 (0.11)          | 0.388 (0.13)             | This work             |
|                      |                            | $(0.1 \times 10^{-3})$                             |                          |                      |                          |                       |
|                      | T > 200 K                  | $4.76 \times 10^{-6}$                              | 3.91 (0.51)              | -                    | -                        | This work             |
|                      |                            | $3.44 \times 10^{-3}$<br>( $1.07 \times 10^{-3}$ ) | 18.09 (0.58)             | 0.76 (0.05)          | 0.25 (0.06)              | This work             |
|                      | T > 220 K                  | $5.91 \times 10^{-6}$                              | 6.04 (0.34)              | -                    | -                        | This work             |
|                      | Cellulose Acetate Film     | $5.13 \times 10^{-6}$<br>( $2.31 \times 10^{-6}$ ) | 6.53 (1.31)              | 0.59 (0.05)          | Essentially Zero         | This work             |

The essential difference between the two expressions is that VHW represents a simple thermally-activated non-radiative route from a 'single' emitting level, whereas 2EXP considers both the dominant non-radiative route at room temperature and the observed luminescence to be thermally activated with energies of  $\Delta E_1$  and  $\Delta E_2$  respectively. At temperatures much below 200 K, the VHW expression gives very poor agreement with experiment<sup>154</sup>.

Table 5.3 presents activation data produced for an extended temperature range (77-298 K) from this work. The fitted curves for the 2EXP expression are given in Figure 5.9 together with the experimental data.

In this work, the estimation of Arrhenius parameters is based on the 2EXP expression, which is generally far superior to VHW when considering an extended temperature range and gives justification to adoption of a more complicated kinetic model to explain the luminescent behaviour of these complexes.

Luminescence from the two systems of *bis*(polypyridyl) ruthenium(II) complexes (bpy- and phen-) shows similar responses towards change of temperature. Both  $[\text{Ru}(\text{bpy})\text{en}]^{2+}$  and its analogue  $[\text{Ru}(\text{phen})\text{en}]^{2+}$  in 9 M LiCl aqueous solution show a near-linear plot of  $\ln k$  against reciprocal temperature from the highest temperature measured ( $\approx 296$  K) down to 200-220 K (Figures 5.9a and f) and the resulting rate parameters are listed in Table 5.3. Below  $\approx 200$  K these plots become smooth curves, rather than straight lines as in the case of the corresponding *tris*(polypyridyl) ruthenium(II) complexes<sup>154</sup>, and it

Figure 5.9

Temperature activation plots for

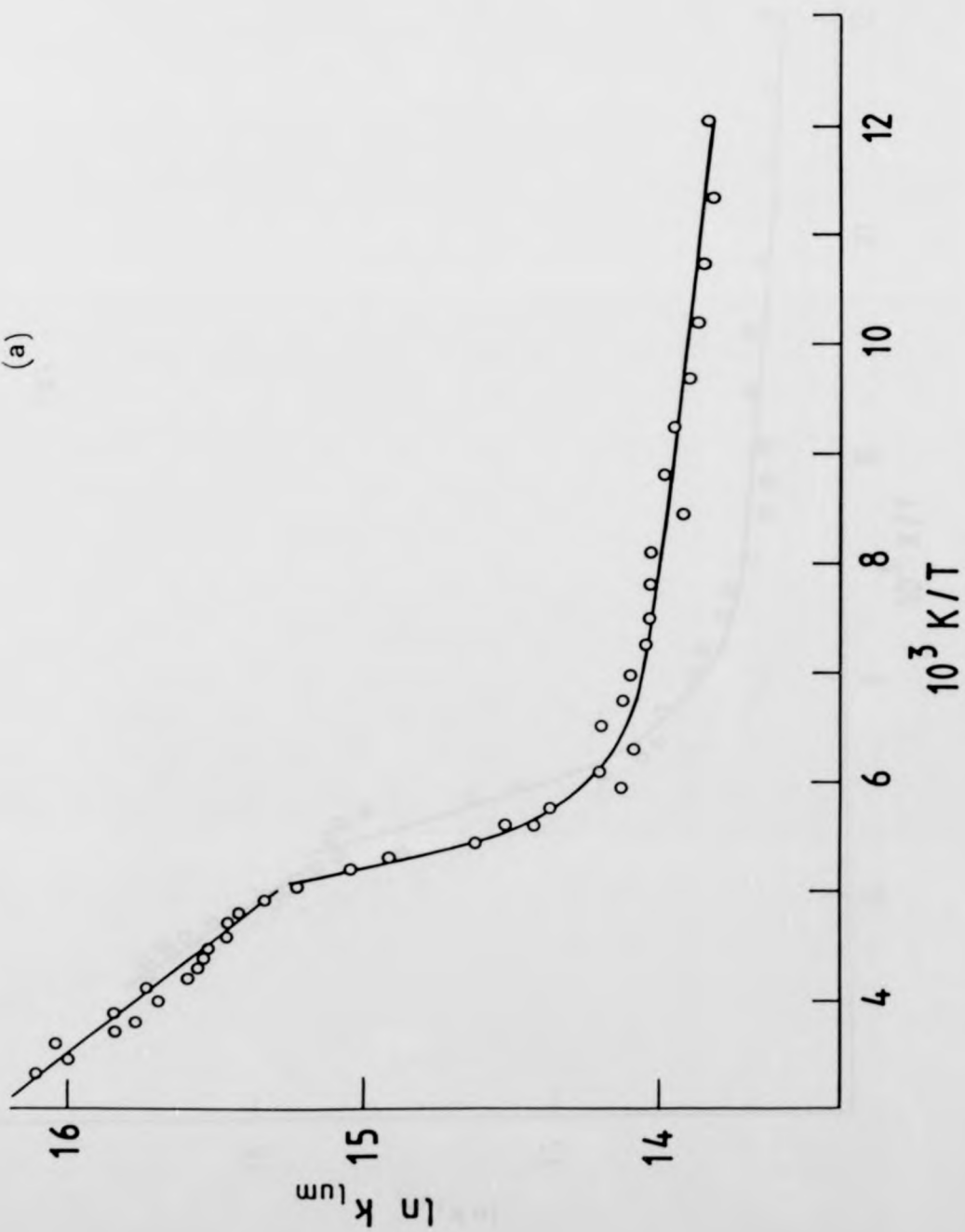
luminescence of bis(polypyridyl)

complexes of Ru(II) in various media.

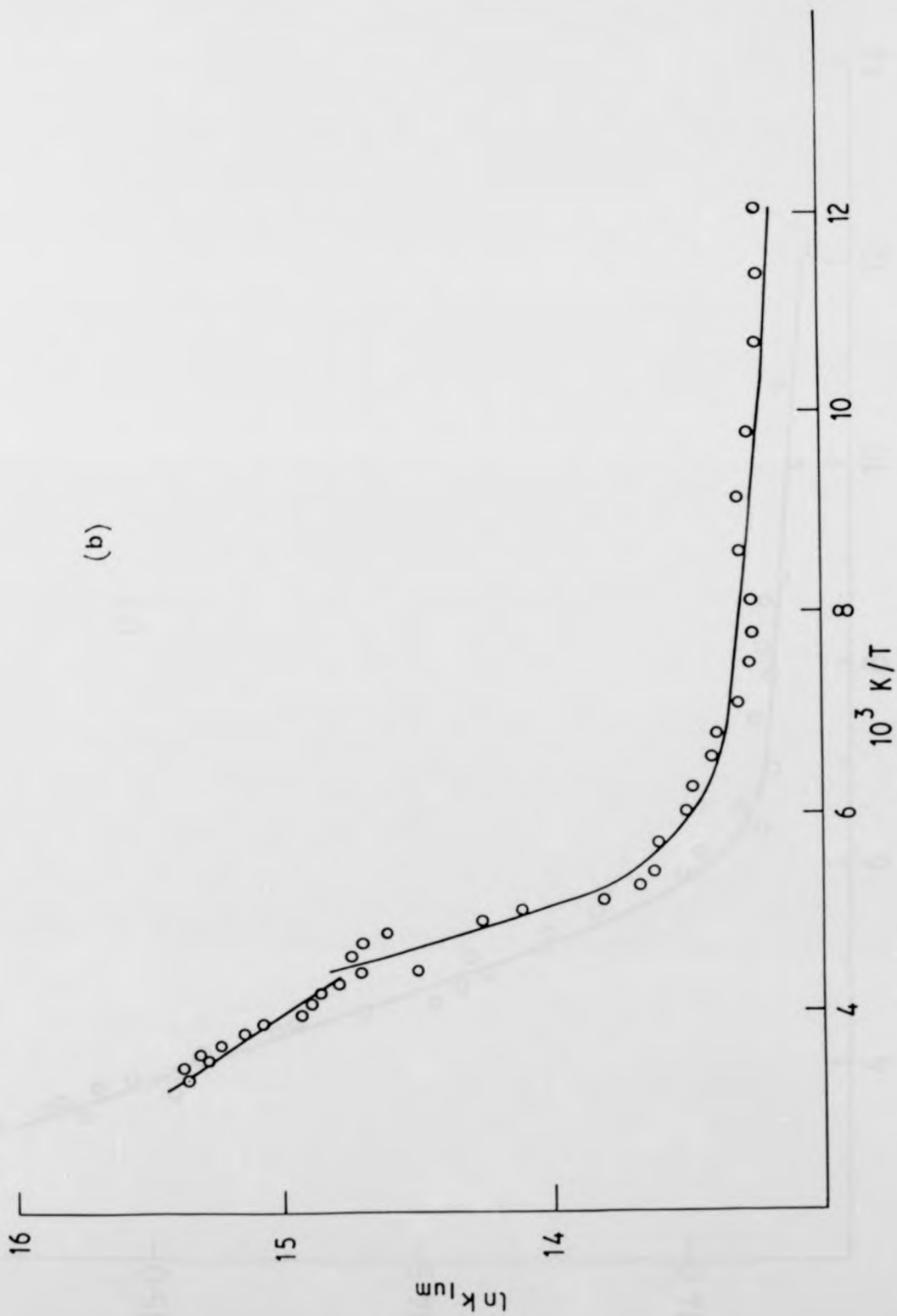
- (a)  $[\text{Ru}(\text{bpy})_2\text{en}]^{2+}$  in  $9 \text{ mol dm}^{-3} \text{ LiCl-H}_2\text{O}$
- (b)  $[\text{Ru}(\text{bpy})_2\text{en}]^{2+}$  in  $9 \text{ mol dm}^{-3} \text{ LiCl-D}_2\text{O}$
- (c)  $[\text{Ru}(\text{bpy})_2\text{en}]^{2+}$  in CA
- (d)  $[\text{Ru}(\text{bpy})_2(\text{NH}_3)_2]^{2+}$  in  $9 \text{ mol dm}^{-3} \text{ LiCl-H}_2\text{O}$
- (e)  $[\text{Ru}(\text{bpy})_2\text{acac}]^+$  in CA
- (f)  $[\text{Ru}(\text{phen})_2\text{en}]^{2+}$  in  $9 \text{ mol dm}^{-3} \text{ LiCl-H}_2\text{O}$
- (g)  $[\text{Ru}(\text{phen})_2\text{acac}]^+$  in CA
- (h)  $[\text{Ru}(\text{phen})_2\text{Cl}_2]$  in EtOH-MeOH (4:1)

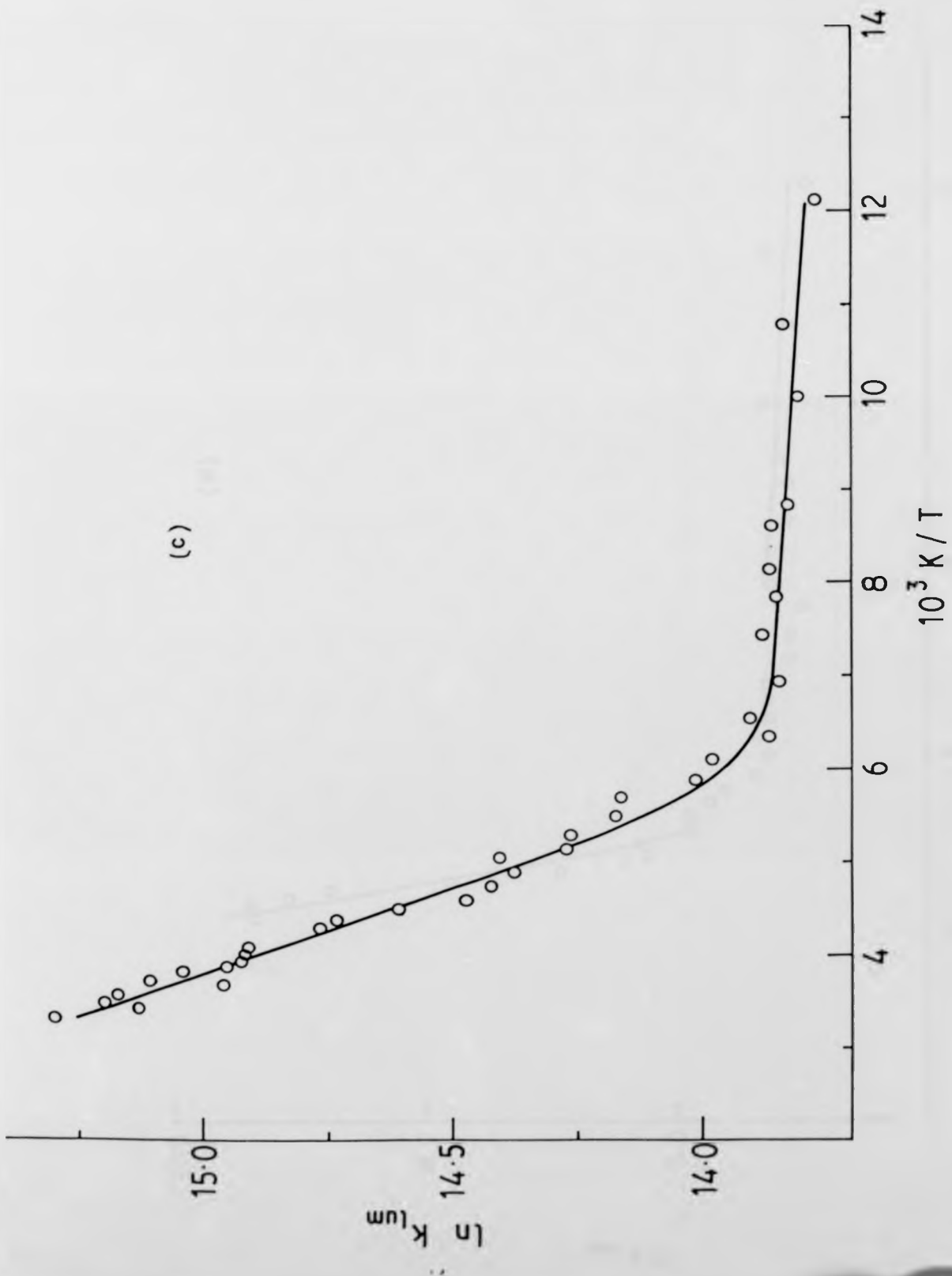
H<sub>2</sub>O

(a)

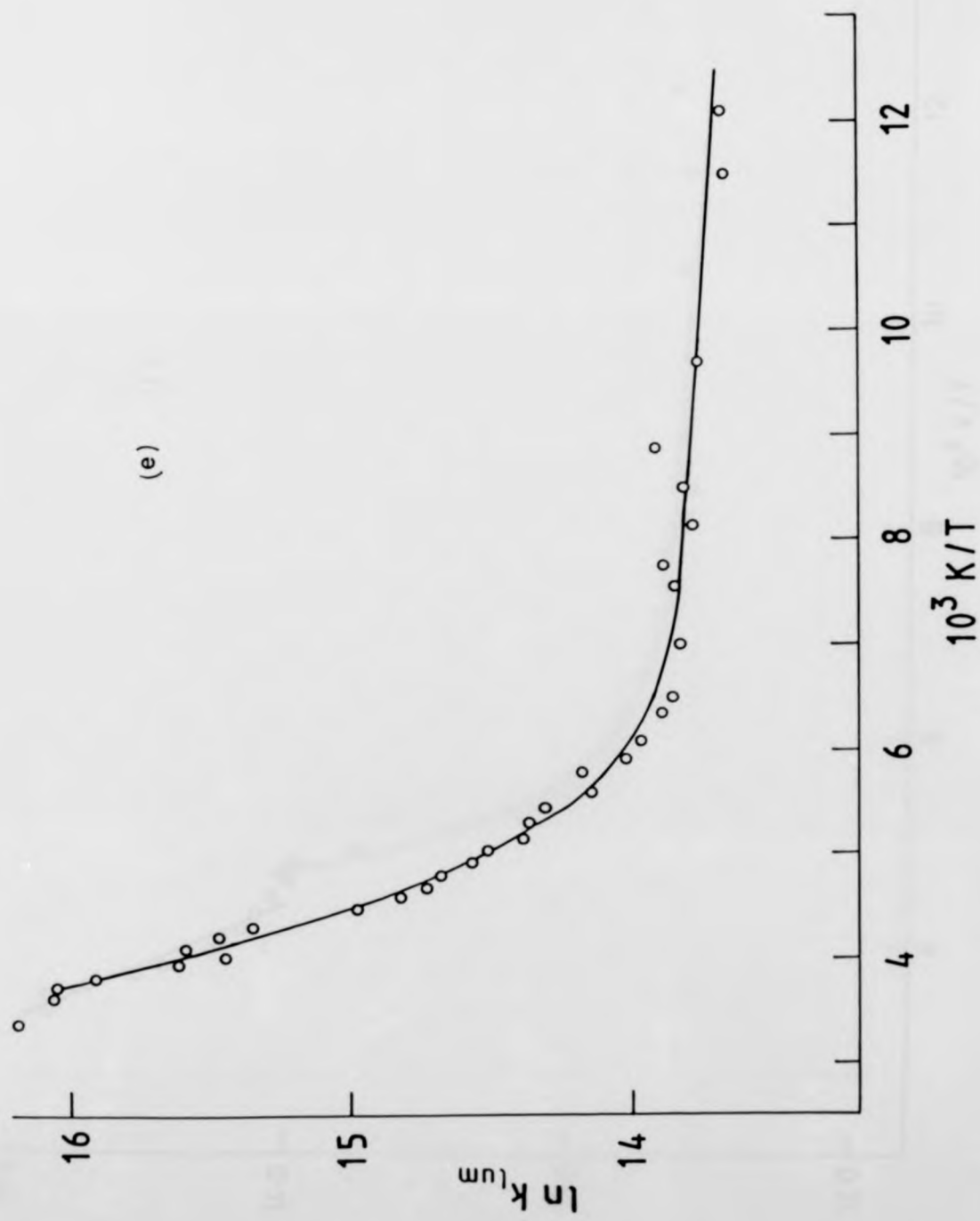


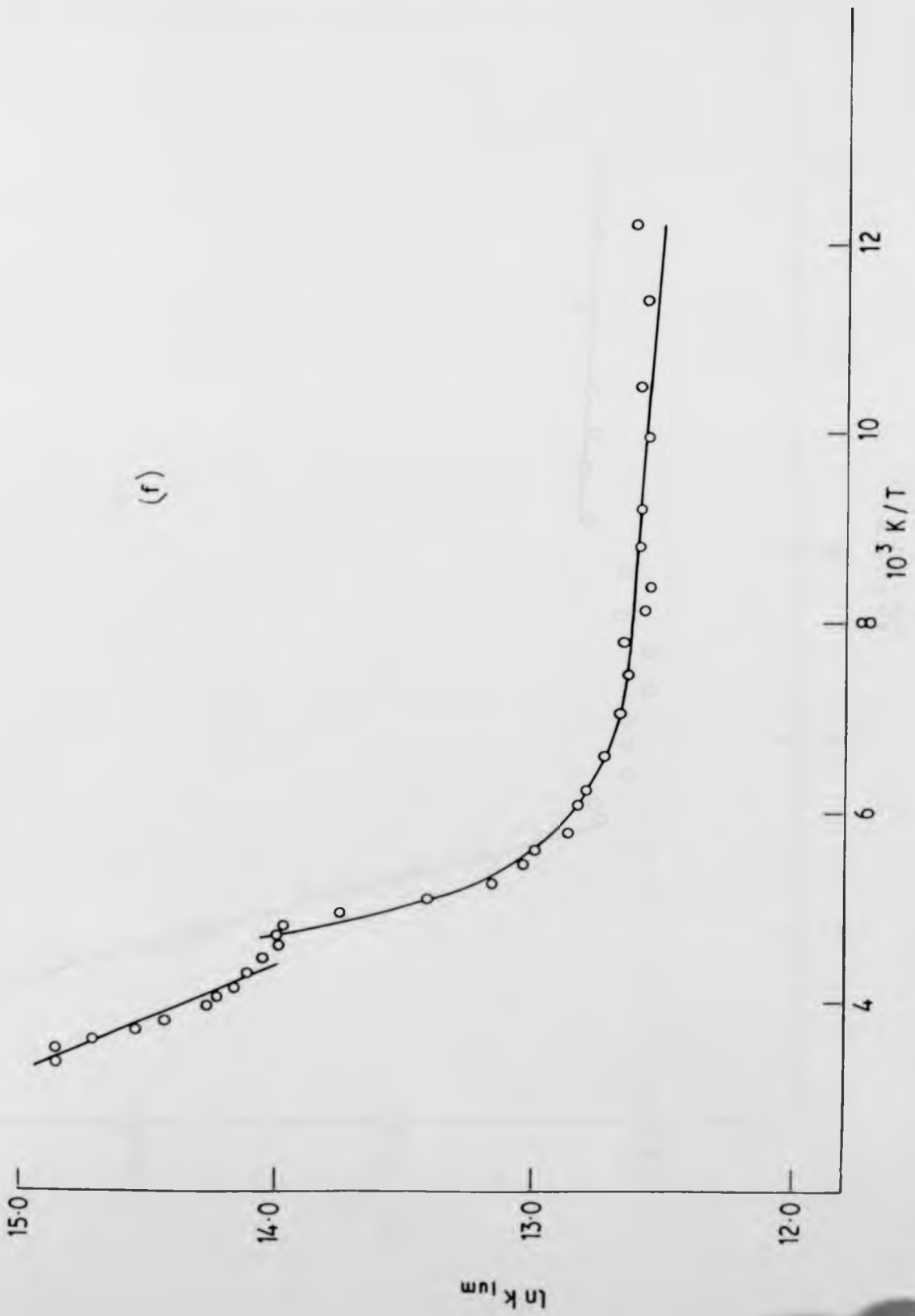
(b)

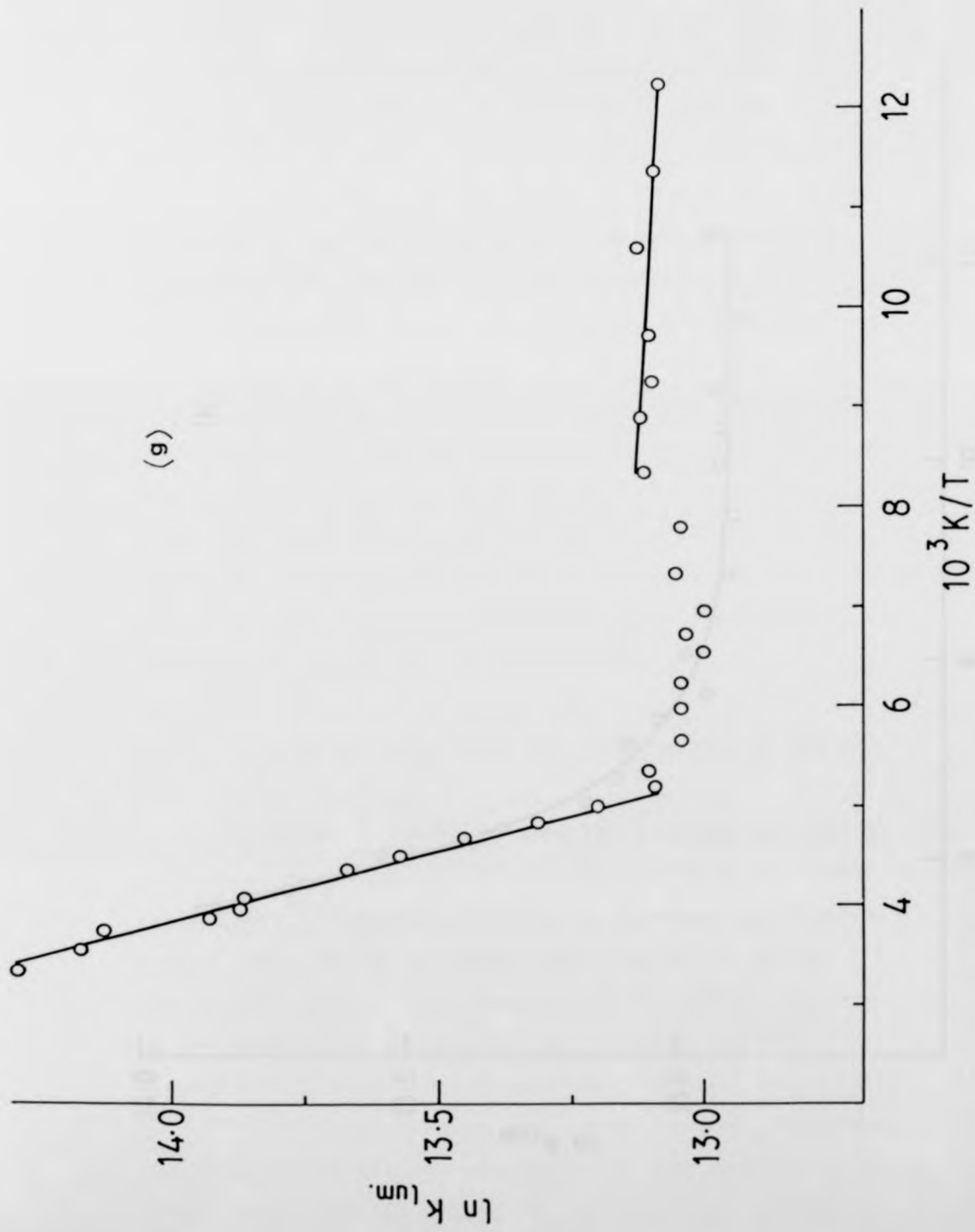


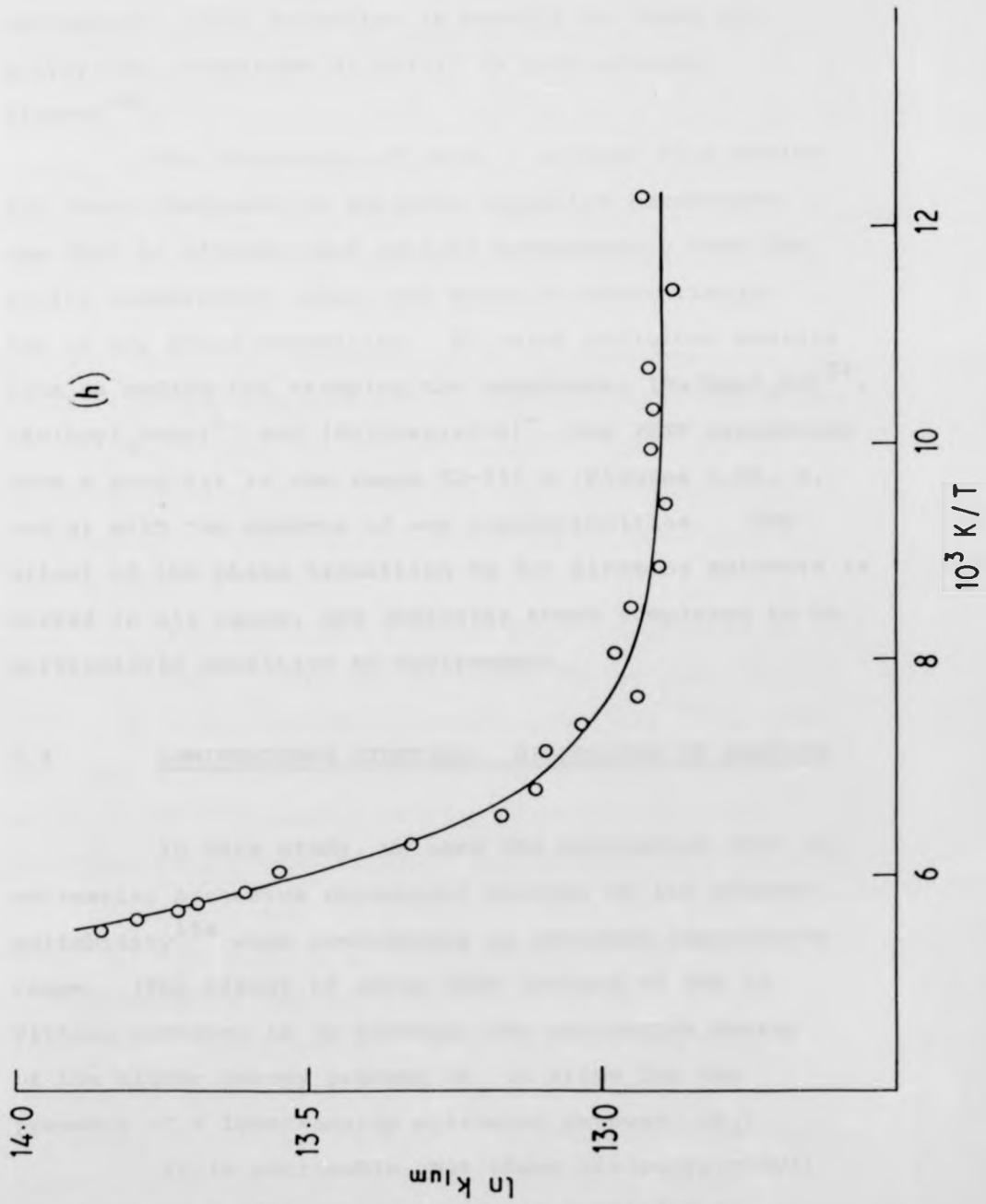












is these sections we have analysed using the 2EXP expression. This situation is exactly as found for polypyridyl complexes of Os(II) in LiCl-aqueous glasses<sup>246</sup>.

The advantages of using a polymer film medium for these complexes to estimate Arrhenius parameters are that it affords good optical transparency over the entire temperature range, and shows no discontinuity due to any phase transition. By using cellulose acetate film as medium for studying the complexes,  $[\text{Ru}(\text{bpy})_2\text{en}]^{2+}$ ,  $[\text{Ru}(\text{bpy})_2\text{acac}]^+$ , and  $[\text{Ru}(\text{phen})\text{acac}]^+$ , the 2EXP expression gave a good fit in the range 82-296 K (Figures 5.9c, e, and g) with the absence of any discontinuities. The effect of the phase transition  $T_g$  for glassing solvents is marked in all cases, and indicates these complexes to be particularly sensitive to environment.

#### 5.4 LUMINESCENCE KINETICS: DISCUSSION OF RESULTS

In this study, we used the expression 2EXP in estimating Arrhenius parameters because of its greater suitability<sup>154</sup> when considering an extended temperature range. (The effect of using 2EXP instead of VHW in fitting routines is to increase the activation energy of the higher energy process  $\Delta E_1$  to allow for the presence of a lower-energy activated pathway,  $\Delta E_2$ ).

It is noticeable that these *bis*(polypyridyl) complexes of Ru(II) are particularly sensitive to environment, and the effect of the phase transition for

glassing solvent is marked in all cases. In low-temperature hydroxylic glasses, it is apparent that there is a considerable isotope effect, indicating that the contribution of the solvent to the deactivation of the excited state of the complex is not diffusional in origin but conforms with the suggestion made by Van Houten and Watts<sup>251</sup>, that there is a weakly-coupled CTTS deactivation of the ligand-field state. The isotope effect in our case for  $[\text{Ru}(\text{bpy})_2\text{en}]^{2+}$  is about 1.7 in  $\text{D}_2\text{O}/\text{H}_2\text{O}$ , and  $\sim 1.3$  in  $\text{CH}_3\text{OD}/\text{CH}_3\text{OH}$  at room temperature, while for  $[\text{Ru}(\text{bpy})_2\text{acac}]^+$  it is  $\sim 2.3$  in  $9\text{ M LiCl} + \text{D}_2\text{O}/9\text{ M LiCl} + \text{H}_2\text{O}$ , and  $\sim 2.1$  in  $\text{CH}_3\text{OD}/\text{CH}_3\text{OH}$  at 80 K, when the  $\Delta E_2$  term is dominant, i.e. isotopic substitution influences both pathways of deactivation.

The Arrhenius plots for 9M LiCl solutions of some *bis*(polypyridyl) complexes of Ru(II) differ from those of the analogous *tris*(polypyridyl) complexes<sup>154</sup> in that the phase transition occurs at a temperature (200-220 K) at which the high energy pathway is still important, resulting in a discontinuity. This phenomenon highlights the different relaxation processes operating above and below  $T_g$ . The simple Arrhenius behaviour exhibited by *bis*(polypyridyl) complexes of Ru(II) in this medium above 200 K indicates the high-energy non-radiative pathway to be the dominant route of deactivation, although the position of this level changes dramatically from  $13.55\text{ kJ mol}^{-1}$  or  $1133\text{ cm}^{-1}$  (below 200 K) to  $3.91\text{ kJ mol}^{-1}$  or  $327\text{ cm}^{-1}$  (above 200 K). For  $[\text{Ru}(\text{bpy})_2\text{en}]^{2+}$  in 9M LiCl/ $\text{H}_2\text{O}$  and from  $10.81\text{ kJ mol}^{-1}$  or  $903\text{ cm}^{-1}$  (below

220 K) to  $6.99 \text{ kJ mol}^{-1}$  or  $584 \text{ cm}^{-1}$  (above 220 K) for  $[\text{Ru}(\text{phen})_2\text{en}]^{2+}$  in  $9\text{M LiCl}/\text{H}_2\text{O}$ . This result exactly parallels the behaviour found with polypyridyl complexes of  $\text{Os}(\text{II})$ <sup>246</sup>, and indicates that besides the large shifts in the levels which are caused by the environment, the nature of the polypyridyl ligand is strongly influential on the individual Arrhenius parameters, which would suggest that the ligand is implicated in the 'forbiddenness' of a transition, possibly through the ordering of the state, which would explain the reduced frequency factors for the more rigid phenanthroline complex. Indeed  $\text{Ru}(\text{II})$  complexes with phenanthroline ligands exhibit longer lifetimes than their analogues with 2,2'-bipyridine ligands under the conditions investigated (see Table 5.2), which seems to be a general trend for polypyridyl complexes<sup>154,246</sup> and may be associated with the relative rigidity of the (phen) ligand which (a) diminishes electronic-vibronic exchange and (b) loss of energy into solvent modes. (Even longer lifetimes are found when methylated and phenylated polypyridyl ligands are used<sup>132</sup>.) All the complexes investigated in this work exhibit much shorter lifetimes than the equivalent *tris*(polypyridyl)ruthenium(II) complexes. This is undoubtedly associated with the much smaller  $\Delta E_1$  term: it may also reflect greater accessibility of the  $\text{Ru}(\text{II})$  centre to solvent modes.

In the case of  $[\text{Ru}(\text{bpy})_2\text{en}]^{2+}$ , the temperature-dependence of the luminescence was investigated in cellulose acetate film to eliminate the acute effect of the phase transition in  $9\text{M LiCl}$  glasses, and the results

shown in Table 5.3 indicate a distinct lowering of  $\Delta E_1$  for the complex in this medium. This peculiarly low value of  $\Delta E_1$  in cellulose acetate film, which was reported before<sup>154</sup>, is unexpected if for  $[\text{Ru}(\text{bpy})_2\text{en}]^{2+}$  loss of energy into solvent modes is significant.

The two thermally-activated pathways for deactivation of *bis*(polypyridyl) complexes of Ru(II) can be generally regarded in terms of a high-energy route which is in the range  $\sim 10$  to  $20 \text{ kJ mol}^{-1}$ , and a second route which is of very small energy (less than  $1 \text{ kJ mol}^{-1}$ ). These values are usually somewhat dependent upon the environment. The high-energy route is due to non-radiative deactivation through a higher state of LF character, as originally assigned by van Houten and Watts<sup>65</sup>.

The low-energy route has been correlated<sup>64</sup> with deactivation through the  $A_2$  level of the Crosby triplet manifold. Most of the energy loss ( $> 90\%$ ) goes through the  $A_2$  level at 70 K and above, giving an explanation of why the non-radiative and radiative decay routes of the lower levels of this manifold can be neglected to give the rate equation 2EXP used in this work.  $A_1$  and E (the lower levels) can be regarded as a single level for the purposes of this work, as they are indistinguishable over the temperature range investigated, and are well-resolved only at temperatures below 30 K according to Crosby *et al.*<sup>64</sup>.

The low-energy term of 2EXP,  $\Delta E_2$ , is susceptible to large errors for data covering a restricted temperature range, since the  $\Delta E_2$  term will make only a relatively

small contribution to the overall rate constant over most of this range, particularly in the case of  $[\text{Ru}(\text{bpy})_2\text{en}]^{2+}$  in cellulose acetate film and  $[\text{Ru}(\text{phen})_2\text{Cl}_2]$  in ethanol-methanol mixture (4:1) (Figures 5.8c and h), where it appears to be essentially zero. At temperatures below 125 K, the rate constant is largely that described by the lower energy route, while above this temperature there is a marked increase in the contribution of the higher energy pathway.

The Jablonski diagram in Figures 5.10 and 5.11 gives the basic scheme for deactivation of our series of excited ruthenium(II) complexes, the specific examples referring to  $[\text{Ru}(\text{phen})_2\text{en}]^{2+}$  and  $[\text{Ru}(\text{bpy})_2(\text{NH}_3)_3]^{2+}$  in 9 M LiCl/H<sub>2</sub>O. It is almost certain that the lower-energy kinetic route corresponds to the upper level,  $A_2$ , of the low-lying Crosby triplet, whereas the lower level can be regarded as the  $A_1, E$  manifold of this triplet (as mentioned in earlier discussions). It is assumed that ISC from the initially populated singlet state to the  $A_1$  level occurs with unitary efficiency.

From these results one can conclude that the luminescence of polypyridyl complexes of Ru(II) occurs mainly through a thermally-activated pathway ( $\Delta E_2$ ) at temperatures  $> 77$  K, representing the highest level of the Crosby<sup>64</sup>  $^3\text{CT}$  model, while deactivation occurs through a higher-energy pathway which dominates at ambient temperature. The magnitude of  $\Delta E_1$ , however, is much less than for the more highly luminescent *tris*(polypyridyl) complexes.

Figure 5.10    Simplified Jablonski diagram for  
[Ru(phen)<sub>2</sub>en]<sup>2+</sup> in 9 M LiCl/H<sub>2</sub>O,  
T > 220 K.

F/cm-1

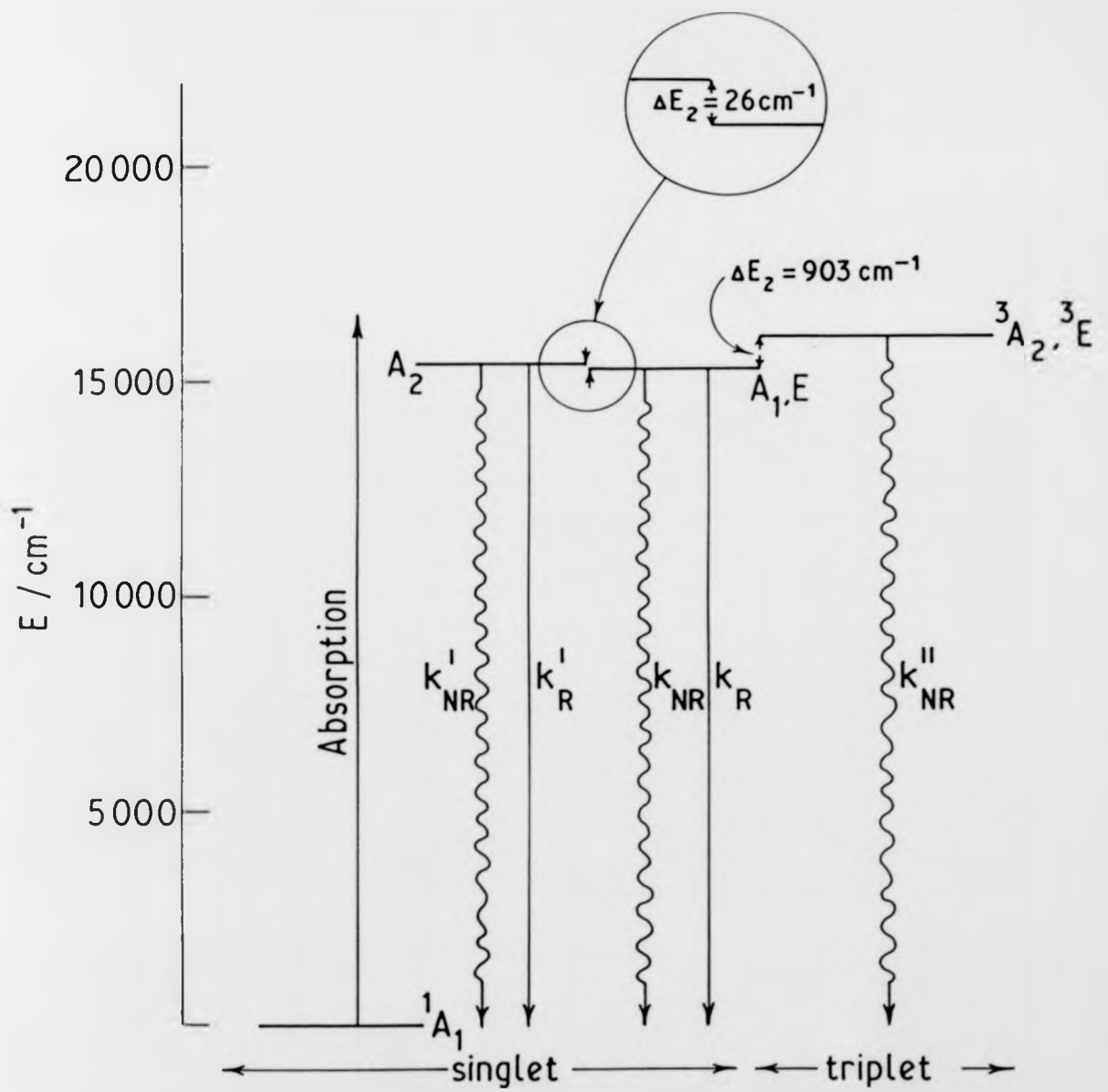
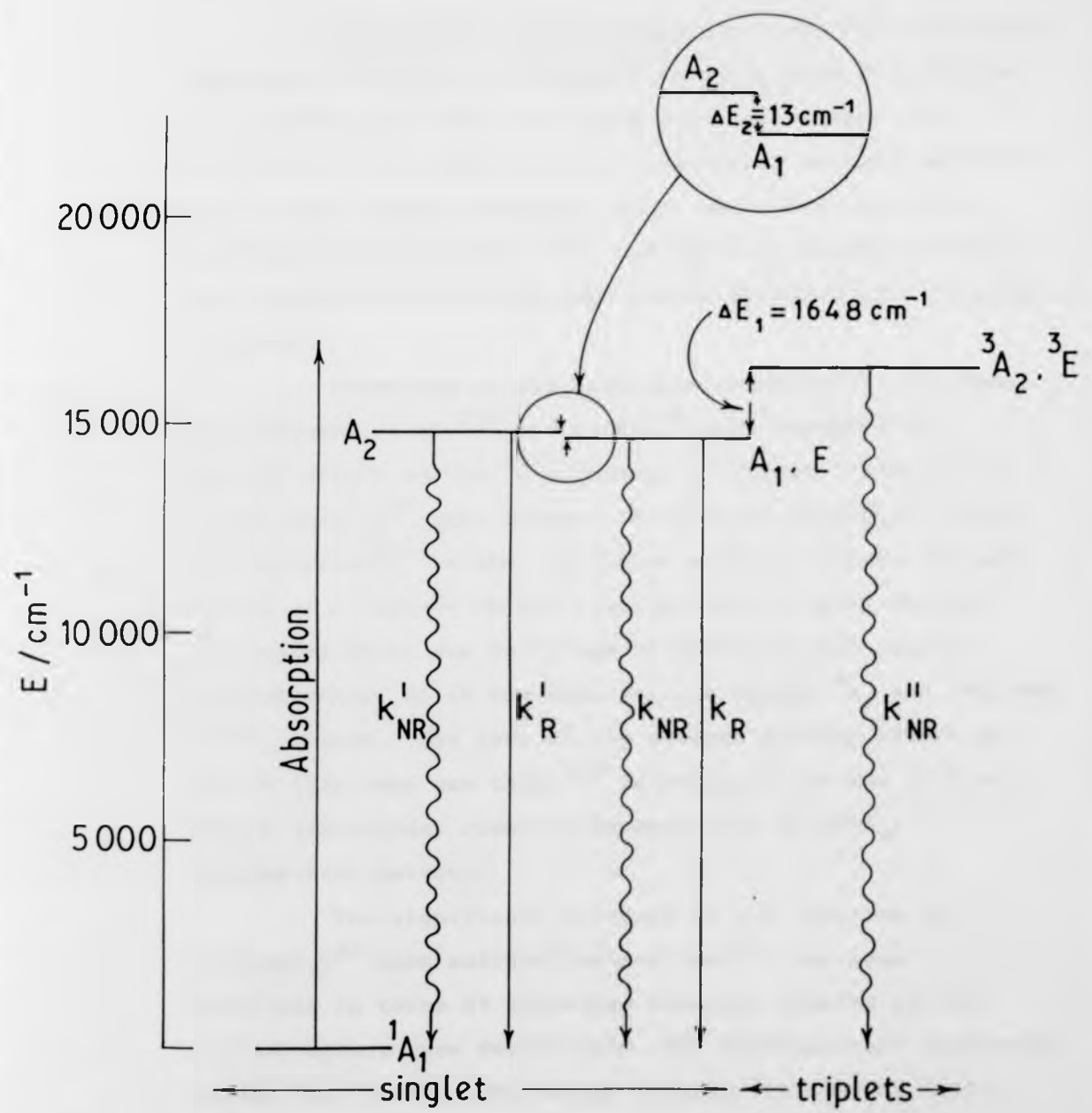


Figure 5.11      Simplified Jablonski diagram for  
[Ru(bpy)<sub>2</sub>(NH<sub>3</sub>)<sub>2</sub>]<sup>2+</sup> in 9 M LiCl/H<sub>2</sub>O,  
T > 220 K.

E / cm<sup>-1</sup>



Finally, the rate constants of some *bis*(polypyridyl) complexes of Ru(II) in different solvents were investigated. It appeared that there is little relation between the lifetime of the complex and any particular solvent parameter such as the Dimroth parameter ( $E_T$ ), which was related to lifetimes of  $[\text{Cr}(\text{CN})_6]^{3-}$ <sup>255</sup>, and the only notable point is the sizeable deuterium isotope effect obtained with hydroxylic solvents.

Referring to the analogous chromium(III) systems, Kane-Maguire *et al.*<sup>252</sup> and Henry<sup>253</sup> have reported no isotope effect on the  $^2E$  lifetimes of either  $[\text{Cr}(\text{bpy})_3]^{3+}$  or  $[\text{Cr}(\text{phen})_3]^{3+}$  upon solvent deuteration ( $\text{H}_2\text{O}/\text{D}_2\text{O}$ ). This was explained<sup>252</sup> on the basis that solvent deuteration has little or no effect on the inter-molecular decay between two states which are relatively undistorted with respect to each other, as is the case for the ground  $^4A_2$  and excited  $^2E/{}^2T_1$  states. The lack of any solvent isotope effect on the  $^2E$  lifetimes was taken<sup>253</sup> as evidence for the lack of direct vibrational coupling between ( $^2E$ )  $[\text{Cr}(\text{NN})_3]^{3+}$  and the bulk solvent.

The significant increase of the lifetime for  $[\text{Ru}(\text{bpy})_3]^{2+}$  upon solvent deuteration<sup>254</sup>, has been explained in terms of increased electron density in the solvent sphere upon deuteration, and consequential increased interaction between the charge-transfer-to-solvent (CTTS) and metal-to-ligand-charge-transfer (MLCT) excited configurations, and clearly this is general for the set of complexes  $[\text{Ru}(\text{bpy})_2\text{X}_2]$  and  $[\text{Ru}(\text{phen})_2\text{X}_2]$ .

5.5 KINETICS OF LUMINESCENCE QUENCHING OF  
POLYPYRIDYL COMPLEXES OF Ru(II) BY  
ELECTRON-TRANSFER - RESULTS

Great interest has been devoted to transition metal complexes of polypyridyl ligands because of the presence of strong electronic transitions of relatively distinct orbital origin in most of the complexes and by reports of strong solution luminescence for some of them<sup>28,54,134,156,165</sup>. Many investigations have been carried out<sup>42,43,131,167</sup> on quenching phenomena and photoreactivity of the strongly luminescent complex  $[\text{Ru}(\text{bpy})_3]^{2+}$ . This complex is reasonably stable towards light except in particular media, and the major consequence of most excited-state quenching is either no permanent reaction or a redox process, but attention was initially drawn to whether quenching of  $[\text{Ru}(\text{bpy})_3]^{2+}$  occurs *via* electron transfer as opposed to excitation energy-transfer<sup>42,94,131,184</sup>. It soon became the most widely investigated material as a component of systems designed to achieve the photochemical splitting of water under solar-type radiation<sup>243</sup>.

This general interest in  $[\text{Ru}(\text{bpy})_3]^{2+}$  has led to many investigations of quenching by both oxidising and reducing species, and this assembly of data has enabled critical evaluation of the recently developed theories of electron-transfer due to Rehm-Weller<sup>49,50</sup>, Marcus<sup>51,52</sup> and Balzani-Scandola<sup>41</sup> to be carried out. Thus, Whitten *et al.*<sup>174</sup> have reported a study of electron-transfer quenching of  $[\text{Ru}(\text{bpy})_3]^{2+}$  by measuring the rates

of oxidative quenching of the excited state of the complex by a series of nitroaromatics, finding a good correlation between  $\log k_q$  and  $E_{1/2}$  for the oxidant. We wished to extend this study to other Ru(II) complexes, particularly the bis(bipyridine) complexes with the following aims: (i) to systematically vary the oxidation potential of the excited state of the complex, and (ii) to note the effect of replacing one (bpy) ligand by another coordinating groups. This study forms the basis of this part of the current chapter.

The complexes selected are  $[\text{Ru}(\text{bpy})_2\text{en}]^{2+}$ ,  $[\text{Ru}(\text{bpy})_2\text{acac}]^+$ , and  $[\text{Ru}(\text{bpy})_2\text{Cl}_2]$ . The ground state oxidation potentials for these complexes are 0.95, 0.61 and 0.31 V respectively, compared with 1.29 V for  $[\text{Ru}(\text{bpy})_3]^{2+}$  itself. To estimate the excited state potentials for these complexes, we measured the luminescence spectra at 77 K in order to estimate  $E_{0,0}$ . The resulting values, together with lifetime measurements for these complexes, are tabulated in Table 5.4 following the procedure of Balzani *et al.*<sup>48</sup>.

Table 5.4 Lifetime measurements, ground and excited state potentials for Ru(II) complexes in acetonitrile

| Complex                                   | Lifetime/ns     | $E_{\text{Ox}}/\text{V}$ | $E_{0-0}/\text{eV}$ | $E_{\text{Ox}}^*/\text{V}$ |
|-------------------------------------------|-----------------|--------------------------|---------------------|----------------------------|
| $[\text{Ru}(\text{bpy})_3]^{2+}$          | $862 \pm 10^a$  | 1.29                     | 2.12                | -0.83                      |
| $[\text{Ru}(\text{bpy})_2\text{en}]^{2+}$ | $111.9 \pm 2.5$ | 0.95                     | 1.92                | -0.97                      |
| $[\text{Ru}(\text{bpy})_2\text{acac}]^+$  | $20.7 \pm 2.0$  | 0.61                     | 1.68                | -1.07                      |
| $[\text{Ru}(\text{bpy})_2\text{Cl}_2]$    | $3.0 \pm 0.5$   | 0.31                     | -                   | -                          |

<sup>a</sup>from reference 174

Table 5.5 Luminescence Quenching of [Ru(bpy)<sub>2</sub>en]<sup>2+</sup>. Quenching Rate Constants and Reduction Potential Data for Organic Acceptors

| Acceptor                          | E <sub>1/2</sub> /V vs SCE | ΔG <sub>23</sub> /kJ mol <sup>-1</sup> | ΔG <sub>23</sub> <sup>‡</sup> /kJ mol <sup>-1</sup> | k <sub>q</sub> (calculated)/<br>dm <sup>3</sup> mol <sup>-1</sup> s <sup>-1</sup> | k <sub>q</sub> (experimental)/<br>dm <sup>3</sup> mol <sup>-1</sup> s <sup>-1</sup> |
|-----------------------------------|----------------------------|----------------------------------------|-----------------------------------------------------|-----------------------------------------------------------------------------------|-------------------------------------------------------------------------------------|
| 1,4-Benzoquinone (1) <sup>a</sup> | -0.51 <sup>b</sup>         | -50.17                                 | 1.94                                                | 2.48 × 10 <sup>10</sup>                                                           | 2.35 × 10 <sup>10</sup>                                                             |
| p-Dinitrobenzene (2)              | -0.69 <sup>c</sup>         | -32.80                                 | 2.83                                                | 1.13 × 10 <sup>10</sup>                                                           | 1.64 × 10 <sup>10</sup>                                                             |
| o-Dinitrobenzene (3)              | -0.83 <sup>c</sup>         | -19.29                                 | 4.28                                                | 8.37 × 10 <sup>9</sup>                                                            | 1.07 × 10 <sup>10</sup>                                                             |
| m-Dinitrobenzene (4)              | -0.91 <sup>c,d</sup>       | -11.59                                 | 5.80                                                | 5.58 × 10 <sup>9</sup>                                                            | 1.03 × 10 <sup>10</sup>                                                             |
| p-Nitrobenzamide (5)              | -1.014 <sup>e</sup>        | -1.54                                  | 9.31                                                | 1.73 × 10 <sup>9</sup>                                                            | 5.41 × 10 <sup>9</sup>                                                              |
| p-Nitrobenzylbromide (6)          | -1.09 <sup>f</sup>         | 5.82                                   | 13.36                                               | 3.50 × 10 <sup>8</sup>                                                            | 3.34 × 10 <sup>9</sup>                                                              |
| m-Nitrotoluene (7)                | -1.17 <sup>f</sup>         | 13.51                                  | 18.86                                               | 3.71 × 10 <sup>7</sup>                                                            | 1.60 × 10 <sup>9</sup>                                                              |
| p-Nitrotoluene (8)                | -1.20 <sup>e</sup>         | 16.40                                  | 21.17                                               | 1.43 × 10 <sup>7</sup>                                                            | 1.24 × 10 <sup>9</sup>                                                              |
| p-Nitroanisole (9)                | -1.25 <sup>f</sup>         | 21.25                                  | 25.25                                               | 2.67 × 10 <sup>6</sup>                                                            | 7.34 × 10 <sup>8</sup>                                                              |
| 2,3-Dimethylnitrobenzene (10)     | -1.318 <sup>g</sup>        | 27.78                                  | 31.03                                               | 2.48 × 10 <sup>5</sup>                                                            | 1.89 × 10 <sup>8</sup>                                                              |
| 2,6-Dimethylnitrobenzene (11)     | -1.402 <sup>g</sup>        | 35.90                                  | 38.52                                               | 1.16 × 10 <sup>4</sup>                                                            | 6.76 × 10 <sup>6</sup>                                                              |

<sup>a</sup>Numbering in Figures 5.13 to 5.17

<sup>b</sup>From reference 263

<sup>c</sup>From reference 265

<sup>d</sup>From reference 264

<sup>e</sup>From reference 267

<sup>f</sup>From reference 266

<sup>g</sup>From reference 268

Table 5.6 Luminescence Quenching of [Ru(bpy)2acac]<sup>2+</sup>. Quenching Rate Constants and Reduction Potential Data for Organic Acceptors

| Acceptor                          | $E_1/V$ vs SCE     | $\Delta G_{23}/\text{kJ mol}^{-1}$ | $\Delta G_{23}^\ddagger/\text{kJ mol}^{-1}$ | $k_q(\text{calculated})/\text{dm}^3 \text{ mol}^{-1} \text{ s}^{-1}$ | $k_q(\text{experimental})/\text{dm}^3 \text{ mol}^{-1} \text{ s}^{-1}$ |
|-----------------------------------|--------------------|------------------------------------|---------------------------------------------|----------------------------------------------------------------------|------------------------------------------------------------------------|
| 1,4-Benzoquinone (1) <sup>a</sup> | -0.51 <sup>b</sup> | -59.83                             | 1.64                                        | $1.35 \times 10^{10}$                                                | $2.32 \times 10^{10}$                                                  |
| p-Dinitrobenzene (2)              | -0.69              | -42.47                             | 2.26                                        | $1.24 \times 10^{10}$                                                | $1.42 \times 10^{10}$                                                  |
| o-Dinitrobenzene (3)              | -0.83              | -28.95                             | 3.14                                        | $1.06 \times 10^{10}$                                                | $8.39 \times 10^9$                                                     |
| m-Dinitrobenzene (4)              | -0.91              | -21.25                             | 4.00                                        | $8.92 \times 10^9$                                                   | $9.26 \times 10^9$                                                     |
| p-Nitrobenzamide (5)              | -1.014             | -11.21                             | 5.90                                        | $5.46 \times 10^9$                                                   | $4.01 \times 10^9$                                                     |
| p-Nitrobenzylbromide (6)          | -1.09              | -3.85                              | 8.30                                        | $2.49 \times 10^9$                                                   | $3.04 \times 10^9$                                                     |
| m-Nitrotoluene (7)                | -1.17              | 3.85                               | 12.15                                       | $5.74 \times 10^8$                                                   | $4.35 \times 10^8$                                                     |
| p-Nitrotoluene (8)                | -1.20              | 6.74                               | 13.96                                       | $2.77 \times 10^8$                                                   | $1.55 \times 10^8$                                                     |
| p-Nitroanisole (9)                | -1.25              | 11.57                              | 17.37                                       | $6.85 \times 10^7$                                                   | $2.17 \times 10^7$                                                     |
| 2,3-Dimethylnitrobenzene (10)     | -1.318             | 18.12                              | 22.58                                       | $8.00 \times 10^6$                                                   | $9.66 \times 10^6$                                                     |

<sup>a</sup>Numbering in Figures 5.13 to 5.17

<sup>b</sup>References for  $E_1$  are listed in Table 5.5

Table 5.7 Luminescence Quenching of  $[\text{Ru}(\text{bpy})_3]^{2+}$ . Quenching Rate Constants and Reduction Potential Data for Nitroaromatics

| Acceptor                              | $E_p^a/V$ vs SCE | $\Delta G_{23}^+/kJ\ mol^{-1}$ | $\Delta G_{23}^+/kJ\ mol^{-1}$ | $k_q(\text{calculated})/$<br>$\text{dm}^3\ \text{mol}^{-1}\ \text{s}^{-1}$ | $k_q^a(\text{experimental})/$<br>$\text{dm}^3\ \text{mol}^{-1}\ \text{s}^{-1}$ |
|---------------------------------------|------------------|--------------------------------|--------------------------------|----------------------------------------------------------------------------|--------------------------------------------------------------------------------|
| p-Nitronitrobenzene (12) <sup>b</sup> | -0.525           | -35.19                         | 2.67                           | $1.158 \times 10^9$                                                        | $9.18 \times 10^9$                                                             |
| p-Dinitrobenzene (13)                 | -0.69            | -19.29                         | 4.28                           | $8.37 \times 10^9$                                                         | $6.56 \times 10^9$                                                             |
| o-Dinitrobenzene (14)                 | -0.81            | -7.70                          | 6.90                           | $4.00 \times 10^9$                                                         | $3.10 \times 10^9$                                                             |
| p-Nitrobenzaldehyde (15)              | -0.863           | -2.59                          | 8.83                           | $2.06 \times 10^9$                                                         | $1.96 \times 10^9$                                                             |
| m-Dinitrobenzene (16)                 | -0.898           | 0.79                           | 10.45                          | $1.12 \times 10^9$                                                         | $1.56 \times 10^9$                                                             |
| Methyl 4-nitrobenzoate (17)           | -0.947           | 5.52                           | 13.18                          | $3.81 \times 10^8$                                                         | $6.56 \times 10^8$                                                             |
| o-8-4,4'-Dinitrostilbene (18)         | -1.00            | 10.63                          | 16.67                          | $9.13 \times 10^7$                                                         | $1.83 \times 10^8$                                                             |
| 4,4'-Dinitrobiphenyl (19)             | -1.004           | 11.00                          | 16.95                          | $8.14 \times 10^7$                                                         | $1.18 \times 10^8$                                                             |
| m-Dinitrobenzaldehyde (20)            | -1.016           | 12.18                          | 17.83                          | $5.67 \times 10^7$                                                         | $4.89 \times 10^7$                                                             |
| Methyl 3-nitrobenzoate (21)           | -1.044           | 14.85                          | 19.92                          | $2.40 \times 10^7$                                                         | $1.66 \times 10^7$                                                             |
| p-Chloronitrobenzene (22)             | -1.063           | 16.69                          | 21.41                          | $1.30 \times 10^7$                                                         | $8.04 \times 10^6$                                                             |
| p-Fluoronitrobenzene (23)             | -1.128           | 22.97                          | 26.74                          | $1.44 \times 10^6$                                                         | $8.32 \times 10^5$                                                             |
| Nitrobenzene (24)                     | -1.148           | 24.81                          | 28.37                          | $7.40 \times 10^5$                                                         | $< 2 \times 10^5$                                                              |
| p-Methylnitrobenzene (25)             | -1.203           | 30.21                          | 33.24                          | $1.00 \times 10^5$                                                         | $< 3 \times 10^5$                                                              |

<sup>a</sup>From reference 174

<sup>b</sup>Numbering in Figures 5.13 to 5.17

Table 5.8 Luminescence Quenching of  $[\text{Ru}(\text{bpy})_3]^{2+}$ . Quenching Rate Constants and Reduction Potential Data for Quinones

| Acceptor                                      | $E_1^a/V$ vs SCE | $\Delta G_{23}/\text{kJ mol}^{-1}$ | $\Delta G_{23}^\ddagger/\text{kJ mol}^{-1}$ | $k_{\text{qdm}}^a(\text{experimental})/\text{mol}^{-1} \text{s}^{-1}$ |
|-----------------------------------------------|------------------|------------------------------------|---------------------------------------------|-----------------------------------------------------------------------|
| o-Chloroanil (26) <sup>b</sup>                | +1.55            | -103.72                            | 0.96                                        | $7.17 \times 10^9$                                                    |
| p-Chloroanil (27)                             | +0.05            | - 93.60                            | 1.05                                        | $6.89 \times 10^9$                                                    |
| p-Benzoquinone (28)                           | -0.455           | - 44.89                            | 2.13                                        | $6.32 \times 10^9$                                                    |
| 3,5-di-Bu <sup>t</sup> -1,2-benzoquinone (29) | -0.49            | - 41.51                            | 2.30                                        | $3.36 \times 10^9$                                                    |
| o-Naphthoquinone (30)                         | -0.50            | - 40.54                            | 2.34                                        | $5.11 \times 10^9$                                                    |
| p-Toluquinone (31)                            | -0.505           | - 40.04                            | 2.38                                        | $5.05 \times 10^9$                                                    |
| o-Phenanthrenequinone (32)                    | -0.59            | -31.84                             | 2.89                                        | $4.10 \times 10^9$                                                    |
| p-Naphthoquinone (33)                         | -0.635           | - 27.53                            | 3.26                                        | $4.36 \times 10^9$                                                    |
| 2,6-di-Bu <sup>t</sup> -1,4-benzoquinone (34) | -0.64            | -27.03                             | 3.31                                        | $2.24 \times 10^9$                                                    |
| p-Duroquinone (35)                            | -0.765           | -14.98                             | 5.02                                        | $2.36 \times 10^9$                                                    |

<sup>a</sup>From reference 249

<sup>b</sup>Numbering in Figure 5.13 to 5.17

Several organic compounds, most of them nitroaromatics, were chosen as quenchers in our study. This series of quenchers was selected because its members undergo reversible one-electron reductions at potentials in the range  $-0.5$  to  $-1.4$  V *versus* SCE in acetonitrile. No spectral evidence for ground-state complexes was detected with either  $[\text{Ru}(\text{bpy})_2\text{en}]^{2+}$  or  $[\text{Ru}(\text{bpy})_2\text{acac}]^+$  for any of the aromatic quenchers. In the case of  $[\text{Ru}(\text{bpy})_2\text{Cl}_2]$ , however, there was clear evidence of ground-state interaction with the quenchers which results in a change of colour of the solution as soon as the quencher is added to the complex. This colour change is associated with the appearance of strong absorption bands which are related to neither the complex nor the quencher.

In the following Tables 5.5, 5.6, 5.7 and 5.8, are set out the quenching rates for each of the complexes in turn, referring to a wide variety of quenchers. All organic compounds listed in Tables 5.5 and 5.6 quench the luminescence of both  $[\text{Ru}(\text{bpy})_2\text{en}]^{2+}$  and  $[\text{Ru}(\text{bpy})_2\text{acac}]^+$  and the rate constants were evaluated from the slopes of the Stern-Volmer plots and the measured lifetime, ( $K^{\text{SV}} = k_q\tau$ ). The Stern-Volmer plots were linear up to rather high quenching values (*ca.*  $I^0/I \sim 4$ ), which is a good indication that there is no static quenching. The plots of  $\log k_q$  *versus* the half-wave reduction potentials for the organic compounds for  $[\text{Ru}(\text{bpy})_2\text{en}]^{2+}$ ,  $[\text{Ru}(\text{bpy})\text{acac}]^+$  and  $[\text{Ru}(\text{bpy})_3]^{2+}$  are shown in Figure 5.12. We have

Figure 5.12 Plots of  $\log k_q$  versus the half-wave potentials for the quenching of the luminescence of  $[\text{Ru}(\text{bpy})_3]^{2+}$  ( $\square$ ),  $[\text{Ru}(\text{bpy})_2\text{en}]^{2+}$  ( $\circ$ ), and  $[\text{Ru}(\text{bpy})_2\text{acac}]^+$  ( $\bullet$ ), by organic compounds in MeCN.

Figure 5.12 Plots of  $\log k_q$  versus the half-wave potentials for the quenching of the luminescence of  $[\text{Ru}(\text{bpy})_3]^{2+}$  ( $\square$ ),  $[\text{Ru}(\text{bpy})_2\text{en}]^{2+}$  ( $\circ$ ), and  $[\text{Ru}(\text{bpy})_2\text{acac}]^+$  ( $\bullet$ ), by organic compounds in MeCN.

lf-  
ning  
)<sub>3</sub>l<sup>2+</sup>  
c

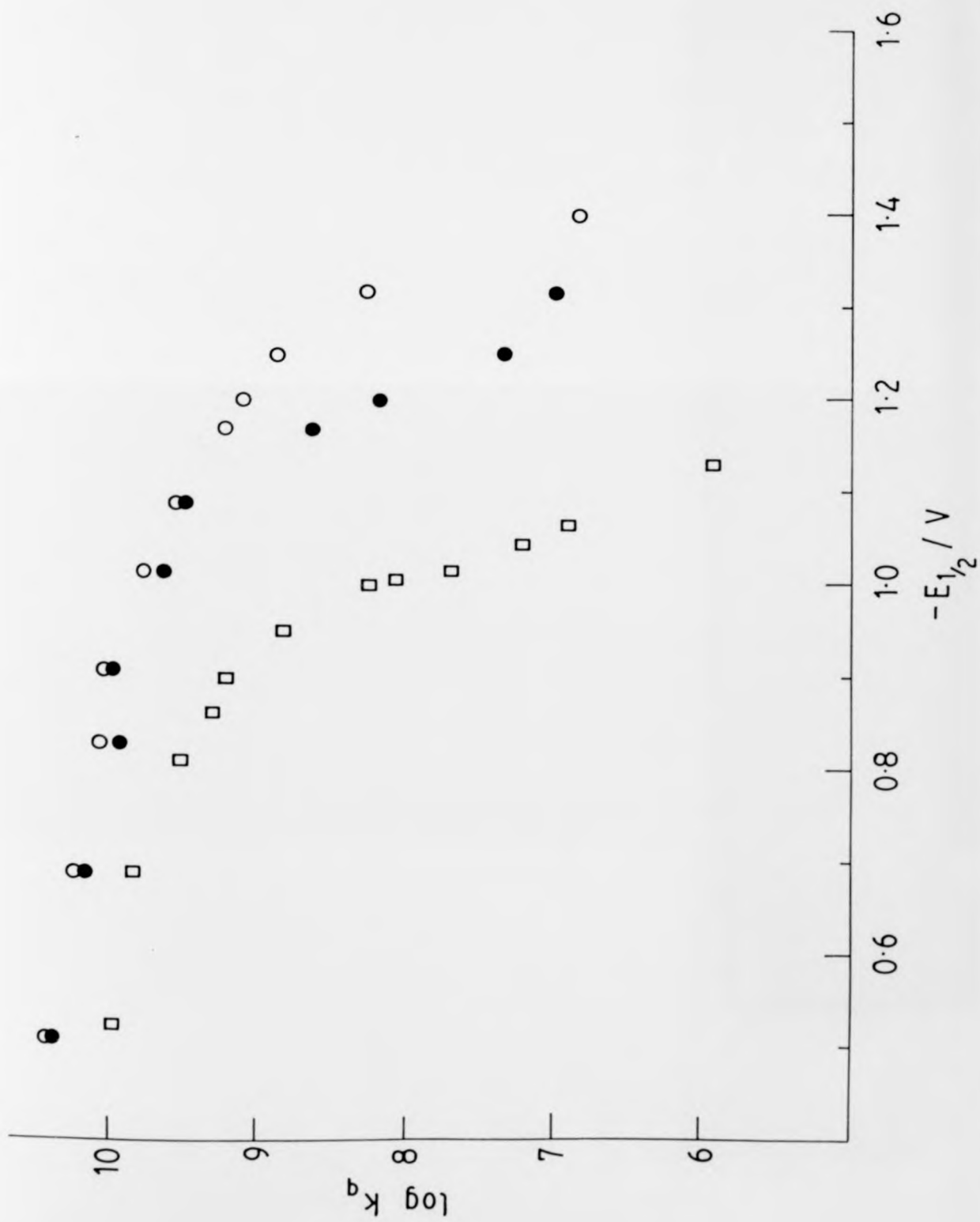


Figure 5.13 Plot of  $\log k_q$  versus  $\Delta G_{23}$  for the electron-transfer quenching of the luminescence of  $[\text{Ru}(\text{bpy})_2\text{acac}]^+$  by organic compounds in MeCN. (The curve is calculated on the basis of Weller theory.)

Figure 5.13 Plot of  $\log k_q$  versus  $\Delta G_{23}$  for the electron-transfer quenching of the luminescence of  $[\text{Ru}(\text{bpy})_2\text{acac}]^+$  by organic compounds in MeCN. (The curve is calculated on the basis of Weller theory.)

the  
the  
+ by  
he  
is

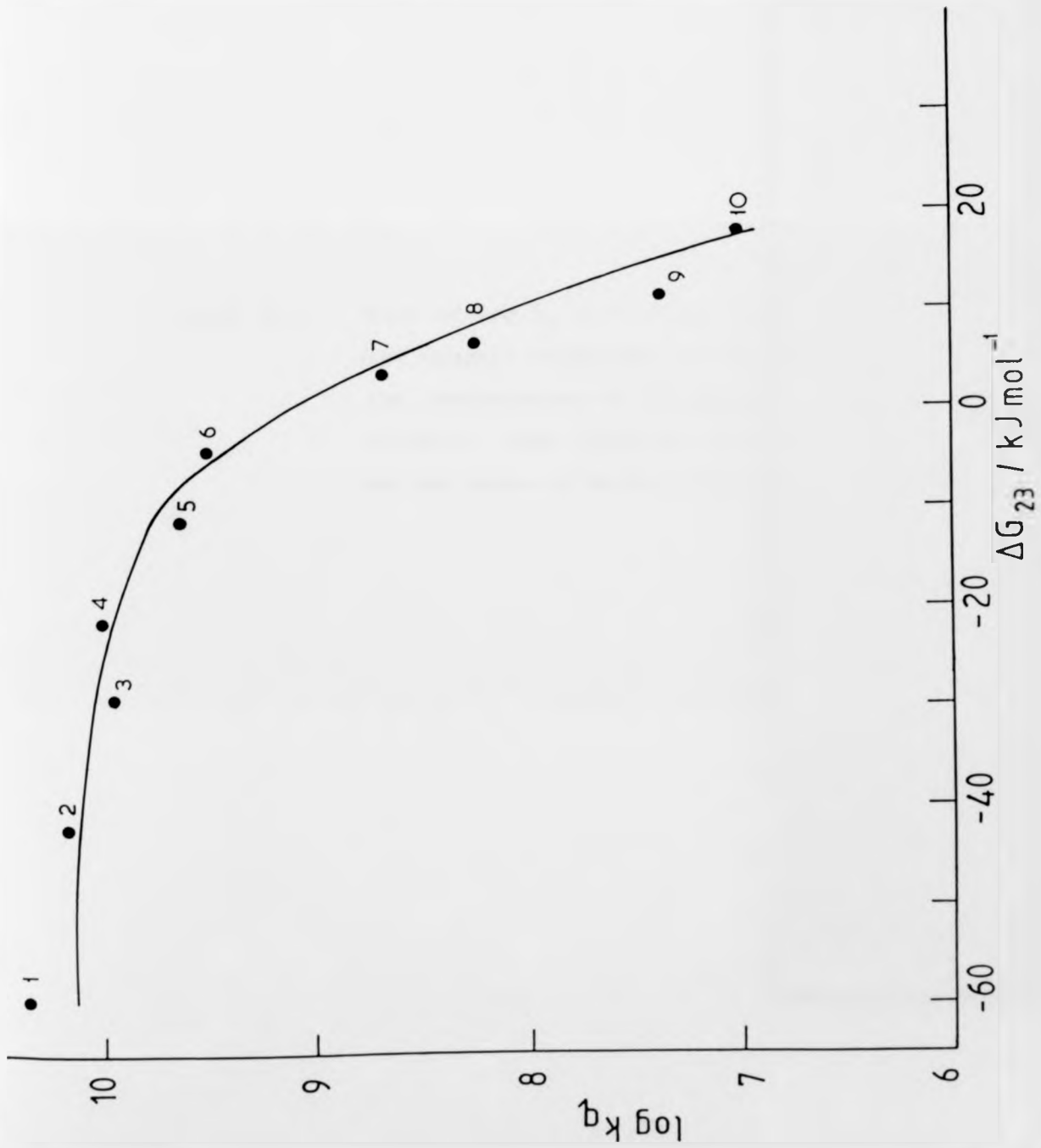


Figure 5.14 Plot of  $\log k_q$  versus  $\Delta G_{23}$  for the organic compounds quenching for the luminescence of  $[\text{Ru}(\text{bpy})_2\text{en}]^{2+}$  in MeCN. (The curve is calculated on the basis of Weller theory.)

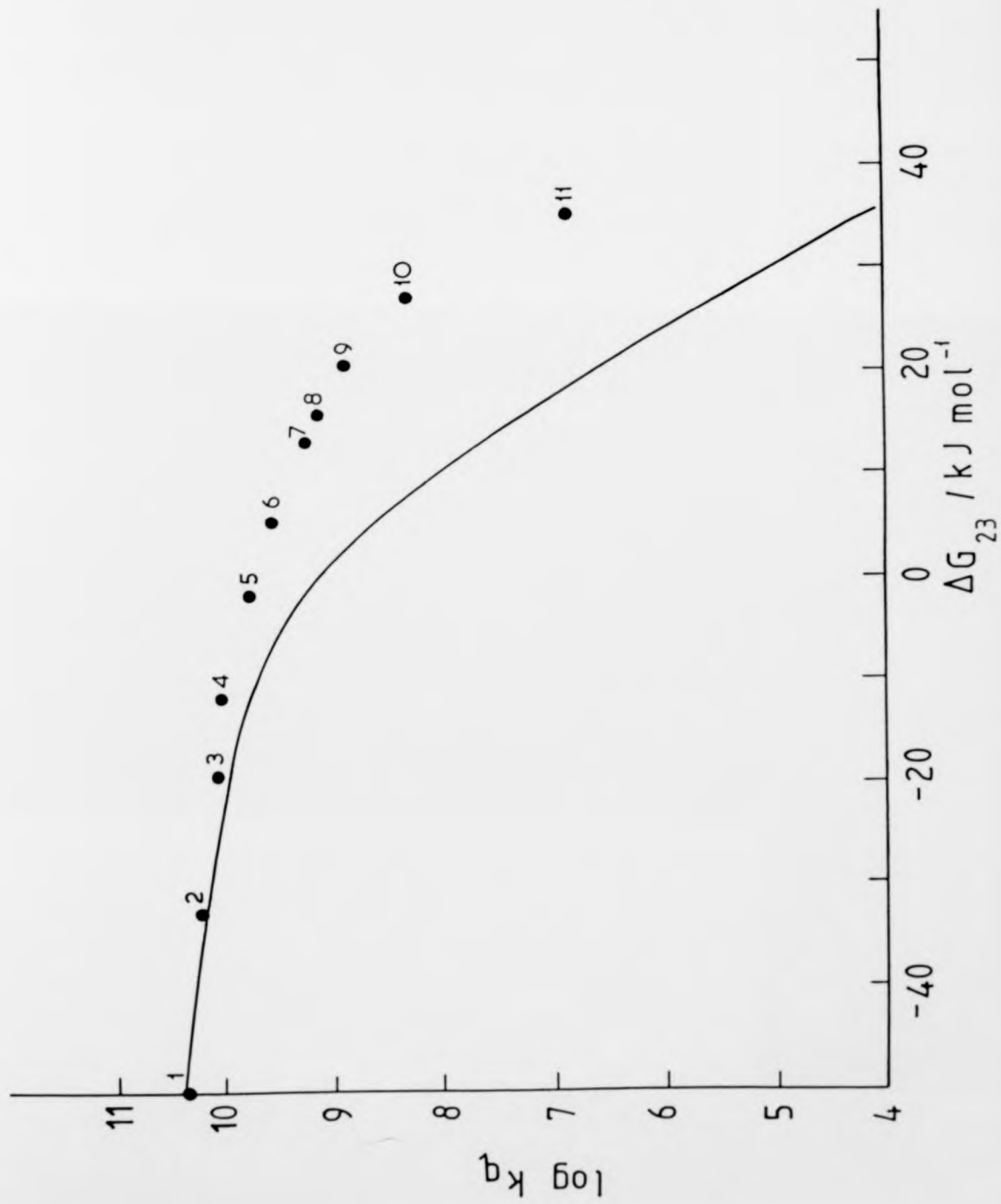


Figure 5.15 Plot of  $\log k_q$  versus  $\Delta G_{23}$  for the electron-transfer quenching of the luminescence of  $[\text{Ru}(\text{bpy})_3]^{2+}$  by organic compounds in MeCN. (The curve is calculated on the basis of Weller theory.)

or the  
of the  
by  
(The  
asis

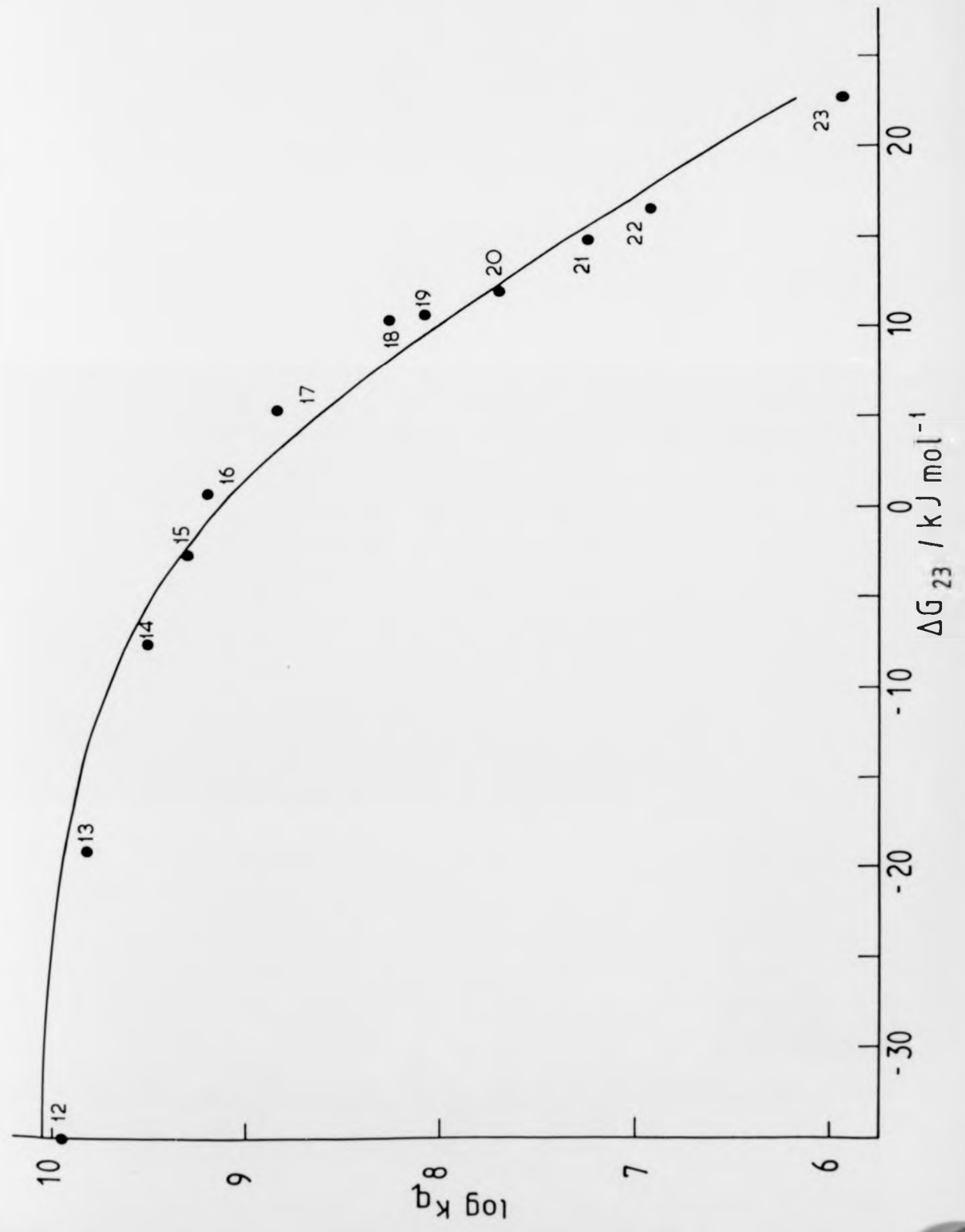


Figure 5.16 Plot of  $\log k_q$  versus  $\Delta G_{23}$  for the electron-transfer quenching by organic compounds of the luminescence of  $[\text{Ru}(\text{bpy})_3]^{2+}$  ( $\square$ ),  $[\text{Ru}(\text{bpy})_2\text{acac}]^+$  ( $\Delta$ ),  $[\text{Ru}(\text{bpy})_2\text{en}]^{2+}$  ( $\bullet$ ) in MeCN.

the  
organic  
of  
cl<sup>+</sup>  
N.

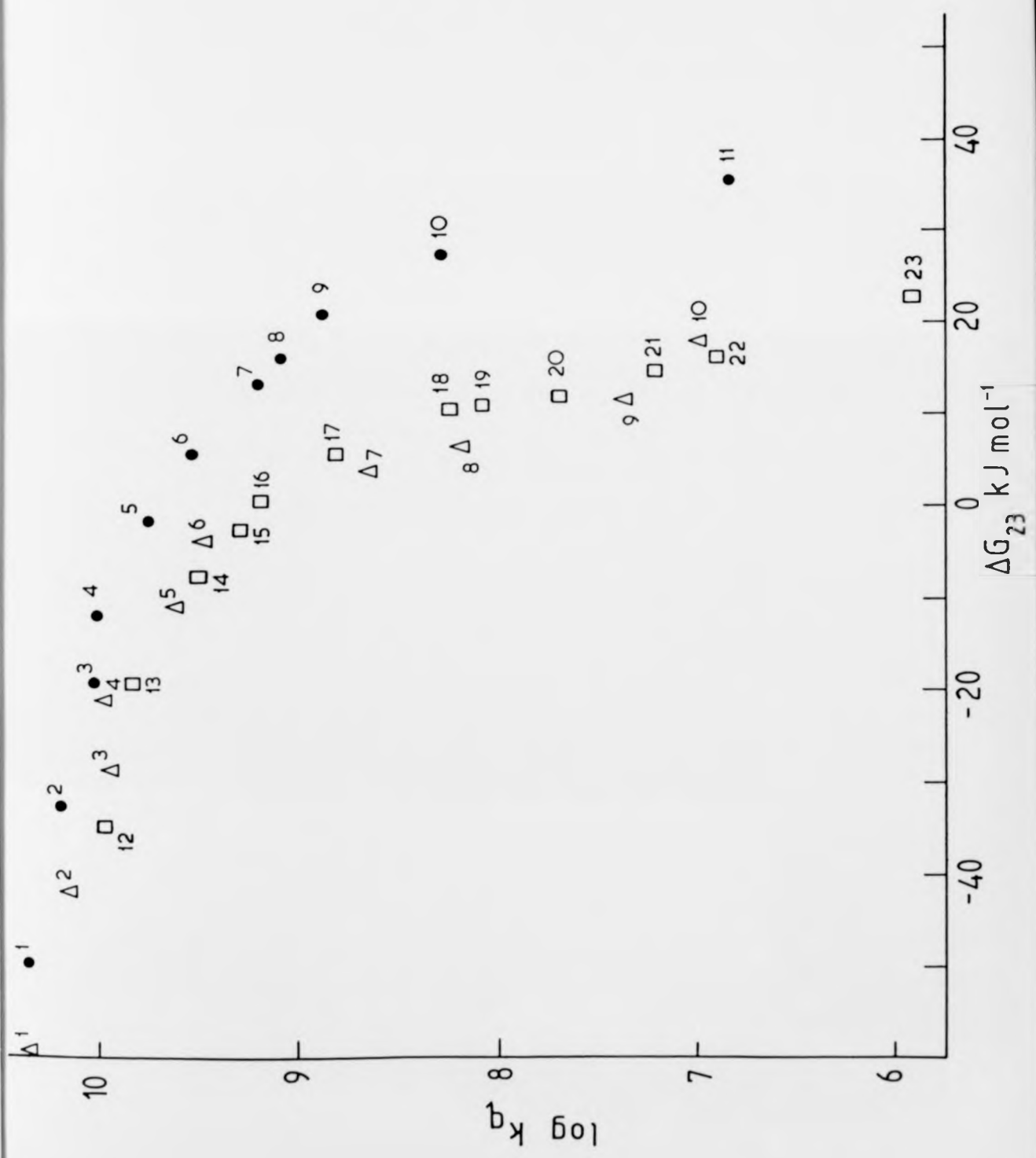
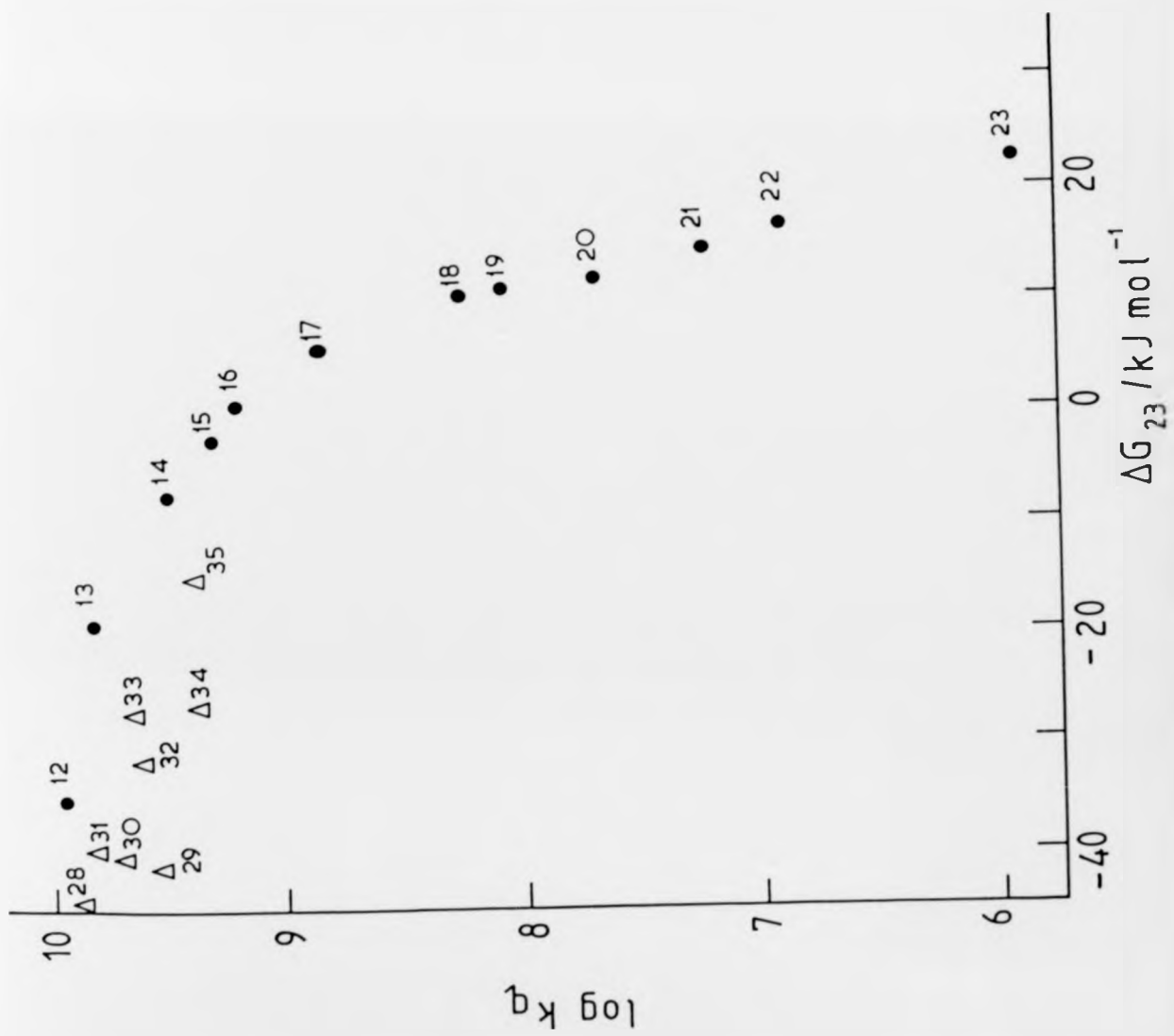


Figure 5.17 Plot of  $\log k_q$  versus  $\Delta G_{23}$  for the electron-transfer quenching of the luminescence of  $[\text{Ru}(\text{bpy})_3]^{2+}$  by nitroaromatics ( $\bullet$ ) and quinones ( $\Delta$ ).

Figure 5.17 Plot of  $\log k_q$  versus  $\Delta G_{23}$  for the electron-transfer quenching of the luminescence of  $[\text{Ru}(\text{bpy})_3]^{2+}$  by nitroaromatics ( $\bullet$ ) and quinones ( $\Delta$ ).

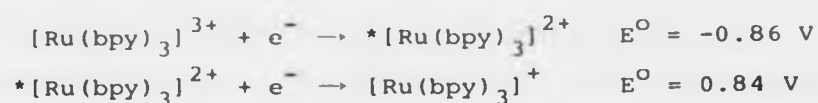
or the  
F  
] 2+



expressed these data for each complex in turn in the form of Weller-type plots (Figures 5.13 to 5.17). Again, we have extended the plot of Whitten *et al.*<sup>174</sup> on  $[\text{Ru}(\text{bpy})_3]^{2+}$  to include the very recent data of Vlček and Bolletta<sup>149</sup> on quinones. Finally, we include in each plot a curve calculated on the basis of Weller theory<sup>49,50</sup> (the relevant calculations being included in Tables 5.5 to 5.8).

#### 5.6 KINETICS OF LUMINESCENCE QUENCHING BY ELECTRON-TRANSFER : DISCUSSION

The conversion and storage of solar energy into real energy resources requires the transformation of an abundant and low cost raw material into a fuel, i.e. into a highly energetic chemical species that can be stored and transported. Simple economical, ecological, and energetic considerations show that water, carbon dioxide, and nitrogen are the most attractive raw materials that can be used as feedstocks of solar reactors, and that hydrogen, methane, ethanal and ammonia are among the most valuable fuels that one would like to obtain<sup>256 257</sup>. Many investigations have been made on quenching phenomena and photoreactivity of the strongly luminescent complex  $[\text{Ru}(\text{bpy})_3]^{2+}$  which can be used as a catalyst for solar energy conversion and it is its electron-transfer processes which are of interest in solar energy applications. The redox potentials for  $[\text{Ru}(\text{bpy})_3]^{2+}$  in aqueous solution are<sup>48</sup>:



Therefore the excited state, which is both a strong reductant and a reasonable oxidant, should be capable of reducing water to hydrogen<sup>258</sup>



being regenerated at moderate to high pH

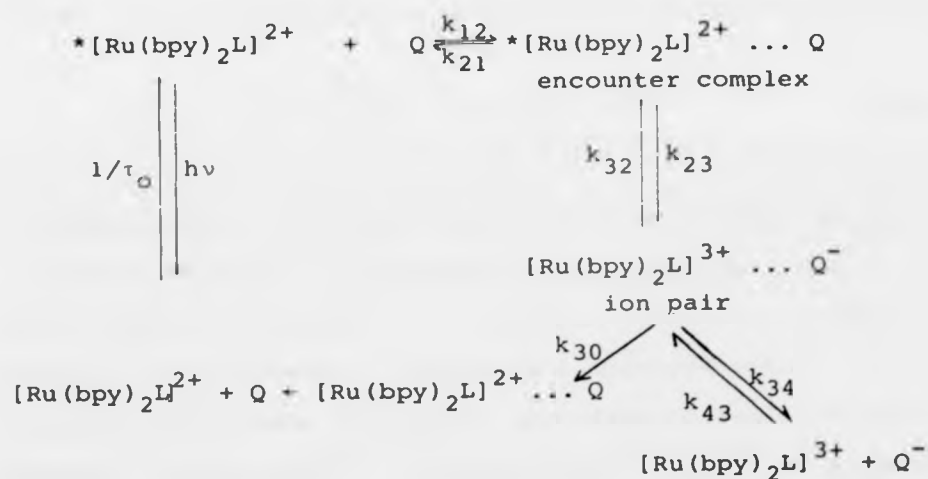


The quenching of long-lived excited states by electron-transfer to yield unstable ground-state products represents a potentially important energy conversion process. This part of the work concerns the oxidation potentials of species such as  $*[\text{Ru}(\text{bpy})_3]^{2+}$  and its analogues  $[\text{Ru}(\text{bpy})_2\text{en}]^{2+}$  and  $[\text{Ru}(\text{bpy})_2\text{acac}]^+$ , and the energy parameters governing the quenching processes. These results present a detailed picture of the excited state electron-transfer process and indicate that energy conversion is an extremely efficient process especially for  $*[\text{Ru}(\text{bpy})_3]^{2+}$ .

All of the organic compounds which were used as acceptors quenched the emission of these three Ru(II) complexes, ( $[\text{Ru}(\text{bpy})_3]^{2+}$ ,  $[\text{Ru}(\text{bpy})_2\text{acac}]^+$  and  $[\text{Ru}(\text{bpy})_2\text{en}]^{2+}$ ) and the rates were found to vary monotonically with the quencher reduction potential,

which clearly supports the quenching mechanism as electron-transfer. In the electron-transfer mechanism (Scheme I), the immediate product is most probably an ion-pair,

Scheme I



where L = bpy or acac<sup>-</sup> and Q = quencher. It is assumed that  $k_{34} \ll k_{30}$ , because it was reported that for the combination,  $[\text{Ru}(\text{bpy})_3]^{3+} \cdots \text{Q}^-$ , the escape probability is very low<sup>174,259</sup>. According to Scheme I the overall rate constant can be obtained using the Stern-Volmer relationship and the steady-state approximation:

$$k_q = \frac{k_{12}}{1 + \frac{k_{21}}{k_{23}} + \frac{k_{21} k_{23}}{k_{23} k_{30}}} \quad (5.3)$$

The equation 5.3 obtained is analogous to that used by

Rehm and Weller<sup>49,50</sup> (equation 1.17). As mentioned in a previous section 1.5, the bimolecular quenching constant of an excited-state electron-transfer reaction (equation 1.22) depends on the free activation energy ( $\Delta G_{23}^\ddagger$ ) and the free energy change ( $\Delta G_{23}$ ) of the electron-transfer step. According to Weller<sup>49,50</sup>, the relationship between these two quantities is as given earlier in equation 1.23.

$$\Delta G_{23}^\ddagger = \frac{\Delta G_{23}}{2} + \left[ \left( \frac{\Delta G_{23}}{2} \right)^2 + (\Delta G_{23}^\ddagger(0))^2 \right]^{1/2} \quad (1.23)$$

In this work we calculated the free energy change ( $\Delta G_{23}$ ) following Weller<sup>49,50</sup> (equation 1.19), and hence the quenching rate constant *via* (equation 1.22). In general there is good agreement between the observed rate constants and those calculated according to Weller theory. However,  $[\text{Ru}(\text{bpy})_2\text{en}]^{2+}$  is exceptional in that the quenching rate constants are consistently faster than expected, (often greatly so) and this unusual result will be discussed later.

The electron-transfer quenching mechanism for the quenching of excited  $[\text{Ru}(\text{bpy})_3]^{2+}$  and  $[\text{Ru}(\text{bpy})_2\text{acac}]^+$  by organic compounds (nitroaromatics and quinones), is implied by the correlation of the quenching rate constant,  $\log k_q$ , with the values of the reduction potentials,  $E_{1/2}$ , for these quenchers (Figures 5.12 to 5.17). The values of  $\log k_q$  approach asymptotically the diffusion-controlled limit as the thermodynamic oxidising power of the quenchers increase. At low  $E_{1/2}(\text{Q}/\text{Q}^-)$  values the plot of  $\log k_q$  versus  $E_{1/2}(\text{Q}/\text{Q}^-)$  should be linear with

a slope =  $-(1/2.3RT)$ . The slope of the linear portion in Figure 5.12 for  $[\text{Ru}(\text{bpy})_3]^{2+}$  and  $[\text{Ru}(\text{bpy})_2\text{acac}]^+$  is  $16.6 \pm 1$  and  $16.1 \pm 1 \text{ V}^{-1}$  respectively which are in good agreement with the theoretical value of  $16.9 \text{ V}^{-1}$ .

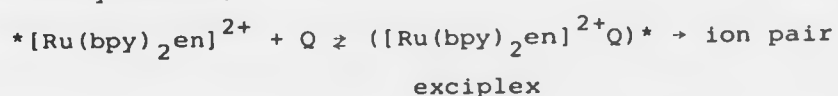
The most useful generalisation, due to Rehm and Weller<sup>49,50</sup>, is that observation of quenching rate constants approaching the diffusion-controlled limit indicate that  $\Delta G_{23}$  is strongly negative, while rate constants a factor of ten below the diffusion-controlled limit indicate that  $\Delta G_{23} \sim 0$  and, finally, that values less than a tenth of the diffusion-controlled limit indicate that  $\Delta G_{23}$  is positive (see Figures 5.13 to 5.17). The limiting slope reached when  $\Delta G_{23}$  is positive which is equal to  $-1/2.3RT = -0.177 \text{ mol kJ}^{-1}$ , is found in the cases of both  $[\text{Ru}(\text{bpy})_3]^{2+}$  and  $[\text{Ru}(\text{bpy})_2\text{acac}]^+$  which give slopes of  $-0.178$  and  $-0.167 \text{ mol kJ}^{-1}$  respectively, which agree well with equation 1.22.

The values of  $E_{\text{ox}}^*$  in Table 5.4 for polypyridyl complexes of Ru(II) can be estimated from the data in Figures 5.12 by extrapolation of the linear portion of the curve to a value of  $\log k_q$  in the range  $10-11$ <sup>49</sup>. The extrapolation, which has been used by Whitten *et al.*<sup>174</sup> to estimate the value of  $E_{\text{ox}}^*$  for  $[\text{Ru}(\text{bpy})_3]^{3+}/[\text{Ru}(\text{bpy})_3]^{2+}$  as  $-0.81 \pm 0.02 \text{ V}$ , agree well with that calculated in Table 5.4. An estimation of  $E_{\text{ox}}^*$  for the  $[\text{Ru}(\text{bpy})_2\text{acac}]^{2+}/[\text{Ru}(\text{bpy})_2\text{acac}]^+$  couple by the same procedure gives a value of  $1.03 \text{ V}$ .

The model behaviour exhibited by the complexes of  $[\text{Ru}(\text{bpy})_3]^{2+}$  and  $[\text{Ru}(\text{bpy})_2\text{acac}]^+$  suggests that an

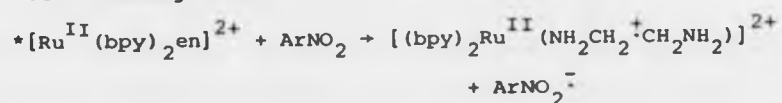
alternative mechanism may operate for  $[\text{Ru}(\text{bpy})_2\text{en}]^{2+}$ , which might be one of the following:

- (a) exciplex quenching of the luminescence by the quencher,



However, there is no evidence of any new emission band at longer wavelengths, although this does not exclude a non-emissive exciplex.

- (b) Semi-oxidation of the electron-rich ligand as opposed to the metal core (followed by a slow secondary electron-transfer from the metal ion to the ligand).



This offers an interesting possibility in the case of  $[\text{Ru}(\text{bpy})_2\text{en}]^{2+}$ , because there are a number of literature reports of metal centres coordinated to organic free radicals, e.g. the species  $[\text{Mn}^{\text{II}}(\text{EDTA})]^-$  found in the photolysis at 77 K of the complex  $[\text{Mn}^{\text{III}}(\text{EDTA})]^-$  following electron transfer from the ligand<sup>260</sup>. Another example is that due to DeArmond and Halper<sup>261</sup>, who found a metal-containing radical in the sensitised photolytic decomposition of certain luminescent rhodium(III) chelates at 77 K by means of e.s.r. spectroscopy (phen refers to an ethanol radical coordinated to the phen ring)



Kohno *et al.*<sup>262</sup> also reported the e.s.r. detection of the  $\pi$ -cation radical at 77 K trapped in a single crystal of chloro(tetraphenylporphyrinato)cobalt(II). (These are just three examples taken from a much wider range.)

Regrettably we could not carry out useful electron-transfer studies on  $[\text{Ru}(\text{bpy})_2\text{Cl}_2]$ , because of ground-state interaction between the complex and the acceptors, as mentioned above (Section 5.4), which suggests a ground-state charge-transfer between the complex and the acceptor which may result in the production of  $[\text{Ru}(\text{bpy})_2\text{Cl}_2^+ \cdot \text{ArNO}_2^-]$  complex in photoexcitation.

In summary, replacement of (bpy) by the ligands (en) or (acac) reduces the luminescence quantum yield of the complex  $[\text{Ru}(\text{bpy})_2(\text{ligand})]^{n+}$ , but not the propensity to participate in photo-electron transfer processes. Both  $[\text{Ru}(\text{bpy})_3]^{2+}$  and  $[\text{Ru}(\text{bpy})_2(\text{acac})]^+$  follow the Weller model to an almost ideal extent, but  $[\text{Ru}(\text{bpy})_2(\text{en})]^{2+}$  shows an interesting discrepancy suggestive of a new type of interaction which we could not completely define and which requires further detailed work.

CHAPTER 6

LUMINESCENCE FROM A BINUCLEAR PLATINUM  
COMPLEX: A PRELIMINARY STUDY

This chapter deals briefly with luminescence from an interesting complex containing a Pt-Pt bond, namely  $[\text{Pt}(\text{PPh}_3)_2]_2$  brought initially to our attention by Professor O. Traverso of the University of Ferrara, Italy. It has been reported<sup>269</sup> that certain polynuclear complexes containing metal-metal bonds possess emissive excited states that undergo oxidation reduction reactions in solution, which include  $d^4-d^4$ ,  $d^8-d^8$ , and  $(d^4)_6$  systems. The emission from  $[\text{Pt}(\text{PPh}_3)_2]_2$  constitutes a useful extension of this series to a  $d^{10}-d^{10}$  system.

Tertiary phosphine complexes of platinum(0) were reported firstly in 1958<sup>270</sup>, and proven to be versatile reagents for the synthesis of a wide variety of compounds<sup>271</sup>. Reactions of the triphenylphosphine complexes of platinum have been extensively studied<sup>271</sup>, because of their reactivity towards unsaturated molecules, utility in oxidative addition reactions, and use as homogeneous catalysts for oxidations by molecular oxygen. In many of these reactions there is evidence of participation by a reactive intermediate<sup>271</sup> which is a coordinatively unsaturated species having the formula  $\text{Pt}(\text{PPh}_3)_2$ . The isolation<sup>272</sup> of yellow material described as  $[\text{Pt}(\text{PPh}_3)_2]_x$  which behaves as a monomer in solution has made easier the investigation of the coordinative reactivity of triphenylphosphine complexes of platinum(0).

Blake and Nyman<sup>273</sup> have reported that photolysis of  $[\text{Pt}(\text{PPh}_3)_2\text{C}_2\text{O}_4]$  in ethanol solution, under an inert atmosphere, yields a complex of empirical formula  $[\text{Pt}(\text{PPh}_3)_2]$  which molecular weight determination in



benzene indicates to be the dimer. Prolonged heating of the dimer with triphenylphosphine in ethanol does not cause its decomposition, and there is no reaction of the dimer in benzene with oxygen and carbon dioxide to give a carbonato complex as exhibited by monomeric platinum(0) complexes of phosphines and arsines<sup>1</sup>.

Our interest in  $[\text{Pt}(\text{PPh}_3)_2]_2$  is that it relates to another highly luminescent complex  $[\text{Pt}_2(\text{P}_2\text{O}_5)_4\text{H}_8]^{4-}$  characterised spectroscopically by Gray *et al.*<sup>274,275</sup> and crystallographically by Sadler *et al.*<sup>276</sup>. It was reported<sup>274</sup> that  $\text{K}_4[\text{Pt}_2(\text{P}_2\text{O}_5)_4\text{H}_8] \cdot 2\text{H}_2\text{O}$  shows remarkable luminescence properties which are attributed to the presence of Pt-Pt bonding. Thus at room temperature it fluoresces at 407 nm and phosphoresces at 517 upon excitation at 367 nm, but it shows phosphorescence exclusively upon excitation at 452 nm.

Traverso reports<sup>277</sup> that  $[\text{Pt}(\text{PPh}_3)_2]_2$  luminesces at room temperature in DMF solution with  $\lambda_{\text{max}}$  in the region 400-500 nm, but in a glassy solvent at 77 K it shows a red luminescence ( $\lambda = 660-670$  nm) in ethanol or MTHF. Also relevant to this discussion are the observations of Vogler *et al.*<sup>278,279</sup> as follows:

- (i) Photolysis of *cis*- $[\text{Pt}(\text{PPh}_3)_2(\text{N}_3)_2]$  and  $[\text{Pt}(\text{PPh}_3)_2\text{C}_2\text{O}_4]$  in ethanol or MTHF at 77 K leads to intense emission at 445 nm but the samples show no e.s.r. signals. On warming the photolysed sample to room temperature

$[\text{Pt}(\text{PPh}_3)_2]_2$  was formed, which was identified by its intensely red luminescence at 77 K ( $\lambda = 665$  nm). They believed that the oxalate and azide complexes form a common photo-product stable only at low temperature and emitting with  $\lambda \sim 445$  nm, which they attribute to  $[\text{Pt}(\text{PPh}_3)_2]$ .

- (ii) Photolysis of  $[\text{Pt}(\text{PPh}_3)_2\text{O}_2]$  at 77 K leads to a blue emission ( $\lambda = 445$  nm) again attributed to the monomer  $[\text{Pt}(\text{PPh}_3)_2]$ <sup>282</sup>.

The results of our study of  $[\text{Pt}(\text{PPh}_3)_2]_2$  (recrystallized from benzene)<sup>273</sup>, are summarised as follows:

(a) Room temperature luminescence: this complex shows an emission as a doublet ( $\lambda$  500 and 520 nm) in DMF in degassed solution upon excitation at 380 nm, which is quenched effectively by oxygen as shown in Figure 6.1. In MTHF solution it shows two emission bands at 450 and 525 nm in degassed solution. In ethanol-methanol (4:1) solvent it emits at 460 nm.

(b) Luminescence at 77 K: as previously reported<sup>278,279</sup>, a red luminescence was observed from  $[\text{Pt}(\text{PPh}_3)_2]_2$  at 77 K with  $\lambda_{\text{max}}$  660-670 nm. In frozen DMF it shows an emission at 663 nm, but as the temperature is raised from 77 K, the emission intensity decreased gradually and at about 140 K the band at 500 nm becomes well-defined;

Figure 6.1 Luminescence spectra of  $[\text{Pt}(\text{PPh}_3)_2]_2$  in DMF at room temperature (curve A) and at 80.5 K (curve C). Quenching of the luminescence by  $\text{O}_2$  at room temperature (curve B).

$3^1 2^1 2$   
Curve A)  
ching of

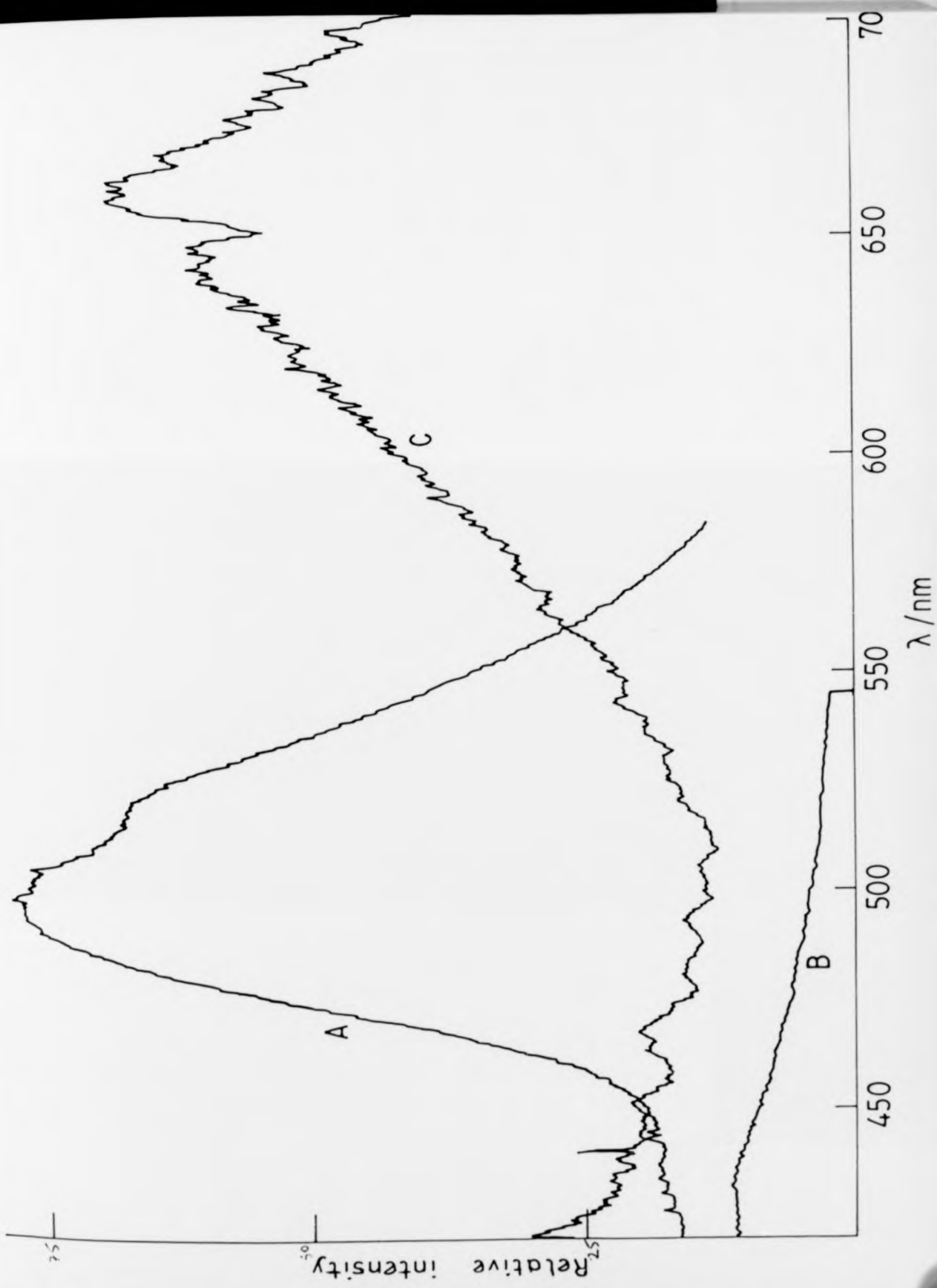
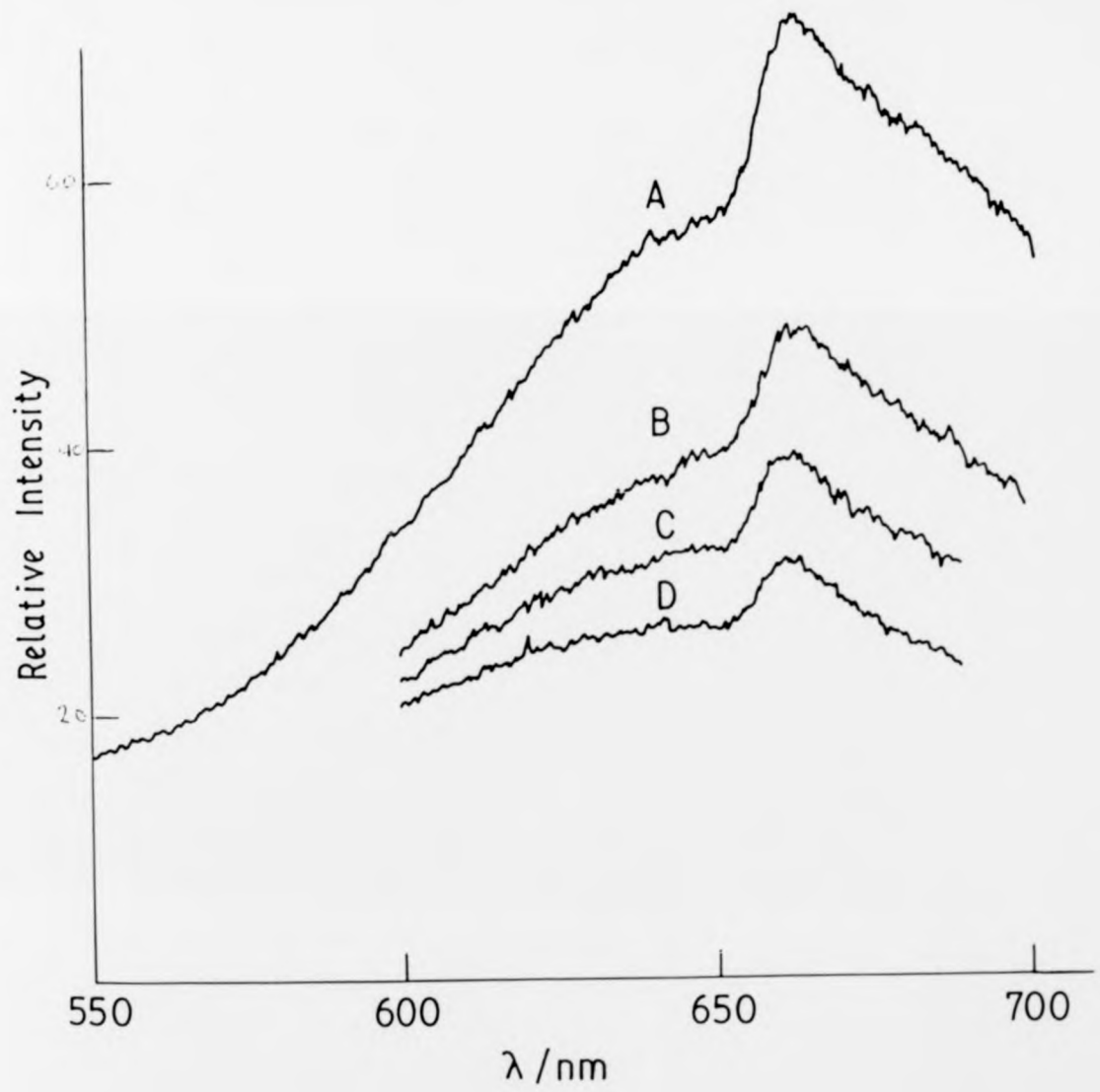


Figure 6.2      The effect of the irradiation by  
u.v. light on the luminescence  
of  $[\text{Pt}(\text{PPh}_3)_2]_2$  in MTHF at 80 K.  
(A) before irradiation  
(B) 5 minutes irradiation  
(C) 10 minutes irradiation  
(D) 60 minutes irradiation

on by  
nce  
80 K.



at room temperature the 663 nm band disappears completely. Using MTHF as a solvent, which gives a very good glass on freezing, the emission at 77 K is situated at 663 and 725 nm. In EtOH-MeOH (4:1), the low-temperature emission is at 660 nm. Photolysis of  $[\text{Pt}(\text{PPh}_3)_2]_2$  with u.v. light (100 W high pressure mercury arc lamp) in MTHF solvent at 77 K induces a decrease in the emission intensity at 663 nm with time (Figure 6.2).

(c) Lifetime measurements: we have measured the emission lifetime of  $[\text{Pt}(\text{PPh}_3)_2]_2$  at 77 K in three different solvents, namely DMF, MTHF, and EtOH-MeOH (4:1) as, respectively,  $(10.1 \pm 0.2)$ ,  $(15.8 \pm 0.4)$ , and  $(12.2 \pm 0.4)$   $\mu\text{s}$ . Lifetimes of both the blue and red emission at room temperature were too short to measure with our instrumentation.

(d) Temperature-dependence studies of the luminescence lifetime: this has been investigated for three media. The temperature profile of the luminescence lifetime has been determined over the range 82 to 220 K for both DMF and EtOH-MeOH (4:1) solvents, and 82 to 165 K for MTHF solvent.

The lifetime data for DMF and EtOH-MeOH solvents were fitted to the two-exponential expression (2EXP) such as we used for ruthenium(II) complexes in the previous chapter (equation 5.1). On the other hand, fitting to 2EXP for lifetime data in MTHF was unsuccessful, and fitting of the two regions to simple Arrhenius expressions was used in this case. The resulting

Table 6.1 [Pt(PPh<sub>3</sub>)<sub>2</sub>]<sub>2</sub>: Activation Parameters for Luminescence Deactivation

| Solvent         | $A_1/s^{-1}$                     | $\Delta E_1/kJ\ mol^{-1}$ | $A_2/s^{-1}$                  | $\Delta E_2/kJ\ mol^{-1}$ |
|-----------------|----------------------------------|---------------------------|-------------------------------|---------------------------|
| DMF             | $(2.89 \pm 0.47) \times 10^8$    | $(12.6 \pm 2.1)$          | $(1.28 \pm 0.31) \times 10^5$ | $(0.07 \pm 0.02)$         |
| EtOH-MeOH (4:1) | $(3.71 \pm 1.12) \times 10^{10}$ | $(20.1 \pm 4.3)$          | $(8.81 \pm 5.20) \times 10^4$ | $(0.04 \pm 0.03)$         |
| MTHF            | $(1.36 \pm 0.32) \times 10^{15}$ | $(27.5 \pm 5.6)$          | $(1.17 \pm 0.4) \times 10^5$  | $(0.55 \pm 0.61)$         |

Arrhenius parameters in these three solvents are given in Table 6.1. The lifetime data together with the fitted 2EXP curves for  $[\text{Pt}(\text{PPh}_3)_2]_2$  in these solvents are shown in Figures 6.3, 6.4 and 6.5.

The fitted values of  $\Delta E_1$  (Table 6.1) show a considerable solvent-dependence, which implies that the thermally-activated route corresponds to deactivation through a higher level the position of which is solvent-sensitive. Figures 6.3, 6.4 and 6.5 indicate the presence of phase transition for DMF at 200 K and for MTHF and EtOH-MeOH at lower temperatures ( $\sim 160$  K).

The low-energy term of 2EXP is susceptible to large errors for data covering a restricted temperature regime, since the  $\Delta E_2$  term will provide only a relatively small contribution to the overall rate constant over this range. The very low values of  $\Delta E_2$  in these solvents suggest that the deactivation is virtually temperature-independent at very low temperatures.

From the luminescence measurements, it is clear that  $[\text{Pt}(\text{PPh}_3)_2]_2$  shows a blue emission at room temperature and a red emission at 77 K. It seems likely that the red luminescence is genuinely due to the dimer  $[\text{Pt}(\text{PPh}_3)_2]_2$ . This is because (a) solutions of this complex luminescence at 660 nm at 77 K, which is in good agreement with the literature<sup>279</sup>, and (b) low-temperature photolysis of the complex leading to the monomeric  $[\text{Pt}(\text{PPh}_3)_2]$ , followed by warming and then recooling to 77 K also results in the red luminescence.

The question of the origin of the blue emission

Figure 6.3 Temperature activation plot for  
luminescence of  $[\text{Pt}(\text{PPh}_3)_2]_2$  in  
DMF at 660 nm.

for  
in

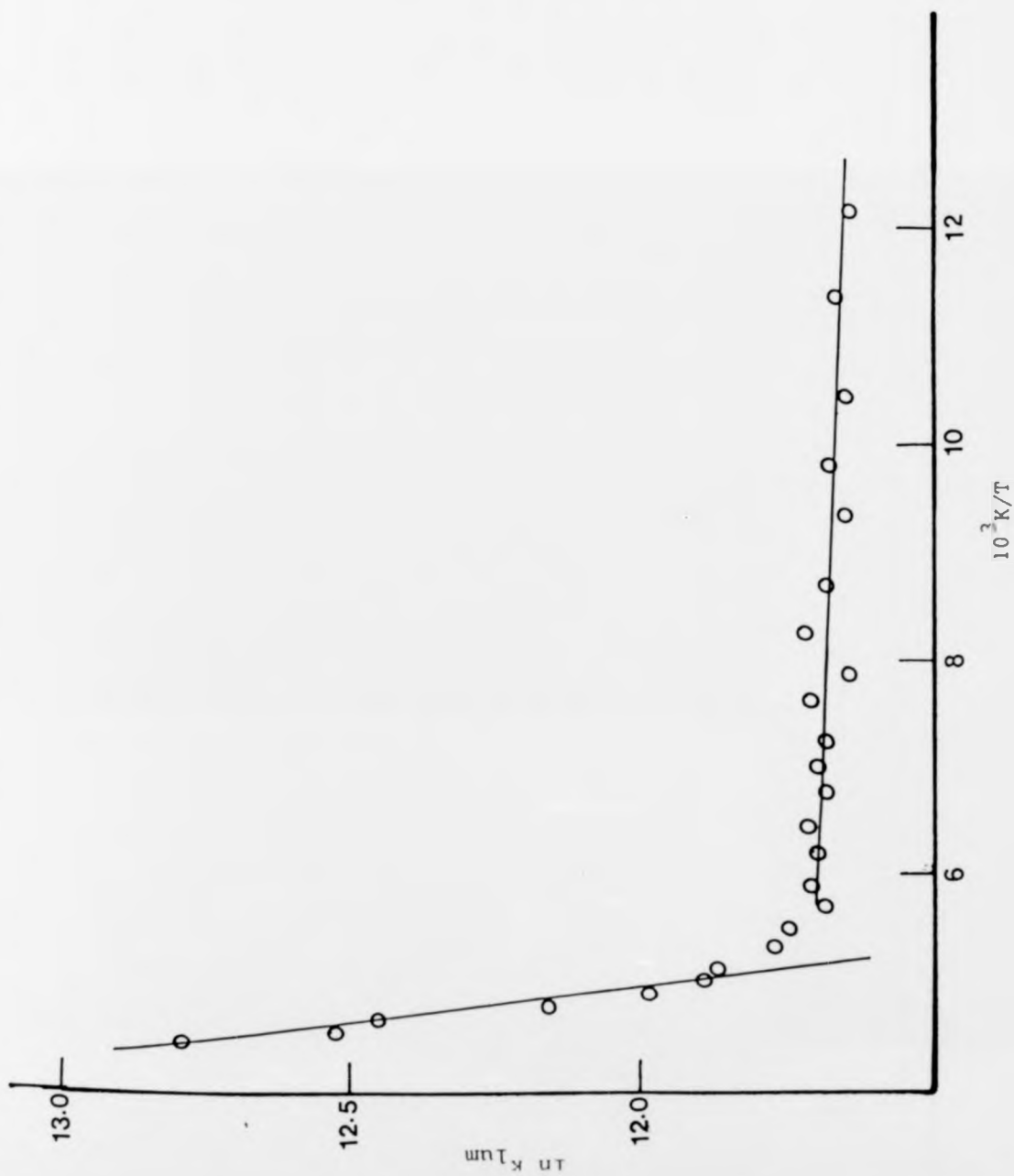


Figure 6.4      Temperature activation plot for  
luminescence of  $[\text{Pt}(\text{PPh}_3)_2]_2$  in  
MTHF at 660 nm.

for  
in

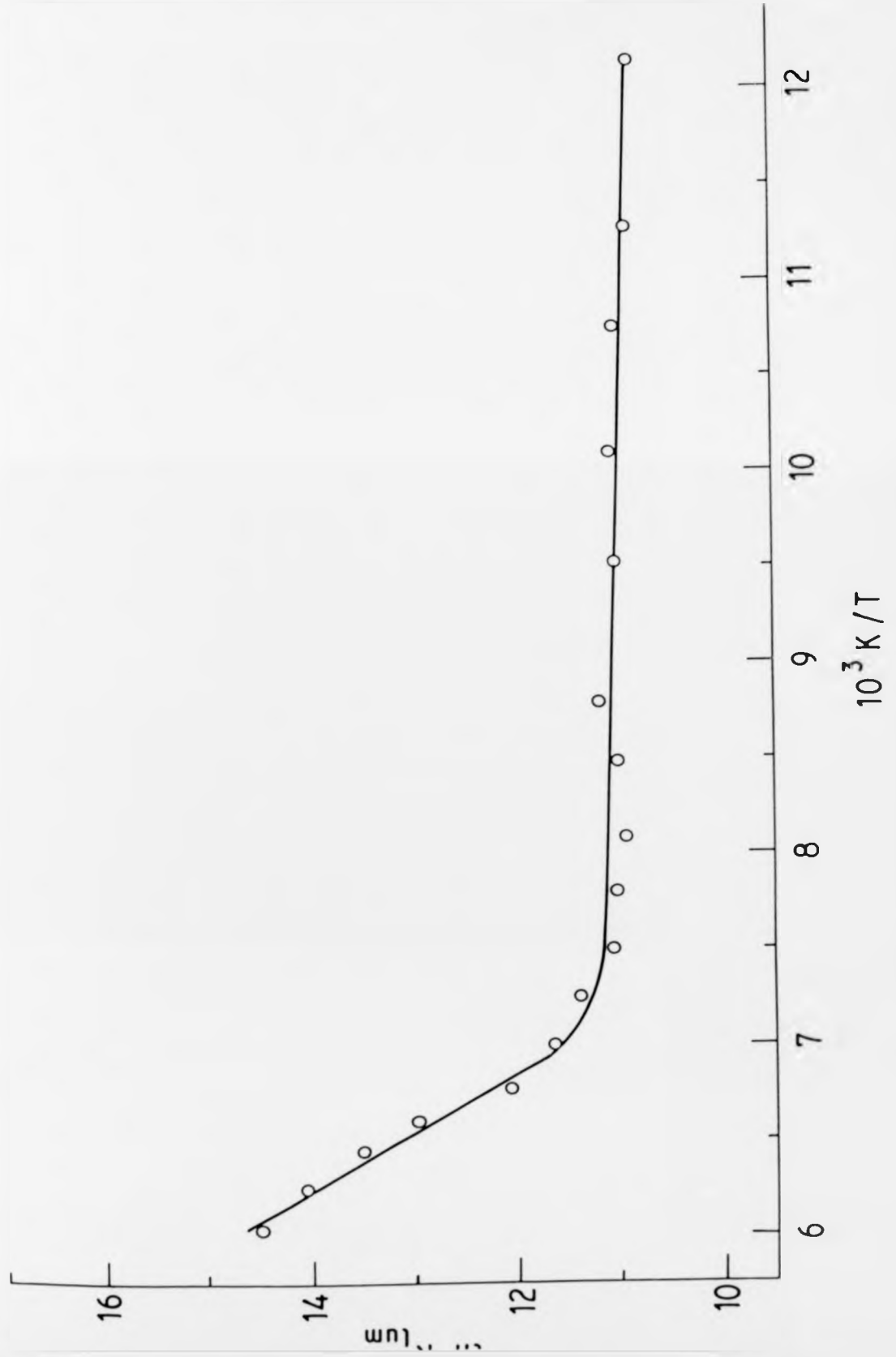
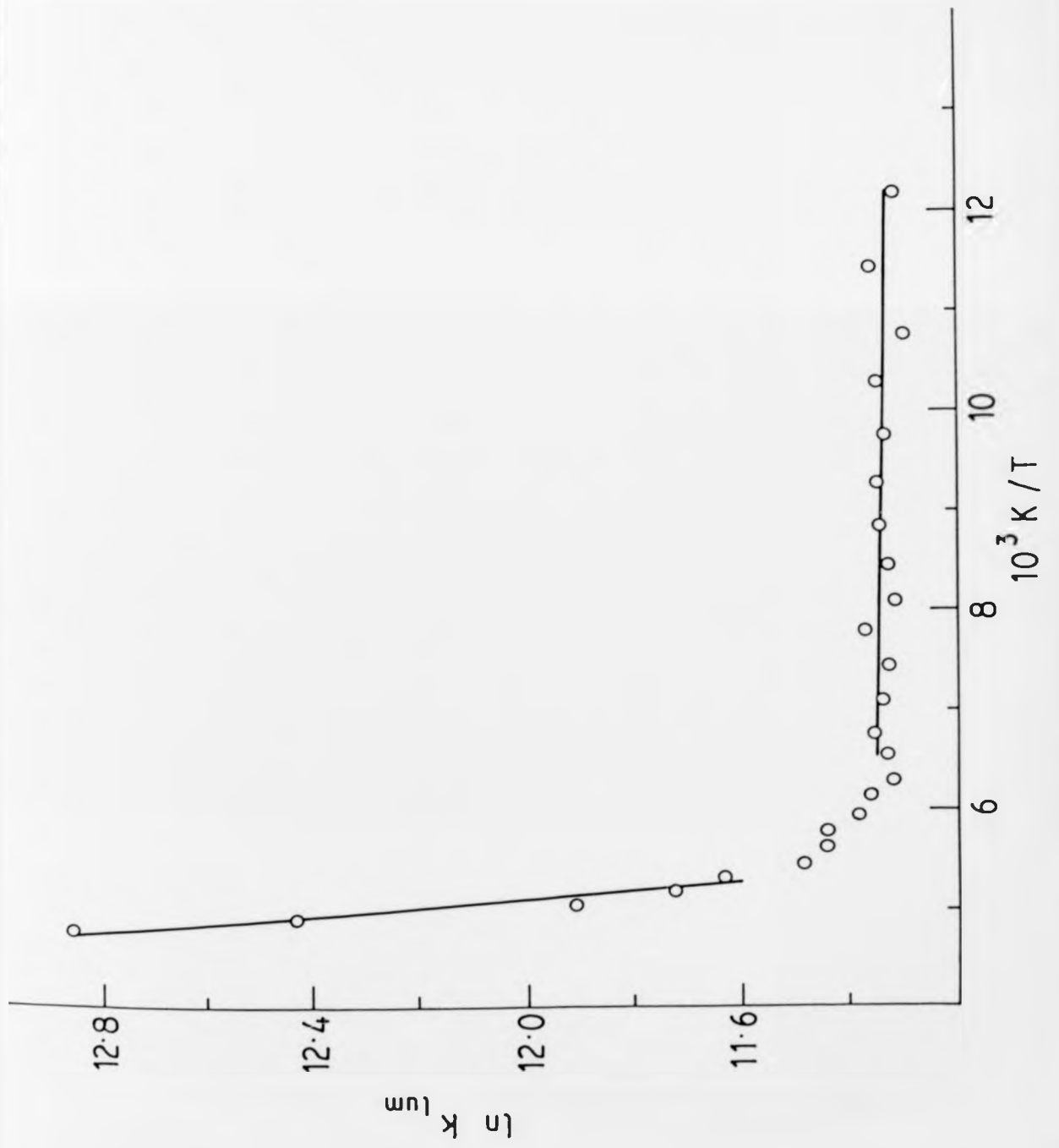


Figure 6.5 Temperature activation plot for  
luminescence of  $[\text{Pt}(\text{PPh}_3)_2]_2$  in  
EtOH-MeOH (4:1) at 660 nm.

t for  
2 in



at room temperature remains open. It can not be due to the monomer as this is believed to be very reactive at room temperature<sup>273</sup>, and it seems unlikely that the dimer can display such a profound temperature-dependence of its emission spectrum. A key observation is the oxygen quenching of the blue emission at room temperature. On this basis we believe the transition responsible for the blue emission to be spin-forbidden, i.e. to be phosphorescence. This would pose the problem that the phosphorescent transition would be at a shorter wavelength than the (presumed) fluorescent transition. However, this situation is not unknown among inorganic species, thus the fluorescence of Cr(III) complexes<sup>7</sup> is at longer wavelengths than the corresponding phosphorescence because of molecular distortion on crossing to the doublet manifold.

REFERENCES

1. A. W. Adamson, W. L. Waltz, E. Zinato, D. W. Watts, P. D. Fleishauer, and R. D. Lindholm, *Chem. Rev.*, 1968, 68, 541
2. J. Franck and G. Scheibe, *Z. Phys. Chem.*, 1928, A139, 22
3. A. W. Adamson and P. D. Fleischauer, in "Concepts of Inorganic Photochemistry", John Wiley, New York, 1975
4. F. S. Dainton, *Chem. Soc. Rev.*, 1975, 4, 323
5. K. Eiben, *Angew Chem. Int. Ed. Engl.*, 1970, 9, 619
6. M. J. Blandamer and M. F. Fox, *Chem. Rev.*, 1970, 70, 59
7. T. J. Kemp, *Progress in Reaction Kinetics*, 1980, 10, 301
8. D. G. Whitten, *Acc. Chem. Res.*, 1980, 13, 83
9. R. Hill, *Nature*, 1937, 139, 881
10. L. P. Vernon and G. R. Seely, in "The Chlorophylls", Academic Press, New York, 1966
11. M. Galvin and J. A. Bassham, in "The Photosynthesis of Carbon Compounds", W. A. Benjamin, New York, 1962
12. V. Balzani and V. Carassiti, in "Photochemistry of Coordination Compounds", Academic Press, London, 1970
13. H. E. White, in "Introduction to Atomic Spectra", McGraw-Hill, Tokyo, 1934
14. Y. Tanabe and S. Sugano, *J. Phys. Soc. Japan*, 1954, 9, 753

15. H. L. Schläfer and G. Gliemann, in "Basic Principles of Ligand Field Theory", John Wiley, London, 1969
16. P. D. Fleischauer and P. Fleischauer, *Chem. Rev.*, 1970, 70, 199
17. T. M. Dunn, in "Modern Coordination Chemistry", Wiley, London, 1960
18. C. K. Jørgenson, *Prog. Inorg. Chem.*, 1962, 4, 73
19. H. H. Schmidtke, in "Physical Methods in Advanced Inorganic Chemistry", Wiley, London 1968
20. R. J. P. Williams, *J. Chem. Soc.*, 1955, 137
21. P. Day and N. Sanders, *J. Chem. Soc.*, 1967, A1530
22. C. K. Jørgenson, *Acta Chem. Scand.*, 1957, 11, 151
23. B. Martin and G. M. Waing, *J. Chem. Soc.*, 1958, 4284
24. R. A. Palmer and T. S. Piper, *Inorg. Chem.*, 1966, 5, 864
25. S. J. Strickler and R. A. Berg, *J. Chem. Phys.*, 1962, 37, 814
26. G. B. Porter and H. L. Schläfer, *Z. Phys. Chem. (Frankfurt)*, 1963, 37, 109
27. T. R. Thomas and G. A. Crosby, *J. Mol. Spec.*, 1971, 38, 118
28. J. N. Demas and G. A. Crosby, *J. Am. Chem. Soc.*, 1971, 93, 2841
29. A. W. Adamson, *J. Phys. Chem.*, 1967, 71, 798

30. H. L. Schläfer, *J. Phys. Chem.*, 1965, 69, 2201
31. K. DeArmond and L. S. Forster, *Spectrochim. Acta*, 1963, 19, 1687
32. T. L. Kelly and J. F. Endicott, *J. Phys. Chem.*, 1972, 76, 1937
33. J. F. Endicott, in "Concepts of Inorganic Photochemistry", edited by A. W. Adamson and P. D. Fleischauer (Wiley, New York, 1975)
34. M. S. Matheson, W. A. Mulac, and J. Rabani, *J. Phys. Chem.*, 1963, 67, 2613
35. J. F. Endicott and M. Z. Hoffman, *J. Am. Chem. Soc.*, 1965, 87, 3348
36. P. P. Zarnegar and D. G. Whitten, *J. Am. Chem. Soc.*, 1971, 93, 3776
37. A. D. Kirk, *Mol. Photochem.*, 1973, 5, 127
38. P. C. Ford, G. Malouf, J. D. Petersen, and V. A. Durante, in "Inorganic Compounds with Unusual Properties", *Adv. Chem. Series*, 1976, 150, 187
39. V. Balzani, L. Moggi, M. F. Manfrin, F. Bolletta, and G. S. Laurence, *Coord. Chem. Rev.*, 1975, 15, 321
40. F. Wilkinson, *Pure App. Chem.*, 1975, 41, 661
41. V. Balzani, F. Bolletta, and F. Scandola, *J. Am. Chem. Soc.*, 1980, 102, 2152
42. H. D. Gafney and A. W. Adamson, *J. Am. Chem. Soc.*, 1972, 94, 8238
43. N. Sabbatini and V. Balzani, *J. Am. Chem. Soc.*, 1972, 94, 7587

44. K. K. Chatterjee and L. S. Forster, *Spectrochim. Acta*, 1974, 33, 63
45. V. Balzani, L. Moggi, F. Bolletta, and M. F. Manfrin, in "Inorganic Compounds with Unusual Properties", Adv. Chem. Series, 1976, 150, 160
46. C. A. Parker, in "Photoluminescence of Solutions", Elsevier, Amsterdam, 1968
47. A. D. Kirk, P. E. Hoggard, G. B. Porter, M. G. Rockley, and M. W. Windsor, *Chem. Phys. Lett.*, 1976, 37, 199
48. V. Balzani, F. Bolletta, M. T. Gaudolfi, and M. Maestri, *Top. Current Chem.*, 1978, 75, 1
49. D. Rehm and A. Weller, *Ber. Bunsenges Phys. Chem.*, 1969, 73, 834
50. D. Rehm and A. Weller, *Isr. J. Chem.*, 1970, 8, 259
51. R. A. Marcus, *Annu. Rev. Phys. Chem.*, 1964, 15, 155
52. R. A. Marcus, *Discuss. Faraday Soc.*, 1960, 29, 21
53. M. Julliard and M. Chanon, *Chemistry in Britain*, 1982, 18, 558
54. J. N. Demas and G. A. Crosby, *J. Am. Chem. Soc.*, 1970, 92, 7262
55. R. Ballardini, M. T. Indelli, G. Varani, C. A. Bignozzi, and F. Scandola, *Inorg. Chim. Acta*, 1978, 31, L423
56. R. F. Ziolo, S. Lipton, and Z. Dori, *J. Chem. Soc., Chem. Commun.*, 1970, 1124
57. M. K. DeArmond, *Acc. Chem. Res.*, 1974, 7, 309

58. R. J. Watts, G. A. Crosby, and J. L. Sansegret, *Inorg. Chem.*, 1972, 11, 1474
59. R. J. Watts and G. A. Crosby, *J. Am. Chem. Soc.*, 1971, 93, 3184
60. D. H. W. Carstens and G. A. Crosby, *J. Mol. Spectr.*, 1970, 34, 113
61. M. K. DeArmond and J. E. Hillis, *J. Chem. Phys.*, 1971, 54, 2247
62. R. Englman and J. Jortner, *Mol. Phys.*, 1970, 18, 145
63. L. S. Forster, in "Inorganic Compounds with Unusual Properties", *Adv. Chem. Series*, 1976, 150, 172
64. G. D. Hager and G. A. Crosby, *J. Am. Chem. Soc.*, 1975, 97, 7031
65. J. Van Houten and R. J. Watts, *J. Am. Chem. Soc.*, 1976, 98, 4853
66. R. W. Harrigan and G. A. Crosby, *J. Chem. Phys.*, 1973, 59, 3468
67. S. C. Pyke and M. W. Windsor, *J. Am. Chem. Soc.*, 1978, 100, 6518
68. M. Mingardi and G. B. Porter, *J. Chem. Phys.*, 1966, 44, 4354
69. G. A. Crosby, *J. Chim. Phys.*, 1967, 64, 160
70. F. Zuloaga and M. Kasha, *Photochem. Photobiol.*, 1968, 7, 549
71. C. K. Jørgensen, *Adv. Chem. Phys.*, 1963, 5, 33
72. C. Furlani, *Coord. Chem. Rev.*, 1966, 1, 51
73. V. Balzani, L. Moggi, F. Scandola, and V. Carassiti, *Inorg. Chim. Acta Rev.*, 1967, 1, 7
74. M. F. Manfrin, G. Varani, L. Moggi, and

- V. Balzani, *Mol. Photochem.*, 1969, 1, 387
75. F. Basolo and R. G. Pearson, in "Mechanism of Inorganic Reactions", Wiley, New York, 1967
76. V. Balzani, R. Ballardini, N. Sabbatini, and L. Moggi, *Inorg. Chem.*, 1968, 7, 1398
77. R. A. Pribush, C. K. Poon, C. M. Bruce, and A. W. Adamson, *J. Am. Chem. Soc.*, 1974, 96, 3027
78. E. R. Kantrowitz, M. Z. Hoffman, and J. F. Endicott, *J. Phys. Chem.*, 1971, 75, 1914
79. G. Ferraudi and J. F. Endicott, *J. Chem. Soc., Chem. Commun.*, 1973, 674
80. A. W. Adamson and A. H. Sporer, *J. Am. Chem. Soc.*, 1958, 80, 3865
81. L. Moggi, F. Bolletta, V. Balzani, and F. Scandola, *J. Inorg. Nucl. Chem.*, 1966, 28, 2589
82. A. W. Adamson, A. Chiang and E. Zinato, *J. Am. Chem. Soc.*, 1969, 91, 5467
83. M. Wrighton and D. Bredesen, *Inorg. Chem.*, 1973, 12, 1707
84. A. W. Adamson, *Coord. Chem. Rev.*, 1968, 3, 169
85. P. D. Fleischauer, A. W. Adamson, and G. Sartori, *Prog. Inorg. Chem.*, 1972, 17, 1
86. A. Vogler and A. W. Adamson, *J. Am. Chem. Soc.*, 1968, 90, 5943
87. N. J. Turro, in "Molecular Photochemistry", Benjamin, New York, 1965
88. D. Valentine, *Adv. Photochem.*, 1968, 6, 123
89. G. B. Porter, *J. Am. Chem. Soc.*, 1969, 91, 3980
90. M. A. Scandola and F. Scandola, *J. Am. Chem. Soc.*, 1972, 94, 1805

91. M. A. Scandola, F. Scandola, and V. Carassiti, *Mol. Photochem.*, 1969, 1, 403
92. M. A. Scandola, *J. Am. Chem. Soc.*, 1970, 92, 7278
93. H. D. Gafney and A. W. Adamson, *J. Phys. Chem.*, 1972, 78, 1105
94. P. Natarajan and J. F. Endicott, *J. Phys. Chem.*, 1973, 77, 1823
95. P. Natarajan and J. F. Endicott, *J. Am. Chem. Soc.*, 1973, 95, 2470
96. J. L. Reed, *Inorg. Chem.*, 1982, 21, 2829
97. S. Arunachalam and P. Natarajan, *J. Chem. Soc., Chem. Commun.*, 1982, 472
98. G. N. Schrauzer, *Angew Chem. Int. Ed. Engl.*, 1976, 15, 417
99. P. G. Lenhert and D. Crowfoot-Hodgkin, *Nature*, 1961, 192, 937
100. G. N. Schrauzer and J. Kohnle, *Chem. Ber.*, 1964, 97, 3056
101. D. Crowfoot-Hodgkin, J. Pickworth, J. H. Robertson, K. N. Trueblood, R. J. Prosen, and J. G. White, *Nature*, 1955, 175, 325
102. D. G. Brown, *Prog. Inorg. Chem.*, 1973, 18, 177
103. P. G. Lenhert, *J. Chem. Soc., Chem. Commun.*, 1967, 980
104. G. N. Schrauzer, E. Deutsch, and R. J. Windgassen, *J. Am. Chem. Soc.*, 1968, 90, 2441
105. G. N. Schrauzer and E. Deutsch, *J. Am. Chem. Soc.*, 1969, 91, 3341

106. G. N. Schrauzer and R. J. Windgassen,  
*Chem. Ber.*, 1966, 99, 602
107. G. N. Schrauzer, *Acc. Chem. Res.*, 1968, 1, 97
108. G. N. Schrauzer and R. J. Windgassen,  
*J. Am. Chem. Soc.*, 1966, 88, 3738
109. E. A. Stadlbauer, R. J. Holland, F. P. Lamm,  
and G. N. Schrauzer, *Bioinorg. Chem.*, 1974,  
4, 67
110. G. N. Schrauzer and R. J. Windgassen,  
*J. Am. Chem. Soc.*, 1967, 89, 1999
111. G. N. Schrauzer, J. H. Weber, and T. M. Beckham,  
*J. Am. Chem. Soc.*, 1970, 92, 7078
112. G. N. Schrauzer, R. J. Windgassen, and  
J. Kohnle, *Chem. Ber.*, 1965, 98, 3324
113. G. N. Schrauzer and L. P. Lee, *J. Am. Chem. Soc.*,  
1968, 90, 6541
114. R. A. Firth, H. A. O. Hill, M. J. Pratt,  
R. J. P. Williams, and W. R. Jackson,  
*Biochemistry*, 1967, 6, 2179
115. G. N. Schrauzer, L. P. Lee, and W. J. Sibert,  
*J. Am. Chem. Soc.*, 1970, 92, 2997
116. G. N. Schrauzer, J. W. Sibert, and R. J. Windgassen,  
*J. Am. Chem. Soc.*, 1968, 90, 6681
117. R. Yamada, S. Shimizu, and S. Fukui,  
*Biochem. Biophys. Acta*, 1966, 124, 195
118. R. Yamada, S. Shimizu, and S. Fukui,  
*Biochem. Biophys. Acta*, 1966, 124, 197
119. C. Giannotti, C. Fontaine, and B. Septe,  
*J. Organomet. Chem.*, 1974, 71, 107

120. C. Giannotti and J. R. Bolton, *J. Organomet. Chem.*, 1974, 80, 379
121. C. Giannotti and J. R. Bolton, *J. Organomet. Chem.*, 1976, 110, 383
122. B. T. Golding, T. J. Kemp, P. J. Sellars, and E. Nocchi, *J. Chem. Soc., Dalton Trans.*, 1977, 1266
123. J. F. Endicott and G. J. Ferraudi, *J. Am. Chem. Soc.*, 1977, 99, 243
124. J. F. Endicott and T. L. Natzel, *J. Am. Chem. Soc.*, 1979, 101, 4000
125. D. W. Barnum, *J. Inorg. Nucl. Chem.*, 1961, 21, 221
126. D. W. Barnum, *J. Inorg. Nucl. Chem.*, 1961, 21, 183
127. N. Filipescu and H. Way, *Inorg. Chem.*, 1969, 8, 1863
128. (a) M. C. R. Symmons, Private Communication
128. (b) D. N. R. Rao and M. C. R. Symmons, *J. Organomet. Chem.*, 1983, 244, C43
129. B. T. Golding, in "B<sub>12</sub>", Vol. 1, edited by D. Dolphin, John Wiley, 1982
130. J. P. Paris and W. W. Brandt, *J. Am. Chem. Soc.*, 1959, 81, 5001
131. J. N. Demas and A. W. Adamson, *J. Am. Chem. Soc.*, 1973, 95, 5159
132. C. T. Lin, W. Böttcher, M. Chou, C. Creutz, and N. Sutin, *J. Am. Chem. Soc.*, 1976, 98, 6536
133. K. Kalyanasundaram, *Coord. Chem. Rev.*, 1982, 46, 159

134. F. E. Lytle and D. M. Hercules, *J. Am. Chem. Soc.*, 1969, 91, 253
135. Q. A. Mulazzani, S. Emmi, P. G. Fuochi, M. Venturi, M. Z. Hoffman, and M. G. Simic, *J. Phys. Chem.*, 1979, 83, 1582
136. A. Harriman, *J. Photochem.*, 1978, 8, 205
137. G. A. Crosby, W. G. Perkins, and D. M. Klassen, *J. Chem. Phys.*, 1965, 43, 1498
138. D. M. Klassen and G. A. Crosby, *J. Chem. Phys.*, 1968, 48, 1853
139. G. B. Porter and H. L. Schläfer, *Ber. Bunsenges Phys. Chem.*, 1964, 68, 316
140. G. A. Crosby and W. H. Elfring, *J. Phys. Chem.*, 1976, 80, 2206
141. J. N. Demas and J. W. Addington, *J. Am. Chem. Soc.*, 1974, 96, 3663
142. S. H. Peterson and J. N. Demas, *J. Am. Chem. Soc.*, 1976, 98, 7880
143. R. J. Watts, R. W. Harrigan, and G. A. Crosby, *Chem. Phys. Lett.*, 1971, 8, 49
144. G. A. Crosby, D. E. Lacky, and B. J. Pankuch, Abstracts of the 169th A.C.S. Meeting (Philadelphia), 1975, No. INOR69
145. R. A. Plane and J. P. Hunt, *J. Am. Chem. Soc.*, 1957, 79, 3343
146. R. W. Harrigan and G. A. Crosby, *J. Am. Chem. Soc.*, 1973, 95, 3468
147. G. D. Hager, R. J. Watts, and G. A. Crosby, *J. Am. Chem. Soc.*, 1975, 97, 7037

148. K. W. Hipps and G. A. Crosby, *J. Am. Chem. Soc.*, 1975, 97, 7042
149. I. Fujita and H. Kobayashi, *Inorg. Chem.*, 1973, 12, 2758
150. I. Hanazaki and S. Nagakura, *Inorg. Chem.*, 1969, 8, 648
151. H. C. Stynes and J. A. Ibers, *Inorg. Chem.*, 1971, 10, 2304
152. D. C. Baker and G. A. Crosby, *Chem. Phys.*, 1974, 4, 428
153. G. A. Crosby, in "Inorganic Compounds with Unusual Properties", *Adv. Chem. Series*, 1976, 150, 149
154. S. R. Allsopp, A. Cox, T. J. Kemp, and W. J. Reed, *J. Chem. Soc., Faraday Trans. I*, 1978, 74, 1275
155. E. E. Mercer and R. R. Buckley, *Inorg. Chem.*, 1965, 4, 1692
156. J. N. Demas and G. A. Crosby, *J. Mol. Spec.*, 1968, 26, 72
157. N. Sabbatini, M. A. Scandola and V. Carassiti, *J. Phys. Chem.*, 1973, 77, 1307
158. N. Sabbatini, M. A. Scandola, and V. Balzani, *J. Phys. Chem.*, 1974, 78, 541
159. I. Fujita and H. Kobayashi, *J. Chem. Phys.*, 1973, 59, 2902
160. F. Bolletta, M. Maestri, and V. Balzani, *J. Phys. Chem.*, 1976, 80, 2499
161. A. Juris, M. T. Gandolfi, M. F. Manfrin, and V. Balzani, *J. Am. Chem. Soc.*, 1976, 98, 1047

162. N. A. P. Kane-Maguire and C. H. Langford, *J. Am. Chem. Soc.*, 1972, 94, 2125
163. J. N. Demas and J. W. Addington, *J. Am. Chem. Soc.*, 1976, 98, 5800
164. C. T. Lin and N. Sutin, *J. Am. Chem. Soc.*, 1975, 97, 3543
165. J. N. Demas and A. W. Adamson, *J. Am. Chem. Soc.*, 1971, 93, 1800
166. A. Juris, M. F. Manfrin, M. Maestri, and N. Serpone, *Inorg. Chem.*, 1978, 17, 2258
167. M. S. Wrighton and J. Markham, *J. Phys. Chem.*, 1973, 77, 3042
168. R. Ballardini, G. Varani, F. Scandola, and V. Balzani, *J. Am. Chem. Soc.*, 1978, 100, 7219
169. C. Creutz and N. Sutin, *J. Am. Chem. Soc.*, 1977, 99, 241
170. D. Meisel, M. S. Matheson, W. A. Mulac, and J. Rabani, *J. Phys. Chem.*, 1977, 81, 1449
171. G. Navon and N. Sutin, *Inorg. Chem.*, 1974, 13, 2976
172. R. C. Young, T. J. Meyer, and D. G. Whitten, *J. Am. Chem. Soc.*, 1976, 98, 286
173. M. I. C. Ferreira and A. Harriman, *J. Chem. Soc., Faraday Trans. II*, 1979, 75, 874
174. C. R. Bock, T. J. Meyer, and D. G. Whitten, *J. Am. Chem. Soc.*, 1975, 97, 2909
175. N. S. Hush, *Prog. Inorg. Chem.*, 1967, 8, 391; *Electrochim. Acta*, 1968, 13, 1005

176. J. K. Nagle, W. J. Dressick, and T. J. Meyer, *J. Am. Chem. Soc.*, 1979, 101, 3993
177. G. S. Laurence and V. Balzani, *Inorg. Chem.*, 1974, 13, 2976
178. F. Bolletta, A. Juris, M. Maestri, and D. Sandini, *Inorg. Chim. Acta*, 1980, 44, L175
179. M. Neumann-Spallart, K. Kalyanasundaram, C. Grätzel, and M. Grätzel, *Helv. Chim. Acta*, 1980, 62, 1111
180. J. N. Demas, E. W. Harris, and R. P. M. McBride, *J. Am. Chem. Soc.*, 1977, 99, 3547
181. J. N. Demas, R. P. M. McBride, and E. W. Harris, *J. Phys. Chem.*, 1976, 80, 2248
182. Y. Kurimura and R. Onimura, *Inorg. Chem.*, 1980, 19, 3516
183. N. Sutin and C. Creutz, *Pure Appl. Chem.*, 1980, 52, 2717
184. P. Natarajan and J. F. Endicott, *J. Phys. Chem.*, 1973, 77, 971
185. P. Natarajan and J. F. Endicott, *J. Am. Chem. Soc.*, 1972, 94, 3635
186. C. R. Bock, J. A. Connor, A. R. Gutierrez, T. J. Meyer, D. G. Whitten, B. P. Sullivan, and J. K. Nagle, *J. Am. Chem. Soc.*, 1979, 101, 4815
187. M. Maestri and M. Grätzel, *Ber. Bunsenges Phys. Chem.*, 1977, 81, 504
188. A. Deronizer and T. J. Meyer, *Inorg. Chem.*, 1980, 19, 2912

176. J. K. Nagle, W. J. Dressick, and T. J. Meyer, *J. Am. Chem. Soc.*, 1979, 101, 3993
177. G. S. Laurence and V. Balzani, *Inorg. Chem.*, 1974, 13, 2976
178. F. Bolletta, A. Juris, M. Maestri, and D. Sandini, *Inorg. Chim. Acta*, 1980, 44, L175
179. M. Neumann-Spallart, K. Kalyanasundaram, C. Grätzel, and M. Grätzel, *Helv. Chim. Acta*, 1980, 62, 1111
180. J. N. Demas, E. W. Harris, and R. P. M. McBride, *J. Am. Chem. Soc.*, 1977, 99, 3547
181. J. N. Demas, R. P. M. McBride, and E. W. Harris, *J. Phys. Chem.*, 1976, 80, 2248
182. Y. Kurimura and R. Onimura, *Inorg. Chem.*, 1980, 19, 3516
183. N. Sutin and C. Creutz, *Pure Appl. Chem.*, 1980, 52, 2717
184. P. Natarajan and J. F. Endicott, *J. Phys. Chem.*, 1973, 77, 971
185. P. Natarajan and J. F. Endicott, *J. Am. Chem. Soc.*, 1972, 94, 3635
186. C. R. Bock, J. A. Connor, A. R. Gutierrez, T. J. Meyer, D. G. Whitten, B. P. Sullivan, and J. K. Nagle, *J. Am. Chem. Soc.*, 1979, 101, 4815
187. M. Maestri and M. Grätzel, *Ber. Bunsenges Phys. Chem.*, 1977, 81, 504
188. A. Deronizer and T. J. Meyer, *Inorg. Chem.*, 1980, 19, 2912

189. R. C. Young, F. R. Keen, and T. J. Meyer, *J. Am. Chem. Soc.*, 1977, 99, 2468
190. H. E. Toma and C. Creutz, *Inorg. Chem.*, 1977, 16, 545
191. E. König and S. Herzog, *J. Inorg. Nucl. Chem.*, 1970, 32, 585
192. N. A. P. Kane-Maguire, J. Conway, and C. H. Langford, *J. Chem. Soc., Chem. Commun.*, 1974, 801
193. P. Belser, A. Von Zelewsky, A. Juris, F. Barigelletti, A. Tucci, and V. Balzani, *Chem. Phys. Lett.*, 1982, 89, 101
194. W. H. Elfring and G. A. Crosby, *J. Am. Chem. Soc.*, 1981, 103, 2683
195. A. T. Cocks, R. D. Wright, and K. R. Seddon, *Chem. Phys. Lett.*, 1982, 85, 369
196. M. G. Kinnaird and D. G. Whitten, *Chem. Phys. Lett.*, 1982, 88, 275
197. R. W. Harrigan and G. A. Crosby, *Spectrochim. Acta*, 1970, 26A, 2225
198. H. L. Schläfer, H. Gausmann, and H. Witzke, *Z. Phys. Chem. (Frankfurt)*, 1967, 56, 55
199. R. G. W. Norrish and G. Porter, *Nature*, 1949, 164, 658
200. G. Porter and M. R. Topp, *Nature*, 1968, 220, 1228
201. G. Porter and E. S. Reid, in "Fast Processes in Radiation Chemistry and Biology", Ed. G. E. Adams, E. M. Fielden, and B. D. Michael, the Institute of Physics, John Wiley, Chichester, 1975, p.33

202. G. C. Hatchard and C. A. Parker, *Proc. Roy. Soc.*, 1956, A235, 518
203. S. L. Murov, in "Handbook of Photochemistry", Marcel Dekker, 1973
204. W. H. Melhuish and R. Hardwick, *Trans. Faraday Soc.*, 1962, 58, 1908
205. F. C. Unterleitner and E. I. Hormats, *J. Phys. Chem.*, 1965, 69, 2516
206. W. Windhager, S. Schneider, and F. Dörr, *J. Photochem.*, 1976, 6, 69
207. G. N. Schrauzer, *Inorg. Synth.*, 1968, 11, 61
208. B. E. Bryant and W. C. Fernelins, *Inorg. Synth.*, 1957, 5, 188
209. F. P. Dwyer, H. A. Goodwin, and E. C. Gyarfas, *Aust. J. Chem.*, 1963, 16, 544
210. B. Bosnich and F. P. Dwyer, *Aust. J. Chem.*, 1966, 19, 2229
211. G. M. Bryant, J. E. Fergusson, and H. K. J. Powell, *Aust. J. Chem.*, 1971, 24, 257
212. T. J. Kemp, J. P. Roberts, G. A. Salmon, and G. F. Thompson, *J. Phys. Chem.*, 1968, 72, 1464
213. F. Wilkinson and A. Farmilo, *J. Chem. Soc., Faraday Trans. II*, 1976, 72, 604
214. J. Postuma and W. Berends, *Biochim. Biophys. Acta*, 1966, 112, 422
215. G. N. Lewis and M. Kasha, *J. Am. Chem. Soc.*, 1944, 66, 2100
216. T. Ohno and S. Kato, *Bull. Chem. Soc. Japan*, 1969, 42, 3385

217. G. Porter and M. W. Windsor, *Proc. Roy. Soc.*, 1958, A245, 238
218. W. G. Herkstroeter and P. B. Merkel, *J. Photochem.*, 1981, 16, 331
219. F. Wilkinson and C. Tsiamis, *J. Chem. Soc., Faraday Trans. II*, 1981, 77, 1681
220. P. Moore, *J. Chem. Soc., Faraday Trans. I*, 1972, 68, 1890
221. K. Itoh and K. Honda, *Chem. Phys. Lett.*, 1982, 87, 213
222. D. K. K. Liu and L. R. Faulkner, *J. Am. Chem. Soc.*, 1977, 99, 4594
223. A. Yildiz, P. T. Kissinger, and C. N. Reilley, *J. Chem. Phys.*, 1968, 49, 1403
224. C. K. Jørgensen, quoted by M. D. Marcantonatos, *J. Chem. Soc., Faraday Trans. I*, 1979, 75, 2252
225. H. D. Burrows and T. J. Kemp, *Chem. Soc. Rev.*, 1974, 3, 139
226. C. Bartocci, S. Sostero, O. Traverso, A. Cox, T. J. Kemp and W. J. Reed, *J. Chem. Soc., Faraday Trans. I*, 1980, 76, 797
227. N. A. P. Kane-Maguire and C. H. Langford, *J. Chem. Soc., Chem. Commun.*, 1971, 895
228. K. Gollnick, *Ann. Acad. Sci. (New York)*, 1970, 171, 89
229. G. Roewer, G. A. Shagisultanova, and I. W. Wojakin, *J. Prakt. Chem.*, 1977, 319, 1031
230. P. Maillard, J. C. Massot, and C. Giannotti, *J. Organomet. Chem.*, 1978, 159, 219

231. V. D. Ghanekar and R. E. Coffman, *J. Phys. Chem.*, 1980, 198, C15
232. G. R. Buettner and R. E. Coffman, *Biochem. Biophys. Acta*, 1977, 480, 495
233. K. L. Schepler, W. R. Dunham, R. H. Sands, J. A. Fee, and R. H. Abeles, *Biochem. Biophys. Acta*, 1975, 397, 510
234. V. D. Ghanekar, R. J. Lin, R. E. Coffman, and R. L. Blakley, *Biochem. Biophys. Res. Commun.*, 1981, 101, 215
235. B. S. Hall, K. F. Dahnke, S. S. Fratoni, and S. P. Perone, *J. Phys. Chem.*, 1977, 80, 866
236. L. L. Constanzo, I. Fragala, S. Giuffrida, and G. Condorelli, *Inorg. Chim. Acta*, 1975, 28, 19
237. P. G. Bowers and G. Porter, *Proc. Roy. Soc.*, 1967, A299, 348
238. F. Bolletta, M. Giera, and V. Balzani, *J. Phys. Chem.*, 1972, 76, 3934
239. Y. L. Chow, G. E. Buono-Core, B. Marciniak, and C. Beddard, *Can. J. Chem.*, 1983, 61, 801
240. G. Navon and N. Sutin, *Inorg. Chem.*, 1974, 13, 2159
241. G. A. Crosby, *Acc. Chem. Res.*, 1975, 8, 23
242. M. K. DeArmond, *Can. J. Chem.*, 1982, 60, 325
243. W. D. K. Clark and N. L. Leiby, *J. Phys. Chem.*, 1977, 99, 4676
244. A. Cox, T. J. Kemp, W. J. Reed, and G. Trapp, *J. Chem. Soc., Faraday Trans. 1*, 1980, 76, 804

260. V. E. Stel'mashok and A. L. Poznyak, *Sov. J. Coord. Chem.*, 1979, 5, 801
261. K. DeArmond and W. Halper, *J. Phys. Chem.*, 1971, 75, 3230
262. M. Kohno, H. Ohya-Nishiguchi, K. Yamamoto, and T. Sakurai, *Bull. Chem. Soc. Japan*, 1983, 56, 822
263. M. E. Peover, *J. Chem. Soc.*, 1962, 4540
264. A. H. Maki and D. H. Geske, *J. Chem. Phys.*, 1960, 33, 825
265. M. E. Peover, *Trans. Faraday Soc.*, 1964, 60, 479
266. J. G. Lawless, D. E. Barkak, and D. M. Hawley, *J. Am. Chem. Soc.*, 1969, 91, 7121
267. A. H. Maki and D. H. Geske, *J. Am. Chem. Soc.*, 1961, 83, 1852
268. D. H. Geske, J. L. Ragle, M. A. Bambenek, and A. L. Balch, *J. Am. Chem. Soc.*, 1964, 86, 987
269. D. G. Nocera, A. W. Maverick, J. R. Winkler, C. M. Che, and H. B. Gray, in "Inorganic Chemistry: Toward the 21st Century", *Am. Chem. Soc.*, Symp. Ser. No. 211, Washington, D.C., 1983, p.21
270. L. Malatesta and C. Cariello, *J. Chem. Soc.*, 1958, 2323
271. R. Ugo, *Coord. Chem. Rev.*, 1968, 3, 319
272. R. Ugo, F. Cariati, and G. La Monica, *J. Chem. Soc., Chem. Commun.*, 1966, 868

273. D. M. Blake and C. J. Nyman, *J. Am. Chem. Soc.*,  
1970, 92, 5359
274. C. M. Che, L. G. Butler, and H. B. Gray,  
*J. Am. Chem. Soc.*, 1981, 103, 7796
275. C. M. Che, L. G. Butler, H. B. Gray, R. M. Crooks,  
and W. H. Woodruff, *J. Am. Chem. Soc.*, 1983,  
105, 5492
276. M. A. Filomena Dos Remedios Pinto and  
P. J. Sadler, *J. Chem. Soc., Chem. Commun.*,  
1980, 13
277. O. Traverso, Private Communication
278. A. Vogler, R. E. Wright, and H. Kunkely,  
*Angew Chem. Int. Ed. Engl.*, 1980, 19, 717
279. A. Vogler and H. Kunkely, *J. Am. Chem. Soc.*,  
1981, 103, 6222

Attention is drawn to the fact that the copyright of this thesis rests with its author.

This copy of the thesis has been supplied on condition that anyone who consults it is understood to recognise that its copyright rests with its author and that no quotation from the thesis and no information derived from it may be published without the author's prior written consent.

**II**

D52